creative commons
COMMONS DEED

저작자표시-비영리-변경금지 2.0 대한민국

이용자는 아래의 조건을 따르는 경우에 한하여 자유롭게

- 이 저작물을 복제, 배포, 전송, 전시, 공연 및 방송할 수 있습니다.

다음과 같은 조건을 따라야 합니다:

저작자표시. 귀하는 원저작자를 표시하여야 합니다.

비영리. 귀하는 이 저작물을 영리 목적으로 이용할 수 없습니다.

변경금지. 귀하는 이 저작물을 개작, 변형 또는 가공할 수 없습니다.

- 귀하는, 이 저작물의 재이용이나 배포의 경우, 이 저작물에 적용된 이용허락조건을 명확하게 나타내어야 합니다.
- 저작권자로부터 별도의 허가를 받으면 이러한 조건들은 적용되지 않습니다.

저작권법에 따른 이용자의 권리는 위의 내용에 의하여 영향을 받지 않습니다.

이것은 이용허락규약(Legal Code)을 이해하기 쉽게 요약한 것입니다.

Disclaimer

dCollection

이학박사학위논문

A Simultaneous 22 GHz Water and 44/95 GHz Methanol Maser Survey toward Massive Star-forming Regions

무거운 별 탄생 영역들에 대한 22 GHz 물 메이저와 44/95 GHz 메탄올 메이저 동시 관측

2016년 8월

서울대학교 대학원

물리·천문학부천문학전공

김 창 희

Abstract

The 22 GHz H_2O and 44 / 95 GHz CH_3OH masers are predominantly associated with high-mass star formation and these signposts would allow us to do statistical studies of high-mass star-forming regions. These molecules are originated from the icy mantle of dust grain and released in shocks. However we do not fully understand the role of those common masers in the process of massive star formation. The main aim of this thesis is to investigate the relationships of those masers with massive star-forming regions in a different evolutionary phase. We carried out simultaneous single-dish surveys of 22 GHz H_2O and 44 and 95 GHz class I CH_3OH maser transitions toward 782 massive star-forming regions. Our samples consist of Infrared Dark Clouds (IRDCs), Red MSX Sources (RMSs), high-mass protostellar objects (HMPOs), Methanol Maser Sources (MMS) and ultra-compact HII regions (UCHIIs). The overall detection rates are 32%, 51%, 61%, 96% and 67% for IRDCs, RMSs, HMPOs, MMSs, and UCHIIs, respectively. There is an increasing trend for each detection rate of 22 GHz and 44 GHz maser emission with

evolution of the central objects from IRDCs to UCHIIs. In samples of RMSs, 138 sources are located in the Methanol Multibeam (MMB) survey area and 25% of them are associated with 6.7 GHz class II CH_3OH masers. We detected H_2O maser of high-velocity (> 30km s^{-1}) features in 99 of 386 H_2O maser sources(26%). We discovered nine sources of being dominant H_2O maser outflow candidates from RMS samples. Both of 44 and 95 GHz class I CH_3OH masers have very similar properties in line parameters, which implies that they hold a common origin of the masing gas. We examined the relationship between the maser luminosity and physical conditions of parental clumps(cores) from ATLASGAL. There were significant ($\rho > 0.5$) correlations between the maser luminosity and the bolometric luminosity and the clump mass for all three masers. For maser sources associated with NH_3 data, we found a increasing trends in the lindwidth and kinetic temperature with the evolution of the central objects. Using the L_{bol}/M_{clump} ratio, we compared the distribution on each type of the central objects. There is no robust difference in the distribution on the combinations with threee maser species. Our investigation on the virial parameter against M_{clump} suggested that ATLASGAL clumps with any maser emission are more gravitationally stable than those with no maser emission in a wide range of clump mass. Like the L_{bol}/M_{clump}, L_{maser}/L_{bol} appear to decrease as the cnetral objects evolve.

Keywords : infrared, ISM; ISM, molecules; masers, ISM; stars, formation

Student Number : 2006-30782

Contents

Abstract **i**

List of Figures **vii**

List of Tables **xvii**

1 Introduction **1**

1.1 Motivations 1

1.2 Star Formation 3

1.2.1 Low Mass Star Formation 4

1.2.2 High Mass Star Formation 9

1.3 Astronomical Masers 14

1.3.1 Radiative Transfer and Population Inversion . 15

1.3.2 Water(H_2O) Masers 19

1.3.3 Methanol(CH_3OH) Masers 19

1.4 Aims and Outlines 22

2 Simultaneous Surveys of Water and Class I Methanol Masers toward Red MSX Sources 27

2.1 Introduction 27

2.2 Source Selection and Observations 30

2.2.1 Source Selection 30

2.2.2 Observations 31

2.3 Result 33

2.3.1 Detection Statistics 33

2.3.2 New Detections 34

2.3.3 Maser Properties 35

2.3.4 Comments on Individual Sources of Interest . . 40

2.4 Analysis and Discussion 44

2.4.1 Masers and the Central Objests 44

2.4.2 Masers and the Parental Clumps 46

2.4.3 NH_3 Linewidth and Kinetic Temperature . . . 49

2.4.4 The Virial Parameters 51

2.4.5 Maser Occurrence and Evolutionary Stage . . . 52

2.5 Summary 54

3 Simultaneous Surveys of Water and Class I Methanol Masers toward High-mass Young stellar Objects in Different Evolutionary Stages 123

3.1 Introduction 123

3.2 Sources and Observations 127

3.2.1 Sources 127
3.2.2 Observations 133
3.3 Results 134
3.3.1 Detection Statistics 134
3.3.2 Maser Line Properties 137
3.3.3 Individual Sources 140
3.4 Analysis and Discussion 141
3.4.1 Luminosity 141
3.4.2 Clump Mass 142
3.4.3 NH_3 Δv(1,1) and T_k 145
3.4.4 Luminosity to Mass Ratio 147
3.4.5 Virial Mass 149
3.4.6 Evolutionary Sequence 151
3.5 Summary 153

4 Summary and Future Work **276**

4.1 Summary 276
4.2 Future work 279

초 록 **281**

List of Figures

1.1 Diagram showing the four different classes of young stellar objects and their respective SEDs. From Isella (2006). 8

1.2 This cartoon illustrates the formation of a cluster of high-mass stars, from molecular cloud to ionised bubble. The sequence places classes of observed objects on a rough time-line. From Dr. Purcell's website 13

1.3 A simple two level system. E_1 , E_2 and E_3 are the first three energy levels and N_1 , N_2 and N_3 are the populations of those levels. 18

2.1 Venn diagram showing the numbers of detected 22 GHz H_2O and 44 and 95 GHz class I CH_3OH maser sources in each epoch. The numbers in blue and black represent the first and second epochs, respectively. The numbers in red are for the subsample of 138 sources in the MMB survey area (see the text for details). 98

2.2 U(Upper panel) The detected 22 GHz H_2O, (Middle panel) 44 GHz CH_3OH, and (Lower panel) 95 GHz CH_3OH maser spectra of the sources detected in all of 3 transitions. Blue and Black colors represent the first and second epochs, respectively. The source name is given in the top-left corner of the upper panel and 'M' is attached for the source associated with 6.7 GHz CH_3OH maser emission from Breen et al. (2015). The observing dates are shown in the top-right corner. The vertical dotted line indicates the systemic velocity. . . 99

2.3 Continued 100

2.4 Continued 101

2.5 Continued 102

2.6 Same as in Figure 2.2except for the source detected both at (Upper) 22 and (Lower) 44 GHz. 103

2.7 Same as in Figure 2.2except for the source detected both at (Upper) 44 and (Lower) 95 GHz. 104

2.8 Same as in Figure 2.2except for the source detected only at 22 GHz. 105

2.9 Continued 106

2.10 Continued 107

2.11 Continued 108

2.12 Continued 109

2.13 Same as in Figure 2.2except for the source detected only at 44 GHz. 110

2.14 (a) Histogram of the relative peak velocities for the 22, 44, and 6.7 GHz maser sources in a bin size of 3 km s^{-1}. Blue, green, and brown colors represent 22, 44, and 6.7 GHz masers, respectively. The 22 and 44 GHz data are from the second epoch survey of this study, while the 6.7 GHz data are from the MMB survey. The mean and median values of each distribution are listed in the top-right corner of each panel. (b) Same as in (a) except for the velocity ranges in 4 km s^{-1} bin. 111

2.15 (Upper) The detected 22 GHz H_2O (*black*) and 44 GHz CH_3OH (*blue*) maser spectra and (Lower) ^{13}CO J=1−0 (*black*) and HCO^+ J=1−0 (*blue*) line spectra of dominant H_2O maser outflow source candidates (^{13}CO J=2−1 line spectrum only for RMS 3936). For each source, the source name is presented at the top-right corner of the upper panel and the systemic velocity is indicated by a vertical dotted line. The lower panel shows spectrum of $^{13}CO(J = 1-0)$(or $^{13}CO(J = 2-1)$ for RMS 3936, refers to Table 2.6.) and $HCO^+(J = 1-0)$ line for 13 H_2O maser sources with high velocity offset (> 30 km s^{-1}) from the systemic velocity. For comparison, corresponding the 22 GHz H_2O and 44 GHz CH_3OH maser spectrum are shown in the upper panel. For each panel, black line represent the ^{13}CO and H_2O maser and blue one stands for HCO^+ line and 44 GHz CH_3OH maser. Because of the systemic velocity modification in RMS database during the observation period, the systemic velocities are presented in two type of vertical line: long-dashed and dashed line for old and current version of them. It is noted that each panel have a different y-axis scale of Jy(upper) and T_A^*(lower). 112

2.16 Continued 113

2.17 Comparison of (a) the relative peak velocities, (b) the peak flux densities, and (c) the isotropic luminosities of the 44 and 95 GHz class I CH_3OH maser sources. In each panel the least-squares fitted relation is displayed by a dashed line with the correlation coefficient in the bottom-right corner. 114

2.18 Comparison of the isotropic maser luminosity with the bolometric luminosity for (a) the 22 GHz, (b) 44 GHz, (c) 95 GHz, and (d) 6.7 GHz maser sources. The 22, 44, and 95 GHz data are from the second-epoch survey of this study, while the 6.7 GHz data are from the MMB survey (Breen et al., 2015). The Pearson correlation coefficient is shown in the bottom-right corner of each panel. 115

2.19 Comparison of the isotropic maser luminosity with the bolometric luminosity for (a) the 22 GHz and (b) 44 GHz maser sources. The data points in low- and intermediate-mass regime are added from the literature. In both panels open circles and asterisks are data points of this study in the second epoch and Bae et al. (2011), respectively. Open squares are data points from Furuya et al. (2003) in (a) and Kalenskii et al. (2013) in (b). The least-sqaures fitted relation is displayed by a dashed line with the correlation coefficient on the bottom-right corner in each panel. 116

2.20 Same as in Figure 2.18except for the associated ATLASGAL clump mass. In each panel the least-sqaures fitted relation is shown by a dashed line with the correlation coefficient on the bottom-right corner. 117

2.21 Same as in Figure 2.18except for the peak H_2 column density. 118

2.22 The peak H_2 column density versus the ATLASGAL clump mass for the four maser species. Open circles and crosses represent the sources with and without maser emission, respectively. In each panel the least-sqaures fitted relation is shown by a dashed line with the correlation coefficient on the bottom-right corner. 119

2.23 The integrated maser flux density versus the peak H_2 column density. In each panel the least-sqaures fitted relation is shown by a dashed line with the correlation coefficient in the bottom-right corner. 120

2.24 Cumulative probability of (a) the NH_3 linewidth and (b) the kinetic temperature for 4 subsamples, which are divided on the bassis of the second-epoch survey results. The subsamples and corresponding colors are displayed on the bottom-right corner in each panel. . 121

2.25 The virial parameter (α) versus the clump mass for the associated ATLASGAL clumps. Open and filled circles represent the sources with and without any maser emission, respectively. The dashed line indicates the critical value (α=1) for an isothermal sphere in hydrostatic equilibrium without magnetic support. The area of $\alpha < 1$ indicates the region where clumps are graviationally unstable and likely to be collapsing without additional support from strong magnetic field. The solid and dotted lines show the least-sqaures fitted relations for the filled and open circles, respectively. The Pearson correlation coefficients are shown in the right upper corner. 122

3.1 A median of (a) the peak flux density, (b) the relative velocity, and (c) the velocity range of the 22 GHz(red), 44 GHz(blue) and 95 GHz(yellow) masers for five type of objects. 221

3.2 Comparison of (a) the relative peak velocities, (b) the peak flux densities, and (c) the isotropic luminosities of the 44 and 95 GHz class I CH_3OH maser sources. Symbols and colors of different type of object are presented in the upper-left corner of panel (a). In each panel the least-squares fitted relation is displayed by a dashed line with the correlation coefficient in the bottom-right corner. 222

3.3 Comparison of the isotropic maser luminosity with the bolometric luminosity for (a) the 22 GHz, (b) 44 GHz, and (c) 95 GHz maser sources. In each panel the least-squares fitted relation is displayed by a dashed line with the correlation coefficient in the bottom-right corner. 223

3.4 Same as in Figure 3.3except for the associated ATLASGAL clump mass. 224

3.5 Same as in Figure 3.3except for the associated ATLASGAL peak H_2 column density. 225

3.6 Same as in Figure 3.3except for the velocity range of the detected maser lines. 226

3.7 Cumulative probability of (Upper panel) the NH_3 linewidth and (Lower panel) the kinetic temperature for 5 type of objects. The detected maser lines are shown in upper-left corners on each panel. The source types and corresponding colors are displayed on the bottom-right corner in (d) panel. 227

3.8 Same as in Figure 3.3except for the NH_3 linewidth of the detected maser lines. 228

3.9 Cumulative probability of L_{bol}/M_{lump} for 5 type of objects regarding to the combinations of three maser detection and non-deection. The parameters of the distribution are displayed in upper-left corners on each panel. The source types and corresponding colors are displayed on the bottom-right corner in (d) and (e) panel. 229

3.10 Histogram of L_{bol}/M_{lump} for the detected maser line of (a) 22 GHz only and (b) 44 GHz only. The source types and corresponding colors are displayed on the bottom-left corner in (a) panel. 230

3.11 The virial parameter (α) versus the clump mass for the associated ATLASGAL clumps. Open and filled symbols represent the sources with and without any maser emission, respectively. The source types and corresponding colors are displayed in the bottom-right corner. The results of linear regression and correlation coefficient for the source with any maser emission and no maser emission are presented on the upper-right corner in the panel. The fitted line for maser detection and non-detection are shown as long-dashed and dashed line, respectively. The horizontal lines in solid and dotted style mark $\alpha = 1$ and $\alpha = 2$ (refer to Sec.4.5. for details) 231

3.12 Comparison of FWHM linewidth of $NH_3(1,1)$ versus M_{clump} (Larson's 2nd law). In each panel the least-squares fitted relation is displayed by a dashed line with the correlation coefficient in the bottom-right corner. The best fit line for source with maser detections and non-detection are displayed in dashed and solid lines. The dotted line is original Larson's result of 0.42 $M^0.2$. The source types and corresponding colors are displayed on the upper-left corner in the panel. . 232

3.13 The maser luminosity to the bolometric luminosity against L_{bol}/M_{clump} for the (a) 22 GHz, (b) 44 GHz, and (c) 95 GHz maser sources. In each panel the least-squares fitted relation is displayed by a dashed line with the correlation coefficient in the bottom-right corner. The source types and corresponding colors are displayed on the upper-left corner in (a) panel. 233

3.14 Same as in Figure 3.13except for the maser luminosity against L_{bol}/M_{clump}. 234

3.15 The peak flux ratio of 44 GHz to 95 GHz($S_{\rm p,44}/S_{\rm p,95}$) against (a) the peak column density and (b) $L_{\rm bol}/M_{\rm clump}$. The source types and corresponding colors are displayed on the upper-left corner in (a) panel. 235

3.16 (Upper panel) The detected 22 GHz H_2O, (Middle panel) 44 GHz CH_3OH, and (Lower panel) 95 GHz CH_3OH maser spectra of the sources detected in all of three transitions. The source name is given in the top-left corner of the upper panel and the observing dates are shown in the top-right corner. The vertical dotted line indicates the systemic velocity. 236

3.17 Continued 237

3.18 Continued 238

3.19 Same as in Figure 3.16except for the source detected both at (Upper) 22 and (Lower) 44 GHz. 239

3.20 Same as in Figure 3.16except for the source detected both at (Upper) 44 and (Lower) 95 GHz. 240

3.21 Same as in Figure 3.16except for the source detected both at (Upper) 22 and (Lower) 95 GHz. 241

3.22 Same as in Figure 3.16except for the source detected only at 22 GHz. 242

3.23 Continued 243

3.24 Same as in Figure 3.16except for the source detected only at 44 GHz. 244

3.25 Same as in Figure 3.16except for the source detected only at 95 GHz. 245

3.26 **HMPOs.** (Upper panel) The detected 22 GHz H_2O, (Middle panel) 44 GHz CH_3OH, and (Lower panel) 95 GHz CH_3OH maser spectra of the sources detected in all of three transitions. Other details are same as in Figure 3.16 246

3.27 Continued 247

3.28 Continued 248

3.29 Same as in Figure 3.26except for the source detected both at (Upper) 22 and (Lower) 44 GHz. 249

3.30 Same as in Figure 3.26except for the source detected both at (Upper) 44 and (Lower) 95 GHz. 250

3.31 Same as in Figure 3.26except for the source detected only at 22 GHz. 251

3.32 Continued 252

3.33 Continued 253

3.34 Same as in Figure 3.26except for the source detected only at 44 GHz. 254

3.35 **MMSs.** (Upper panel) The detected 22 GHz H_2O, (Middle panel) 44 GHz CH_3OH, and (Lower panel) 95 GHz CH_3OH maser spectra of the sources detected in all of three transitions. Other details are same as in Figure 3.16 255

3.36 Continued 256

3.37 Continued 257

3.38 Continued 258

3.39 Continued 259

3.40 Same as in Figure 3.35except for the source detected both at (Upper) 22 and (Lower) 44 GHz. 260

3.41 Continued 261

3.42 ame as in Figure 3.35except for the source detected both at (Upper) 44 and (Lower) 95 GHz. 262

3.43 Continue 263

3.44 Same as in Figure 3.35except for the source detected only at 22 GHz. 264

3.45 Same as in Figure 3.35except for the source detected only at 44 GHz. 265

3.46 **UCHIIs.** Upper panel) The detected 22 GHz H_2O, (Middle panel) 44 GHz CH_3OH, and (Lower panel) 95 GHz CH_3OH maser spectra of the sources detected in all of three transitions. Other details are same as in Figure 3.16 266

3.47 Continued 267

3.48 Continued 268

3.49 Same as in Figure 3.46except for the source detected both at (Upper) 22 and (Lower) 44 GHz. 269

3.50 Same as in Figure 3.46except for the source detected both at (Upper) 44 and (Lower) 95 GHz. 270

3.51 Same as in Figure 3.46except for the source detected both at (Upper) 22 and (Lower) 95 GHz. 271

3.52 Same as in Figure 3.46except for the source detected only at 22 GHz. 272

3.53 Continued 273

3.54 Continued 274

3.55 Same as in Figure 3.46except for the source detected only at 44 GHz. 275

List of Tables

2.1 Summary of Target Sources 62

2.1 Summary of Target Sources 63

2.1 Summary of Target Sources 64

2.1 Summary of Target Sources 65

2.1 Summary of Target Sources 66

2.1 Summary of Target Sources 67

2.1 Summary of Target Sources 68

2.1 Summary of Target Sources 69

2.1 Summary of Target Sources 70

2.1 Summary of Target Sources 71

2.1 Summary of Target Sources 72

2.1 Summary of Target Sources 73

2.2 Summary of Observations 74

2.3 Summary of Detections 75

2.4 Detected Maser Line Parameters 76

2.4 Detected Maser Line Parameters 77
2.4 Detected Maser Line Parameters 78
2.4 Detected Maser Line Parameters 79
2.4 Detected Maser Line Parameters 80
2.4 Detected Maser Line Parameters 81
2.4 Detected Maser Line Parameters 82
2.4 Detected Maser Line Parameters 83
2.4 Detected Maser Line Parameters 84
2.4 Detected Maser Line Parameters 85
2.4 Detected Maser Line Parameters 86
2.4 Detected Maser Line Parameters 87
2.4 Detected Maser Line Parameters 88
2.4 Detected Maser Line Parameters 89
2.4 Detected Maser Line Parameters 90
2.4 Detected Maser Line Parameters 91
2.4 Detected Maser Line Parameters 92
2.4 Detected Maser Line Parameters 93
2.4 Detected Maser Line Parameters 94
2.4 Detected Maser Line Parameters 95
2.5 Statistics of Maser Line Parameters 96
2.6 Dominant Shifted H_2O Maser Source Candidates . . . 97

3.1 Summary of Observations with KVN 21m telescopes . 164

3.2 Summary of Targets 165

3.3 List of Physical Properties 166

3.4 Summary of Detections 167

3.5 Summary of target sources(IRDC) 168

3.5 Summary of target sources(IRDC) 169

3.5 Summary of target sources(IRDC) 170

3.5 Summary of target sources(IRDC) 171

3.5 Summary of target sources(IRDC) 172

3.6 Summary of target sources(HMPO) 173

3.6 Summary of target sources(HMPO) 174

3.6 Summary of target sources(HMPO) 175

3.6 Summary of target sources(HMPO) 176

3.6 Summary of target sources(HMPO) 177

3.6 Summary of target sources(HMPO) 178

3.7 Summary of target sources(MMS) 179

3.7 Summary of target sources(MMS) 180

3.7 Summary of target sources(MMS) 181

3.7 Summary of target sources(MMS) 182

3.7 Summary of target sources(MMS) 183

3.8 Summary of target sources(UCHII) 184

3.8 Summary of target sources(UCHII) 185

3.8 Summary of target sources(UCHII) 186

3.8 Summary of target sources(UCHII) 187
3.9 Detected Maser Line Parameters(IRDC) 188
3.9 Detected Maser Line Parameters(IRDC) 189
3.9 Detected Maser Line Parameters(IRDC) 190
3.9 Detected Maser Line Parameters(IRDC) 191
3.9 Detected Maser Line Parameters(IRDC) 192
3.9 Detected Maser Line Parameters(IRDC) 193
3.10 Detected Maser Line Parameters(MMS) 194
3.10 Detected Maser Line Parameters(MMS) 195
3.10 Detected Maser Line Parameters(MMS) 196
3.10 Detected Maser Line Parameters(MMS) 197
3.10 Detected Maser Line Parameters(MMS) 198
3.10 Detected Maser Line Parameters(MMS) 199
3.10 Detected Maser Line Parameters(MMS) 200
3.10 Detected Maser Line Parameters(MMS) 201
3.10 Detected Maser Line Parameters(MMS) 202
3.10 Detected Maser Line Parameters(MMS) 203
3.10 Detected Maser Line Parameters(MMS) 204
3.11 Detected Maser Line Parameters(HMPO) 205
3.11 Detected Maser Line Parameters(HMPO) 206
3.11 Detected Maser Line Parameters(HMPO) 207
3.11 Detected Maser Line Parameters(HMPO) 208

3.11 Detected Maser Line Parameters(HMPO) 209

3.11 Detected Maser Line Parameters(HMPO) 210

3.11 Detected Maser Line Parameters(HMPO) 211

3.12 Detected Maser Line Parameters(UCHII) 212

3.12 Detected Maser Line Parameters(UCHII) 213

3.12 Detected Maser Line Parameters(UCHII) 214

3.12 Detected Maser Line Parameters(UCHII) 215

3.12 Detected Maser Line Parameters(UCHII) 216

3.13 Summary of ATLASGAL 217

3.14 Summary of NH_3 218

3.15 Summary of Maser Line Parameters 219

3.16 Summary of Linear Regression Analyses 220

Chapter 1

Introduction

1.1 Motivations

Massive ($> 8M_{\odot}$) stars play a pivotal role in astrophysics. In the early Universe, the first generation of stars were predominantly massive stars (Bleomhof et al., 1989). They produced copious amounts of UV photons, leading to the reionisation of the Universe, while their prodigious energy output had important effects on subsequent galaxy formation (Carr et al. 1984). Today, the only phenomena sufficiently bright to be seen from those times are due to massive stars (e.g. Salvaterra et al. 2006). In the local Universe, massive stars are the powerhouses driving the cycles of matter and energy in the Milky Way. Formed from quiescent gas and dust, they evolve swiftly, develop energetic winds of charged particles and emit intense UV radiation. During their short lifetimes they actively reshape their environment, triggering the birth of new stars and possibly solar systems. They

end their lives in violent supernova explosions that return much of their mass to interstellar space, where the cycle begins again. To understand the physics of the evolving Universe on both small and large scales, it is essential we first understand the nearest examples of massive star formation.

Understanding the process of the formation of high mass stars with masses remains a challenge in modern astronomy. There are observational difficulties associated with high mass stars. High mass stars are rare, they form at large distances from the Earth where their birth is enshrouded in dust and gas. They begin the process of nuclear fusion even as they are accreting matter. They form on relatively short timescales and in clusters. Clustering is an issue as it causes confusion when observing a star forming region and the feedback effects of neighbouring stars also adds to the complexity of their formation.

Interstellar maser transitions at centimeter and millimeter wavelength enable us to study these regions unaffected by obscuration from dust. Being compact and bright sources, masers offer a unique opportunity to peer into the deep interior of high mass star forming regions. There are four interstellar masers of H_2O, class I/II CH_3OH, and OH that are commonly observed in high-mass star forming regions(SFRs). Class I CH_3OH masers (e.g., at 44 GHz and 95 GHz) and H_2O masers (22 GHz) are collisionally pumped in a shocked gas, while class II CH_3OH (e.g., at 6.7GHz and 12.2 GHz) and OH masers (ground state mainline at 1.6 GHz) are radiatively pumped by infrared emission from warm dust (e.g. Elitzur et al., 1989; Cragg et al., 2002). Ellingsen et al. (2007) suggested that the common maser species (H_2O, class I and II CH_3OH, and OH masers) may help iden-

tify the evolutionary phase of the central objects, and proposed a possible evolutionary sequence of these maser species. This proposed sequence has been improved upon by Breen et al. (2010b) (in their Figure 6). However, there remains significant uncertainty about where in SFRs the different maser species arise and which evolutionary phase they are associated with. The motivation for the work presented in this thesis is the quest for an empirical evolutionary sequence of massive star formation using common maser species.

1.2 Star Formation

Stars of all masses begin their lives as contracting clouds of dense gas and dust embedded in the interstellar medium. Low and high mass stars are distinguished from each other by the timescales over which they form. The timescale for collapse is given by the free-fall time (Shu et al., 1987)

$$t_{\rm ff} = \left(\frac{3\pi}{32{\rm G}_\rho}\right)^{0.5} = 3.4 \times 10^7 n^{-0.5} \text{ years}, \tag{1.1}$$

where $\mathrm{G} = 6.673 \times 10^{-11} \mathrm{N} \cdot \mathrm{m}^2 \cdot \mathrm{kg}^{-2}$ is the gravitational constant, ρ is the average mass density in $\mathrm{kg} \cdot \mathrm{cm}^{-3}$ and n is the number density in cm^{-3}. In typical molecular clouds $n \geq 50$ cm^{-3} and the free fall time is $t_{\rm ff} \leq 5 \times 10^6$ yrs, which gives a lower limit on the timescale for stellar evolution. Contraction of a mass of gas under self gravity results in gravitational potential energy being converted to heat. The timescale on which this process occurs is given by the Kelvin-Helmholtz time $t_{\rm KH}$, which provides an estimate of the time taken for

pre-fusion burning objects to evolve

$$t_{\rm KH} \approx \frac{\rm GM_*^2}{\rm R_* L_*} \tag{1.2}$$

In Equation 2 $\rm R_*$ is the stellar radius and $\rm L_*$ is the stellar luminosity. For a 1 $\rm M_\odot$ star this time is relatively long at $t_{\rm KH} \approx 3\times10^7$ yrs, but for a massive star of 50 $\rm M_*$($\rm L_* \approx 10^4 L_\odot$) collapse takes place extremely rapidly and $t_{\rm KH} \approx 10^4$ yrs. For stars with masses $>$ 8 $\rm M_\odot$ we find $t_{\rm KH} < t_{\rm ff}$, implying that fusion ignites before the collapse has ceased. Thus keey fact has important implications for the process of forming a star via accretion.

1.2.1 Low Mass Star Formation

Low mass stars are known to form in molecular clouds with masses greater than $\sim$ 0.3 $\rm M_\odot$. Although they form in clusters with their more massive counterparts, many examples also form in relative isolation where they can be studied without concern for the disruptive effects of surrounding stars. The closest complexes forming low mass stars are a mere few hundred parsecs away (e.g., Ophiuchus 119 pc (Lumbardi et al., 2008), Taurus 140 pc (Kenyon et al., 1994), Perseus 320 pc (Hirota et al., 2008)) and alleviating the investigation of the physics and chemistry on scales down to a few hundred astronomical units (AU).

Theoretically, the process of low mass star formation is well understood and has a clear evolutionary scenario (e.g., Shu et al., 1987, 1991). The fundamental event leading to star formation is the cllapse

of a dense ($10^2 - 10^4 \mathrm{cm}^{-3}$), cool ($\sim$ 10 K) knots at the intersection filaments of gas and dust within a molecular cloud. Initially the gravitational force acting towards the center of the cloud is ounterbalanced by rotation, thermal pressure and weak magnetic fields, or turbulence. Over time this support is lost as neutral particles slip through the ions (via ambipolar diffusion) and the central region increases in density. The core undergoes an 'inside-out' collapse and the collapse front expands outwards at the speed of sound in the gas. An accretion phase follows in which material from the extended envelope rains down onto the central condensation. The envelope, which was previously optically thin, becomes opaque to cooling radiation and the temperature of the central object increases. Residual angular momentum in the infalling material causes it to spin down into a dusty circumstellar disk as it contracts. Highly collimated jets and outflows are often detected at this stage as angular momentum is shed into the surrounding medium. After approximately 10^7 years the material in the vicinity of the protostar is exhausted and accretion ceases. By this time the pressure and temperature has increased enough to ignite fusion in the core and the young star begins life on the main sequence.

Observationally, low-mass young stellar objects have been divided into four distinct evolutionary classes on the basis of their spectral energy distributions (SEDs) (e.g., Lada & Wilking , 1984; Andre et al., 1993). Radiation from the powering central source is scattered, absorbed and re-emitted by the dusty protostellar envelope before escaping to interstellar space. The variation in the shape of the resultant SED reflects the conditions in the envelope at each stage of evolution. Figure 1.1 represents the evolutionary sequence and the associated spectral energy distributions for the classes 0 to III. The

SEDs of each class are shown in Figure 1.1.

Class 0: Collapse has commenced at this stage raising the temperature and luminosity of the core. The SED resembles a single blackbody, with a temperature between 20 and 30 K, and so peaks in the sub-millimetre band, at $\lambda > 150\ \mu m$. Many Class 0 sources drive energetic bipolar outflows (Lada 1999; Andre et al. 1993), implying that the infall is not spherical and disks-like structures have already formed.

Class I: As accretion proceeds the dust temperature rises and the peak of the SED moves to the far-IR (100 μm). Residual rotation causes the infalling material to form an accretion disk around the central protostellar object. Bipolar outflows and jets are formed as momentum and energy is bled off into the surroundings. The SED profile corresponds to a 50–100 K blackbody, originating in the accreting envelope, plus additional 200–400 K components, originating in the disk. A silicate absorption feature is often present at 10 μ m, indicating an optically thick envelope of dust. Observationally these sources are deeply embedded and invisible at wavelengths shortward of 1 μm.

Class II: After $\sim 10^6$ years, winds and molecular outflows have swept away much of the natal envelope, exposing the dusty disk. The peak of the SED falls in the near-infrared band, around 2 μm. Flux longward of 2 μm is dominated by excess emission from the disk. At this stage, the pre-main-sequence core is often visible in the optical and near-infrared, and is typically identified as a T-Tauri star.

Class III: These objects are visible as stars in the near-infrared and

optical, where their SED peaks. Some circumstellar material may be present in the form of a thin disk, however, the SED is generally well fit by a reddened blackbody with little or no IR excess emission. This is consistent with a reddened stellar photosphere of a star on the zero-age-main-sequence.

The evolution of the SED is due to gradual dissipation of gas and dust from the natal envelope. A quantitative classification scheme is based on the spectral index between 10 μm and 100 μm, according to (Lada , 1987)

$$\mathrm{a} = \frac{\mathrm{dlog}(\lambda \mathrm{F}_\lambda)}{\mathrm{dlog}(\lambda)} \tag{1.3}$$

For class I sources $0 < a \leq 3$, for class II sources $-2 \leq a \leq 0$, and for class III sources $-3 \leq a \leq -2$.

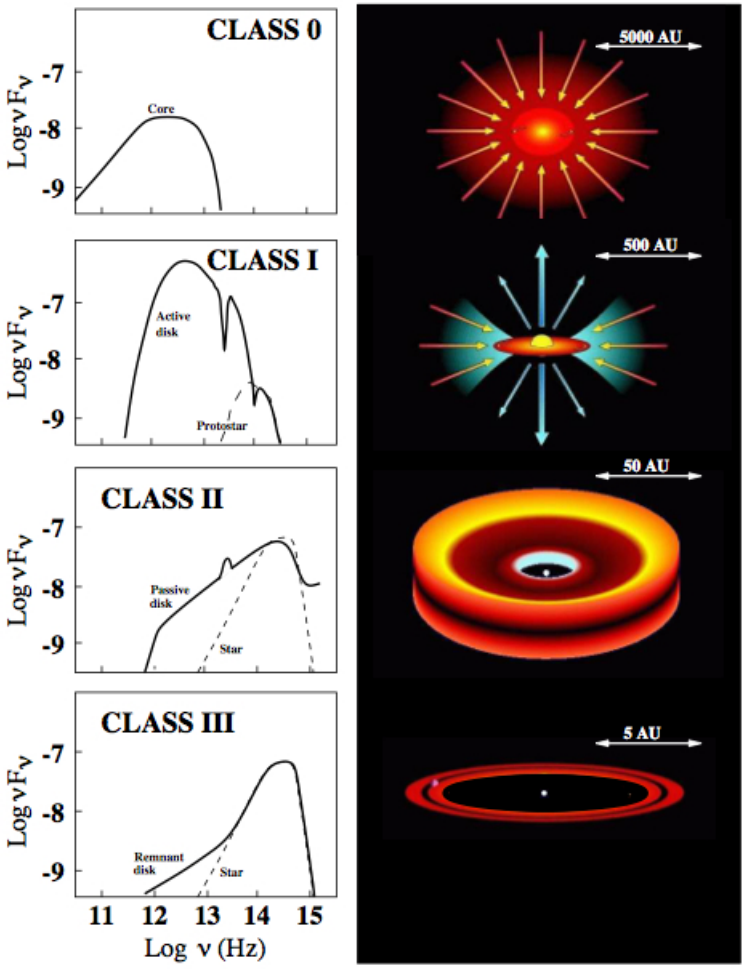

Figure 1.1: Diagram showing the four different classes of young stellar objects and their respective SEDs. From Isella (2006).

1.2.2 High Mass Star Formation

High mass stars form within dense cores containing at least 10 $M_{\odot}$ of gas concentrated in a region ≤ 0.05 pc ,which is the mean separation between stars observed in clusters (Hillenbrand et al., 1997; Kurtz et al., 2000).

The processes leading to the formation of massive stars are poorly understood for a number of reasons. Massive stars, due to the steep dependence on mass in the initial mass function (IMF), are much less common than their low mass counterpats. Consequently, most examples of massive star forming regions are located at distances of several kiloparsecs and require interferometric techniques to resolve them. Obtaining a clear picture of the earliest stages is further confounded by the short timescales over which they evolve. Forming deep within molecular clouds, their birth is obscured by optically thick layers of dust and gas, from which they emerge only after having evolved onto the main sequence.

Massive stars are gregarious, that is they tend to form in clusters, giving rise to OB associations. A single region may contain several massive stars at varying stages of development. This means that energetic processes, such as outflows, from the more evolved massive young stellar objects (MYSOs) may disrupt the evolutionary sequence of the younger members. For observers it is nearly impossible to disentangle cause and effect in such a feedback loop.

If we try to apply the low-mass formation scenario to high mass stars we encounter a number of limiting problems which make the scenario implausible. As mentioned before, $t_{\rm KH} < t_{\rm ff}$ for massive

protostellar objects, meaning that they begin emitting intense ultraviolet radiation and winds of energetic particles while still accreting material. Neglecting feedback from other members of protoclusters, the radiation pressure exerted by a single massive star later than B3 (~ 150 $M_\odot$) is capable of halting or reversing the accretion of material from a spherical envelope. This suggests there should be an upper limit to stars formed through this process, yet stars with masses up to 150 $M_\odot$ have been detected (e.g., Figer et al., 2002). Two solutions have been proposed to overcome the apparent limitations:

Enhanced accretion. Recently 3-D hydrodynamic simulations have shown that massive stars can form via accretion if the accretion rate is significantly enhanced over the low-mass scenario. Enhanced accretion via a disk is capable of overcoming the extreme radiation pressure to build stars up to 100 $M_\odot$ (e.g., Yorke & Sonnhalter , 2002; Tan & Mckee , 2004; Krumholz , 2006).

Dynamical interaction and mergers. Massive stars may form through mergers of low-mass protostellar condensations at the heart of a cluster (e.g., Bonnel & Bate , 2006). Support for this theory comes from the fact that massive stars tend to form in clusters. Simulations have shown that the merger must take place early on in the evolution of the cluster.

Currently, there is no generally accepted scenario for high-mass star formation. However, if it really is a scaled-up version of low-mass star formation one would expect the evolutionary sequence to be the following (Beuther et al., 2007; Tan , 2008): high- mass starless core (HMSC) $\rightarrow$ massive dense core containing accreting low- to intermediate- mass protostars destined to become high-mass proto-

stars → massive core containing high-mass protostar(s), i.e., high-mass protostellar object (HMPO) → final massive star(s).

The formation process of high-mass stars is hard to observe and the embedded phases are only visible in optical wavelengths during 15 % of an OB-type stars lifetime. Mid-infrared to radio wavelength observations have, however, shown that the embedded phase of a massive proto-star can be divided into three groups of objects representing their evolutionary stages. In what follows is an overview of what we have learned about high-mass star formation, the emphasis being in the topics relevant for the present thesis.

Infrared dark clouds (IRDCs) are typically observed in extinction against bright mid-infrared emission of the Galactic plane (at $8\mu m$) or as a faint envelope of emission from cold dust at 850 μm. Each of the IRDCs contain at least one, if not multiple, compact 0.5 pc dust cores with masses of $\sim 10^2 - 10^4 \mathrm{M}_\odot$. Their dense ($10^2 - 10^4 cm^{-3}$) and cold (10 - 20 K) internal regions are believed to have the initial conditions needed to form high-mass stars (Rathborne et al., 2006).

HMPOs can be defined as protostars with masses of $\geq 8\mathrm{M}_\odot$; furthermore, at some point they form a detectable hot molecular core (HMC) and hyper-/ultra-compact H II region around themselves.

Hot molecular cores (HMCs) are internally heated and centrally dense massive molecular gas clouds with diameters of 0.1 pc. Their high gas phase abundances of complex organic molecules are thought to result from evaporation of ices from the dust grains at the elevated temperatures. In addition, HMCs are therefore signposted by methanol emission and water masers. Their strong emission lines

are excited at temperatures > 100 K and densities $> 10^6 \mathrm{cm}^{-3}$ often tracing an outflow or a disk. These objects are often observed to be associated with nearby, or in some cases embedded, ultra-compact H II regions described below (Kurtz et al., 2000).

Hyper/ultra-compact H II regions (HCHIIs or UCHIIs) are small but growing pockets of ionized gas that very likely represent the evolutionary stage which follows the natal environment of high-mass stars (the HMC phase). A HCHII region is believed to represent individual photoevapo- rating disks, while UCHII regions probably represent disk-less stars that photoionize their own cocoons and massive envelopes. UCHII regions are also known as the most luminous objects in the Galaxy at far-infrared wavelengths (Kurtz et al., 2000; Peeters et al., 2002).

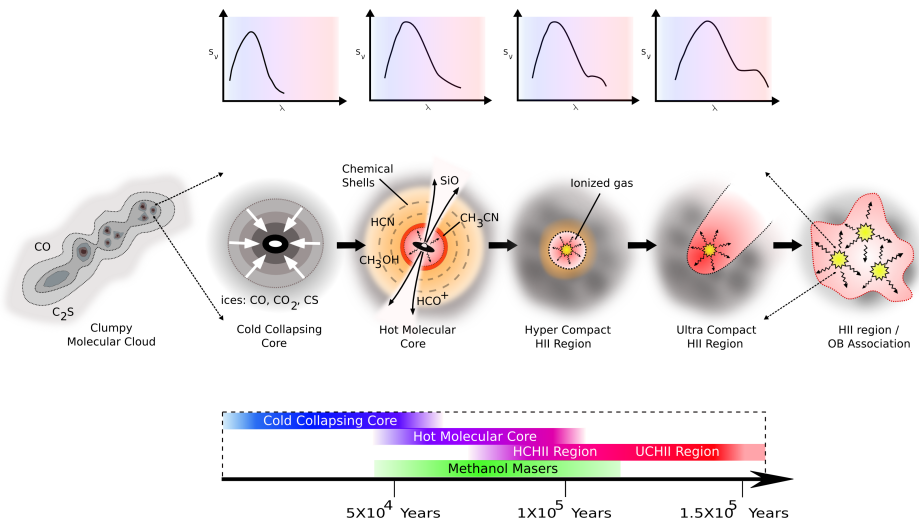

Figure 1.2: This cartoon illustrates the formation of a cluster of high-mass stars, from molecular cloud to ionised bubble. The sequence places classes of observed objects on a rough time-line. From Dr. Purcell's website[1].

[1] http://www.physics.usyd.edu.au/ cpurcell/professional/figures.php

1.3 Astronomical Masers

Observations of maser lines are ideal for studying high mass star forming regions at high angular resolution, as masers are compact and bright sources. Masers are compact sites of molecular emission where certain transitions can be enormously amplified by the process of population inversion, giving rise to intense and narrow spectral lines. Physically, the emitting regions must be dense ($10^6 - 10^{11} cm^{-3}$), be near an exciting source, and the masing transition must contain a high-excitation metastable level to facilitate population inversion. In a simplified 2-level case, population inversion occurs when the exciting source pumps more molecules into the upper metastable state than there are in the ground state. Photons emitted due to a transition from upper to lower state stimulate further emission from nearby molecules and a cascade succeeds. The intensity of a ray passing through the masing gas is amplified exponentially with distance travelled, until the pumping source cannot re-stock the metastable level fast enough and the maser saturates. Other factors which limit the amplification are the path length through the gas, the abundance of the molecule and the velocity dispersion of the gas. The requirement for a long column of gas means that the maser may operate efficiently in only one dimension and the emission will be beamed out over a very narrow opening angle. Alternatively, the structure of the maser sites may allow beaming in multiple directions, the so-called 'hedgehog' model (Sobolev et al., 1997). Determining which model applies is one of the major unanswered questions in maser research.

The first observation of an astrophysical maser was by Weaver et al. (1965). Since then maser lines have been observed in a variety of

molecules like H_2O, SiO, CO, HCN, CS, and complex molecules such as CH_3OH. At first these observations were performed with single dish radio telescopes at angular resolutions on the order of arcminutes. Interferometers like the Very Large Array (VLA), and particularly the technique of Very Long Baseline Interferometry (VLBI), with many dishes spread out over a wide area, have allowed imaging of masers at sub-arcsecond resolution.

1.3.1 Radiative Transfer and Population Inversion

To understand how masers form, we must start with the equation of radiative transfer.

$$\frac{dI_\nu}{ds} = -\kappa_\nu I_\nu + \epsilon_\nu \tag{1.4}$$

where I_ν is the specific intensity of radiation, ϵ_ν is the emissivity, and κ_ν is the absorption coefficient.

We consider a two level system(Figure 1.3), with populations n_1 and n_2 in the respective levels (Cohen 1995). The emissivity is

$$\epsilon_\nu = n_2 A_{21} \frac{h\nu_{21}}{4} f(\nu) \tag{1.5}$$

A_{21} is the Einstein coefficient of spontaneous emission, ν_{21} is the frequency of the emitted photons, $f(\nu)$ is the normalised line profile. The absorption coefficient:

$$\kappa_\nu = (n_1 B_{12} - n_2 B_{21}) \frac{h\nu_{21}}{c} f(\nu) \tag{1.6}$$

B_{12} is the Einstein coefficient for absorption and B_{21} is the coefficient

for stimulated emission. They are related by

$$A_{21} = B_{21}\frac{8h\nu^3}{\pi c^3} \tag{1.7}$$

$$B_{12} = \frac{g_2}{g_1}B_{21} \tag{1.8}$$

where g_1 and g_2 are the statistical weights of the upper and lower states. The ratio of stimulated emission to spontaneous emission increases with the cube of the wavelength, therefore it is $\sim 10^{18}$ times larger for radio waves than visible light (Cohen 1989). Stimulated emission has the effects of reducing the absorption coefficient κ_ν, which is quite substantial at radio wavelengths.

The populations of each level are calculated by:

$$\frac{n_2}{n_1} = \frac{g_2}{g_1}\exp\left(-\frac{h\nu_{21}}{kT_{ex}}\right) \tag{1.9}$$

where T_{ex} is the excitation temperature. At radio frequencies h/k is the order of 0.1K so for a gas at local thermal equilibrium (LTE) the factor is very small and stimulated emission almost cancels absorption. The net absorption of the system is the difference of two very large numbers, this causes the radiative transfer to be very sensitive to very small changes.

A very small shift from Maxwell-Boltzman distribution, which describes the speed, or kinetic energy, of a molecular specie at thermodynamic equilibrium, can cause a population inversion ($n_2/n_1 > g_2/g_1$) and absorption becomes negligible. The radiation passing through the gas becomes amplified and a maser is created. The solution to the equation of radiative transfer is:

$$I_\nu = I_\nu(0)\exp(-\tau_\nu) + \int_\tau^0 \frac{j_\nu}{\kappa_\nu}\exp[-(\tau_\nu - \tau'_\nu)]d\tau'_\nu \tag{1.10}$$

where $I_\nu(0)$ is the intensity entering the gas, τ_ν is the optical depth and j_ν is the total radiation emitted per unit mass per until time (Cohen 1989).

Normally the optical depth is positive and the radiation reaching the observer would be background radiation $I_\nu(0)$, which is attenuated by a factor exponential τ_ν plus the emission/absorption of the cloud. For a maser, the absorption coefficient is negative along with the optical depth. The optical depth can reach -25 magnitudes, which leads to gain factors 10^{10}. Growth will continue as long as population inversion can be maintained against the losses by stimulated emission.

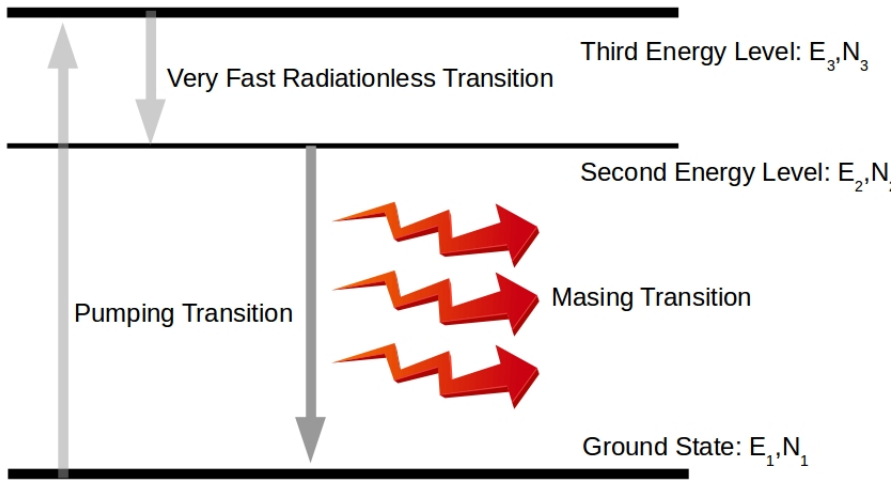

Figure 1.3: A simple two level system. E_1 , E_2 and E_3 are the first three energy levels and N_1 , N_2 and N_3 are the populations of those levels.

1.3.2 Water(H_2O) Masers

Masing transitions of H_2O and OH have been known to be associated with regions of massive star formation for some time (e.g., Mader et al., 1975; Reid et al., 1980; Brand et al., 1994). In the IRAS era these phenomenon were postulated to be physically connected to UCH II regions, but derived from different positions in relation to exciting sources. OH masers appeared to be confined close to the radio continuum emission and the spread in velocity of the maser spectrum rarely exceeded $\sim$ 15 km s^{-1}. Proper motion observations by Bleomhof et al. (1989) clearly showed that the general OH maser motion was expansion, lending support to an earlier theory by Elitzer & de Jong (1994) that the masers were located in the compressed shell between the shock and the ionisation fronts around H II regions. Unlike OH masers, H_2O masers are found at greater separations from the exciting source and their spectra have large velocity dispersions. The relatively high temperatures ($>$ 100 K) and densities ($\sim 10^9 cm^{-3}$) required for their excitation have been successfully modelled by highly supersonic mass outflows interacting with the clumpy ambient medium of the surrounding cloud (Genzel et al., 1986). VLBI observations capable of resolving the maser spots grant confidence to an origin in outflows, as the maser spots are often seen to form lines and arcs.

1.3.3 Methanol(CH_3OH) Masers

Maser emission from interstellar CH_3OH was first observed by Barret et al. (1971) towards Orion-KL. This transition near 25 GHz was the only known CH_3OH maser transition until Wilson et al. (1984)

discovered two new transitions, near 23 and 19 GHz, towards the star forming region W3(OH). Shortly after, new maser lines were discovered at 6.67 GHz (Menten et al., 1991b), 12 GHz (Bartrla et al., 1987), 36 GHz and 44 GHz (Morimoto et al., 1985), prompting fresh interest in the field. In particular, the 6.67 GHz $J_K = 5_1 - 6_0A^+$ transition of CH_3OH has proven to be comparable in strength to OH and is widespread towards massive star forming regions. OH and H_2O masers are not exclusive signposts of massive star formation, they are also found in the environments surrounding evolved stars. In contrast, the 6.67 GHz CH_3OH masers have been observed solely towards massive star forming regions. To test this transition's reliability as a tracer of massive stars Minier et al. (2003) conducted a sensitive survey of 13 low-mass young stellar objects. No detections were reported down to a 4 σ sensitivity of 400 mJy, supporting the hypothesis that 6.67 GHz CH_3OH masers are exclusively associated with high-mass star formation.

From an observational perspective methanol masers have been divided into two groups: Class I and Class II (see Menten et al., 1991a). Class I masers are found offset from the UCHII regions and luminous infrared sources that trace young massive stars. Transitions in this class include the 25 GHz $J_2 - J_1$ E lines, which have Orion-KL as their prototype, and the 36, 44, 84 and 95 GHz lines. The pumping mechanism for class I masers is thought to be related to shocks associated with mass outflows (Plambeck & Menten , 1990), and they are frequently found coincident with H_2O masers. Class II masers include the 6.67, 12, 19, 23, 37 and 38 GHz lines. They are typically found close to UCHII regions, at the same positions as OH maser emission (Norris et al. 1988). Unlike OH masers, individual maser spots some-

times appear to be distributed along lines or arcs suggesting origins in disks, jets or shock fronts.

The 6.7 GHz transition is the strongest and most common Class II CH_3OH maser and numerous searches have shown that these masers are not found toward low-mass YSOs (e.g., Minier et al. 2003; Bourke et al. 2005; Xu et al. 2008; Pandian et al. 2008). A number of surveys have been conducted for the 6.7 GHz class II methanol maser, resulting in the detection of 1600 sources in the Galaxy to date. The surveys include those that are summarized in the compilation of Pestalozzi et al. (2005) and the recent searches of Pandian et al. (2007), Ellingsen (2007), Xu et al. (2008), and the Parkes Methanol Multibeam (MMB) blind survey (Green et al. 2009). In contrast to class II, class I CH_3OH masers are usually found offset by 0.1–1.0 pc from UCHII regions, infrared sources, and OH masers (e.g., Plambeck & Menten , 1990; Kurtz et al., 2004). Surveys have revealed that class I methanol maser are associated not only with high-mass star formation, but also with lower mass counterparts (Kalenskii et al., 2013). Compared to class II masers, class I methanol masers are relatively poorly studied and understood. There have only been a few large surveys for class I masers (mainly at 44 and 95 GHz), primarily undertaken with single-dish telescopes (e.g., Haschick et al. 1990; Slysh et al. 1994; Val'tts et al. 2000; Ellingsen 2005) along with a few smaller scale interferometric searches (e.g., Kurtz et al. 2004; Cyganowski et al. 2009). These have resulted in the detection of about 500 class I maser sources in the Galaxy to date (Kim et al., 2016).

1.4 Aims and Outlines

The broad aim of this work is to investigate the relation between the properties of common maser species and the central objects with a evolutionary sequence. These include:

• How are the common species of H_2O and CH_3OH class I maser relate to the evolutionary phase of massive star formation?

• Can we discern the evolutionary effect and the intrinsic properties of central sources on a correlation between the maser lines and physical parameter of parental clumps/cores?

• Is there any relation between common masers with the evolutionary stages?

To answer these questions we have conducted the 22 GHz H_2O and 44/95 GHz CH_3OH class I maser survey towards 783 sources of massive star forming regions in a different evolutionary phase from IRDCs up to UCHIIs. To assess the properties of central sources, we used the bolometric luminosity from the literature or calculated in this work, 870 μm continuum from APEX Telescope Large Area Survey of the Galaxy(ATLASGAL: Schuller et al. (2009); Contreras et al. (2013)), and NH_3 parameter available from other surveys. In Chapter 2 we describe the maser survey toward RMSs and present results. In Chapter 3 we introduce 2nd maser survey and discuss the result. Summary and Conclusion are presented in Chapter 4.

Bibliography

Andre P., Ward-Thompson D., & Barsony M., 1993, ApJ, 406, 122

Barrett, A. H., Schwartz, P. R., & Waters, J. W., 1971, ApJ, 168, 101

Batrla, W., Matthews, H. E., Menten, K. M., & Walmsley, C. M. 1987, Nature, 326, 49

Beuther, H., Churchwell, E. B., McKee, C. F., & Tan, J. C. 2007, in Protostars

Bloemhof E. E., Reid M. J., & Moran J. M., 1989, LNP Vol. 331: The Physics and Chemistry of Interstellar Molecular Clouds - mm and Sub-mm Observations in Astrophysics, 331, 228

Bonnell I. A., Bate M. R., 2006, MNRAS, 370, 488

Brand J., Cesaroni R., Caselli P., et al. 1994, A&AS, 103, 541

Breen, S. L., Ellingsen, S. P., Caswell, J. L., et al. 2010b, MNRAS, 401, 2219

Contreras, Y., Schuller, F., Urquhart, J. S., et al. 2013, A&A, 549, A45

Cragg, D. M., Sobolev, A. M., & Godfrey, P. D. 2002, MNRAS, 331, 521

Cyganowski, C. J., Brogan, C. L., Hunter, T. R., et al. 2009, ApJ, 702, 1615

Elitzur, M., Hollenbach, D. J., & McKee, C. F. 1989, ApJ, 346, 983

Elitzur M. & de Jong T., 1978, A&A, 67, 323

Ellingsen, S. P., Voronkov, M. A., Cragg, D. M., et al. 2007, in IAU Symp. 242, Astrophysical Masers and their Environments, ed. J. M. Chapman & W. A. Baan (Cambridge: Cambridge Univ. Press), 213

Figer D. F., Najarro F., Gilmore D., et al. 2002, ApJ, 581, 258

Genzel R., 1986, in Masers, Molecules, and Mass Outflows in Star Formation Regions. p. 233

Hill T., Burton M. G., Minier V., et al. 2005, MNRAS, 363, 405

Hillenbrand L. A., 1997, AJ, 113, 1733

Hirota, T., Bushimata, T., Choi, Y. K., et al. 2008, PASJ, 60, 37

Kenyon, S. J., Dobrzycka, D., & Hartmann, L. 1994, AJ, 108, 1872

Kim, C,-H, Kim, K.-T., Park, Y.-S., 2016, ApJS, 00, 00

Krumholz M. R., 2006, ApJ, 641, L45 Protostars and Planets IV, ed. V. Mannings, A. P. Boss, & S. S. Russell (Tucson, AZ: Univ. Arizona Press), 299

Kurtz, S., Cesaroni, R., Churchwell, E., Hofner, P., & Walmsley, C. M. 2000,

Lada C. J., Wilking B. A., 1984, ApJ, 287, 610

Lada C. J., 1987, in IAU Symp. 115: Star Forming Regions. p. 1

Lada, C. J., Lombardi, M., & Alves, J. F. 2010, ApJ, 724, 687

Lombardi, M., Lada, C. J., & Alves, J. 2008, A&A, 480, 785

Mader G. L., Johnston K. J., Knowles S. H., et al. 1975, ApJ, 200, L111

Menten K., 1991a, in Haschick A. D., Ho P. T. P., eds, ASP Conf. Ser. 16: Atoms, Ions and Molecules: New Results in Spectral Line Astrophysics. p. 119

Menten K. M., 1991b, ApJ, 380, L75

Minier V., Ellingsen S. P., Norris R. P., & Booth R. S., 2003, A&A, 403, 1095

Morimoto, M., Kanzawa, T., & Ohishi, M. 1985, ApJ, 288, L11

Peeters, E., Martín-Hernández, N. L., Damour, F., et al. 2002, A&A, 381, 571

Plambeck R. L., & Menten K. M., 1990, ApJ, 364, 555

Rathborne, J. M., Jackson, J. M., & Simon, R. 2006, ApJ, 641, 389

Reid M. J., Haschick A. D., Burke B. F., et al. 1980, ApJ, 239, 89

Schuller, F., Menten, K. M., Contreras, Y., et al. 2009, A&A, 504, 415

Shu F. H., Adams F. C., & Lizano S., 1987, ARA&A, 25, 23

Shu F. H., Ruden S. P., Lada C. J., & Lizano S., 1991, ApJ, 370, L31

Sobolev A. M., Cragg D. M., & Godfrey P. D., 1997, A&A, 324, 211

Tan J. C., McKee C. F., 2004, ApJ, 603, 383

Tan, J. C. 2008a, in ASP Conf. Ser. 387, Massive Star Formation: Observations Confront Theory, ed. H. Beuther, H. Linz, & T. Henning (San Francisco, CA: ASP), 346

Yorke H. W., Sonnhalter C., 2002, ApJ, 569, 846

Weaver, H., Dieter, N. H., Williams, D. R. W., & Lum, W. T. 1965, Nature, 208, 29

Wilson, T. L., Walmsley, C. M., Snyder, L. E., & Jewell, P. R. 1984, A&A, 134, L7

Chapter 2

Simultaneous Surveys of Water and Class I Methanol Masers toward Red MSX Sources

2.1 Introduction

Interstellar masers of H_2O, CH_3OH, and OH are considered excellent probes of high-mass star formation regions (SFRs). Because these masers at radio frequencies are quite common, intense, and rarely affected by dust extinction in massive SFRs, they allow us to investigate such regions. The different maser species favor different physical conditions for their production and survival, which has led to propose tracing different evolutionary phases of massive star formation (e.g.,

Ellingsen et al., 2007; Breen et al., 2010a; Fontani et al., 2010). Since many sources of massive SFRs show emission from multiple maser species or transitions, there must be significant overlap for the evolutionary stage traced by the most common types of masers (Breen et al., 2010a). H_2O masers are known to occur in both low- and high-mass SFRs (e.g., Furuya et al., 2003; Szymczak et al., 2005), and are thus an important signpost of ongoing star formation. The evolutionary stage associated with 22 GHz H_2O maser emission has been investigated through extensive single-dish and interferometric observations (e.g., Torrelles et al., 1997; Urquhart et al., 2011), which have indicated that this type of maser is closely associated with high-mass young stellar objects (YSOs) in various evolutionary stages. Although it has been claimed in a few cases that H_2O masers could trace circumstellar disks around (proto)stellar objects (e.g., Torrelles et al., 1997; Seth et al., 2002), connected-array and VLBI observations toward high-mass YSOs have shown that H_2O masers are predominantly associated with jets and outflows (e.g., Torrelles et al., 2001; Codella et al., 2004).

Methanol masers are commonly observed in massive SFRs. They have been empirically classified into two categories: class I and class II. The initial classification was based on the sources toward which the different transitions were detected (Batrla et al., 1988; Menten et al., 1991). Class I CH_3OH masers (e.g., the 7_0–6_1 A^+ and 8_0–7_1 A^+ at 44 and 95 GHz, respectively) are often observed significantly offset from high-mass YSOs (e.g., Kurtz et al., 2004; Voronkov et al., 2006; Cyganowski et al., 2009). In contrast, class II CH_3OH masers (e.g., the 5_1–6_0 A^+ and 2_0–3_1 E at 6.7 and 12.2 GHz, respectively) are usually very close to high-mass YSOs (e.g., Caswell et al., 2010). These

observational findings were supported by early theoretical models of CH_3OH masers, which suggest that the class I masers are pumped by collisions with molecular hydrogen, while the class II masers are pumped by external far infrared radiation (Cragg et al., 1992). Compared to class II masers, class I CH_3OH masers are relatively poorly studied and understood. There have only been a few large surveys of class I masers (mainly at 44 and 95 GHz), primarily undertaken with single-dish telescopes (e.g., Slysh et al., 1994; Val'tts et al., 2000; Ellingsen et al., 2005) along with interferometric searches (e.g, Kurtz et al., 2004; Cyganowski et al., 2009). Presently, the catalog from these surveys comprises of about 200 class I CH_3OH maser sources (Bayandina et al., 2012).

Ellingsen et al. (2007) suggested that the common maser species (H_2O, class I and II CH_3OH, and OH masers) may help identify the evolutionary phase of the central objects, and proposed a possible evolutionary sequence of these maser species. This proposed sequence has been improved upon by Breen et al. (2010b) (in their Figure 6). However, there remains significant uncertainty about where in SFRs the different maser species arise and which evolutionary phase they are associated with.

In this study, we performed simultaneous 22 GHz H_2O and 44 and 95 GHz class I CH_3OH maser surveys toward high-mass protostellar objects (HMPOs) using single-dish telescopes. Our aim is to find new maser sources and to investigate the relationship between the different maser species and between the maser activity and the properties of the central objects and the natal clumps. In Section 2 we describe the source selection and the observations. In Section 3 we present

the results of the survey. Discussion of analyses is given in Section 4, followed by a summary in Section 5.

2.2 Source Selection and Observations

2.2.1 Source Selection

Lumsden et al. (2002) identified about 2000 candidates for young massive stars with 21 μm flux densities of >2.5 Jy and infrared colors consistent with known massive YSOs, using the color-color plots of the Midcourse Space Experiment (MSX) and Two Micron All Sky Survey (2MASS) data (see also Lumsden et al., 2013). They carried out follow-up observations and manipulated the complementary data from other surveys to differentiate HMPOs and ultracompact HII regions (UCHIIs) (e.g., Urquhart et al., 2014a). From this so-called Red MSX Source (RMS) catalog[1], we selected 299 HMPO candidates, which are very likely under active accretion and so have not yet developed detectable UCHIIs, because they have bolometric luminosities of $> 10^3 L_{\odot}$ and declinations of $> -30°$. Table 2.1 lists their information as extracted from the RMS catalog, including their RMS ID, MSX name, equatorial coordinates, source type, distance, bolometric luminosity, and systemic velocity.

[1] http://rms.leeds.ac.uk/cgi-bin/public/RMS_DATABASE.cgi.

2.2.2 Observations

We surveyed the 299 sources in three maser transitions: H_2O $6_{16} - 5_{23}$ (22.235080 GHz), CH_3OH $7_0 - 6_1$ A^+ (44.069430 GHz), and $8_0 - 7_1$ A^+ (95.169463 GHz). The observations were undertaken using the Korean VLBI Network (KVN) 21 m telescopes from 2011 April to 2014 May. The telescopes were equipped with multi-frequency receiving systems which made it possible to observe in the 22, 43, 86, and 129 GHz bands simultaneously (Han et al., 2008). The first-epoch observations were made only at 22 and 44 GHz in 2011 because the 86 and 129 GHz receivers were not then installed, while the second-epoch observations were conducted at 22, 44, and 95 GHz in 2012. Supplementary observations were performed toward 15 sources in 2013 April and May and 2015 May to confirm their detections. We observed dual polarization both at 22 and 44 GHz in the first epoch, and single polarization at 22 and 44 GHz and dual polarization at 95 GHz in the second epoch. The backend was a digital spectrometer that provided 4096 channels and 64 MHz bandwidth for each stream.

The full widths at half maximum (FWHMs) of the telescopes were about $130''$ at 22 GHz, $65''$ at 44 GHz, and $32''$ at 95 GHz. The telescope pointing and focus were checked every $\sim$2 hr by observing strong SiO maser sources at 43 or 86 GHz. The pointing accuracy was better than $5''$. Each spectrum was obtained in position-switching mode usually with an offset of +2 minutes in the right ascension. The total (ON+OFF) integration time was typically 30 minutes for each source, which yielded rms noise levels of about 0.7 Jy (σ), 0.8 Jy, and 1.3 Jy at about 0.2 km s^{-1} resolution after smoothing for 22, 44, and 95 GHz, respectively. The data were calibrated with the stan-

dard chopper wheel method to provide the line intensity on the $T_{\rm A}^{*}$ scale, which were converted to flux density using the conversion factors in Table 2.2. The KVN telescopes are of shaped Cassegraign type and hence have quite high first-sidelobe levels of $\sim$ 14 dB at $\sim$ 1.5 times FWHM away from the pointing center (Kim et al., 2011; Lee et al., 2011). We thus mapped each detected source at the observing frequency to investigate contamination from nearby bright maser sources. The mapping area was 1.5 FWHM $\times$ 1.5 FWHM around a source with half-beam spacing at each frequency.

We also surveyed 10 sources in our sample in the ^{13}CO J=1–0 and HCO^{+} J=1–0 lines in 2013 June. The ^{13}CO line observations were conducted with the Taeduk Radio Astronomy Observatory (TRAO) 14 m telescope, while the HCO^{+} line observations were made with the KVN telescope at the Tamna station. The observed sources were H_2O maser sources with maser features largely offset from the systemic velocities (see Section 3.3.1). These observations aimed to search for dense molecular cores associated with those features. The TRAO telescope was equipped with the 15-beam receiver, QUARRY (QUabbin ARRaY) (Erickson et al., 1992). The backends were autocorrelators, each of which had 427 channels and a bandwidth of 100 MHz. We utilized the position switching mode. Table 2.2 summarizes the observational details. All the spectral data were reduced and analyzed with the GILDAS/CLASS package.

2.3 Result

2.3.1 Detection Statistics

Our search toward the 299 RMSs resulted in the detection of 151 (51%) sources at least in one of the three maser transitions. Table 2.1 presents the detection summary: detection (y), nondetection (n), and new detection (Y). All the detected maser lines were limited to signals stronger than the 3σ rms noise level. Table 2.3 lists the numbers of observed and detected sources and the corresponding detection rates for each transition and epoch (see also Figure 2.1). We detected 22, 44, and 95 GHz maser emission in 135 (45%), 83 (28%), and 68 (23%) sources, respectively. The detection rates (42% and 37%) of H_2O maser emission are a little different in the first and second epochs, although the difference is not substantial, while those (25% and 27%) of 44 GHz CH_3OH maser emission are practically the same. All detected maser spectra are shown in Figures 2.2−2.13: sources detected in all three masers in Figure 2.2; sources detected in 22 and 44 GHz masers in Figure 2.6; sources detected in 44 and 95 GHz masers in Figure 2.7; sources detected only in 22 GHz maser in Figure 2.8; sources detected only in 44 GHz maser in Figure 2.13.

There are several maser surveys of HMPO candidates with various sensitivities. Sridharan et al. (2002) detected 22 GHz H_2O maser emission toward 42 % of 69 HMPOs at a rms noise level of ∼0.4 Jy. Urquhart et al. (2011) searched for H_2O maser emission toward 597 RMSs with a detection rate of ∼52% for 275 HMPOs. The survey had a mean rms noise level of ∼0.12 Jy at a velocity resolution of ∼0.33 km s^{-1}. If its sensitivity is similar to ours, ∼0.7 Jy, neglecting

the difference in the velocity resolution, the detection rate would be 38%. Fontani et al. (2010) surveyed 88 HMPOs in the 44 GHz CH_3OH maser with a twice better sensitivity to ours, and obtained a detection rate of 31 %. Gan et al. (2013) detected 95 GHz maser emission in 22% (62) of 288 outflow sources. Val'tts et al. (2007) also found that 24 % of the outflow sources are associated with class I CH_3OH maser sources, including 36, 44, and 95 GHz masers, within $2'$. Thus the detection rates of the three masers in this study seem to be comparable to those of the previous surveys.

In our sample, 138 sources are distributed in the Methanol Multibeam (MMB) survey area of 6.7 GHz class II CH_3OH maser with the Parkes 64 m telescope (Green et al., 2009; Breen et al., 2015). We found that 24% (34), 34% (47), and 33% (46) of them are associated with 6.7, 22, and 44 GHz masers, respectively. Of the 34 sources with 6.7 GHz maser, 13 (39%) are related to 22 GHz maser while 12 (36%) are related to 44 GHz maser. Szymczak et al. (2005) obtained a slightly higher detection rate (52%) in the survey of H_2O maser toward seventy nine 6.7 GHz maser sources at a slightly lower rms noise level of $\sim$0.45 Jy.

2.3.2 New Detections

We compared our results with the previous surveys of H_2O and class I CH_3OH masers to identify newly detected sources. In this comparison we used a criterion of $65''$. For 22 GHz H_2O masers, we examined the catalogs of Han et al. (1995), Han et al. (1998), Valdettaro et al. (2001), Sunada et al. (2007), Urquhart et al. (2009), and Urquhart

et al. (2011). In particular, Urquhart et al. (2011) observed ∼600 RMSs using the Green Bank Telescope (GBT) in 2009 and 2010 and detected 308 sources (∼50%). Their sample contains the 257 sources in our sample, 145 (56%) of which were detected. For 44 and 95 GHz class I CH_3OH masers, we investigated the catalogs of Val'tts et al. (1995), Kurtz et al. (2004), Val'tts et al. (2007), Chen et al. (2011), Chen et al. (2012), and Bayandina et al. (2012). We identified 15, 56, and 52 new maser sources at 22, 44, and 95 GHz, respectively. Five of the new 95 GHz maser sources have been observed but not detected in the previous surveys.

2.3.3 Maser Properties

We determined the line parameters of the observed maser spectra, including the peak velocity, the peak flux density, the integrated flux density, and the minimum and maximum values of the velocity range over which the maser lines are distributed. Table 2.4 summarizes the measurements. Table 2.5 presents the mean, median, minimum, and maximum values of the peak flux density ($S_{\rm p}$), the relative peak velocity with respect to the systemic velocity ($V_{\rm rel}$), and the velocity range ($V_{\rm range}$) of 22, 44, and 95 GHz masers for the detected sources. The mean and median values of 44 and 95 GHz CH_3OH masers are very similar for all the three parameters, while they are much smaller than those of the 22 GHz H_2O masers (see also Figure 2.14).

The isotropic luminosity of maser emission can be estimated from the integrated flux density using the following equations

$$L_{22} = 2.30 \times 10^{-8}\ L_{\odot} \left(\frac{\int S_{22} dv}{\mathrm{Jykms^{-1}}} \right) \left(\frac{D}{\mathrm{kpc}} \right)^2, \tag{2.1}$$

$$L_{44} = 4.60 \times 10^{-8}\ L_{\odot} \left(\frac{\int S_{44} dv}{\mathrm{Jykms^{-1}}} \right) \left(\frac{D}{\mathrm{kpc}} \right)^2, \tag{2.2}$$

$$L_{95} = 9.92 \times 10^{-8}\ L_{\odot} \left(\frac{\int S_{95} dv}{\mathrm{Jykms^{-1}}} \right) \left(\frac{D}{\mathrm{kpc}} \right)^2. \tag{2.3}$$

$$L_{6.7} = 6.95 \times 10^{-9}\ L_{\odot} \left(\frac{\int S_{6.7} dv}{\mathrm{Jykms^{-1}}} \right) \left(\frac{D}{\mathrm{kpc}} \right)^2, \tag{2.4}$$

where D is the distance to the source. We adopted the distances from Urquhart et al. (2014a), who gathered well-determined distances from the literature or derived kinematic distances using available molecular and HI line data for the individual sources. The integrated flux densities given by Breen et al. (2015) were used for 6.7 GHz CH_3OH masers. The derived isotropic maser luminosities are listed in the 11th column of Table 2.4.

H_2O maser

We detected 22 GHz H_2O maser emission toward 135 sources in our sample: 126 in the first epoch and 112 in the second epoch. The median of the peak flux densities is 15.5 Jy with the minimum and maximum values of 0.8 and 4552 Jy, respectively. The vast majority (78%) of the detected sources have velocity ranges smaller than 20 km s^{-1}. RMS 3555 exhibits the largest velocity range, 230 km s^{-1}. Twenty seven sources (19%) have one or more high-velocity features,

which are defined to be offset from the systemic velocity by more than 30 km s^{-1} as in Breen et al. (2010a). These high-velocity sources fall into three categories: eighteen with only blueshifted features, three with both blue- and redshifted ones, and six with only redshifted ones. For comparison, Breen et al. (2010a) detected high-velocity features toward 33% (77) of 223 detected H_2O maser sources in their sample. This higher detection rate might be due to their nearly six times better sensitivity compared to ours. The mean offset of the peak velocities from the systemic velocities is slightly blueshifted, -3.2 km s^{-1}, for all the 135 sources.

Caswell & Phillips (2008) reported four so-called blue dominant H_2O maser sources, which show blueshifted high-velocity maser features with no or very weak features around the systemic velocities, and suggested that the features can be generated by pole-on jets. We found 9 blue and 2 red dominant H_2O maser source candidates. To examine whether the dominant maser feature candidates are associated with other YSOs in the same lines of sight, we observed 10 of them in the ^{13}CO J=1–0 line and found that 3 of them have weak ^{13}CO lines around the candidate features. For the remaining one (RMS 3936), no ^{13}CO J=2–1 line emission near the candidate feature was confirmed using the JCMT archive. We observed the 3 candidates in the HCO^+ J=1–0 line, which is known to be a good tracer of massive star-forming cores (Purcell et al. 2006), and detected the line emission toward 2 of them (RMS 2716, 3360). These two appear to originate from other YSOs than target sources in the same lines of sight. The remaining 9 are very likely to be dominant shifted H_2O maser sources. Table 2.6 summarizes the survey results and Figure 2.15 shows the detected molecular spectra together with the 22

and 44 GHz maser spectra. Urquhart et al. (2011) also detected H_2O maser emission in 8 of the 9 sources. However, only 3 of them showed dominant blue- or redshifted features (RMS 2547, 2584, 3936).

Class I CH_3OH maser

We detected 44 and 95 GHz class I CH_3OH maser emission toward 83 and 68 sources, respectively, in the two epochs. It should be noted that 95 GHz maser emission was detected only in 44 GHz maser sources (Figure. 2.1). The peak flux densities range from 1.1 to 253 Jy at 44 GHz and between 1.1 and 147 Jy at 95 GHz. The peak velocities are always very close to the systemic velocities with $\pm$5 km s^{-1} (Figure 2.17). The mean values of the relative peak velocities are $<$0.1 km s^{-1} for both masers (Table 2.5). The measured velocity ranges limited by 3 σ noise levels are 0.21–15.5 km s^{-1} at 44 GHz and 0.20–13.4 km s^{-1} at 95 GHz. The median values are 2.3 and 2.4 km s^{-1} for 44 and 95 GHz masers, respectively. With a criterion of 1 km s^{-1} velocity range by Ellingsen et al. (2005), the broad spectral features appear in the majority (75%) of detected 44 and 95 GHz maser sources. The broad emission features have been reported by previous surveys of class I CH_3OH masers (e.g., Ellingsen et al., 2005; Chen et al., 2011). They might include quasi-thermal emission, which means maser emission may be blended with the thermal component. We compared the first-epoch spectra with the second-epoch ones for seventy four 44 GHz CH_3OH maser sources that were detected in both epochs. Only 11 sources show significant variations in the peak flux density by factors of 1.5–2.

Figure 2.17 compares 44 GHz masers with 95 GHz masers in the relative peak velocity, the peak flux density, and the isotropic maser luminosity. There appear to be strong correlations between the two masers. The least-squares fitting results are as follows:

$$\mathrm{V_{rel}} = 0.98(\mathrm{V_{rel}}) - 0.01 \ (\rho = 0.73), \tag{2.5}$$

$$\log(\mathrm{S_{p,95}}) = 0.98\log(\mathrm{S_{p,44}}) - 0.12 \ (\rho = 0.89), \tag{2.6}$$

$$\log(\mathrm{L_{95}}) = 0.93\log(\mathrm{L_{44}}) - 0.09 \ (\rho = 0.91). \tag{2.7}$$

Four sources (RMS 2445, 3963, 3982 and 3998) show a difference of >1 km s^{-1} between the 44 and 95 GHz relative peak velocities. They have two or more velocity components and/or broad spectral features. Thus the peak velocity measurements could be affected by the combination of the positional offsets from the pointing center and the different beam sizes at 44 and 95 GHz. If the four are excluded, the correlation becomes stronger with a correlation coefficient of 0.96. Val'tts et al. (2000) and Jordan et al. (2015) estimated the peak flux density ratio of 44 and 95 GHz masers to be 0.31−0.32, while Kang et al. (2015) derived the ratio to be about 0.71. Our result of best fit in linear scale plot is $S_{\mathrm{p,95}}$=0.56 $\times$ $S_{\mathrm{p,44}} + 2.16$ ($\rho = 0.91$), and this is consistent with Kang et al. (2015). It is worth noting that the former two studies established datasets using different telescopes in epochs separated by several years while this study and Kang et al. (2015) utilized the datasets simultaneously taken from the same telescopes at the same velocity resolution. We also found a strong correlation between the isotropic maser luminosities of the two masers. But there is no correlation in the isotropic maser luminosity between 44 GHz masers and 22 GHz H_2O or 6.7 GHz class II CH_3OH masers.

Class II CH_3OH maser

As mentioned in § 3.1, 34 of the 138 sources in the MMB survey area are associated with 6.7 GHz class II CH_3OH maser emission. Breen et al. (2015) measured the line parameters of the 6.7 GHz maser spectra. The peak flux densities range from 0.9 to 163 Jy. Table 2.5 presents the mean, median, minimum, and maximum values of $S_{\rm p}$, $V_{\rm rel}$, and $V_{\rm range}$ of four maser species for the maser-detected sources in the MMB survey area. The median values of $S_{\rm p}$ and $V_{\rm range}$ of 6.7 GHz masers are comparable to those of 22 GHz masers, while they are (2−3) times larger than those of 44 and 95 GHz masers. The median value of $V_{\rm rel}$ for 6.7 GHz masers is in the middle of the values of 22 and 44/95 GHz masers. These trends are well displayed in Figure 2.14. We could *not* find any correlation in the isotropic maser luminosity between 6.7 GHz masers and the other maser species.

2.3.4 Comments on Individual Sources of Interest

RMS 121. Strong H_2O maser emissions were detected in the first and second epochs with peak flux densities of 53 and 25 Jy, respectively. During the observing period of 2 years, the peak velocity changed from redshifted (7.2 km s^{-1}) to blueshifted (−3.1 km s^{-1}) relative to the systemic velocity (3.1 km s^{-1}). While there is a considerable variation in the H_2O maser line, the 44 GHz CH_3OH maser lines are invariable in peak flux density and peak velocity.

RMS 145. As noted in § 3.3.1, this new H_2O maser source can be classified as a red dominant source (Table 6; Figure 2.15). A high-

velocity feature appears at 125 km s^{-1} without any feature near the systemic velocity, 46.6 km s^{-1}. Both ^{13}CO (1–0) and HCO^+ (1–0) lines were detected only around the systemic velocity. The peak flux density practically remained constant, ∼8 Jy, between the two epochs. Neither 44 GHz nor 95 GHz CH_3OH maser emission was detected toward this object.

RMS 2490. This is located in the W33A massive star-forming region. H_2O maser lines were detected near the systemic velocity of 35.8 km s^{-1} in both epochs. The peak flux density of them increased from 11.4 Jy in the first epoch to 15.6 Jy in the second epoch. A high-velocity maser feature was also detected at −7.9 km s^{-1} in the second epoch. The peak flux was 15.8 Jy. Urquhart et al. (2011) detected only maser features around the systemic velocity.

RMS 2547. This is a blue dominant H_2O maser source (Table 6; Figure 2.15). High-velocity features were detected at −70.9 and −65.5 km s^{-1} in the first and second epochs, respectively, with no emission around the systemic velocity of 20.9 km s^{-1}. Urquhart et al. (2011) also detected this source in 2009–2010. The peak flux density rapidly increased from 13.5 Jy in 2009–2010 to 128 Jy in 2011 April and 945 Jy in 2012 June, while the velocity range remained very similar over the three epochs. Weak 44 GHz CH_3OH maser emission was detected near the systemic velocity in both epochs.

RMS 2584. This source showed strong dominant blue-shifted H_2O maser features in both epochs (Table 6; Figure 2.15). Urquhart et al. (2011) also detected them. The peak flux density rapidly faded out from 165 Jy in 2009–2010 to 75 Jy in 2011 March and 5 Jy in 2012 June, while the velocity range appeared similar in three epochs.

RMS 3236. Two weak 44 GHz CH_3OH maser features were detected toward this source. One is at the systemic velocity, while the other is offset by -29 km s^{-1}. From the Galactic Ring Survey (GRS) ^{13}CO J=1$-$0 line data archive (Jackson et al., 2006), we examined whether there are ^{13}CO lines associated with both maser features or not. As a result, we found that the latter feature in the offset is related to another YSO in the same line of sight.

RMS 3555. This source is located within G49.5–0.4 in the W51 A complex. H_2O maser emission toward this is the broadest (188 and 230 km s^{-1}) in velocity range at each epoch. The peak flux density was about 3600 Jy at 57.0 km s^{-1} in the second epoch. The emission of CH_3OH maser was detected near the systemic velocity (60.1 km s^{-1}) at 44 and 95 GHz. Interestingly, weak 44 GHz maser emission was also detected at 50 km s^{-1} far from the systemic velocity in both epochs. The grid mapping result suggests that this emission may result from W51 IRS 1 in a sidelobe.

RMS 3587. In the first epoch, H_2O maser emission showed blue dominant-shifted features (Table 6; Figure 2.15). High-velocity features were detected around –44 km s^{-1} in both epochs, although the peak flux density decreased from 4.2 Jy in 2011 March to 2.2 Jy in 2012 May by a factor of 2. The H_2O maser emission near the systemic velocity (16.1 km s^{-1}) emerged in the second epoch with a peak flux of 6.7 Jy. Urquhart et al. (2011) detected multiple features only near the systemic velocity.

RMS 3735. The emission of CH_3OH maser was marginally detected only at 44 GHz in the second epoch, with a peak flux density of 1.4 Jy near the systemic velocity. As for the H_2O maser, a single velocity

component was detected in both epochs, and the peak flux density increased by a factor of 6 in a period of two years : from 5 Jy in 2011 April to 30 Jy in 2013 April. There is no significant change in velocity position of peak flux density.

RMS 3749. The emission of H_2O maser was detected in both epochs. The peak flux density varied from 73 Jy in 2011 April to 266 Jy in 2012 October. Also, the velocity of peak flux density moved from blueshifted (1.7 km s^{-1}) to redshifted (15.6 km s^{-1}) relative to the systemic velocity (7.9 km s^{-1}). Urquhart et al. (2011) detected a peak flux density of 175 Jy at -2.4 km s^{-1}.

RMS 3766. A dominant blueshifted H_2O maser feature with a peak flux of 5.0 Jy was detected at –25.7 km s^{-1} in the first epoch (Table 6; Figure 2.15), while a 1.2 Jy feature solely appeared around the systemic velocity of 5.6 km s^{-1} in the second epoch. In both epochs 44 GHz CH_3OH maser emission ($\sim$2 Jy) was detected near the systemic velocity.

RMS 3846. In both epochs, 44 GHz CH_3OH maser spectra consisted mainly of two strong features of about 25 Jy at –5.2 km s^{-1} and –3.1 km s^{-1}. These lines appeared to have a symmetrical profile with respect to the systemic velocity (-4.4 km s^{-1}). Contrasting with the 44 GHz CH_3OH maser, 95 GHz maser spectrum showed a red-skewed profile in a similar velocity range of 44 GHz maser.

RMS 3911. A dominant high-velocity H_2O maser feature was detected at -75.0 km s^{-1} and -65.8 km s^{-1} in the first and second epochs, respectively (Table 6; Figure 2.15). The peak flux density decreased by a factor of 2 from 6.4 Jy to 3.2 Jy. In comparison, Urquhart

et al. (2011) detected multiple features around the systemic velocity, -46.6 km s^{-1}, as well as a high-velocity feature around -75.0 km s^{-1}.

RMS 3936 Weak H_2O maser features were detected between -75 and -55 km s^{-1} in the first epoch, while a red dominant feature was detected at -10.1 km s^{-1} with a peak flux of 3.2 Jy in the second epoch (Table 6; Figure 2.15). Urquhart et al. (2011) detected the peak flux density of $\sim$19 Jy at the systemic velocity (-87.5 km s^{-1}) and multiple high-velocity features from -88.6 to -27.6 km s^{-1}. No class I CH_3OH maser emission was detected in our survey.

RMS 3958. Blue dominant H_2O maser features were detected around -96.4 km s^{-1} without any feature near the systemic velocity (-51.2 km s^{-1}) in the first epoch, while no maser emission was detected in the second epoch (Table 6; Figure 2.15). The peak flux density was 11.7 Jy. Urquhart et al. (2011) detected H_2O maser features only near the systemic velocity. The 44 GHz and 95 GHz CH_3OH maser emission were detected at the systemic velocity.

2.4 Analysis and Discussion

2.4.1 Masers and the Central Objests

In Figure 2.18, the isotropic luminosities of four maser species are plotted against the bolometric luminosity ($L_{\rm bol}$) of the central protostar. In our sample, as marked in Table 2.1, 62 sources have one or two nearby RMSs within 20″ radius. By considering the FWHMs of the KVN telescopes, we integrated the bolometric luminosities of the

individual members and use the total luminosity for this comparison. The total bolometric luminosity is less than 5 times larger than the luminosity of a target source for 90% of them. Thus this integration may not significantly affect the derived relationship here. The maser luminosity tends to increase with the bolometric luminosity for all maser species, although the correlations seem to be moderate. Linear least-square fittings result in the following relations with correlation coefficients of 0.34–0.54:

$$\log(\mathrm{L}_{22}) = 1.48\ \log(\mathrm{L}_{\mathrm{bol}}) - 11.05\ (\rho = 0.29\ 0.54), \tag{2.8}$$

$$\log(\mathrm{L}_{44}) = 1.31\ \log(\mathrm{L}_{\mathrm{bol}}) - 10.59\ (\rho = 0.20\ 0.45), \tag{2.9}$$

$$\log(\mathrm{L}_{95}) = 1.22\ \log(\mathrm{L}_{\mathrm{bol}}) - 9.93\ (\rho = 0.27\ 0.44), \tag{2.10}$$

$$\log(\mathrm{L}_{6.7}) = 1.39\ \log(\mathrm{L}_{\mathrm{bol}}) - 11.59\ (\rho = 0.34). \tag{2.11}$$

The relationship between the isotropic maser luminosity and the bolometric luminosity has been investigated in several previous studies of H_2O and CH_3OH masers in SFRs. For H_2O masers, the correlation between L_{H_2O} and L_{bol} has been proposed by Furuya et al. (2003) for low-mass YSOs ($L_{\mathrm{bol}} \sim 0.1 - 10^2 L_\odot$), Bae et al. (2011) for intermediate-mass YSOs ($L_{\mathrm{bol}} \sim 10^2 - 10^4 L_\odot$), and Felli et al. (1992) for low- to high-mass YSOs ($L_{\mathrm{bol}} \sim 10 - 10^6 L_\odot$). The slopes of their fit lines are close to 1 (0.81 − 1.02). For comparison, we plot our data together with H_2O maser data of low- and intermediate-mass YSOs from Furuya et al. (2003) and Bae et al. (2011). We obtain a relation of $L_{22} = 6.02 \times 10^{-10} (L_{\mathrm{bol}})^{1.07}$ with a much higher correlation coefficient ($\rho = 0.76$), which is consistent with previous studies (Figure 2.19*a*).

In the case of 44 CH_3OH masers, the relation between L_{CH_3OH} and

$L_{\rm bol}$ has been investigated by Kalenskii et al. (2013) for low-mass YSOs ($L_{\rm FIR} \sim 0.1 - 10^2 L_{\odot}$) and Bae et al. (2011) for intermediate-mass YSOs ($L_{\rm bol} \sim 10^2 - 10^3 L_{\odot}$). We combine our data with the data of Kalenskii et al. (2013) and Bae et al. (2011) to widen the range of $L_{\rm bol}$. The best-fit line of 44 GHz data is $L_{44} = 1.68 \times 10^{-10} (L_{\rm bol})^{1.12}$ ($\rho = 0.71$) (Figure 2.19*b*). For the 95 GHz CH_3OH masers, Gan et al. (2013) presented a relation of $L_{95} = 1.74 \times 10^{-8} (L_{\rm bol})^{0.51}$ ($\rho = 0.66$) from low to high-mass YSOs ($L_{\rm bol} \sim 10^1 - 10^6 L_{\odot}$).

2.4.2 Masers and the Parental Clumps

We search for molecular clumps associated with our target sources using the 870 μm continuum data of the APEX Telescope Large Area Survey of the Galaxy (ATLASGAL) (Schuller et al., 2009; Contreras et al., 2013). We find that 135 sources are located in the survey area and that 116 (86%) of them are associated with the ATLASGAL clumps within a search radius of 30$''$, in which ∼90% of ATLASGAL−RMS matches are distributed (Urquhart et al., 2014b). The maser detection rates of the 116 sources are 35%, 36%, and 31% at 22, 44, and 95 GHz, respectively, in the second epoch. These values are higher than the maser detection rates of the remaining 19 sources: 26%, 26%, and 10%. Assuming that dust emission is optically thin at 870 μm, we derive the clump mass in a similar way to Urquhart et al. (2014b) using the following equation

$$M_{\rm clump} = \frac{S_{\rm int} D^2}{k_{\nu} B_{\nu}(T_{\rm d}) R_{\rm d}}. \tag{2.12}$$

Here $S_{\rm int}$ is the integrated flux density, D is the distance to the source,

k_ν is the mass absorption coefficient per unit mass of dust, $B_\nu(T)$ is the Planck function, $T_{\rm d}$ is the dust temperature, and $R_{\rm d}$ is the dust−to−gas mass ratio. We take $S_{\rm int}$ from the ATLASGAL catalog and adopt k_ν=1.85 cm^2 g^{-1}, $T_{\rm d}$=20 K, and $R_{\rm d}$=0.01 as in Urquhart et al. (2014b). The effective radii of the associated clumps range from 7″ to 154″ with a median of 31″.

Figure 2.20 shows the maser luminosity versus the estimated clump mass for the detected maser sources. The maser luminosity appears to correlate with the clump mass for all four maser species, especially 44 and 95 GHz CH_3OH masers. Linear least-squares fittings result in the following relations with correlation coefficients of 0.55 to 0.81.

$$\log(\mathrm{L}_{22}) = 1.47\ \log(\mathrm{M}_{\rm clump}) - 9.47\ (\rho = 0.55), \tag{2.13}$$

$$\log(\mathrm{L}_{44}) = 1.31\ \log(\mathrm{M}_{\rm clump}) - 9.21\ (\rho = 0.78), \tag{2.14}$$

$$\log(\mathrm{L}_{95}) = 1.30\ \log(\mathrm{M}_{\rm clump}) - 8.82\ (\rho = 0.81), \tag{2.15}$$

$$\log(\mathrm{L}_{6.7}) = 1.63\ \log(\mathrm{M}_{\rm clump}) - 10.67\ (\rho = 0.58). \tag{2.16}$$

Chen et al. (2012) also found a strong (ρ=0.84) correlation between L_{95} and the clump mass for the Bolocam Galactic Plane Survey (BGPS) sources. However, the slope was much lower, 0.81. Chen et al. (2011) and Gan et al. (2013) obtained even lower (0.5−0.6) slopes of the best linear fits between L_{95} and $M_{\rm clump}$ for the BGPS clumps associated with EGOs and molecular outflows, respectively. In our sample, twenty 95 GHz maser sources are associated both with the ATLASGAL clumps and BGPS clumps. After deriving the mass of the BGPS clumps as in Chen et al. (2012), we examine the $M_{\rm clump}$−L_{95} relations for the two groups and find no significant difference. The slopes of the best linear fits are 1.3 and 1.2 for the ATLASGAL and BGPS clumps with correlation coefficients of 0.89 and 0.74, respectively.

The peak H_2 column density can be calculated from the peak flux density of each clump using the equation

$$N_{\rm H_2} = \frac{S_{\rm p}}{\Omega_{\rm b}\mu\ m_{\rm H} k_\nu B_\nu(T_{\rm d}) R_{\rm d}}, \tag{2.17}$$

where $S_{\rm p}$ is the peak flux density, $\Omega_{\rm b}$ is the beam solid angle, μ is the mean molecular weight, and $m_{\rm H}$ is the mass of hydrogen atom. We adopt $\Omega_{\rm b}$=2.0 $\times$ 10^{-8} Sr and μ=2.8 (e.g., Urquhart et al. 2014b). Figure 2.21 plots the maser luminosity against $N_{\rm H_2}$ for four maser species. No correlation appears for 22 and 6.7 GHz masers while very weak correlations exist with $\rho \simeq$0.3 for 44 and 95 GHz masers. Figure 2.22 compares $N_{\rm H_2}$ with $M_{\rm clump}$. There are moderate correlations between the two parameters for all four maser species. Linear least-squares fittings yield correlation coefficients of 0.38 to 0.48. For 22, 44, and 95 GHz masers, most sources ($>$ 90%) without maser emission have lower $N_{\rm H_2}$'s than 10^{23} cm^{-2}. For 6.7 GHz masers, there is no clear difference in the distributions of $M_{\rm clump}$ and $N_{\rm H_2}$ between the sources with and without the maser emission.

Figure 2.23 plots the integrated flux density of each maser ($\int S_\nu dv$) versus $N_{\rm H_2}$. The relationship might be meaningful for the future maser survey because the two parameters are independent of the distance and other intrinsic physical parameters (Chen et al., 2012). We

perform least-squares fit and obtain the following relations:

$$\log(\int S_{22}\ dv) = 2.00\ \log(N_{H_2}) - 44.37\ (\rho = 0.42), \tag{2.18}$$

$$\log(\int S_{44}\ dv) = 1.69\ \log(N_{H_2}) - 37.86\ (\rho = 0.71), \tag{2.19}$$

$$\log(\int S_{95}\ dv) = 1.80\ \log(N_{H_2}) - 40.50\ (\rho = 0.71), \tag{2.20}$$

$$\log(\int S_{6.7}\ dv) = 1.81\ \log(N_{H_2}) - 40.26\ (\rho = 0.35). \tag{2.21}$$

The slopes of linear fits are similar (1.7−2.0) for all four maser species. However, there is a significant difference in the correlation coefficient in that 44 and 95 GHz masers show quite high correlation coefficients of 0.71, while 22 and 6.7 GHz masers have considerably lower coefficients of ∼0.4. The derived correlation coefficient of 95 GHz masers is consistent with the value (0.69) of Chen et al. (2012), although they used 40″ beam-averaged column density of the BGPS data.

2.4.3 NH_3 Linewidth and Kinetic Temperature

Urquhart et al. (2011) surveyed about 600 RMSs in the NH_3 lines as well, and detected the line emission toward 479 (∼80%) sources. They derived some line and physical parameters using the NH_3 line data, including the line width (FWHM) of each transition and the kinetic temperature of gas. The line widths range from 0.49 to 8.23 km s^{-1} with mean and median values of 1.85 and 1.73 km s^{-1}, respectively. These values are similar to the line widths (1.7−1.9 km s^{-1}) of infrared dark clouds (IRDCs) measured by Wienen et al. (2012) and Chira et al. (2013) from the NH_3 line observations. We compare the line widths of four subsamples: none, only 22 GHz, only 44 GHz, and both maser-detected sources. The median values are 1.5, 1.8, 1.7, and

2.2 km s^{-1} for none, only 22 GHz, only 44 GHz, and both maser-detected sources, respectively. The line width tends to increase from none to only 22 or 44 GHz to both maser-detected subsamples. This tendency is more clearly displayed in Figure 2.24, which presents cumulative probabilities of the line width for the four subsamples. The difference between none and both maser-detected subsamples seems to be distinct. We perform a Kolmogorov-Smirnov(K-S) test for combinations of the four subsamples in order to examine the statistical difference in their distributions. The K-S test shows that both maser-detected subsample has a significantly different distribution from the other three subsamples, namely, the p-values being 1.2×10^{-10}, 0.001, and 0.02 for none, only 22 GHz, and only 44 GHz maser-detected subsamples, respectively.

The estimated kinetic temperatures are in the range of 12−45 K with mean and median values of 21.6 and 21.1 K. The values are comparable to the temperatures (16−45 K) of IRDCs (Chira et al., 2013). The median values are 19.2, 23.0, 21.3, and 23.1 K for none, only 22 GHz, only 44 GHz, and both maser-detected sources, respectively. The kinetic temperature tends to increase from none to only 44 GHz to only 22 GHz and both maser-detected subsamples. Figure 2.24 shows this tendency. The K-S test also shows that both maser-detected sources have a different distribution from none ($p=1.3\times10^{-7}$) and only 44 GHz ($p=0.005$) maser-detected sources.

2.4.4 The Virial Parameters

We estimate the virial masses of the molecular clumps associated with our RMSs using the NH_3 line widths. Following Fuller et al. (1992) (see also Urquhart et al. 2015), we first derive the average line width of the total column of gas from the observed NH_3 line width using the equation below

$$\Delta v^2_{\rm avg} = \Delta v^2_{\rm T} + \Delta v^2_{\rm NT} = \Delta v^2_{\rm corr} + 8{\rm ln}2\ \frac{{\rm k_b T_{kin}}}{\rm m_H}\left(\frac{1}{\mu_{\rm p}} - \frac{1}{\mu_{\rm NH_3}}\right). \quad (2.22)$$

Here $\Delta v_{\rm corr}$ is the observed line width corrected for the resolution of the spectrometer, k_b is the Boltzmann constant, $T_{\rm kin}$ is the kinetic temperature of gas, taken to be 20 K, $\mu_{\rm p}$ and $\mu_{\rm NH_3}$ are the mean molecular mass of molecular hydrogen and ammonia taken as 2.33 and 17, respectively.

Assuming the associated clumps are self-gravitating, we calculate the virial mass from

$$M_{\rm vir} = \frac{5}{8{\rm ln}2{\rm G}}\frac{R_{eff}\Delta v^2_{\rm avg}}{a_1 a_2} = 210 M_\odot \frac{(R_{eff}/{\rm pc})(\Delta {\rm v_{avg}/kms^{-1}})^2}{a_1 a_2}, \quad (2.23)$$

$$a_1 = \frac{1-p/3}{1-2p/5}\ {\rm for\ p} < 2.5, \quad {\rm a_2} = {\rm y}\frac{{\rm arcsinh}({\rm y}^2-1)^{\frac{1}{2}}}{({\rm y}^2-1)^{\frac{1}{2}}}, \quad (2.24)$$

where R_{eff} is the effective radius of the clump, G is the gravitational constant, a_1 is the correction for the power-law density distribution $\rho(r) \sim r^{-p}$, a_2 accounts for the effect of the clump ellipticity, and y is the aspect ratio of the clump (Bertoldi et al., 1992). We adopt the mean power value determined by Mueller et al. (2002), <p>=1.8 (i.e. a_1=1.43), by modeling the 350 mum continuum emission maps of 31 massive star-forming clumps, and the mean aspect ratio of the 99 associated ATLASGAL clumps, y=1.54 (i.e., a_2∼1.3).

Figure 2.25 shows the virial parameter α ($\equiv M_{\rm vir}/M_{\rm clump}$) versus $M_{\rm clump}$ for the clumps with and without maser emission. The virial parameter tends to decrease with increasing clump mass. This implies that more massive clumps are more gravitationally unstable. Linear regression fittings to the clumps with and without maser emission give slopes of about -0.54 and -0.63, respectively. These values are similar to the slopes from -0.37 to -0.79 reported by Kauffmann et al. (2013) for 260 other massive star-forming clumps. In addition, the maser-detected clumps appear to have higher α's than the non-detected clumps with similar masses, which suggests that the former are more stable than the latter. This may be because of more active feedback in the clumps with maser emission.

2.4.5 Maser Occurrence and Evolutionary Stage

IRDCs are generally believed to be the best candidates of birthplaces for high-mass stars and clusters (e.g., Rathborne et al., 2006). UCHIIs are produced by young massive stars that have reached the main sequence stage. Thus IRDCs, HMPOs, and UCHIIs represent the evolutionary sequence of massive star formation. We investigate how the occurrence rates of H_2O and class I CH_3OH masers vary with the evolution of the central objects. Wang et al. (2006) surveyed H_2O maser emission toward 140 IRDC cores with the Very Large Array (VLA) at a typical rms noise level of $\sim$0.1 Jy, and detected the emission in 12% of them. Chambers et al. (2009) also observed the 140 and 50 more IRDC cores using the GBT with a twice lower noise level ($\sim$0.05 Jy) and obtained a detection rate of 35% . As mentioned earlier, the previous surveys of H_2O maser emission toward HMPOs

showed a detection rate of 42% at a similar sensitivity to ours (Sridharan et al., 2002), and a slightly higher rate of $\sim$ 52% with a better sensitivity ($\sim$0.12 Jy) (Urquhart et al., 2011). Although Urquhart et al. (2011) obtained the same detection rate of H_2O maser emission toward UCHIIs as that for HMPOs, other surveys showed significantly higher detection rates for UCHIIs. Churchwell et al. (1990) surveyed 84 UCHIIs and detected H_2O maser emission in 67% of them, and Kim et al. (2016, in prep.) also observed 103 UCHIIs and obtained a similar detection rate with the KVN telescopes at a similar detection limit to this study. Therefore, the detection rate of H_2O maser emission tends to increase as the central objects evolve.

As for 44 GHz CH_3OH masers, as mentioned in § 3.1, Fontani et al. (2010) detected the emission in 31% of 88 HMPO candidates at a rms noise level of about 0.3 Jy. Kim et al. (2016) observed 103 UCHIIs in the 44 GHz maser tranisition at a similar sensitivity to this study, and obtained a significantly higher detection rate of 48%. In actual, Fontani et al. (2010) also acquired the same value for the *high* group of their sample, which has similar $IRAS$ colors to UCHIIs, but a considerably lower detection rate (17%) for the *low* group, which may be in an earlier evolutionary phase than the *high* group. Thus the detection rates of 44 GHz CH_3OH maser emission also appear to increase as the central objects evolve. Moreover, Fontani et al. (2010) found a similar evolutionary trend for 95 GHz masers of which the detection rate increase from the *low* group (6%) to the *high* group (20%), although the number of the detected sources is just 11.

These trends are in contrast to the findings in low- and intermediate-mass star-forming regions. Furuya et al. (2003) found in low-mass

YSOs that the detection rate of H_2O masers dramatically decreases from Class 0 to Class I to Class II objects. Bae et al. (2011) also found similar trends in the detection rates of both H_2O and 44 GHz CH_3OH masers toward intermediate-mass YSOs. Bae et al. (2011) suggested that this difference can be caused by the different environments of low- and high-mass star-forming regions. UCHIIs are still deeply embedded in the natal molecular clouds although the central stars have already reached the main sequence stage. On the contrary, low-mass stars in the pre-main sequence phase are usually visible. Therefore, the occurrence of 22 GHz H_2O and 44 GHz class I CH_3OH masers is closely related to the surrounding environments as well as the evolutionary stage of the central objects.

2.5 Summary

We have simultaneously surveyed 22 GHz H_2O and 44 and 95 GHz class I CH_3OH masers toward 299 HMPOs in the RMS catalog. The main results are summarized as follows.

1. The overall detection rates are 45%, 28%, and 23% for 22, 44, and 95 GHz masers, respectively. We found 123 new maser sources: 15 at 22 GHz, 56 at 44 GHz, and 52 at 95 GHz. In our sample, 138 sources are distributed in the MMB survey area and 34 (25%) of them are associated with 6.7 GHz class II CH_3OH maser emission. We detected high-velocity (>30 km s^{-1}) features in 27 H_2O maser sources. Nine of them are very likely to be dominant H_2O maser outflow sources, 7 blueshifted and 2 redshifted ones.

2. The 44 and 95 GHz class I CH_3OH masers have very similar properties. The 95 GHz maser emission was detected only in 44 GHz maser sources. The two transitions have strong correlations with each other in the peak velocity, the peak flux density, and the isotropic luminosity. The peak flux density ratio ($S_{\rm p,95}/S_{\rm p,44}$) was estimated to be 0.56. Both of these masers always have the peak velocities within 5 km s^{-1} from the systemic velocities. Therefore, 44 and 95 GHz masers might be produced by the same mechanisms in the same sites. On the other hand, they show no significant correlation with 22 GHz H_2O or 6.7 GHz class II CH_3OH masers in the isotropic luminosity.

3. The 44 GHz class I CH_3OH masers have much narrower distributions than 22 GHz H_2O masers in the relative peak velocity and the velocity range. The 6.7 GHz class II CH_3OH masers have intermediate distributions between the two maser species. As for the peak flux density, 44 GHz masers have a significantly smaller median value than those of 6.7 and 22 GHz masers, which are comparable.

4. We investigated for 22, 44, 95, and 6.7 GHz masers whether the isotropic luminosity of each maser species correlates with the physical properties of the central objects and the parental clumps. The maser luminosity shows significant correlations with the clump mass and moderate correlations with the bolometric luminosity for all the four maser species, but does *not* correlate with the peak H_2 column density. Furthermore, quite strong correlations appeared between the two parameters for 22 and 44 GHz masers in the case where the data points of low- and intermediate mass YSOs from the previous studies were added.

5. The linewidth and kinetic temperature of NH_3 line emission tend

to increase from none to only 22 GHz or 44 GHz to both maser-detected sources. The investigation of the virial mass suggests that the ATLASGAL clumps with any maser emission could be more gravitationally stable than those associated with no maser emission.

6. The detection rates of 22 GHz H_2O and 44 GHz CH_3OH maser emission appear to increase as the central objects evolve in massive star-forming regions. This is contrary to the results of low-mass and intermediate-mass cases. Therefore, the occurrence of both masers might depend on the encompassing environments as well as on the evolutionary stage of the central objects.

We are grateful to all staff members in KVN who helped to operate the array and to correlate the data. The KVN is a facility operated by KASI (Korea Astronomy and Space Science Institute). The KVN operations are supported by KREONET (Korea Research Environment Open NETwork) which is managed and operated by KISTI (Korea Institute of Science and Technology Information). This paper made use of information from the Red MSX Source survey database at $http://rms.leeds.ac.uk/cgi-bin/public/RMS_DATABASE.cgi$ which was constructed with support from the Science and Technology Facilities Council of the UK.

Bibliography

Bae, J.-H., Kim, K.-T., Youn, S.-Y., et al. 2011, ApJS, 196, 21

Batrla W., Menten K. M. 1988, ApJ, 329, L117

Bayandina O. S., Val'tts I. E., Larionov G. M. 2012, Astron. Rep., 56, 553

Bertoldi, F., & McKee, C. F. 1992, ApJ, 395, 140

Breen, S. L., Caswell, J. L., Ellingsen, S. P., et al. 2010a, MNRAS, 406, 1487

Breen, S. L., Ellingsen, S. P., Caswell, J. L., et al. 2010b, MNRAS, 401, 2219

Breen, S. L., Fuller, G. A., Caswell, J. L., et al. 2015, MNRAS, 450, 4109

Caswell, J. L., & Phillips, C. J. 2008, MNRAS, 386, 1521

Caswell J. L., Breen S. L., 2010, MNRAS, 407, 2599

Chambers, E. T., Jackson, J. M., Rathborne, J. M., et al. 2009, ApJ, 181, 360

Chen X., Ellingsen S. P., Shen Z.-Q., et al. 2011, ApJS, 196, 9

Chen, X., Ellingsen, S. P., He, J.-H., et al. 2012, ApJS, 200, 5

Chira R.-A., Beuther H., Linz H., et al. 2013, A&A, 552, A40

Churchwell, E., Walmsley, C. M., & Cesaroni, R. 1990, A&AS, 83, 119

Codella C., Lorenzani A., Gallego A. T., et al. 2004, A&AS, 417, 615

Contreras, Y., Schuller, F., Urquhart, J. S., et al. 2013, A&A, 549, A45

Cragg, D. M., Johns, K. P., Godfrey, P. D., et al. 1992, MNRAS, 259, 203

Cyganowski, C. J., Brogan, C. L., Hunter, T. R., et al. 2009, ApJ, 702, 1615

Ellingsen, S. P. 2005, MNRAS, 359, 1498

Ellingsen, S. P., Voronkov, M. A., Cragg, D. M., et al. 2007, in IAU Symp. 242, Astrophysical Masers and their Environments, ed. J. M. Chapman & W. A. Baan (Cambridge: Cambridge Univ. Press), 213

Erickson, N. R., Goldsmith, P. F., Novak, G., Viscuso, P. J., Erickson, R. B., & Predmore, C. R. 1992, IEEE Trans. Microwave Theory Tech., MTT-40, 1

Felli, M., Palagi, F., & Tofani, G. 1992, A&A, 255, 293

Fontani, F., Cesaroni, R., & Furuya, R. S. 2010, A&A, 517, A56

Fuller G. A., Myers P. C. 1992, ApJ, 384, 523

Furuya, R. S., Kitamura, Y., Wootten, A., et al. 2003, ApJS, 144, 71

Gan C.-G., Chen X., Shen Z.-Q., et al. 2013, ApJ, 763, 2

Green J. A., Caswell, J. L., Fuller, G. A., et al. 2009, MNRAS, 392, 783

Han, F., Mao, R. Q., Lei, C. M., et al. 1995, PPMtO, 14, 185

Han, F., Mao, R. Q., Lu, J., et al. 1998, A&AS, 127, 181

Han, S.-T., Lee, J.-W., Kang, J., et al. 2008, IJIMW, 29, 69

Jackson, J. M., Rathborne, J. M.; Shah, R. Y., et al. 2006, ApJS, 163, 145

Jordan, C. H., Walsh, A. J., Lowe, V., et al. 2015, MNRAS, 448, 2344

Kim, K.-T., Byun, D.-Y., Je, D.-H., et al. 2011, JKAS, 44, 81

Kalenskii, S. V., Kurtz, S., & Bergman, P. 2013, ARep, 57, 120

Kang, H., Kim, K.-T., Byun, D.-Y., et al. 2015, ApJS, 221, 6

Kauffmann J., Pillai T., Goldsmith P. F. 2013, ApJ, 779, 185

Kurtz, S., Hofner, P., & Alvarez, C. V. 2004, ApJS, 155, 149

Lee, S.-S., Byun, D.-Y., Oh, C. S., et al. 2011, PASP, 123, 1398

Lumsden, S. L., Hoare, M. G., Oudmaijer, R. D., & Richards, D. 2002, MNRAS, 336, 621

Lumsden, S. L., Hoare, M. G., Urquhart, J. S., et al. 2013, ApJS, 208, 11

Menten K. M., 1991, ApJ, 380, L75

Mueller, K. E., Shirley, Y. L., Evans, N. J., II, et al. 2002, ApJS, 143, 469

Rathborne, J. M., Jackson, J. M., & Simon, R. 2006, ApJ, 641, 389

Schuller, F., Menten, K. M., Contreras, Y., et al. 2009, A&A, 504, 415

Seth, A. C., Greenhill, L. J., & Holder, B. P. 2002, ApJ, 581, 325

Slysh V. I., Kalenskii S. V., Val'tts I. E., et al. 1994, MNRAS, 268, 464

Sridharan T. K., Beuther H., Schilke P., et al. 2002,ApJ, 566, 931

Sunada, K., Nakazato, T., Ikeda, N., et al. 2007, PASJ, 59, 1185

Szymczak, M., Pillai, T., & Menten, K. M. 2005, A&A, 434, 613

Testi, L., Palla, F., & Natta, A. 1998, A&AS, 133, 81

Torrelles, J. M., Gómez, J. F., Rodríguez, L. F., et al. 1997, ApJ, 489, 744

Torrelles, J. M., Patel, N. A., Gómez, J. F., et al. 2001, ApJ, 560, 853

Urquhart, J. S., Hoare, M. G., Purcell, C. R., et al. 2009, A&A, 501, 539

Urquhart, J. S., Morgan, L. K., Figura, C. C., et al. 2011, MNRAS, 418, 1689

Urquhart J. S., Figura C. C., Moore T. J. T., et al. 2014a, MNRAS, 437, 1791

Urquhart J. S., Moore, T. J. T., Csengeri, T., et al., 2014b, MNRAS, 443, 1555

Urquhart, J. S., Moore, T. J. T., Menten, K. M., et al. 2015, MNRAS, 446, 3461

Valdettaro, R., Palla, F., Brand, J., et al. 2001, A&A, 368, 845

Val'tts, I. E., Dzyura, A. M., Kalenskii, S. V., et al. 1995, AZh, 72, 22

Val'tts I. E., Ellingsen S. P., Slysh V. I., et al. 2000, MNRAS, 317, 315

Val'tts, I. E., & Larionov, G. M. 2007, Astron. Rep., 51, 519

Voronkov, M. A., Brooks, K. J., Sobolev, A. M., et al. 2006, MNRAS, 373, 411

Wang, Y., Zhang, Q., Rathborne, J. M., et al. 2006, ApJ, 651, L125

Wienen, M., Wyrowski F., Schuller F., et al. 2012, A&A, 544, A146

Table 2.1. Summary of Target Sources

RMS[a] ID	MSX name	R.A. (J2000.0)	Decl. (J2000.0)	Distance (kpc)	$L_{\rm bol}$ ($L_\odot$)	$V_{\rm sys}$[b] (km s^{-1})	Detection[c] 22 GHz	44 GHz	95 GHz	MMB Coverage
4	G118.6172-01.3312	00:15:27.83	+61:14:18.9	2.8	4900	-39.20	Y[11]	n	n	...
7	G120.1483+03.3745	00:23:57.04	+66:05:51.5	5.6	21000	-68.90	y[4]	n	n	...
11	G121.3479-03.3705	00:38:59.37	+59:27:48.2	3.0	1100	-41.90	n	n	n	...
12	G122.4459-00.7815	00:47:17.05	+62:05:09.3	3.1	1600	-42.80	n	n	n	...
14	G123.2836+03.0307	00:54:52.79	+65:53:57.4	4.9	4300	-62.10	n	n	n	...
15	G123.8059-01.7805	00:58:39.99	+61:04:43.0	2.1	2400	-31.90	n	n	n	...
16	G124.0144-00.0267	01:00:55.41	+62:49:30.4	3.1	1800	-43.40	n	n	n	...
18[H]	G125.6045+02.1038B	01:16:36.21	+64:50:38.4	4.1	8400	-53.70	y[4]	n	n	...
20	G125.7795+01.7285	01:17:53.03	+64:27:14.3	5.2	5400	-64.50	n	n	n	...
23	G126.7144-00.8220	01:23:33.17	+61:48:48.2	0.7	2600	-13.90	n	n	n	...
35[H]	G133.6945+01.2166A	02:25:30.99	+62:06:20.9	2.0	45000	-43.40	y[4,11]	Y	Y	...
37	G133.7150+01.2155	02:25:40.77	+62:05:52.4	2.0	140000	-39.20	y[1,4,6,11]	n	n	...
46	G134.2792+00.8561	02:29:01.93	+61:33:30.5	2.0	5200	-51.20	y[1]	n	n	...
49	G135.2774+02.7981	02:43:28.64	+62:57:08.7	6.0	29000	-71.50	y[4,6,11]	n	n	...
50	G136.3542+00.9543	02:45:10.70	+60:49:38.0	5.5	3700	-61.50	n	n	n	...
53	G136.3833+02.2666	02:50:08.57	+61:59:52.1	3.2	7800	-42.40	y[11]	n	n	...
54	G136.5370+02.8934	02:53:43.47	+62:29:23.2	3.9	1200	-48.00	n	n	n	...
56	G138.2957+01.5552	03:01:31.32	+60:29:13.2	2.9	17000	-38.00	n	n	n	...
58[H]	G139.9091+00.1969A	03:07:24.52	+58:30:43.3	3.2	21000	-39.80	y[6,11]	n	n	...
61	G143.8118-01.5699	03:24:50.95	+54:57:32.7	2.4	9200	-31.10	Y[11]	n	n	...
63	G141.9996+01.8202	03:27:38.76	+58:47:00.1	0.8	5500	-13.10	y[1,6,11]	n	n	...
65	G145.1975+02.9870	03:52:27.32	+57:48:31.7	6.5	4500	-58.60	n	n	n	...
66	G148.1201+00.2928	03:56:15.36	+53:52:13.0	3.2	3400	-34.60	n	n	n	...
71	G151.6120-00.4575	04:10:11.86	+50:59:54.4	6.4	61000	-49.70	n	n	n	...
84	G160.1452+03.1559	05:01:39.89	+47:07:21.7	1.9	2100	-16.50	y[4,6,11]	n	n	...
88	G168.0627+00.8221	05:17:13.69	+39:22:19.4	2.0	1700	-25.00	y[1,4,6,11]	n	n	...

Table 2.1 (cont'd)

RMS[a] ID	MSX name	R.A. (J2000.0)	Decl. (J2000.0)	Distance (kpc)	$L_{\rm bol}$ ($L_\odot$)	$V_{\rm sys}$[b] (km s^{-1})	Detection[c] 22 GHz	44 GHz	95 GHz	MMB Coverage
90[†]	G176.4661-01.6758	05:30:20.82	+31:01:28.7	2.0	1200	-18.90	n	n	n	...
91	G174.1974-00.0763	05:30:46.06	+33:47:54.1	2.0	5900	-3.50	y[1,4,6,11]	y[12]	Y	...
97	G177.7291-00.3358	05:38:47.16	+30:41:18.1	2.0	2300	-16.10	n	n	n	...
106	G173.6339+02.8218	05:41:11.02	+35:50:01.7	2.0	5400	-19.70	Y[4,11]	n	n	...
110	G178.7540+01.1609	05:47:12.27	+30:36:12.2	2.0	2100	-18.00	n	n	n	...
111	G184.8704-01.7329	05:50:13.89	+23:52:17.7	2.0	2000	2.30	n	n	n	...
113	G188.9696-01.9380	05:58:24.43	+20:13:57.6	2.0	1900	-1.20	y[1,3,6]	n	n	y
114	G178.8454+04.2936	06:00:04.99	+32:06:31.8	1.1	2200	0.60	n	n	n	...
119	G189.0307+00.7821	06:08:40.52	+21:31:00.4	2.0	24000	2.50	n	n	n	y
120	G189.0323+00.8092	06:08:46.73	+21:31:44.1	2.0	11000	1.90	n	n	n	y
121	G188.9479+00.8871	06:08:53.40	+21:38:28.1	1.8	2200	3.10	y[1,4,6]	Y	Y	y
124	G188.8120+01.0686	06:09:17.90	+21:50:49.9	2.0	664	-0.30	n	n	n	y
125[H]	G189.8557+00.5011A	06:09:19.82	+20:39:31.5	2.0	1622	8.20	Y[6,8]	n	n	y
128	G192.9089-00.6259	06:11:23.74	+17:26:28.5	2.0	1400	22.60	n	n	n	y
131	G192.6005-00.0479	06:12:54.01	+17:59:23.1	2.0	45000	7.40	y[1,4,6]	y[7,12]	Y	y
133	G194.9349-01.2224	06:13:16.14	+15:22:43.3	2.0	3000	15.90	Y[6,8]	y[12]	Y	y
135	G196.4542-01.6777	06:14:37.06	+13:49:36.4	5.3	94000	18.00	y[1,4,6]	n	n	y
136	G196.1620-01.2546	06:15:34.71	+14:17:03.2	1.5	2400	10.80	n	n	n	y
140	G201.3419+00.2914	06:31:06.92	+10:26:04.9	0.8[d]	1100	-1.40	n	n	n	y
141[H]	G206.7804-01.9395B	06:33:16.21	+04:34:53.0	1.2	912	14.00	n	n	n	y
145	G212.2344-03.5038	06:37:41.59	-00:58:37.7	5.0	2500	46.60	y[4]	n	n	...
146	G203.7637+01.2705	06:39:09.95	+08:44:09.7	0.8	483	9.50	n	n	n	y
149	G203.3166+02.0564	06:41:10.15	+09:29:33.6	0.6	1100	7.40	y[1,6]	y[7,12]	Y	...
151	G211.8957-01.2025	06:45:16.00	+00:22:24.9	4.8	5800	45.00	n	n	n	y
153	G212.0641-00.7395	06:47:13.36	+00:26:06.5	4.7	16000	45.00	y[4,6]	Y	Y	y
154[Y]	G214.4934-01.8103A	06:47:50.26	-02:12:51.3	2.1	1980	26.80	n	n	n	y

Table 2.1 (cont'd)

RMS[a] ID	MSX name	R.A. (J2000.0)	Decl. (J2000.0)	Distance (kpc)	$L_{\rm bol}$ ($L_\odot$)	$V_{\rm sys}$[b] (km s^{-1})	Detection[c] 22 GHz	44 GHz	95 GHz	MMB Coverage
155	G215.8902-02.0094	06:49:40.23	-03:32:52.4	6.1	4100	57.60	n	n	n	...
156	G217.6047-02.6170	06:50:37.41	-05:21:00.9	6.8	4200	63.30	n	n	n	...
157	G211.5350+01.0053	06:52:28.23	+01:42:06.5	4.8	7400	44.80	n	n	n	y
158	G213.9180+00.3786	06:54:35.14	-00:42:17.8	3.9	1200	41.60	n	n	n	y
160	G212.9626+01.2954	06:56:06.32	+00:33:47.7	4.2	1300	42.50	n	n	n	y
167	G217.3020-00.0567	06:59:13.13	-03:54:53.2	1.3	799	26.70	n	n	n	y
172[Y]	G218.0230-00.3139A	06:59:37.48	-04:40:23.5	1.9	3000	25.70	n	n	n	y
174	G221.9605-01.9926	07:00:50.94	-08:56:30.1	3.2	5500	41.10	n	n	n	y
175	G220.4587-00.6081	07:03:03.06	-06:58:25.9	2.2	2100	29.60	y[1,4,11]	n	n	y
176	G224.6065-02.5563	07:03:43.16	-11:33:06.2	0.8	1200	13.80	n	n	n	...
181	G224.6075-01.0063	07:09:20.55	-10:50:28.1	1.0	596	16.20	n	n	n	y
184	G232.0766-02.2767	07:18:59.91	-18:02:41.6	3.0	5000	42.10	n	n	n	...
188	G231.7986-01.9682	07:19:35.93	-17:39:18.0	3.2	5600	43.50	n	n	n	y
189	G229.5711+00.1525	07:23:01.80	-14:41:32.2	4.1	4700	52.80	y[4,6,8,11]	n	n	y
193	G233.8306-00.1803	07:30:16.72	-18:35:49.1	3.3	13000	44.60	n	n	n	y
196	G232.6207+00.9959	07:32:09.73	-16:58:13.4	1.7	11000	16.60	n	n	n	y
203[Y]	G236.8158+01.9821A	07:44:28.02	-20:08:31.2	4.0	3600	52.80	y[4,6,8,11]	n	n	y
205	G242.9402-00.4501	07:48:43.25	-26:39:30.9	5.1	3200	63.50	n	n	n	y
2360	G010.5067+02.2285	18:00:34.53	-18:45:17.9	2.9	1700	21.80	y[6,8,11]	n	n	...
2384	G011.9019+00.7265	18:08:58.78	-18:16:29.8	2.9	502	24.30	n	n	n	y
2389	G010.8856+00.1221	18:09:07.98	-19:27:24.0	2.7	5500	19.70	y[4,11,14]	n	n	y
2434[Y]	G012.8909+00.4938A	18:11:51.13	-17:31:21.1	2.4	20600	33.80	y[1,4,9,11,14]	y[7]	y[13]	y
2437	G012.0260-00.0317	18:12:01.88	-18:31:55.7	11.1	35000	110.80	n	n	n	y
2445[H]	G012.1993-00.0342B	18:12:23.43	-18:22:51.0	12.0	143000	50.90	n	Y	y[10]	y
2489[H]	G013.1840-00.1069A	18:14:38.98	-17:33:07.5	11.9	32000	54.40	n	n	n	y
2490	G012.9090-00.2607	18:14:39.56	-17:52:02.3	2.4	32000	36.70	y[4,9,11,14]	Y	y[10]	y

Table 2.1 (cont'd)

RMS[a] ID	MSX name	R.A. (J2000.0)	Decl. (J2000.0)	Distance (kpc)	$L_{\rm bol}$ ($L_\odot$)	$V_{\rm sys}$[b] (km s^{-1})	Detection[c] 22 GHz	44 GHz	95 GHz	MMB Coverage
2491	G013.3310-00.0407	18:14:41.80	-17:23:27.7	4.5	3700	54.70	n	Y	n	y
2512	G016.7122+01.3119	18:16:26.38	-13:46:24.4	2.1	1800	20.30	n	n	n	y
2529	G014.6087+00.0127	18:17:02.71	-16:14:28.0	2.6	4900	24.40	y[4,9,11,14]	y[12]	Y	y
2535	G015.0939+00.1913	18:17:20.87	-15:43:45.9	2.9	1600	29.90	y[8,11,14]	Y	n	y
2536	G013.6562-00.5997	18:17:24.38	-17:22:14.8	4.1	14000	47.40	y[4,11,14]	y[7,12]	Y	y
2540	G014.0329-00.5155	18:17:50.63	-16:59:57.3	1.1	1000	20.30	n	n	n	y
2545	G018.3412+01.7681	18:17:58.11	-12:07:24.8	2.8	22000	33.10	y[4,6,11,14]	n	n	y
2547	G016.9270+00.9599	18:18:08.62	-13:45:07.0	2.1	7600	20.90	y[4,8,11]	Y	Y	y
2577	G016.9512+00.7806	18:18:50.31	-13:48:53.9	2.4	945	24.90	n	n	n	y
2583[H]	G017.0332+00.7476A	18:19:07.33	-13:45:23.6	2.4	2734	24.90	n	n	n	y
2584	G010.8411-02.5919	18:19:12.09	-20:47:30.9	1.9	24000	12.30	y[4,6,9,11]	y[7,12]	Y	...
2586	G014.4335-00.6969	18:19:18.21	-16:43:56.1	1.1	1300	17.50	n	n	n	y
2591[Y]	G017.4507+00.8118A	18:19:41.88	-13:21:35.4	2.1	2084	21.30	n	Y	Y	y
2611	G014.9958-00.6732	18:20:19.47	-16:13:29.8	2.0	13000	19.40	y[8,11]	Y	Y	y
2642	G015.1288-00.6717	18:20:34.60	-16:06:28.2	2.0	12000	19.00	n	n	n	y
2645	G016.9261+00.2854	18:20:35.44	-14:04:13.9	2.4	1300	24.20	y[11]	n	n	y
2659	G016.7981+00.1264	18:20:55.28	-14:15:30.8	1.7	956	15.20	n	n	n	y
2690	G017.6380+00.1566	18:22:26.37	-13:30:12.0	2.2	100000	22.10	y[4,6,11,14]	n	n	y
2698[Y]	G017.9642+00.0798A	18:23:20.94	-13:15:05.5	2.2	2835	22.60	y[11]	n	n	y
2716[H]	G018.6608+00.0372A	18:24:50.24	-12:39:22.4	11.0	22300	81.10	y[11,14]	Y	y[10]	y
2739	G018.3706-00.3818	18:25:48.36	-13:06:29.2	3.5	5200	44.60	n	n	n	y
2757	G019.8922+00.1023	18:26:57.37	-11:32:09.6	3.4	3700	45.90	n	n	n	y
2760	G018.8319-00.4788	18:27:02.34	-12:44:38.3	4.5	4300	65.20	n	Y	n	y
2785	G019.9386-00.2079	18:28:10.03	-11:38:21.8	4.2	3400	63.40	n	n	n	y
2788	G019.9224-00.2577	18:28:18.96	-11:40:36.7	4.3	3100	64.90	n	Y	y[13]	y
2799[Y]	G020.7617-00.0638B	18:29:12.11	-10:50:36.2	11.8	62000	56.90	y[11]	Y	Y	y

Table 2.1 (cont'd)

RMS[a] ID	MSX name	R.A. (J2000.0)	Decl. (J2000.0)	Distance (kpc)	L_{bol} ($L_{\odot}$)	V_{sys}[b] (km s^{-1})	Detection[c] 22 GHz	44 GHz	95 GHz	MMB Coverage
2810	G016.8689-02.1552	18:29:24.23	-15:15:48.3	2.0	6600	18.60	y[1,4,6,11]	y[7,12]	y[2]	...
2817	G028.5483+03.7649	18:30:01.36	-02:10:25.6	0.7	132	6.70	n	n	n	...
2821	G021.5624-00.0329	18:30:36.06	-10:07:11.0	9.7	48000	113.60	y[11]	n	n	y
2822[H]	G021.3570-00.1795B	18:30:44.95	-10:22:12.6	10.5	47000	91.20	n	n	n	y
2837	G022.3554+00.0655	18:31:44.08	-09:22:18.5	4.9	11000	84.20	y[4,9,11]	Y	Y	y
2844	G023.3891+00.1851	18:33:14.32	-08:23:57.4	4.5	24000	75.50	n	Y	Y	y
2846	G023.8176+00.3841	18:33:19.54	-07:55:37.8	4.5	3900	76.50	y[11]	Y	y[10]	y
2853	G026.4207+01.6858	18:33:30.55	-05:01:02.0	2.9	19000	42.20	y[4,6,11]	n	n	y
2858[H]	G024.0946+00.4565B	18:33:34.67	-07:38:49.0	5.2	2497	94.10	n	n	n	y
2879	G025.6498+01.0491	18:34:20.89	-05:59:42.5	3.0	41000	42.80	y[1,4,6,9,11]	y[12]	Y	y
2881[H]	G026.3819+01.4057A	18:34:25.67	-05:10:50.2	2.9	21400	42.10	y[4,6,11]	n	n	y
2901	G023.6566-00.1273	18:34:51.56	-08:18:21.6	3.2	10000	80.40	n	n	n	y
2920	G024.7320+00.1530	18:35:50.91	-07:13:27.2	7.7	12000	108.90	Y[11]	Y	n	y
2963[Y]	G026.4958+00.7105A	18:37:07.30	-05:23:58.2	11.8	22300	48.60	n	Y	Y	y
2966[E]	G025.4118+00.1052B	18:37:16.99	-06:38:24.3	5.2	10493	95.30	n	y[12]	Y	y
2967	G024.6343-00.3233	18:37:22.68	-07:31:41.5	3.0	6800	42.80	n	n	n	y
2970[H]	G025.3953+00.0336B	18:37:30.30	-06:41:17.8	16.3	310000	-13.00	y[8,11]	n	n	y
2978	G029.8129+02.2195	18:37:50.54	-01:45:37.5	3.0	1300	45.40	y[4,11]	n	n	...
2994	G026.2020+00.2262	18:38:18.51	-05:52:57.4	7.5	3600	112.40	n	n	n	y
3003[H]	G025.4948-00.2990A	18:38:52.85	-06:45:07.8	...	...	...	n	n	n	y
3028[H]	G026.5254-00.2667A	18:40:40.25	-05:49:12.9	7.5	9144	105.80	Y[11]	n	n	y
3032[H]	G027.1852-00.0812B	18:41:13.26	-05:08:57.7	13.0	280000	25.80	y[4,11]	n	n	y
3044	G027.7571+00.0500	18:41:47.98	-04:34:52.9	5.4	13000	99.60	n	n	n	y
3049	G028.3373+00.1189	18:42:37.10	-04:02:02.1	4.6	7600	81.00	n	Y	Y	y
3051	G028.2325+00.0394	18:42:42.50	-04:09:45.9	7.4	8600	107.10	n	n	n	y
3056	G027.7954-00.2772	18:43:02.25	-04:41:48.8	3.1	5100	45.90	n	n	n	y

Table 2.1 (cont'd)

RMS[a] ID	MSX name	R.A. (J2000.0)	Decl. (J2000.0)	Distance (kpc)	$L_{\rm bol}$ ($L_\odot$)	$V_{\rm sys}$[b] (km s^{-1})	Detection[c] 22 GHz	44 GHz	95 GHz	MMB Coverage
3075	G028.8621+00.0657	18:43:46.24	-03:35:29.2	7.4	94000	103.10	y[4,11]	Y	Y	y
3077[D]	G028.3046-00.3871A	18:44:21.96	-04:17:39.5	10.0	191000	85.50	n	n	n	y
3094	G030.9727+00.5620	18:45:51.68	-01:29:13.0	12.6	27000	23.70	y[11]	n	n	y
3099	G029.8620-00.0444	18:45:59.55	-02:45:06.5	4.9	28000	101.20	n	Y	n	y
3105	G029.8390-00.0980	18:46:08.44	-02:47:45.2	4.9	3300	99.20	n	n	n	y
3117[†]	G030.2971+00.0549	18:46:25.79	-02:19:13.7	4.9	3300	108.10	n	n	n	y
3119	G030.8185+00.2729	18:46:36.58	-01:45:22.4	4.9	8800	97.50	n	n	n	y
3126	G030.1981-00.1691	18:47:03.06	-02:30:36.1	4.9	30000	103.10	n	n	n	y
3145	G029.5904-00.6144	18:47:31.65	-03:15:13.8	4.4	2600	76.50	y[11]	n	n	y
3146[H]	G030.9585+00.0862B	18:47:31.83	-01:42:59.6	11.7	70000	39.60	Y[4,11]	n	n	y
3155	G030.5942-00.1273	18:47:37.53	-02:08:19.6	4.9	2000	84.50	n	n	n	y
3158	G030.4117-00.2277	18:47:38.95	-02:20:51.8	4.9	2500	104.80	y[8,11]	Y	n	y
3186	G030.9959-00.0771	18:48:10.65	-01:45:25.3	4.9	1700	81.20	n	Y	n	y
3187[H]	G031.2803+00.0615A	18:48:12.38	-01:26:30.3	4.9	56000	109.00	y[11]	Y	Y	y
3205	G032.0451+00.0589	18:49:36.56	-00:45:45.4	4.9	24000	95.30	y[4,11]	Y	Y	y
3212	G032.0518-00.0902	18:50:09.25	-00:49:29.1	4.2	3400	70.20	n	n	n	y
3221[H]	G032.9957+00.0415A	18:51:24.45	+00:04:34.0	9.2	34000	83.80	n	y[12]	n	y
3223	G033.3891+00.1989	18:51:33.82	+00:29:51.0	5.0	13000	85.30	n	n	n	y
3236	G033.3933+00.0100	18:52:14.63	+00:24:52.6	7.0	17000	103.60	y[11]	Y	n	y
3241	G033.5237+00.0198	18:52:26.74	+00:32:08.9	7.0	13000	103.50	n	Y	Y	y
3254	G034.8211+00.3519	18:53:37.88	+01:50:30.5	3.5	24000	56.90	n	n	n	y
3261	G034.0126-00.2832	18:54:25.05	+00:49:56.6	12.9	31000	11.80	n	n	n	y
3263	G034.0500-00.2977	18:54:32.29	+00:51:32.9	12.9	23000	11.50	n	n	n	y
3265	G035.3449+00.3474	18:54:36.14	+02:18:20.2	6.8	24000	94.30	n	n	n	y
3266	G034.7569+00.0247	18:54:40.72	+01:38:06.8	4.6	12000	76.90	n	n	n	y
3279	G035.8546+00.2663	18:55:49.27	+02:43:20.3	2.0	1600	29.20	n	n	n	y

Table 2.1 (cont'd)

RMS[a] ID	MSX name	R.A. (J2000.0)	Decl. (J2000.0)	Distance (kpc)	$L_{\rm bol}$ ($L_\odot$)	$V_{\rm sys}$[b] (km s^{-1})	Detection[c] 22 GHz	44 GHz	95 GHz	MMB Coverage
3282[H]	G040.5451+02.5961B	18:56:04.57	+07:57:29.2	2.3	40000	33.10	n	n	n	...
3291	G034.7123-00.5946	18:56:48.26	+01:18:47.1	2.9	9700	44.50	n	n	n	y
3292[H]	G036.9194+00.4825A	18:56:59.78	+03:46:03.9	15.8	26100	-30.50	Y[11]	n	n	y
3304	G037.4974+00.5301	18:57:53.37	+04:18:17.5	12.8	923	10.90	y[4,11]	Y	Y	y
3308	G035.1979-00.7427	18:58:12.99	+01:40:31.2	2.2	35000	33.70	y[4,6,11]	y[12]	y[10]	y
3314	G037.5536+00.2008	18:59:09.94	+04:12:15.6	6.7	120000	85.10	y[11]	Y	Y	y
3316[H]	G037.3412-00.0600A	18:59:42.28	+03:53:49.1	9.8	25400	55.80	n	n	n	y
3319	G036.8780-00.4728	19:00:19.81	+03:17:42.9	3.8	5200	60.90	n	n	n	y
3335[H]	G038.1208-00.2262B	19:01:44.15	+04:30:37.7	6.6	10400	82.30	n	n	n	y
3336	G035.3778-01.6405	19:01:44.54	+01:25:39.6	3.3	5900	43.60	n	n	n	y
3360	G038.9365-00.4592	19:04:03.67	+05:07:53.2	2.8	1500	41.90	y[11]	Y	n	y
3371[D]	G039.9284-00.3741A	19:05:35.27	+06:03:01.3	9.0	7713	60.00	n	n	n	y
3373	G040.2849-00.2378	19:05:45.66	+06:25:52.3	6.4	5300	72.40	Y[11]	n	n	y
3381	G039.4943-00.9933	19:06:59.68	+05:22:53.4	3.5	8700	53.40	n	n	n	y
3382[Y]	G042.0977+00.3521A	19:07:00.50	+08:18:44.1	10.9	62000	20.80	y[4,11]	n	n	y
3386[H]	G042.0341+00.1905A	19:07:28.20	+08:10:53.2	11.1	27000	17.80	n	n	n	y
3390	G041.0780-00.6365	19:08:39.25	+06:57:07.7	6.3	3500	73.70	n	n	n	y
3402[H]	G043.0786+00.0033A	19:10:05.01	+09:01:15.6	11.1	10600	14.40	n	n	n	y
3414	G043.1635-00.0697A	19:10:30.28	+09:03:45.4	11.1	4900	4.40	n	n	n	y
3427	G043.9956-00.0111	19:11:51.64	+09:49:40.4	6.0	21000	65.40	Y[11]	n	n	y
3429	G043.8152-00.1172	19:11:54.20	+09:37:12.7	3.3	795	46.90	y[11]	n	n	y
3436	G043.5216-00.6476	19:13:15.46	+09:06:48.9	8.1	1900	58.30	n	n	n	y
3446	G044.2836-00.5249	19:14:14.92	+09:50:43.5	6.0	9800	66.30	n	n	n	y
3448[H]	G045.4543+00.0600A	19:14:21.31	+11:09:11.7	7.3	152000	59.00	y[11]	n	n	y
3457	G045.1894-00.4387	19:15:39.00	+10:41:14.3	5.9	5600	67.30	n	n	n	y
3483	G050.0721+00.5591	19:21:24.82	+15:28:04.4	10.8	14000	-4.50	y[11]	Y	Y	y

Table 2.1 (cont'd)

RMS[a] ID	MSX name	R.A. (J2000.0)	Decl. (J2000.0)	Distance (kpc)	$L_{\rm bol}$ ($L_\odot$)	$V_{\rm sys}$[b] (km s^{-1})	Detection[c] 22 GHz	44 GHz	95 GHz	MMB Coverage
3489	G049.2982-00.0582	19:22:09.43	+14:29:46.9	5.4	4300	59.30	n	n	n	y
3503$^{\rm H}$	G048.9897-00.2992A	19:22:26.66	+14:06:46.2	5.4	45000	67.70	y[4,11]	Y	Y	y
3504	G049.2015-00.1876	19:22:26.55	+14:20:59.2	5.4	4800	64.90	n	n	n	y
3546	G049.5993-00.2488	19:23:26.61	+14:40:16.9	5.4	1800	56.90	y[11]	n	n	y
3550†	G049.4227-00.3715	19:23:32.65	+14:27:28.5	5.4	25000	66.60	n	n	n	y
3555$^{\rm H}$	G049.4883-00.3545B	19:23:36.79	+14:31:16.4	5.4	10800	60.10	y[4,11]	y[7,12]	Y	y
3580	G050.7796+00.1520	19:24:17.41	+15:54:01.8	5.3	2900	42.30	n	n	n	y
3585$^{\rm H}$	G052.2025+00.7217A	19:24:59.84	+17:25:18.1	10.0	29000	0.80	y[11]	n	n	y
3586	G052.2078+00.6890	19:25:08.53	+17:24:47.4	9.8	13000	3.80	y[11]	Y	Y	y
3587$^{\rm H}$	G050.2844-00.3925A	19:25:17.79	+15:12:24.5	9.3	190000	16.10	y[11]	n	n	y
3588	G049.0431-01.0787	19:25:22.24	+13:47:19.6	3.0	4000	38.70	y[6,11]	Y	Y	y
3593	G050.2213-00.6063	19:25:57.77	+15:02:59.6	3.3	13000	40.60	n	n	n	y
3597	G052.9217+00.4142	19:27:34.98	+17:54:38.0	5.1	7300	45.00	n	n	n	y
3603$^{\rm Y}$	G053.0366+00.1110A	19:28:55.65	+17:51:59.5	9.5	11900	4.80	y[11]	y[12]	Y	y
3608	G053.1417+00.0705	19:29:17.59	+17:56:23.0	1.9	8700	21.70	y[11]	Y	y[13]	y
3609$^{\rm H}$	G051.4006-00.8893A	19:29:19.70	+15:57:05.5	5.2	5600	62.80	n	n	n	y
3611	G053.6185+00.0376	19:30:23.04	+18:20:26.6	7.9	19000	23.00	n	n	n	y
3621	G052.5405-00.9272	19:31:45.03	+16:55:59.1	5.1	4000	64.70	n	n	n	y
3625	G053.5343-00.7943	19:33:16.40	+17:52:04.8	5.0	7300	58.50	n	n	n	y
3635	G056.4120-00.0277	19:36:21.53	+20:45:17.9	9.3	22000	-4.40	n	n	n	y
3641	G056.3694-00.6333	19:38:31.63	+20:25:18.7	5.9	8700	32.40	y[4,11]	n	n	y
3642	G058.7087+00.6607	19:38:36.83	+23:05:43.5	4.4	3300	30.90	n	n	n	y
3648$^{\rm H}$	G057.5474-00.2717A	19:39:39.61	+21:37:31.7	8.3	39300	4.30	n	n	n	y
3659	G059.7831+00.0648	19:43:11.23	+23:44:03.6	2.2	22000	22.40	y[4,11]	y[12]	y[2]	y
3661	G059.9997+00.1167	19:43:27.78	+23:56:53.0	9.3	9000	-15.20	n	n	n	y
3663	G059.6403-00.1812	19:43:48.53	+23:29:17.9	2.2	1500	27.40	y[11]	Y	y[13]	y

Table 2.1 (cont'd)

RMS[a] ID	MSX name	R.A. (J2000.0)	Decl. (J2000.0)	Distance (kpc)	L_{bol} ($L_\odot$)	V_{sys}[b] (km s^{-1})	Detection[c] 22 GHz	44 GHz	95 GHz	MMB Coverage
3671[H]	G060.8828-00.1295B	19:46:20.14	+24:35:29.2	2.2	50000	21.70	n	n	n	...
3683	G063.1140+00.3416	19:49:32.11	+26:45:15.0	4.7	5500	20.00	y[4,6,11]	Y	Y	...
3712	G068.2040+00.2387	20:01:59.95	+31:03:10.3	9.0	7000	-35.50	n	n	n	...
3722	G071.8944+01.3107	20:07:04.79	+34:44:42.6	1.4	1500	11.60	n	n	n	...
3724	G073.0633+01.7958	20:08:10.08	+35:59:24.0	1.4	3500	0.60	y[4,11]	y[12]	Y	...
3733[H]	G072.2479+00.2617A	20:12:17.28	+34:28:11.0	11.3	10700	-71.00	n	n	n	...
3734	G077.5671+03.6911	20:12:33.70	+40:47:40.7	5.7	4500	-21.90	n	n	n	...
3735	G071.5219-00.3854	20:12:57.87	+33:30:26.8	1.4	1700	10.30	y[4,6,11]	Y	n	...
3739	G078.1224+03.6320	20:14:25.86	+41:13:36.3	1.4	4000	-3.90	y[1,4,6,11]	y[7,12]	Y	...
3741	G075.6014+01.6394	20:15:48.15	+38:01:31.2	11.2	8800	-77.50	n	n	n	...
3742	G073.6525+00.1944	20:16:21.96	+35:36:06.2	11.2	100000	-73.40	y[4,11]	n	n	...
3746	G072.5056-01.1708	20:18:44.19	+33:53:08.8	7.2	6100	-26.00	n	Y	n	...
3748[H]	G078.4373+02.6584B	20:19:38.49	+40:56:33.7	1.4	12100	0.90	n	n	n	...
3749	G078.8699+02.7602	20:20:30.60	+41:21:26.6	1.4	6500	7.90	y[4,11]	y[12]	Y	...
3752	G073.6952-00.9996	20:21:18.88	+34:57:50.9	7.4	17000	-31.30	n	n	n	...
3757	G077.8999+01.7678	20:21:55.01	+39:59:45.5	1.4	741	-2.50	n	n	n	...
3760	G079.1272+02.2782	20:23:23.83	+41:17:39.3	1.4	1600	-2.00	n	n	n	...
3761	G076.0902+00.1412	20:23:27.29	+37:34:53.9	1.4	1400	-0.10	y[4]	n	n	...
3764	G080.0251+02.6933	20:24:20.00	+42:16:01.8	1.4	751	5.20	n	n	n	...
3765[Y]	G079.8855+02.5517B	20:24:31.68	+42:04:22.4	1.4	2440	5.90	n	n	n	...
3766	G080.1710+02.7450	20:24:33.42	+42:24:58.2	1.4	1300	5.60	Y[6,11]	Y	n	...
3767	G078.7641+01.6862	20:24:51.66	+40:39:25.2	10.5	13000	-76.30	y[11]	n	n	...
3774	G078.3762+01.0191	20:26:32.33	+39:57:20.7	1.4	461	-0.90	n	n	n	...
3775	G078.4754+01.0421	20:26:44.44	+40:02:57.8	1.4	4300	-3.70	Y[11]	n	n	...
3796	G078.8867+00.7087	20:29:24.86	+40:11:19.4	3.3	200000	-6.00	y[1,4,6,11]	Y	Y	...
3808	G079.3398+00.3417	20:32:22.08	+40:20:17.1	1.4	1700	0.20	n	n	n	...

Table 2.1 (cont'd)

RMS[a] ID	MSX name	R.A. (J2000.0)	Decl. (J2000.0)	Distance (kpc)	$L_{\rm bol}$ ($L_\odot$)	$V_{\rm sys}$[b] (km s^{-1})	Detection[c] 22 GHz	44 GHz	95 GHz	MMB Coverage
3816	G083.7071+03.2817	20:33:36.51	+45:35:44.0	1.4	3900	-3.60	y[11]	n	n	...
3830[H]	G080.8282+00.5670A	20:36:07.53	+41:40:09.0	1.4	3979	11.50	n	n	n	...
3832	G080.8624+00.3827	20:37:00.93	+41:34:55.8	1.4	2000	-1.90	y[11]	Y	Y	...
3838	G081.8652+00.7800	20:38:35.36	+42:37:13.7	1.4	3600	9.40	y[1,4,6,11]	y[7,12]	y[2]	...
3841	G081.7131+00.5792	20:38:57.19	+42:22:40.9	1.4	4900	-3.60	y[1,4,11]	y[12]	y[2]	...
3846	G081.7624+00.5916	20:39:03.72	+42:25:29.6	1.4	2600	-4.40	y[1,4,11]	y[7,12]	Y	...
3856	G084.3065+01.8933	20:41:58.51	+45:14:00.4	10.5	8200	-86.50	n	n	n	...
3859[H]	G082.5682+00.4040A	20:42:33.76	+42:56:51.3	1.4	7600	-4.10	n	n	n	...
3865	G082.5828+00.2014	20:43:28.49	+42:50:01.8	1.4	654	11.00	y[11]	Y	Y	...
3866	G084.1940+01.4388	20:43:36.70	+44:51:54.2	1.4	2100	-1.80	y[11]	n	n	...
3878[H]	G085.4102+00.0032A	20:54:14.36	+44:54:04.5	5.5	42000	-35.80	y[11]	n	n	...
3880	G084.9505-00.6910	20:55:32.47	+44:06:10.1	5.5	13000	-34.90	y[11]	n	n	...
3887	G090.2095+02.0405	21:03:41.76	+49:51:47.1	7.4	7600	-65.10	n	n	n	...
3892	G089.6368+00.1732	21:09:45.75	+48:10:58.1	6.5	26000	-54.60	n	n	n	...
3894	G095.0531+03.9724	21:15:55.63	+54:43:31.0	8.7	12000	-84.10	y[4,6,11]	Y	Y	...
3895	G093.1610+01.8687	21:17:14.17	+51:54:23.0	6.8	8800	-63.10	n	n	n	...
3906	G094.3228-00.1671	21:31:45.11	+51:15:35.3	4.4	5700	-38.40	n	n	n	...
3910[Y]	G097.5268+03.1837B	21:32:11.29	+55:53:39.9	7.0	84000	-70.00	y[1,4,11]	Y	Y	...
3911	G094.2615-00.4116	21:32:30.59	+51:02:16.0	5.2	9000	-46.60	y[4,6,11]	y[7,12]	n	...
3914	G094.4637-00.8043	21:35:09.11	+50:53:09.6	5.0	21000	-44.60	y[4,6,11]	n	n	...
3915[H]	G096.4353+01.3233A	21:35:21.23	+53:47:12.0	7.0	18700	-68.90	n	n	n	...
3916	G096.5438+01.3592	21:35:43.82	+53:53:09.3	7.0	18000	-69.40	n	n	n	...
3917	G094.6028-01.7966	21:39:58.25	+50:14:20.9	4.9	43000	-43.90	y[4,6,11]	n	n	...
3919[Y]	G095.0026-01.5779A	21:40:57.34	+50:39:58.5	4.5	4546	-40.00	n	n	n	...
3922	G097.9978+01.4688	21:42:43.19	+54:55:51.9	6.5	5000	-65.80	n	n	n	...
3927	G100.1685+02.0266	21:52:02.77	+56:44:59.7	6.0	8400	-62.40	n	n	n	...

Table 2.1 (cont'd)

RMS[a] ID	MSX name	R.A. (J2000.0)	Decl. (J2000.0)	Distance (kpc)	$L_{\rm bol}$ ($L_\odot$)	$V_{\rm sys}$[b] (km s^{-1})	Detection[c] 22 GHz	44 GHz	95 GHz	MMB Coverage
3928	G100.2124+01.8829	21:52:57.15	+56:39:54.2	5.9	8300	-61.90	n	n	n	...
3933	G101.2490+02.5764	21:55:45.55	+57:51:05.6	6.1	4300	-65.00	n	n	n	...
3935	G102.3533+03.6360	21:57:25.19	+59:21:56.6	8.4	110000	-88.60	y[4,11]	n	n	...
3936	G102.3340+03.6094	21:57:26.08	+59:19:54.1	8.3	6600	-87.50	y[11]	n	n	...
3939	G103.8744+01.8558	22:15:09.08	+58:49:07.8	1.6	6800	-18.30	n	n	n	...
3940	G100.3779-03.5784	22:16:10.35	+52:21:34.7	3.7	17000	-37.60	y[4,11]	n	n	...
3941[Y]	G102.8051-00.7184B	22:19:09.11	+56:05:00.3	4.0	5900	-43.50	n	n	n	...
3945	G103.8034+00.4062	22:20:46.17	+57:34:17.2	5.7	4200	-63.40	y[11]	n	n	...
3949	G105.5072+00.2294	22:32:23.85	+58:18:59.8	4.6	7000	-52.30	n	n	n	...
3958[Y]	G108.5955+00.4935C	22:52:38.09	+60:01:01.1	4.3	9700	-51.20	y[1,4,6,11]	y[12]	Y	...
3960[H]	G107.6823-02.2423A	22:55:29.82	+57:09:24.9	4.7	8200	-55.10	n	n	n	...
3963	G109.8715+02.1156	22:56:17.98	+62:01:49.7	0.7	15000	-11.10	y[1,4,6,11]	Y	Y	...
3968	G108.7575-00.9863	22:58:47.25	+58:45:01.6	4.3	14000	-51.50	y[4,11]	n	n	...
3970	G109.0775-00.3524	22:58:59.08	+59:27:36.4	4.0	2400	-48.10	y[11]	n	n	...
3972	G108.4714-02.8176	23:02:32.07	+56:57:51.3	4.5	5100	-53.80	y[1,4,11]	n	n	...
3976	G110.0931-00.0641	23:05:25.16	+60:08:15.4	4.3	17000	-53.10	y[6,11]	y[12]	Y	...
3980[Y]	G111.5234+00.8004A	23:13:32.39	+61:29:06.2	2.6	6700	-58.60	y[11]	n	n	...
3982	G111.5320+00.7593	23:13:43.91	+61:26:57.7	2.6	4600	-56.10	y[1,4,6,11]	y	y[2]	...
3985	G111.5851+00.7976	23:14:01.71	+61:30:17.8	2.6	1800	-56.60	Y[11]	n	n	...
3986	G111.5671+00.7517	23:14:01.75	+61:27:19.8	2.6	23000	-57.20	y[11]	Y	Y	...
3991	G111.8904+00.9894	23:15:50.03	+61:47:39.7	2.6	6600	-48.50	Y[11]	n	n	...
3992[H]	G111.2824-00.6639A	23:16:04.00	+60:02:00.6	3.5	48000	-44.10	y[4,6,11]	n	n	...
3996	G111.2552-00.7702	23:16:10.39	+59:55:28.2	3.5	11000	-44.70	y[1,4,6,11]	Y	Y	...
3998	G111.2348-01.2385	23:17:21.01	+59:28:48.0	4.4	42000	-54.40	y[4,6,11]	y[12]	Y	...
3999	G110.8038-02.5649	23:17:52.26	+58:05:11.0	2.7	654	-34.60	n	n	n	...
4004	G114.0835+02.8568	23:28:27.76	+64:17:38.4	4.2	7100	-53.20	n	n	n	...

Table 2.1 (cont'd)

RMS[a] ID	MSX name	R.A. (J2000.0)	Decl. (J2000.0)	Distance (kpc)	$L_{\rm bol}$ ($L_\odot$)	$V_{\rm sys}$[b] (km s^{-1})	Detection[c] 22 GHz	44 GHz	95 GHz	MMB Coverage
4365	G032.8205-00.3300	18:52:24.60	-00:14:57.7	4.7	10000	79.30	y[11]	Y	Y	y
4741[Y]	G136.8283+01.0635B	02:49:04.04	+60:43:17.0	2.5	562	-34.30	n	n	n	...
4745	G173.4815+02.4459	05:39:13.02	+35:45:51.3	2.0	7600	-16.20	y[1,4,6,11]	y[7,12]	y[2]	...
4747	G183.3485-00.5751	05:51:11.15	+25:46:16.4	2.0	3800	-9.40	y[6]	y[12]	Y	...
4748	G197.1387-03.0996	06:10:49.94	+12:32:45.2	3.4	1000	21.00	n	n	n	...
4751	G238.9590-01.6835	07:35:15.23	-23:48:45.9	7.2	1200	82.30	n	n	n	y
4888	G019.8817-00.5347	18:29:14.68	-11:50:23.6	3.3	4700	43.50	y[11,14]	Y	y[10]	y
4905	G030.8786+00.0566	18:47:28.85	-01:48:07.1	4.9	2200	75.10	n	n	n	y
4910	G030.9726-00.1410	18:48:22.03	-01:48:30.3	4.9	2700	77.50	y[11]	Y	n	y
4924[H]	G039.3880-00.1421B	19:03:45.15	+05:40:44.4	4.3	14400	66.30	n	Y	y[10]	y
4941	G059.8329+00.6729	19:40:59.32	+24:04:44.1	2.2	570	34.40	y[4,11]	y[12]	Y	y
4952[†]	G093.0166+02.4953	21:13:39.09	+52:14:05.1	...	...	...	n	n	n	...
4954	G100.0141+02.3591	21:49:38.26	+56:54:36.5	5.9	1300	-61.70	n	n	n	...

[a]For presence of multiple RMSs in a 20 $''$, the superscript Y H D and E indicate the type of neaby sources as YSO, HII region, Diffuse HII region and Evolved souces, repectively. Dagger symbol represents the single source finally classified with HII region, of which it's tpye was YSO at the observation time.

[b]The systemic velocity from the RMS archives.

[c]Y: New detection, y: detection, n: non-detection

[d]Adopted distance from nearby known YSO, VV Mon(Testi et al., 1998).

References. — 1. Han et al. (1995), 2. Val'tts et al. (1995), 3. Han et al. (1998), 4. Valdettaro et al. (2001), 5. Kurtz et al. (2004), 6. Sunada et al. (2007), 7. Val'tts et al. (2007), 8. Urquhart et al. (2009), 9. Breen et al. (2011), 10. Chen et al. (2011), 11. Urquhart et al. (2011), 12. Bayandina et al. (2012), 13. Chen et al. (2012), 14 **?**)

Table 2.2. Summary of Observations

Telescope	Maser Transition	Frequency (GHz)	FWHM ($''$)	η_A	Velocity Resolution (km s^{-1})	Velocity Coverage (km s^{-1})	T_{sys} (K)	f[a] (Jy K^{-1})
KVN 21m	H_2O 6_{16}–5_{23}	22.235080	120	0.6	0.105	431	60–200	13.3
	CH_3OH 7_0–6_1 A^+	44.069430	62	0.6	0.053	218	120–350	13.3
	CH_3OH 8_0–7_1 A^+	95.169463	32	0.5	0.025	101	160–470	16.0
	HCO^+ J=1–0	89.188523	32	0.4[b]	0.026	108	170–200	
TRAO 14m	^{13}CO J=1–0	110.201353	48	0.5[b]	0.703	300	600–700	

[a]The conversion factor from T_A^* to flux density.

[b]The main-beam efficiency.

Table 2.3. Summary of Detections

Maser	Epoch	Number	Detection Rate (%)
22 GHz	2011	126	42
	2012	112	37
	Subtotal	135	45
44 GHz	2011	76	25
	2012	81	27
	Subtotal	83	28
95 GHz	2012	68	23
Any	Both	151	51

Table 2.4. Detected Maser Line Parameters

RMS ID	Maser	Epoch (yyyymmdd)	Station[a]	$V_{\rm p}$ (km s^{-1})	$S_{\rm p}$ (Jy)	$\int S_\nu dv$ (Jy km s^{-1})	$V_{\rm min}$ (km s^{-1})	$V_{\rm max}$ (km s^{-1})	$V_{\rm range}$ (km s^{-1})	$L_{\rm maser}$ ($L_\odot$)	Notes[b]
4	22	20110326	YS	-43.00	6.4	4.7	-43.42	-42.58	0.84	8.55E-07	
7	22	20110324	YS	-83.03	3.6	1.7	-83.24	-82.82	0.42	1.26E-06	
		20120212	YS	-81.56	5.1	3.0	-81.56	-81.13	0.42	2.18E-06	
18	22	20110411	US	-52.96	4.1	2.9	-53.17	-52.54	0.63	1.12E-06	
35	22	20110322	YS	-39.04	1221.6	4519.8	-56.10	-24.71	31.39	4.19E-04	
		20120521	YS	-42.62	841.7	4096.1	-62.21	-25.56	36.66	3.80E-04	
	44	20110322	YS	-42.55	1.2	1.0	-42.55	-42.55	0.21	1.92E-07	
		20120521	YS	-42.55	2.2	5.2	-43.62	-40.64	2.98	9.50E-07	
	95	20120521	YS	-43.24	3.0	6.0	-43.63	-41.27	2.36	2.39E-06	
37	22	20110322	YS	-39.02	3432.2	12782.0	-56.29	-24.48	31.81	1.19E-03	
		20120212	YS	-42.39	4552.1	14832.7	-54.82	-25.11	29.70	1.38E-03	
46	22	20110327	YS	-65.93	13.5	7.6	-66.35	-65.51	0.84	7.02E-07	
		20121012	TN	-42.34	4.3	2.8	-42.55	-41.91	0.63	2.63E-07	
49	22	20110322	YS	-72.45	17.4	47.9	-80.66	-63.60	17.06	4.00E-05	
		20120214	YS	-69.08	24.2	70.1	-78.14	-64.02	14.11	5.85E-05	
53	22	20110323	YS	-45.88	6.8	3.8	-46.30	-45.67	0.63	8.99E-07	
		20120521	YS	-41.03	3.2	4.6	-46.30	-40.61	5.69	1.08E-06	
58	22	20110323	YS	-35.39	2.3	3.6	-35.39	-25.70	9.69	8.55E-07	
		20120214	YS	-22.75	9.7	7.1	-23.17	-22.12	1.05	1.68E-06	
61	22	20110322	YS	-31.84	2.5	1.5	-31.84	-31.42	0.42	1.99E-07	
63	22	20110411	US	-6.42	4.3	2.4	-6.63	-6.00	0.63	3.61E-08	
		20120216	YS	-7.26	11.4	7.7	-7.47	-6.84	0.63	1.14E-07	
84	22	20110327	YS	-15.96	6.6	6.0	-17.02	-12.80	4.21	5.00E-07	
		20120521	YS	-20.81	12.4	18.0	-21.23	-14.07	7.16	1.51E-06	
88	22	20110325	YS	-29.82	233.8	211.7	-30.87	-28.77	2.11	1.96E-05	
		20120301	YS	-30.03	216.0	194.4	-30.87	-26.03	4.85	1.80E-05	

Table 2.4 (cont'd)

RMS ID	Maser	Epoch (yyyymmdd)	Station[a]	$V_{\rm p}$ (km s^{-1})	$S_{\rm p}$ (Jy)	$\int S_\nu dv$ (Jy km s^{-1})	$V_{\rm min}$ (km s^{-1})	$V_{\rm max}$ (km s^{-1})	$V_{\rm range}$ (km s^{-1})	$L_{\rm maser}$ ($L_\odot$)	Notes[b]
91	22	20110331	YS	-5.50	135.8	297.1	-10.14	5.66	15.80	2.76E-05	
		20120310	YS	-0.87	234.5	335.3	-13.30	5.66	18.96	3.11E-05	
	44	20110331	YS	-3.34	6.2	8.2	-3.98	-1.64	2.34	1.51E-06	
		20120310	YS	-3.13	7.0	2.4	-3.34	-3.13	0.21	4.35E-07	
	95	20120310	YS	-3.33	5.8	5.5	-3.92	-2.74	1.18	2.16E-06	
106	22	20120320	YS	-19.57	1.8	0.4	-19.57	-19.57	0.21	3.57E-08	
113	22	20110412	US	-3.83	3.4	1.8	-4.04	-3.41	0.63	1.66E-07	
121	22	20110401	YS	7.21	53.3	84.6	-3.75	12.05	15.80	6.36E-06	
		20130430	YS	-3.11	24.8	45.5	-3.75	7.84	11.59	3.42E-06	
	44	20110401	YS	3.05	7.0	11.7	1.56	4.11	2.55	1.75E-06	
		20130430	YS	3.05	6.4	14.5	1.13	4.75	3.61	2.16E-06	
	95	20130430	YS	3.08	6.4	13.4	1.50	4.45	2.95	4.32E-06	
	6.7		MMB			444.0				1.00E-05	
125	22	20110402	YS	18.42	4.4	3.3	18.00	18.63	0.63	3.08E-07	
131	22	20110322	YS	6.03	394.3	671.7	-9.56	11.72	21.28	6.23E-05	
		20120215	YS	3.29	251.0	577.6	-0.29	15.30	15.59	5.36E-05	
	44	20110322	YS	7.35	5.9	7.1	6.50	7.98	1.49	1.30E-06	
		20120215	YS	7.35	6.7	5.6	6.92	8.41	1.49	1.03E-06	
	95	20120215	YS	7.18	4.4	11.6	5.21	9.54	4.33	4.61E-06	
	6.7		MMB			64.0				1.78E-06	
133	22	20110402	YS	17.90	5.7	2.4	17.69	18.11	0.42	2.23E-07	
	44	20110402	YS	16.48	3.4	2.3	16.48	17.33	0.85	4.28E-07	
		20130421	US	16.48	2.4	1.4	14.57	16.70	2.13	2.59E-07	
	95	20130421	US	16.47	5.9	7.5	13.32	17.65	4.33	2.97E-06	
135	22	20110324	YS	19.58	363.6	204.0	18.11	20.42	2.32	1.33E-04	
		20120215	YS	19.58	301.1	170.1	18.32	20.21	1.90	1.11E-04	

Table 2.4 (cont'd)

RMS ID	Maser	Epoch (yyyymmdd)	Station[a]	$V_{\rm p}$ (km s^{-1})	$S_{\rm p}$ (Jy)	$\int S_\nu dv$ (Jy km s^{-1})	$V_{\rm min}$ (km s^{-1})	$V_{\rm max}$ (km s^{-1})	$V_{\rm range}$ (km s^{-1})	$L_{\rm maser}$ ($L_\odot$)	Notes[b]
	6.7		MMB			16.0				3.12E-06	
145	22	20110402	YS	125.07	7.5	19.9	122.34	127.18	4.85	1.15E-05	D
		20121011	TN	125.71	8.6	30.0	121.70	127.81	6.11	1.74E-05	D
149	22	20110329	YS	-8.29	2.4	1.1	-8.29	-8.08	0.21	9.31E-09	
		20120310	YS	7.72	6.7	2.4	7.51	7.93	0.42	2.01E-08	
	44	20110329	YS	7.35	136.4	91.7	6.07	9.47	3.40	1.52E-06	
		20120310	YS	7.35	100.2	59.2	7.13	7.98	0.85	9.78E-07	
	95	20120310	YS	7.18	43.4	32.7	5.80	8.56	2.76	1.17E-06	
153	22	20110325	YS	45.53	10.0	14.1	44.26	47.42	3.16	7.22E-06	H
		20120215	YS	46.58	7.9	13.0	40.05	76.71	36.66	6.65E-06	
	44	20110325	YS	44.73	23.4	15.7	44.31	45.37	1.06	1.59E-05	
		20120215	YS	44.73	18.2	11.9	44.52	45.16	0.64	1.21E-05	
	95	20120215	YS	44.58	12.0	7.1	44.38	45.17	0.79	1.56E-05	
175	22	20110327	YS	27.82	7.2	14.7	24.87	30.56	5.69	1.65E-06	
		20120303	YS	26.13	15.5	29.0	24.87	34.56	9.69	3.25E-06	
189	22	20110325	YS	46.79	35.6	42.0	45.94	59.21	13.27	1.64E-05	
		20120215	YS	46.79	19.9	31.9	42.78	57.53	14.75	1.24E-05	
196	6.7		MMB			87.0				1.75E-06	
203	22	20110327	YS	42.07	25.9	58.4	37.44	60.40	22.96	2.17E-05	
		20121009	TN	41.65	80.0	116.5	39.54	59.98	20.44	4.32E-05	
2360	22	20110410	US	11.45	25.7	24.4	4.29	12.08	7.79	4.76E-06	
		20120606	YS	14.19	2.8	1.4	13.77	14.19	0.42	2.76E-07	
2389	22	20110321	YS	17.19	10.7	30.0	13.40	25.40	12.01	5.08E-06	
		20120621	YS	23.51	10.5	30.4	13.19	24.14	10.95	5.14E-06	
2434	22	20110321	YS	29.27	42.0	54.7	28.01	32.85	4.85	7.31E-06	
		20120605	YS	29.27	121.4	174.7	28.22	32.64	4.42	2.33E-05	

Table 2.4 (cont'd)

RMS ID	Maser	Epoch (yyyymmdd)	Station[a]	$V_{\rm p}$ (km s^{-1})	$S_{\rm p}$ (Jy)	$\int S_\nu dv$ (Jy km s^{-1})	$V_{\rm min}$ (km s^{-1})	$V_{\rm max}$ (km s^{-1})	$V_{\rm range}$ (km s^{-1})	$L_{\rm maser}$ ($L_\odot$)	Notes[b]
	44	20110321	YS	31.41	19.4	23.1	31.20	34.60	3.40	6.10E-06	
		20120605	YS	31.41	20.5	25.9	30.77	34.38	3.61	6.85E-06	
	95	20120605	YS	31.41	21.9	30.8	31.22	34.17	2.95	1.76E-05	
2437	6.7		MMB			114.0				9.76E-05	
2445	44	20110321	YS	52.65	3.2	5.2	49.03	52.86	3.83	3.42E-05	
		20130426	US	52.65	4.3	6.5	48.82	52.86	4.04	4.29E-05	
	95	20130426	US	49.40	4.0	7.5	48.81	52.94	4.13	1.07E-04	
	6.7		MMB			17.0				1.70E-05	
2490	22	20110322	YS	34.43	11.4	33.2	-8.34	60.13	68.47	4.43E-06	H
		20120618	YS	-7.91	15.8	40.1	-8.55	36.96	45.50	5.36E-06	H
	44	20110322	YS	36.60	10.8	27.0	35.75	40.00	4.25	7.15E-06	
		20120618	YS	36.38	9.6	23.4	35.75	39.79	4.04	6.19E-06	
	95	20120618	YS	36.37	9.3	18.6	35.38	39.52	4.13	1.06E-05	
2491	44	20110410	US	54.05	5.1	2.3	53.83	54.26	0.43	2.14E-06	
		20120621	YS	53.83	2.5	2.4	53.41	54.26	0.85	2.19E-06	
2529	22	20110322	YS	26.19	24.9	53.9	7.65	33.56	25.91	8.45E-06	
		20120605	YS	26.19	25.0	45.1	21.13	33.56	12.43	7.07E-06	
	44	20110322	YS	24.98	28.8	51.9	20.95	27.54	6.59	1.61E-05	
		20120605	YS	24.98	27.9	47.1	22.86	27.54	4.68	1.46E-05	
	95	20120605	YS	25.16	24.7	46.6	22.60	26.15	3.54	3.13E-05	
2535	22	20110411	US	27.99	20.3	45.0	-7.83	30.52	38.34	8.78E-06	H
		20130419	YS	28.20	17.2	32.7	-7.83	30.31	38.13	6.38E-06	H
	44	20130419	YS	30.36	3.5	1.4	30.15	30.36	0.21	5.42E-07	
	6.7		MMB			8.0				4.68E-07	
2536	22	20110322	YS	42.00	7.7	48.5	36.31	54.85	18.54	1.89E-05	
		20120605	YS	49.16	25.2	61.1	37.57	50.00	12.43	2.38E-05	

Table 2.4 (cont'd)

RMS ID	Maser	Epoch (yyyymmdd)	Station[a]	$V_{\rm p}$ (km s^{-1})	$S_{\rm p}$ (Jy)	$\int S_\nu dv$ (Jy km s^{-1})	$V_{\rm min}$ (km s^{-1})	$V_{\rm max}$ (km s^{-1})	$V_{\rm range}$ (km s^{-1})	$L_{\rm maser}$ ($L_\odot$)	Notes[b]
	44	20110322	YS	48.37	50.5	67.0	45.82	49.65	3.83	5.17E-05	
		20120605	YS	48.58	52.4	67.2	46.25	49.65	3.40	5.19E-05	
	95	20120605	YS	48.37	40.5	51.6	46.20	48.76	2.56	8.60E-05	
2545	22	20110322	YS	12.26	16.8	64.0	7.20	46.39	39.18	1.16E-05	
		20120613	YS	31.85	5.8	3.0	31.64	32.06	0.42	5.49E-07	
	6.7		MMB			49.0				2.67E-06	
2547	22	20110411	US	-70.93	128.4	364.2	-75.56	-60.60	14.96	3.73E-05	D
		20120620	YS	-65.45	945.0	2113.3	-71.98	-61.02	10.95	2.16E-04	D
	44	20110411	US	19.50	4.6	1.9	19.28	19.50	0.21	3.79E-07	
		20120620	YS	19.50	2.8	3.8	19.07	21.62	2.55	7.66E-07	
	95	20120620	YS	19.98	2.3	1.6	19.78	21.56	1.77	7.14E-07	
2584	22	20110321	YS	-82.03	75.1	246.2	-87.93	-78.66	9.27	2.06E-05	D
		20120605	YS	-69.39	4.8	14.1	-82.66	-68.34	14.33	1.18E-06	D
	44	20110321	YS	13.26	118.3	104.0	11.98	14.75	2.76	1.72E-05	
		20120605	YS	13.26	146.3	126.4	11.98	14.32	2.34	2.10E-05	
	95	20120605	YS	13.15	111.8	84.4	11.97	13.74	1.77	3.02E-05	
2591	44	20110412	US	20.96	14.0	6.5	20.53	21.17	0.64	1.31E-06	
		20120618	YS	20.96	8.2	3.6	20.75	21.17	0.43	7.39E-07	
	95	20120618	YS	20.90	5.4	2.1	20.70	21.10	0.39	9.29E-07	
2611	22	20110322	YS	21.90	29.8	102.6	-0.43	35.17	35.60	9.52E-06	
		20120623	YS	21.06	20.7	38.5	19.58	22.53	2.95	3.57E-06	
	44	20110322	YS	19.00	8.4	9.1	17.30	19.21	1.91	1.68E-06	
		20120623	YS	19.00	5.2	6.4	16.66	19.21	2.55	1.17E-06	
	95	20120623	YS	19.09	3.2	4.5	17.91	19.09	1.18	1.79E-06	
2645	22	20120612	YS	27.25	6.4	3.8	27.04	27.47	0.42	5.09E-07	
2690	22	20110322	YS	23.03	10.2	35.3	16.50	30.19	13.69	3.96E-06	

Table 2.4 (cont'd)

RMS ID	Maser	Epoch (yyyymmdd)	Station[a]	$V_{\rm p}$ (km s^{-1})	$S_{\rm p}$ (Jy)	$\int S_\nu dv$ (Jy km s^{-1})	$V_{\rm min}$ (km s^{-1})	$V_{\rm max}$ (km s^{-1})	$V_{\rm range}$ (km s^{-1})	$L_{\rm maser}$ ($L_\odot$)	Notes[b]
		20120613	YS	23.45	29.0	43.0	16.50	26.40	9.90	4.83E-06	
	6.7		MMB			5.9				1.98E-07	
2698	22	20110412	US	26.59	4.3	5.9	21.74	26.80	5.06	6.59E-07	
2716	22	20110322	YS	26.68	3.3	14.8	26.26	78.09	51.82	4.16E-05	H
		20130427	US	42.48	5.6	13.5	40.80	82.51	41.71	3.79E-05	H
	44	20110322	YS	79.18	5.6	12.2	78.55	82.16	3.61	6.80E-05	
		20130427	US	79.40	7.0	16.9	77.48	82.16	4.68	9.42E-05	
	95	20130427	US	80.28	4.0	9.6	78.11	82.05	3.94	1.16E-04	
2760	44	20110412	US	64.90	2.8	2.6	64.90	65.96	1.06	2.46E-06	
2788	44	20110412	US	64.02	25.1	44.6	61.26	65.72	4.46	3.79E-05	
		20120607	YS	64.45	22.5	36.9	61.90	65.51	3.61	3.13E-05	
	95	20120607	YS	64.01	14.6	25.8	62.43	65.19	2.76	4.73E-05	
2799	22	20110323	YS	59.61	49.8	70.0	55.81	60.87	5.06	2.26E-04	
		20120605	YS	59.82	19.9	37.4	55.81	60.45	4.63	1.21E-04	
	44	20110323	YS	55.83	5.7	12.1	54.98	58.60	3.61	7.73E-05	
		20120605	YS	56.05	6.0	7.4	55.83	57.75	1.91	4.75E-05	
	95	20120605	YS	56.33	7.9	11.3	55.93	57.51	1.58	1.57E-04	
2810	22	20110411	US	22.84	72.4	119.2	-1.18	25.79	26.97	1.11E-05	
		20120605	YS	19.47	77.3	141.2	-10.02	33.58	43.61	1.31E-05	
	44	20110411	US	17.62	126.3	293.6	13.58	29.10	15.52	5.39E-05	
		20120605	YS	17.62	113.8	250.4	14.65	22.51	7.87	4.60E-05	
	95	20120605	YS	17.48	55.5	142.0	16.30	21.42	5.12	5.64E-05	
2821	22	20120613	YS	114.13	7.8	3.1	113.92	114.55	0.63	6.69E-06	
	6.7		MMB			18.3				1.20E-05	
2837	22	20110323	YS	87.32	15.6	21.4	75.31	88.17	12.85	1.19E-05	
		20120605	YS	87.32	25.9	40.2	8.53	89.01	80.48	2.24E-05	H

Table 2.4 (cont'd)

RMS ID	Maser	Epoch (yyyymmdd)	Station[a]	$V_{\rm p}$ (km s^{-1})	$S_{\rm p}$ (Jy)	$\int S_\nu dv$ (Jy km s^{-1})	$V_{\rm min}$ (km s^{-1})	$V_{\rm max}$ (km s^{-1})	$V_{\rm range}$ (km s^{-1})	$L_{\rm maser}$ ($L_\odot$)	Notes[b]
	44	20110323	YS	84.00	49.9	29.5	82.51	84.42	1.91	3.25E-05	
		20120605	YS	84.00	57.1	30.8	83.15	84.42	1.28	3.39E-05	
	95	20120605	YS	83.89	42.9	22.8	83.69	84.28	0.59	5.42E-05	
2844	44	20110323	YS	77.72	5.5	3.2	76.23	77.72	1.49	2.98E-06	
		20120621	YS	77.72	7.2	5.0	76.23	77.93	1.70	4.65E-06	
	95	20120621	YS	77.78	9.5	4.1	76.21	77.78	1.58	8.20E-06	
	6.7		MMB			66.9				9.42E-06	
2846	22	20120621	YS	68.19	7.9	9.0	66.93	68.61	1.69	4.25E-06	
	44	20110413	US	75.38	9.3	14.7	71.34	78.36	7.02	1.37E-05	
		20120621	YS	75.38	7.5	11.1	71.56	75.60	4.04	1.03E-05	
	95	20120621	YS	75.03	2.6	8.1	72.66	77.39	4.73	1.63E-05	
2853	22	20110324	YS	58.95	5.5	6.1	58.53	60.00	1.47	1.20E-06	
	6.7		MMB			2.6				1.52E-07	
2879	22	20110323	YS	41.91	2573.3	2314.1	-14.55	67.40	81.95	4.83E-04	H
		20140521	TN	41.07	272.5	435.7	-12.02	67.40	79.42	9.10E-05	H
	44	20110323	YS	41.73	58.7	56.6	40.46	45.35	4.89	2.34E-05	
		20140521	TN	41.73	59.6	58.7	40.46	45.77	5.31	2.43E-05	
	95	20140521	TN	41.71	50.2	79.8	38.75	45.77	7.28	7.12E-05	
	6.7		MMB			48.7				3.05E-06	
2881	22	20120612	YS	40.73	13.0	9.8	40.10	41.15	1.05	1.91E-06	
2901	6.7		MMB			37.8				2.69E-06	
2920	22	20110323	YS	102.92	2.6	4.2	102.71	105.66	2.95	5.74E-06	
	44	20110323	YS	109.50	1.4	2.2	109.50	110.35	0.85	6.10E-06	
2963	44	20110324	YS	47.87	10.3	10.3	47.66	49.15	1.49	6.57E-05	
		20120611	YS	47.87	7.8	7.1	47.66	48.94	1.28	4.53E-05	
	95	20120611	YS	48.46	3.8	5.8	47.48	49.64	2.17	7.97E-05	

Table 2.4 (cont'd)

RMS ID	Maser	Epoch (yyyymmdd)	Station[a]	$V_{\rm p}$ (km s^{-1})	$S_{\rm p}$ (Jy)	$\int S_\nu dv$ (Jy km s^{-1})	$V_{\rm min}$ (km s^{-1})	$V_{\rm max}$ (km s^{-1})	$V_{\rm range}$ (km s^{-1})	$L_{\rm maser}$ ($L_\odot$)	Notes[b]
2966	44	20110413	US	95.33	10.7	14.1	94.91	97.46	2.55	1.75E-05	
		20120616	YS	95.33	9.8	10.3	94.70	96.40	1.70	1.27E-05	
	95	20120616	YS	95.38	7.9	8.9	95.18	97.15	1.97	2.38E-05	
2967	6.7		MMB			4.5				2.82E-07	
2970	22	20110322	YS	-15.88	16.4	23.6	-17.14	-10.19	6.95	1.46E-04	
		20120613	YS	-15.88	14.2	16.8	-17.14	-13.35	3.79	1.03E-04	
2978	22	20110414	US	56.74	5.1	6.4	56.32	60.53	4.21	1.33E-06	
3028	22	20110324	YS	109.29	3.7	3.5	108.24	109.71	1.47	4.53E-06	
	6.7		MMB			3.5				1.37E-06	
3032	22	20110324	YS	17.31	473.9	1737.1	12.89	64.29	51.40	6.81E-03	H
		20120616	YS	19.21	386.0	1333.7	14.99	50.81	35.81	5.23E-03	
3044	6.7		MMB			0.5				1.01E-07	
3049	44	20110324	YS	81.52	6.8	9.1	80.46	83.01	2.55	8.85E-06	
		20120611	YS	81.52	5.5	4.9	81.31	82.37	1.06	4.75E-06	
	95	20120611	YS	82.12	3.4	3.4	81.33	82.12	0.79	7.17E-06	
3075	22	20110325	YS	105.19	161.5	502.9	84.75	108.14	23.38	6.39E-04	
		20120605	YS	105.19	125.2	399.9	88.75	106.87	18.12	5.08E-04	
	44	20110325	YS	103.36	15.2	13.8	102.72	104.85	2.13	3.47E-05	
		20120605	YS	103.36	17.5	17.1	102.08	104.64	2.55	4.30E-05	
	95	20120605	YS	103.25	24.7	20.6	102.85	103.84	0.98	1.12E-04	
3077	6.7		MMB			54.7				3.80E-05	
3094	22	20110325	YS	27.65	3.2	6.4	14.38	30.81	16.43	2.37E-05	
	6.7		MMB			0.3				3.31E-07	
3099	44	20110325	YS	100.86	4.0	6.8	98.31	102.13	3.83	7.53E-06	
		20120614	YS	100.86	4.1	1.7	100.86	101.07	0.21	1.91E-06	
3119	6.7		MMB			2.2				3.67E-07	

Table 2.4 (cont'd)

RMS ID	Maser	Epoch (yyyymmdd)	Station[a]	$V_{\rm p}$ (km s^{-1})	$S_{\rm p}$ (Jy)	$\int S_\nu dv$ (Jy km s^{-1})	$V_{\rm min}$ (km s^{-1})	$V_{\rm max}$ (km s^{-1})	$V_{\rm range}$ (km s^{-1})	$L_{\rm maser}$ ($L_\odot$)	Notes[b]
3126	6.7		MMB			30.4				5.07E-06	
3145	22	20110413	US	80.97	5.7	4.1	80.55	81.39	0.84	1.83E-06	
		20130421	YS	74.65	6.8	4.8	74.23	75.07	0.84	2.17E-06	
3146	22	20110325	YS	39.02	22.8	59.0	-58.31	41.76	100.07	1.87E-04	H
		20130427	US	-53.26	11.0	75.6	-65.90	58.40	124.30	2.40E-04	H
3158	22	20110419	US	58.26	9.0	33.4	52.99	60.15	7.16	1.86E-05	D
		20120623	YS	51.94	12.4	38.5	48.57	111.56	62.99	2.14E-05	H
	44	20110414	US	104.87	9.3	21.8	102.11	107.00	4.89	2.41E-05	
		20120623	YS	104.66	5.3	11.9	102.11	106.79	4.68	1.31E-05	
3186	44	20110414	US	82.35	3.0	4.4	80.86	82.77	1.91	4.89E-06	
		20120612	YS	82.77	2.7	3.1	81.50	82.77	1.28	3.47E-06	
3187	22	20110325	YS	113.90	24.2	20.1	101.26	114.54	13.27	1.12E-05	
		20130426	US	106.74	10.1	28.7	104.21	113.06	8.85	1.60E-05	
	44	20110325	YS	109.12	13.8	39.5	105.72	111.67	5.95	4.36E-05	
		20130426	US	109.33	11.9	38.4	105.72	113.80	8.08	4.23E-05	
	95	20130426	US	109.25	10.4	38.5	104.92	111.62	6.69	9.18E-05	
	6.7		MMB			158.6				2.65E-05	
3205	22	20110325	YS	97.33	6.7	15.9	94.38	102.59	8.22	8.88E-06	
		20120606	YS	92.90	7.3	10.8	92.69	94.59	1.90	6.02E-06	
	44	20110325	YS	95.26	16.9	30.3	92.71	98.02	5.31	3.34E-05	
		20120606	YS	95.26	12.0	22.3	93.77	98.02	4.25	2.45E-05	
	95	20120606	YS	94.81	6.7	10.8	94.02	95.99	1.97	2.57E-05	
	6.7		MMB			139.1				2.32E-05	
3221	44	20110325	YS	83.22	4.7	3.5	82.58	83.43	0.85	1.37E-05	
		20120623	YS	83.22	5.6	3.7	82.58	83.43	0.85	1.43E-05	
3236	22	20110326	YS	98.06	2.3	3.4	74.04	98.06	24.02	3.91E-06	

Table 2.4 (cont'd)

RMS ID	Maser	Epoch (yyyymmdd)	Station[a]	$V_{\rm p}$ (km s^{-1})	$S_{\rm p}$ (Jy)	$\int S_\nu dv$ (Jy km s^{-1})	$V_{\rm min}$ (km s^{-1})	$V_{\rm max}$ (km s^{-1})	$V_{\rm range}$ (km s^{-1})	$L_{\rm maser}$ ($L_\odot$)	Notes[b]
	44	20110326	YS	103.17	2.5	2.2	103.17	104.24	1.06	5.05E-06	
		20120606	YS	103.17	2.3	2.5	103.17	104.02	0.85	5.54E-06	
	6.7		MMB			35.4				1.21E-05	
3241	44	20110414	US	104.87	3.7	1.4	104.87	105.08	0.21	3.08E-06	
		20120623	YS	104.87	3.8	1.6	104.66	105.08	0.43	3.54E-06	
	95	20120623	YS	105.26	1.1	0.2	105.07	105.07	0.20	1.04E-06	
3266	6.7		MMB			0.8				1.18E-07	
3292	22	20110323	YS	-30.80	5.1	6.2	-31.86	-30.17	1.69	3.59E-05	
	6.7		MMB			0.4				6.94E-07	
3304	22	20110326	YS	11.32	49.5	169.5	-5.54	27.75	33.29	6.44E-04	
		20130421	YS	11.53	47.3	159.7	-14.18	27.33	41.50	6.07E-04	
	44	20130421	YS	12.44	3.0	1.0	12.22	12.44	0.21	7.76E-06	
	95	20130421	YS	12.16	2.6	4.0	9.99	12.94	2.95	6.57E-05	
3308	22	20110322	YS	23.30	75.9	58.6	22.67	23.72	1.05	6.58E-06	
		20120518	YS	20.77	13.2	8.0	20.35	20.98	0.63	8.95E-07	
	44	20110322	YS	34.93	27.2	58.0	31.75	36.85	5.10	1.29E-05	
		20120518	YS	34.93	23.2	50.0	30.26	36.00	5.74	1.11E-05	
	95	20120518	YS	34.98	18.6	50.4	29.47	37.34	7.88	2.42E-05	
3314	22	20110326	YS	84.37	128.1	138.9	83.74	89.43	5.69	1.45E-04	
		20130427	US	86.06	18.5	17.4	83.53	86.48	2.95	1.81E-05	
	44	20110326	YS	86.55	3.9	5.5	85.48	87.19	1.70	1.13E-05	
		20130427	US	86.33	3.6	4.8	85.06	86.97	1.91	9.91E-06	
	95	20130427	US	85.27	3.4	6.1	83.89	87.04	3.15	2.71E-05	
	6.7		MMB			8.4				2.62E-06	
3335	6.7		MMB			7.0				2.12E-06	
3360	22	20110326	YS	66.99	5.1	3.8	66.14	67.20	1.05	6.90E-07	

Table 2.4 (cont'd)

RMS ID	Maser	Epoch (yyyymmdd)	Station[a]	$V_{\rm p}$ (km s^{-1})	$S_{\rm p}$ (Jy)	$\int S_\nu dv$ (Jy km s^{-1})	$V_{\rm min}$ (km s^{-1})	$V_{\rm max}$ (km s^{-1})	$V_{\rm range}$ (km s^{-1})	$L_{\rm maser}$ ($L_\odot$)	Notes[b]
	44	20110326	YS	42.18	3.8	0.8	42.18	42.18	0.21	2.94E-07	
		20121010	TN	42.40	2.9	1.2	42.18	42.40	0.21	4.25E-07	
3373	22	20110412	US	73.36	35.2	84.8	59.24	76.10	16.85	8.06E-05	
		20120521	YS	73.78	48.8	98.3	70.83	86.84	16.01	9.34E-05	
3382	22	20110402	YS	17.86	5.3	19.6	10.27	25.02	14.75	5.41E-05	
		20120611	YS	23.12	3.9	2.4	23.12	23.54	0.42	6.60E-06	
3386	6.7		MMB			27.2				2.33E-05	
3427	22	20110402	YS	83.43	3.2	3.0	82.80	83.85	1.05	2.54E-06	
3429	22	20110415	US	41.07	265.2	477.2	35.17	49.29	14.11	1.21E-04	
		20120521	YS	41.07	200.6	370.1	33.28	49.71	16.43	9.35E-05	
3448	22	20110414	US	51.56	17.3	22.3	19.54	51.99	32.44	2.76E-05	H
		20120520	YS	51.35	12.5	11.7	50.51	52.20	1.69	1.45E-05	
3483	22	20110331	YS	-7.94	3.0	2.1	-8.36	-6.88	1.47	5.75E-06	
	44	20110331	YS	-4.33	2.9	2.0	-4.33	-3.69	0.64	1.07E-05	
		20130421	YS	-4.33	4.0	1.5	-4.97	-4.33	0.64	7.94E-06	
	95	20130421	YS	-4.47	2.7	1.6	-5.07	-4.47	0.59	1.86E-05	
3503	22	20110414	US	65.53	63.5	136.8	30.98	68.06	37.08	9.25E-05	H
		20120520	YS	66.38	57.1	106.4	64.27	68.69	4.42	7.19E-05	
	44	20110414	US	66.41	105.7	129.9	65.13	70.02	4.89	1.74E-04	
		20120520	YS	66.41	80.3	101.4	65.13	69.60	4.46	1.36E-04	
	95	20120520	YS	66.41	36.3	84.4	65.03	70.15	5.12	2.44E-04	
3546	22	20110416	US	58.69	9.7	23.7	40.78	68.17	27.39	1.60E-05	
		20120512	YS	58.06	18.4	20.7	55.32	59.53	4.21	1.40E-05	
	6.7		MMB			66.9				1.36E-05	
3555	22	20110416	US	50.90	1652.5	14673.1	-42.64	145.49	188.13	9.92E-03	H
		20120519	YS	57.01	3623.0	10923.7	-79.93	150.75	230.68	7.39E-03	H

Table 2.4 (cont'd)

RMS ID	Maser	Epoch (yyyymmdd)	Station[a]	$V_{\rm p}$ (km s^{-1})	$S_{\rm p}$ (Jy)	$\int S_\nu dv$ (Jy km s^{-1})	$V_{\rm min}$ (km s^{-1})	$V_{\rm max}$ (km s^{-1})	$V_{\rm range}$ (km s^{-1})	$L_{\rm maser}$ ($L_\odot$)	Notes[b]
	44	20110416	US	60.04	30.5	62.2	54.08	66.63	12.54	8.33E-05	
		20120519	YS	60.04	21.8	43.8	55.36	66.63	11.27	5.86E-05	
	95	20120519	YS	60.03	10.9	25.1	58.84	66.52	7.68	7.26E-05	
3580	6.7		MMB			2.9				5.66E-07	
3585	22	20110329	YS	-3.93	1.6	1.3	-5.20	-3.93	1.26	3.10E-06	
	6.7		MMB			3.9				2.71E-06	
3586	22	20110324	YS	-7.09	11.8	26.8	-8.78	4.28	13.06	5.97E-05	
	44	20110324	YS	6.67	4.6	9.2	2.21	6.89	4.68	4.06E-05	
		20121011	TN	6.67	4.5	6.7	2.42	6.89	4.46	2.97E-05	
	95	20121011	TN	6.74	2.0	3.7	4.77	7.13	2.36	3.53E-05	
3587	22	20110331	YS	-44.71	4.2	20.6	-52.51	19.54	72.05	4.14E-05	D
		20120502	YS	10.48	6.7	21.4	-47.24	10.48	57.72	4.29E-05	H
3588	22	20110415	US	39.65	3.4	6.5	29.54	44.07	14.54	1.36E-06	
		20130422	YS	42.18	2.6	1.4	41.97	42.18	0.21	2.97E-07	
	44	20110415	US	39.28	7.7	7.3	38.01	40.13	2.13	3.00E-06	
		20130422	YS	39.28	5.7	5.1	38.43	39.71	1.28	2.11E-06	
	95	20130422	YS	39.27	1.9	0.6	39.07	39.27	0.20	4.95E-07	
	6.7		MMB			52.4				3.28E-06	
3597	6.7		MMB			4.5				8.14E-07	
3603	22	20110416	US	0.26	1.8	0.8	0.26	0.26	0.21	1.63E-06	
		20121011	TN	3.21	6.9	4.3	2.79	3.63	0.84	8.98E-06	
	44	20110416	US	5.58	6.1	12.8	3.03	6.65	3.61	5.29E-05	
		20121011	TN	6.22	4.5	10.5	3.03	6.86	3.83	4.37E-05	
	95	20121011	TN	5.37	3.1	6.9	3.60	6.94	3.35	6.15E-05	
3608	22	20120513	YS	23.79	3.3	0.7	23.58	23.58	0.21	5.89E-08	
	44	20110415	US	21.95	19.9	21.4	18.12	22.37	4.25	3.55E-06	

Table 2.4 (cont'd)

RMS ID	Maser	Epoch (yyyymmdd)	Station[a]	$V_{\rm p}$ (km s^{-1})	$S_{\rm p}$ (Jy)	$\int S_\nu dv$ (Jy km s^{-1})	$V_{\rm min}$ (km s^{-1})	$V_{\rm max}$ (km s^{-1})	$V_{\rm range}$ (km s^{-1})	$L_{\rm maser}$ ($L_\odot$)	Notes[b]
		20120513	YS	21.95	16.6	16.7	19.40	26.84	7.44	2.77E-06	
	95	20120513	YS	21.98	13.4	14.3	20.60	22.96	2.36	5.13E-06	
	6.7		MMB			0.6				1.51E-08	
3611	6.7		MMB			3.6				1.56E-06	
3641	22	20110413	US	40.72	418.5	539.2	38.19	41.77	3.58	4.35E-04	H
		20120509	YS	40.30	10.3	14.8	-95.37	72.95	168.33	1.20E-05	H
3659	22	20110416	US	26.72	93.7	260.1	15.97	33.04	17.06	2.92E-05	
		20121011	TN	10.08	39.3	145.0	6.92	32.62	25.70	1.63E-05	
	44	20110416	US	22.56	20.3	18.7	20.86	23.62	2.76	4.17E-06	
		20121011	TN	22.56	19.7	16.3	21.71	24.05	2.34	3.63E-06	
	95	20121011	TN	22.57	14.5	15.6	20.60	23.75	3.15	7.47E-06	
	6.7		MMB			27.0				9.08E-07	
3663	22	20110412	US	28.03	25.9	40.6	24.45	38.56	14.11	4.56E-06	
		20120623	YS	25.92	13.1	24.3	24.02	41.93	17.91	2.73E-06	
	44	20110412	US	27.23	3.1	4.4	26.38	28.72	2.34	9.86E-07	
		20120623	YS	27.23	6.6	9.3	26.17	28.72	2.55	2.07E-06	
	95	20120623	YS	26.69	1.8	1.4	25.90	26.69	0.79	6.64E-07	
3683	22	20110411	US	1.94	1.7	3.2	1.94	2.78	0.84	1.66E-06	
	44	20110411	US	21.19	11.4	19.0	19.27	21.40	2.13	1.93E-05	
		20120317	YS	21.19	4.0	5.4	18.85	21.19	2.34	5.43E-06	
	95	20120317	YS	21.04	6.7	8.7	19.27	21.43	2.17	1.90E-05	
3724	22	20121011	TN	19.13	19.4	17.8	18.29	23.56	5.27	8.07E-07	
	44	20110414	US	0.12	12.7	9.3	-0.73	0.76	1.49	8.34E-07	
		20121011	TN	0.22	11.3	6.8	-0.20	0.65	0.85	6.10E-07	
	95	20121011	TN	0.08	8.0	6.8	-0.51	0.87	1.38	1.31E-06	
3735	22	20110413	US	14.28	4.8	3.9	14.07	15.96	1.90	1.76E-07	

Table 2.4 (cont'd)

RMS ID	Maser	Epoch (yyyymmdd)	Station[a]	$V_{\rm p}$ (km s^{-1})	$S_{\rm p}$ (Jy)	$\int S_\nu dv$ (Jy km s^{-1})	$V_{\rm min}$ (km s^{-1})	$V_{\rm max}$ (km s^{-1})	$V_{\rm range}$ (km s^{-1})	$L_{\rm maser}$ ($L_\odot$)	Notes[b]
		20130422	YS	14.07	30.0	27.2	13.22	14.91	1.69	1.24E-06	
	44	20130422	YS	9.68	1.4	0.7	9.68	9.90	0.21	5.93E-08	
3739	22	20110412	US	-5.60	22.8	31.1	-17.19	-3.71	13.48	1.41E-06	
	44	20110412	US	-3.23	11.2	18.6	-4.50	-1.74	2.76	1.67E-06	
		20120311	YS	-3.23	10.7	3.3	-3.44	-3.23	0.21	2.96E-07	
	95	20120311	YS	-3.23	13.9	24.5	-4.81	-0.08	4.73	4.76E-06	
3742	22	20110330	YS	-76.24	52.5	96.5	-92.04	-70.98	21.07	2.81E-04	
		20120318	YS	-76.24	73.3	107.0	-93.10	-70.98	22.12	3.11E-04	
3746	44	20110413	US	-26.59	3.6	1.4	-26.80	-26.59	0.21	3.38E-06	
		20130422	YS	-26.59	3.0	1.1	-26.80	-26.59	0.21	2.73E-06	
3749	22	20110416	US	1.66	73.3	118.8	-2.55	17.04	19.59	5.40E-06	
		20121010	TN	15.57	265.7	328.3	1.66	17.25	15.59	1.49E-05	
	44	20110416	US	8.88	40.1	17.1	8.46	9.31	0.85	1.54E-06	
		20121010	TN	8.88	48.0	20.5	8.46	9.31	0.85	1.84E-06	
	95	20121010	TN	8.87	38.6	21.5	8.08	9.85	1.77	4.18E-06	
3761	22	20110414	US	6.79	1.7	0.7	6.79	6.79	0.21	3.31E-08	
		20120318	YS	0.62	9.8	9.1	0.19	3.35	3.16	4.12E-07	
3766	22	20110416	US	-25.68	5.0	6.6	-26.53	-24.84	1.69	3.01E-07	D
		20120317	YS	4.23	1.2	0.3	4.02	4.02	0.21	1.16E-08	
	44	20110416	US	4.91	2.5	2.0	4.91	5.55	0.64	1.76E-07	
		20121012	TN	5.55	1.9	0.7	5.12	5.55	0.43	6.64E-08	
3767	22	20120419	YS	-70.51	9.5	8.7	-73.88	-69.03	4.85	2.23E-05	
3775	22	20110416	US	8.71	6.1	6.3	8.08	9.35	1.26	2.85E-07	
		20120318	YS	10.40	14.9	8.7	9.98	10.82	0.84	3.94E-07	
3796	22	20110323	YS	-9.18	74.9	193.1	-29.19	-3.49	25.70	4.88E-05	
		20121012	TN	-23.92	115.2	444.7	-31.51	11.26	42.77	1.12E-04	

Table 2.4 (cont'd)

RMS ID	Maser	Epoch (yyyymmdd)	Station[a]	$V_{\rm p}$ (km s^{-1})	$S_{\rm p}$ (Jy)	$\int S_\nu dv$ (Jy km s^{-1})	$V_{\rm min}$ (km s^{-1})	$V_{\rm max}$ (km s^{-1})	$V_{\rm range}$ (km s^{-1})	$L_{\rm maser}$ ($L_\odot$)	Notes[b]
	44	20121012	TN	-5.97	3.5	0.7	-5.97	-5.97	0.21	3.70E-07	
	95	20121012	TN	-6.32	2.5	1.8	-6.71	-5.92	0.79	1.95E-06	
3816	22	20110413	US	-4.57	8.1	8.7	-7.10	-4.15	2.95	3.95E-07	
		20120317	YS	-4.36	27.7	24.6	-6.25	-3.94	2.32	1.12E-06	
3832	22	20110415	US	-3.39	15.3	10.4	-4.02	-3.18	0.84	4.72E-07	
		20130421	YS	-2.97	34.9	30.5	-3.60	6.51	10.11	1.39E-06	
	44	20110415	US	-2.08	4.5	2.5	-2.29	-1.87	0.43	2.24E-07	
		20130421	YS	-2.93	3.9	3.8	-2.93	-2.08	0.85	3.46E-07	
	95	20130421	YS	-2.22	4.0	4.5	-3.00	-0.64	2.36	8.81E-07	
3838	22	20110411	US	10.42	3540.6	5874.2	-11.07	20.11	31.18	2.67E-04	
		20121010	TN	15.05	463.0	1328.3	-11.70	22.00	33.71	6.04E-05	
	44	20110411	US	8.77	12.9	27.6	6.43	10.90	4.46	2.49E-06	
		20121010	TN	8.77	13.6	23.5	6.22	10.68	4.46	2.11E-06	
	95	20121010	TN	8.89	6.8	22.0	5.94	12.63	6.69	4.27E-06	
3841	22	20110415	US	-4.53	809.4	1635.8	-10.64	31.71	42.34	7.44E-05	H
		20121012	TN	0.72	128.9	390.2	-19.93	7.04	26.97	1.77E-05	
	44	20110415	US	-0.01	242.9	268.2	-5.75	0.84	6.59	2.41E-05	
		20121012	TN	-0.04	218.0	248.9	-9.18	1.45	10.63	2.24E-05	
	95	20121012	TN	0.31	52.7	59.9	-5.59	0.90	6.50	1.16E-05	
3846	22	20110416	US	10.45	18.6	66.3	4.97	11.51	6.53	3.01E-06	
		20120321	YS	3.50	7.0	12.5	0.76	3.92	3.16	5.66E-07	
	44	20110416	US	-3.18	30.1	43.5	-5.52	-2.33	3.19	3.92E-06	
		20120321	YS	-3.18	24.5	43.1	-5.94	1.50	7.44	3.88E-06	
	95	20120321	YS	-3.24	10.8	31.7	-7.18	6.21	13.39	6.17E-06	
3865	22	20110411	US	28.48	6.3	19.9	-12.60	29.11	41.71	9.03E-07	
		20121011	TN	28.69	8.5	15.0	27.64	34.59	6.95	6.82E-07	

Table 2.4 (cont'd)

RMS ID	Maser	Epoch (yyyymmdd)	Station[a]	$V_{\rm p}$ (km s^{-1})	$S_{\rm p}$ (Jy)	$\int S_\nu dv$ (Jy km s^{-1})	$V_{\rm min}$ (km s^{-1})	$V_{\rm max}$ (km s^{-1})	$V_{\rm range}$ (km s^{-1})	$L_{\rm maser}$ ($L_\odot$)	Notes[b]
	44	20110411	US	10.41	252.5	157.2	9.77	11.26	1.49	1.41E-05	
		20121011	TN	10.41	236.5	149.1	9.77	11.26	1.49	1.34E-05	
	95	20121011	TN	10.29	146.9	100.1	9.50	12.26	2.76	1.95E-05	
3866	22	20110412	US	3.25	63.6	111.3	0.30	6.20	5.90	5.06E-06	
		20120317	YS	0.09	43.0	55.4	-0.96	3.25	4.21	2.52E-06	
3878	22	20110326	YS	-33.45	87.6	129.9	-38.08	-18.07	20.01	9.12E-05	
		20120310	YS	-33.66	63.7	77.8	-38.29	-16.17	22.12	5.46E-05	
3880	22	20110322	YS	-41.33	3.7	1.4	-41.54	-41.11	0.42	9.67E-07	
3894	22	20110326	YS	-87.05	10.9	16.8	-88.53	-80.73	7.79	2.95E-05	
		20130418	TN	-85.60	6.6	3.5	-85.80	-85.21	0.59	6.06E-06	
	44	20110326	YS	-85.54	9.1	4.1	-85.75	-85.33	0.43	1.42E-05	
		20130418	TN	-85.54	6.7	3.7	-87.88	-84.48	3.40	1.30E-05	
	95	20130418	TN	-85.60	6.6	3.5	-85.80	-85.21	0.59	2.59E-05	
3910	22	20110330	YS	-77.56	411.8	867.7	-99.68	-60.70	38.97	9.86E-04	
		20120419	YS	-77.14	87.4	388.6	-107.89	-64.71	43.19	4.42E-04	H
	44	20120419	YS	-68.85	2.7	1.1	-69.07	-68.85	0.21	2.50E-06	
	95	20120419	YS	-68.95	1.1	1.9	-70.52	-68.16	2.36	9.42E-06	
3911	22	20110323	YS	-75.04	6.5	6.2	-76.09	-74.61	1.47	3.86E-06	D
		20120303	YS	-65.77	3.4	1.6	-65.98	-65.34	0.63	9.85E-07	
	44	20121011	TN	-47.60	1.1	0.5	-47.60	-47.60	0.21	5.97E-07	
3914	22	20110322	YS	-40.39	3.2	4.8	-45.45	-40.18	5.27	2.80E-06	
		20120301	YS	-47.77	2.9	1.1	-47.98	-47.77	0.21	6.22E-07	
3917	22	20110322	YS	-54.54	124.9	202.8	-56.22	-40.00	16.22	1.13E-04	
		20120216	YS	-53.70	17.4	22.4	-54.33	-40.63	13.69	1.25E-05	
3935	22	20110325	YS	-85.55	7.0	8.1	-87.23	-85.12	2.11	1.33E-05	
		20120420	YS	-86.39	19.0	15.8	-92.92	-85.55	7.37	2.59E-05	

Table 2.4 (cont'd)

RMS ID	Maser	Epoch (yyyymmdd)	Station[a]	$V_{\rm p}$ (km s^{-1})	$S_{\rm p}$ (Jy)	$\int S_\nu dv$ (Jy km s^{-1})	$V_{\rm min}$ (km s^{-1})	$V_{\rm max}$ (km s^{-1})	$V_{\rm range}$ (km s^{-1})	$L_{\rm maser}$ ($L_\odot$)	Notes[b]
3936	22	20110326	YS	-60.22	1.8	6.0	-70.75	-60.22	10.53	9.52E-06	H
		20130429	YS	-10.08	3.2	6.0	-65.70	-9.45	56.25	9.52E-06	D
3940	22	20110326	YS	-28.76	94.4	133.7	-44.98	-27.70	17.27	4.25E-05	
		20120215	YS	-35.08	26.7	37.8	-41.40	-34.45	6.95	1.20E-05	
3945	22	20110410	US	-56.02	4.5	11.4	-67.61	-54.76	12.85	8.59E-06	
		20130430	YS	-57.29	2.8	2.8	-69.71	-57.07	12.64	2.10E-06	
3958	22	20110410	US	-96.39	11.7	25.8	-109.45	-91.75	17.70	1.11E-05	D
	44	20110410	US	-51.89	4.4	9.1	-53.17	-48.49	4.68	7.76E-06	
		20130430	YS	-51.89	4.2	7.4	-52.74	-49.34	3.40	6.31E-06	
	95	20130430	YS	-51.82	3.6	6.0	-52.80	-50.04	2.76	1.10E-05	
3963	22	20110410	US	-9.52	730.5	1548.5	-44.07	29.24	73.31	1.76E-05	H
		20121010	TN	-9.73	1084.3	2754.7	-41.12	31.14	72.26	3.13E-05	H
	44	20110410	US	-13.07	5.8	4.0	-13.70	-11.58	2.13	8.97E-08	
		20121010	TN	-13.07	6.1	2.6	-13.28	-13.07	0.21	5.75E-08	
	95	20121010	TN	-10.34	1.6	3.4	-11.91	-9.55	2.36	1.64E-07	
3968	22	20110322	YS	-49.85	57.0	51.8	-50.48	-48.80	1.69	2.22E-05	
		20120303	YS	-49.85	70.3	47.2	-50.48	-26.47	24.02	2.02E-05	
3970	22	20110410	US	-52.83	3.7	2.5	-53.25	-52.62	0.63	9.35E-07	
		20120316	YS	-47.77	2.5	4.5	-54.30	-47.56	6.74	1.67E-06	
3972	22	20110410	US	-60.96	78.1	209.6	-69.81	-50.00	19.80	9.84E-05	
		20120310	YS	-55.27	25.1	84.7	-66.22	-50.00	16.22	3.98E-05	
3976	22	20110403	YS	-54.89	3.9	22.9	-73.43	-31.51	41.92	9.81E-06	
		20120311	YS	-57.42	34.3	50.1	-62.90	-38.04	24.86	2.15E-05	
	44	20110403	YS	-54.43	25.7	15.3	-54.85	-53.79	1.06	1.30E-05	
		20120311	YS	-54.43	13.7	5.5	-54.64	-54.43	0.21	4.65E-06	
	95	20120311	YS	-54.50	7.1	3.8	-54.70	-53.91	0.79	6.90E-06	

Table 2.4 (cont'd)

RMS ID	Maser	Epoch (yyyymmdd)	Station[a]	$V_{\rm p}$ (km s^{-1})	$S_{\rm p}$ (Jy)	$\int S_\nu dv$ (Jy km s^{-1})	$V_{\rm min}$ (km s^{-1})	$V_{\rm max}$ (km s^{-1})	$V_{\rm range}$ (km s^{-1})	$L_{\rm maser}$ ($L_\odot$)	Notes[b]
3980	22	20110323	YS	-75.17	19.2	57.8	-78.33	-51.57	26.75	9.07E-06	
		20121012	TN	-58.11	6.4	13.9	-70.32	-57.89	12.43	2.18E-06	
3982	22	20110403	YS	-56.66	30.5	186.0	-78.57	-35.60	42.98	2.92E-05	H
		20120216	YS	-54.35	37.5	173.2	-76.68	-7.58	69.10	2.72E-05	
	44	20110403	YS	-57.24	41.9	91.3	-59.37	-51.93	7.44	2.83E-05	
		20120216	YS	-57.24	26.0	53.1	-57.88	-52.99	4.89	1.65E-05	
	95	20120216	YS	-53.49	10.9	41.4	-58.61	-52.90	5.71	2.77E-05	
3985	22	20110403	YS	-48.18	8.9	5.3	-48.60	-47.97	0.63	8.27E-07	
		20120216	YS	-48.39	6.6	4.3	-48.60	-47.97	0.63	6.82E-07	
3986	22	20110323	YS	-72.26	114.4	250.9	-77.53	-49.72	27.81	3.93E-05	
		20121012	TN	-69.95	123.5	127.7	-72.47	-53.51	18.96	2.00E-05	
	44	20110323	YS	-57.68	15.5	18.1	-58.32	-55.98	2.34	5.62E-06	
		20121012	TN	-57.68	12.7	18.3	-58.32	-55.76	2.55	5.69E-06	
	95	20121012	TN	-57.62	12.9	18.6	-58.60	-55.26	3.35	1.24E-05	
3991	22	20110403	YS	-93.47	5.0	8.1	-93.68	-39.75	53.93	1.27E-06	H
		20121011	TN	-50.70	7.8	19.7	-51.75	-39.33	12.43	3.09E-06	
3992	22	20110322	YS	-43.36	5.0	2.6	-43.78	-43.15	0.63	7.30E-07	
		20120612	YS	-44.21	9.6	11.9	-46.52	-43.78	2.74	3.39E-06	
3996	22	20110331	YS	-47.12	90.4	108.6	-53.02	-39.33	13.69	3.09E-05	
		20130430	YS	-47.12	33.9	59.7	-58.50	-39.96	18.54	1.70E-05	
	44	20110331	YS	-45.82	2.8	3.9	-45.82	-44.12	1.70	2.19E-06	
		20130430	YS	-45.60	1.3	1.1	-45.60	-45.39	0.21	6.00E-07	
	95	20130430	YS	-44.53	2.2	3.9	-46.50	-43.94	2.56	4.78E-06	
3998	22	20110322	YS	-53.24	32.6	60.3	-54.29	-41.87	12.43	2.71E-05	
		20121010	TN	-51.35	54.0	85.0	-60.40	-50.08	10.32	3.82E-05	
	44	20110322	YS	-52.75	6.9	5.4	-54.88	-52.54	2.34	4.77E-06	

Table 2.4 (cont'd)

RMS ID	Maser	Epoch (yyyymmdd)	Station[a]	$V_{\rm p}$ (km s^{-1})	$S_{\rm p}$ (Jy)	$\int S_\nu dv$ (Jy km s^{-1})	$V_{\rm min}$ (km s^{-1})	$V_{\rm max}$ (km s^{-1})	$V_{\rm range}$ (km s^{-1})	$L_{\rm maser}$ ($L_\odot$)	Notes[b]
		20121010	TN	-52.75	5.5	4.3	-54.88	-52.54	2.34	3.84E-06	
	95	20121010	TN	-54.82	4.2	3.5	-54.82	-52.46	2.36	6.68E-06	
4365	22	20110325	YS	79.31	0.8	1.9	77.62	79.31	1.69	9.67E-07	
		20120613	YS	73.41	9.0	8.5	73.20	78.89	5.69	4.37E-06	
	44	20110325	YS	79.77	5.7	8.9	78.28	81.47	3.19	9.05E-06	
		20120613	YS	79.98	5.0	9.3	78.28	82.11	3.83	9.42E-06	
	95	20120613	YS	79.89	2.8	1.8	79.50	79.89	0.39	3.88E-06	
4745	22	20110326	YS	-19.89	238.7	331.0	-21.99	-15.04	6.95	3.07E-05	
		20120303	YS	-21.78	123.4	222.6	-22.63	-14.62	8.01	2.07E-05	
	44	20110326	YS	-16.68	29.2	33.6	-19.23	-14.55	4.68	6.18E-06	
		20120303	YS	-16.68	31.2	32.3	-18.80	-14.98	3.83	5.94E-06	
	95	20120303	YS	-16.82	19.6	23.5	-18.78	-14.65	4.13	9.32E-06	
4747	22	20110329	YS	-10.98	40.4	21.6	-11.61	-10.56	1.05	2.01E-06	
		20120303	YS	-10.98	14.2	6.9	-11.40	-10.77	0.63	6.38E-07	
	44	20110329	YS	-10.30	6.4	2.5	-10.52	-10.09	0.43	4.63E-07	
		20120303	YS	-10.30	8.2	3.2	-10.30	-10.09	0.21	5.89E-07	
	95	20120303	YS	-10.21	6.7	4.1	-10.80	-10.02	0.79	1.61E-06	
4888	22	20110322	YS	33.46	52.2	98.0	8.18	47.79	39.61	2.48E-05	H
		20120605	YS	34.51	38.6	169.5	13.45	62.32	48.88	4.28E-05	H
	44	20110322	YS	43.62	31.0	50.9	41.28	45.32	4.04	2.54E-05	
		20120605	YS	43.62	31.9	44.9	42.56	44.90	2.34	2.25E-05	
	95	20120605	YS	43.09	64.8	117.6	41.12	46.04	4.92	1.27E-04	
4910	22	20120619	YS	71.77	3.9	2.7	71.56	71.99	0.42	1.48E-06	
	44	20120619	YS	76.87	1.9	0.8	76.87	76.87	0.21	9.07E-07	
	6.7		MMB			23.8				3.97E-06	
4924	44	20110410	US	66.38	3.7	4.4	65.32	66.81	1.49	3.73E-06	

Table 2.4 (cont'd)

RMS ID	Maser	Epoch (yyyymmdd)	Station[a]	$V_{\rm p}$ (km s^{-1})	$S_{\rm p}$ (Jy)	$\int S_\nu dv$ (Jy km s^{-1})	$V_{\rm min}$ (km s^{-1})	$V_{\rm max}$ (km s^{-1})	$V_{\rm range}$ (km s^{-1})	$L_{\rm maser}$ ($L_\odot$)	Notes[b]
		20120607	YS	66.60	2.5	4.9	64.05	66.60	2.55	4.14E-06	
	95	20120607	YS	66.37	5.7	3.2	65.58	66.37	0.79	5.95E-06	
4941	22	20110411	US	35.77	4.4	3.8	34.93	35.77	0.84	4.26E-07	
		20130422	YS	36.82	10.2	18.9	35.14	40.40	5.27	2.12E-06	
	44	20110411	US	35.20	8.1	2.9	34.98	35.20	0.21	6.43E-07	
		20130422	YS	35.20	4.7	1.6	34.98	35.20	0.21	3.54E-07	
	95	20130422	YS	35.16	2.8	3.7	33.78	35.36	1.58	1.77E-06	

[a]YS, US, and TN are the KVN Yonsei, Ulsan, and Tamna stations, respectively. MMB is the MMB survey of 6.7 GHz class II CH_3OH masers.

[b]D: H_2O maser with a dominant shifted feature at that epoch, H: presence of H_2O maser emission with high velocity(>30 km s^{-1}) component

Table 2.5. Statistics of Maser Line Parameters

Maser	Number	S_p (Jy)				V_{rel} (km s^{-1})				V_{range} (km s^{-1})			
		mean	median	min	max	mean	median	min	max	mean	median	min	max
1st Epoch													
22	126	156.6 ± 525.5	13.5	0.8	3540.6	-3.73 ± 18.63	-0.93	-94.33	78.47	17.37 ± 24.21	12.01	0.21	188.13
44	76	24.9 ± 46.0	9.1	1.2	252.5	0.02 ± 1.05	-0.05	-2.39	3.59	2.92 ± 2.60	2.34	0.21	15.52
2nd Epoch													
22	112	144.4 ± 563.6	17.2	1.2	4552.1	-2.69 ± 20.05	-0.11	-92.86	79.11	19.70 ± 32.59	9.69	0.21	230.68
44	81	21.5 ± 41.6	6.7	1.1	236.5	0.05 ± 1.06	-0.05	-2.39	3.56	2.54 ± 2.41	2.13	0.21	11.27
95	68	16.2 ± 25.0	6.7	1.1	146.9	0.09 ± 1.08	-0.02	-2.39	3.91	2.96 ± 2.31	2.36	0.20	13.39
Either Epoch													
22	135	150.9 ± 542.6	15.5	0.8	4552.1	-3.24 ± 19.28	-0.89	-94.33	79.11	18.46 ± 28.42	9.90	0.21	230.68
44	83	23.1 ± 43.7	7.0	1.1	252.5	0.03 ± 1.05	-0.05	-2.39	3.59	2.72 ± 2.50	2.34	0.21	15.52
95	68	16.2 ± 25.0	6.7	1.1	146.9	0.09 ± 1.08	-0.02	-2.39	3.91	2.96 ± 2.31	2.36	0.20	13.39
MMB Survey Area													
2nd Epoch													
22	54	130.3 ± 506.1	15.8	2.6	3623.0	-7.52 ± 19.65	-1.70	-92.86	7.90	25.47 ± 42.98	10.95	0.21	230.68
44	50	13.3 ± 16.6	6.6	1.9	80.3	0.15 ± 1.01	0.12	-2.39	2.87	2.77 ± 2.26	2.55	0.21	11.27
95	50	12.3 ± 14.7	6.4	1.1	64.8	0.04 ± 1.02	0.03	-2.39	2.94	2.80 ± 2.06	2.56	0.20	7.88
6.7	38	48.7 ± 90.2	18.6	0.9	517.3	-0.40 ± 4.70	-0.90	-12.00	7.70	7.80 ± 4.72	6.80	0.90	17.00

Note. — Upper : Maser sources for KVN observations

Lower : Maser sources combining the current work with 6.7 GHz in an region covered with MMB survey

Table 2.6. Dominant Shifted H_2O Maser Source Candidates

RMS ID	^{13}CO[a] J=1–0	HCO^+[a] J=1-0	Note[b]
145	n	–	R
2547	n	–	B
2584	n	–	B
2716	y	y	N
3158	y	n	B
3360	y	y	N
3587	n	–	B
3766	n	–	B
3911	n	–	B
3936	n[c]	–	R
3958	n	–	B

[a]The presence of molecular line emission associated with the dominant blue- or redshifted H_2O maser feature candidates.

[b]B: dominant blueshifted, R: dominant redshifted, N: no dominant maser emission

[c]The ^{13}CO J=2–1 line data from the JCMT archives.

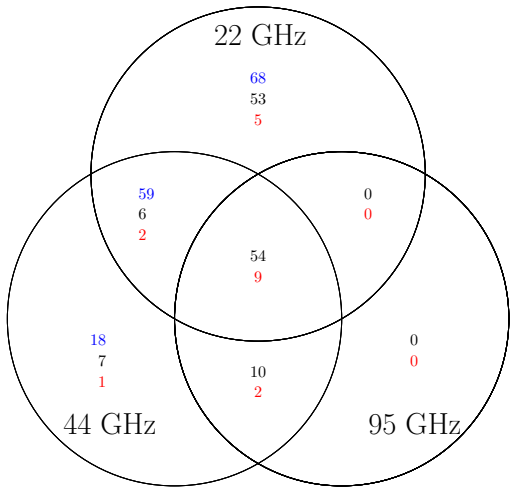

Figure 2.1: Venn diagram showing the numbers of detected 22 GHz H_2O and 44 and 95 GHz class I CH_3OH maser sources in each epoch. The numbers in blue and black represent the first and second epochs, respectively. The numbers in red are for the subsample of 138 sources in the MMB survey area (see the text for details).

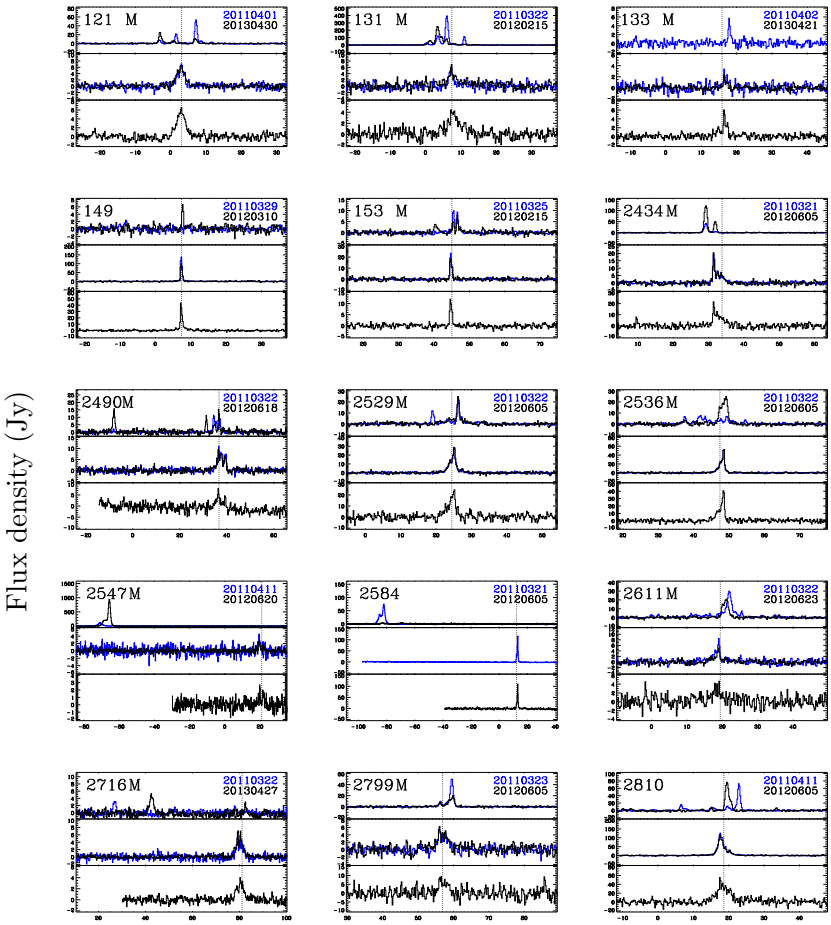

Figure 2.2: U(Upper panel) The detected 22 GHz H_2O, (Middle panel) 44 GHz CH_3OH, and (Lower panel) 95 GHz CH_3OH maser spectra of the sources detected in all of 3 transitions. Blue and Black colors represent the first and second epochs, respectively. The source name is given in the top-left corner of the upper panel and 'M' is attached for the source associated with 6.7 GHz CH_3OH maser emission from Breen et al. (2015). The observing dates are shown in the top-right corner. The vertical dotted line indicates the systemic velocity.

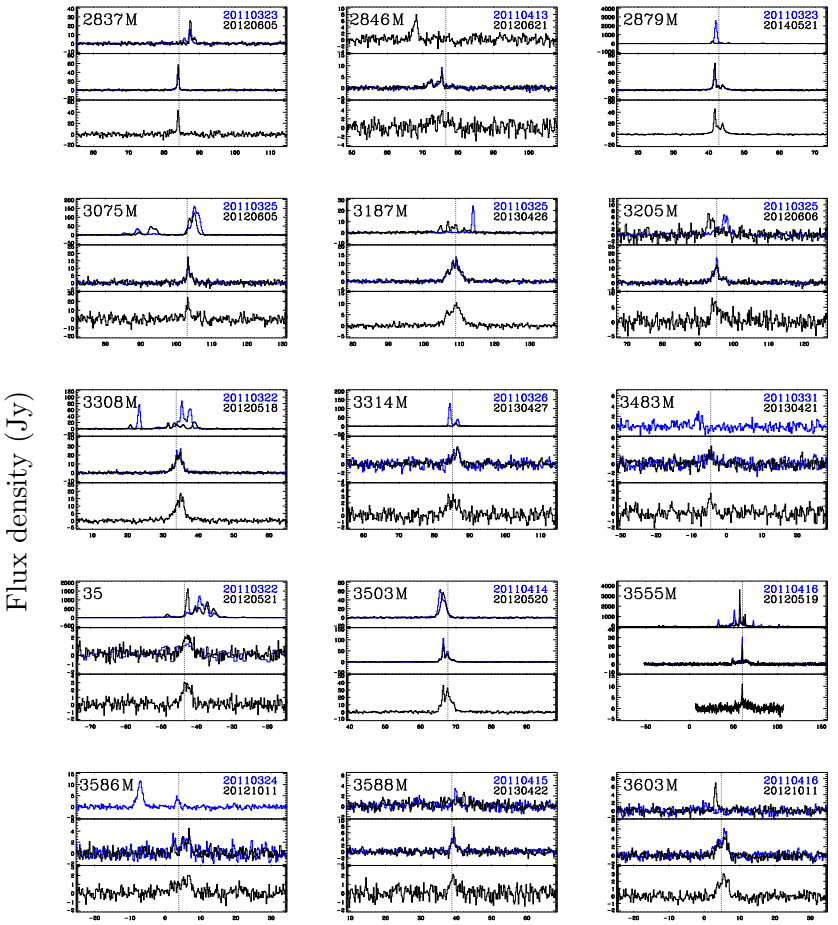

Figure 2.3: Continued

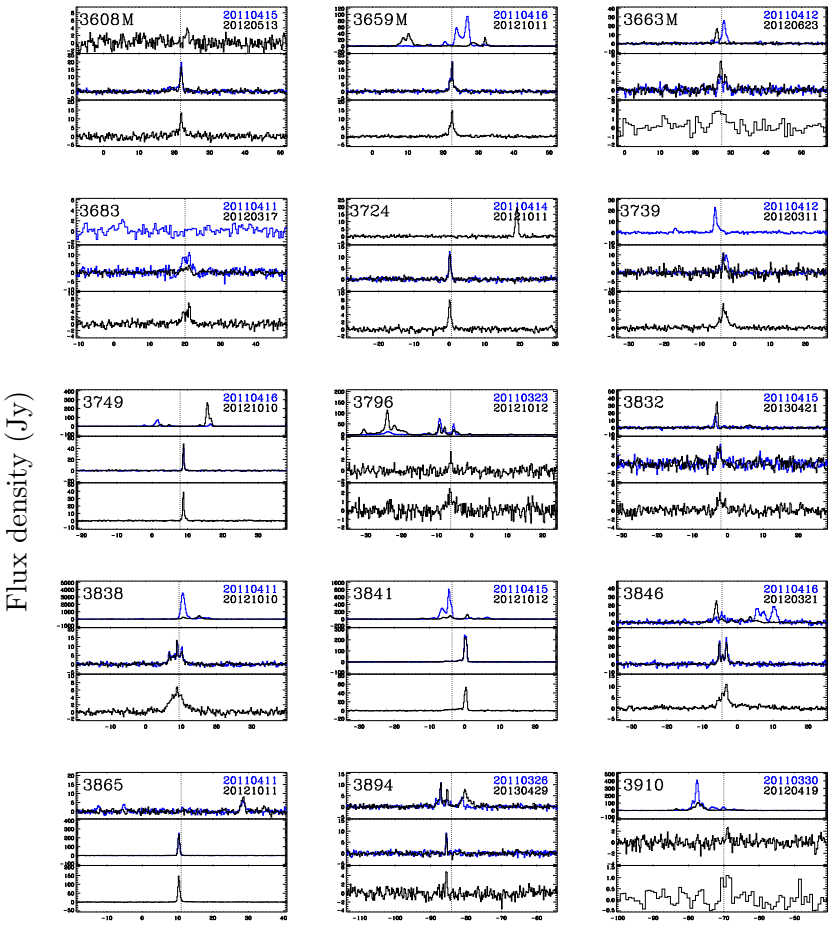

Figure 2.4: Continued

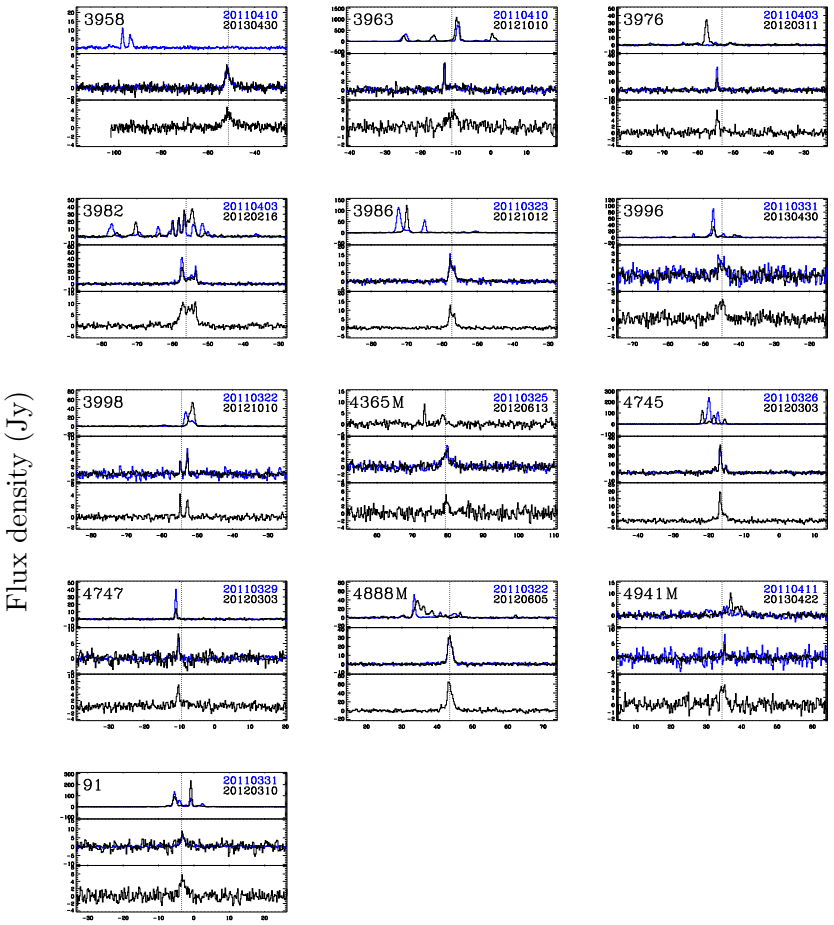

Figure 2.5: Continued

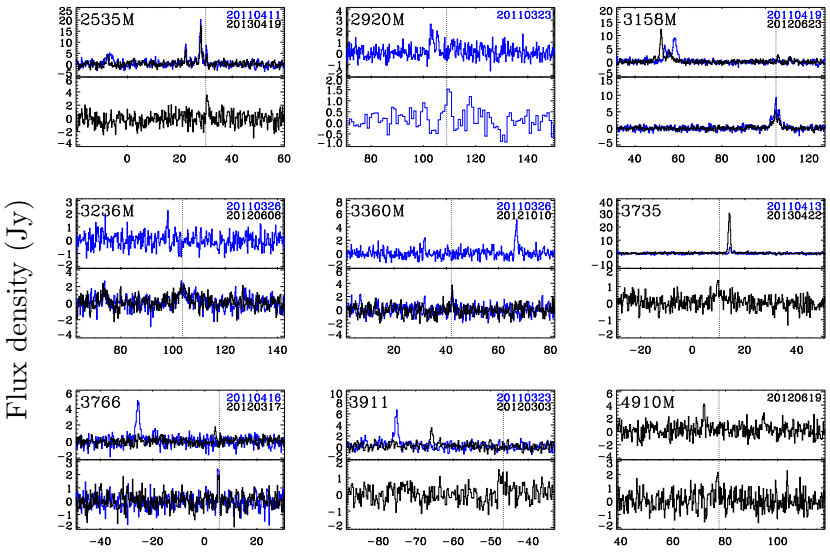

Figure 2.6: Same as in Figure 2.2 except for the source detected both at (Upper) 22 and (Lower) 44 GHz.

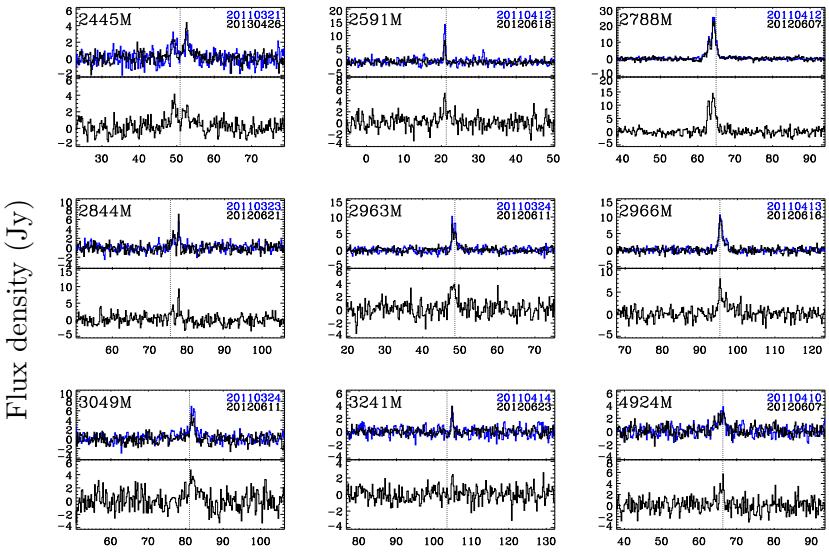

Figure 2.7: Same as in Figure 2.2 except for the source detected both at (Upper) 44 and (Lower) 95 GHz.

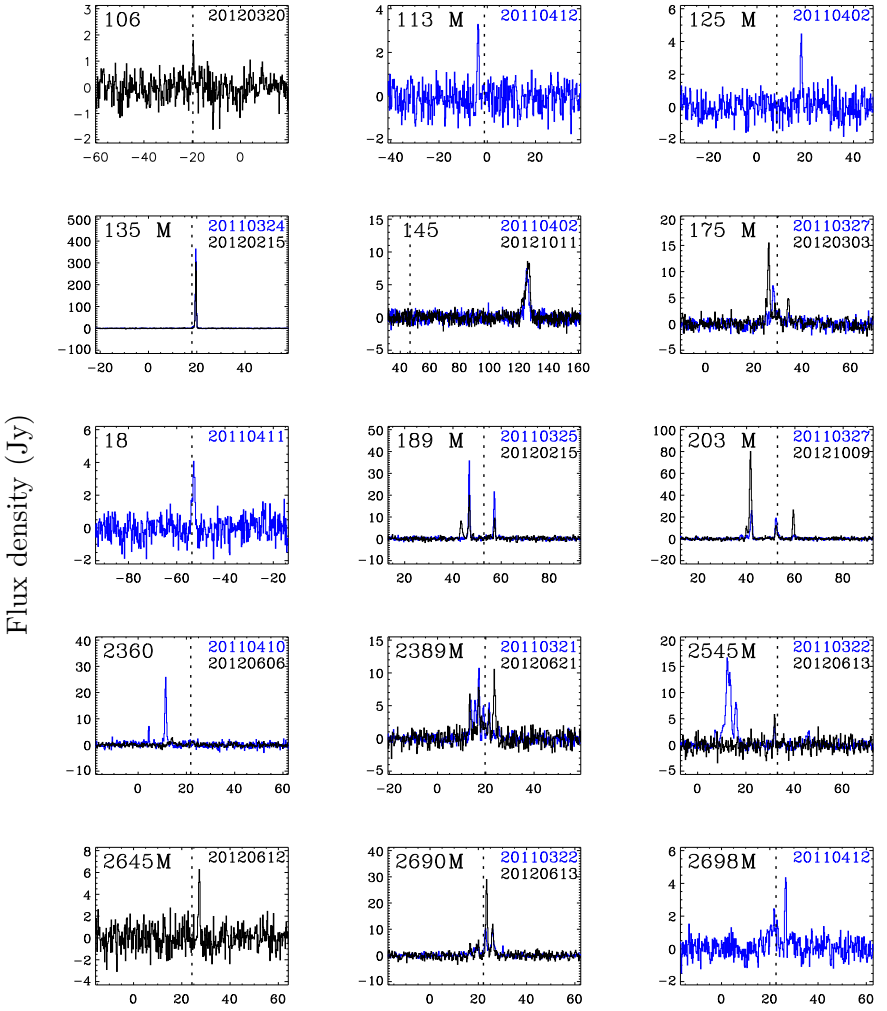

Figure 2.8: Same as in Figure 2.2 except for the source detected only at 22 GHz.

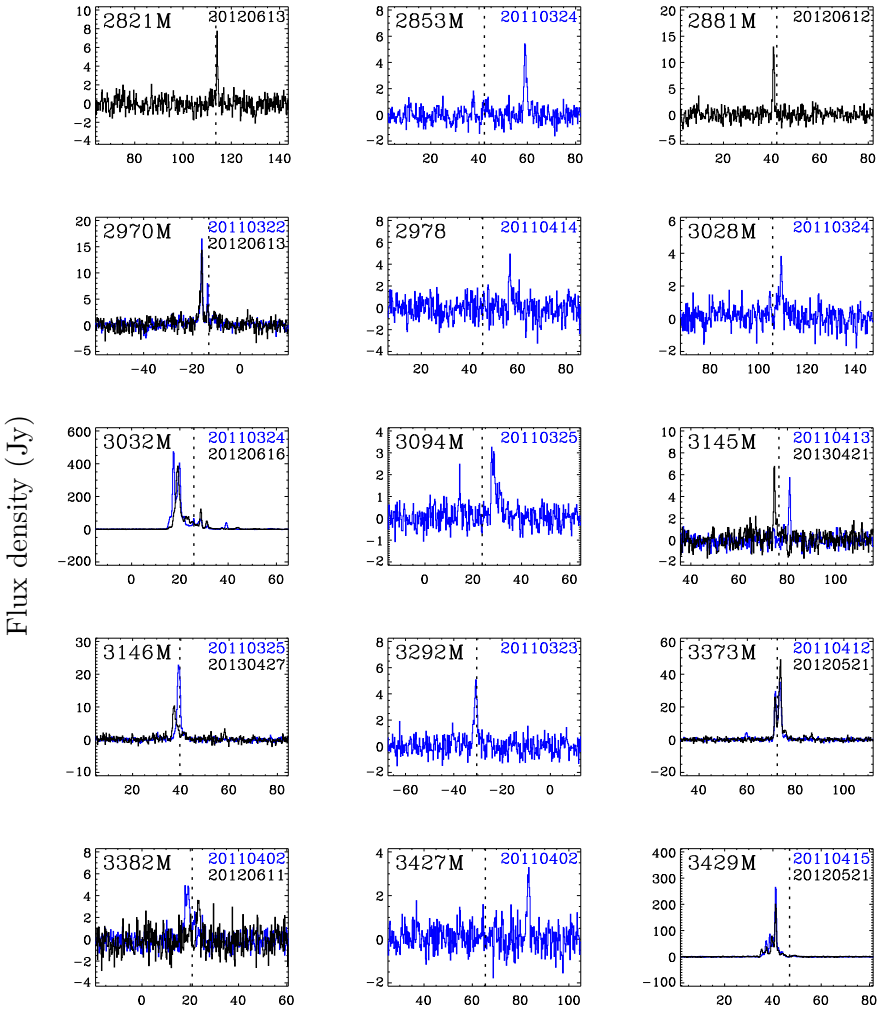

Figure 2.9: Continued

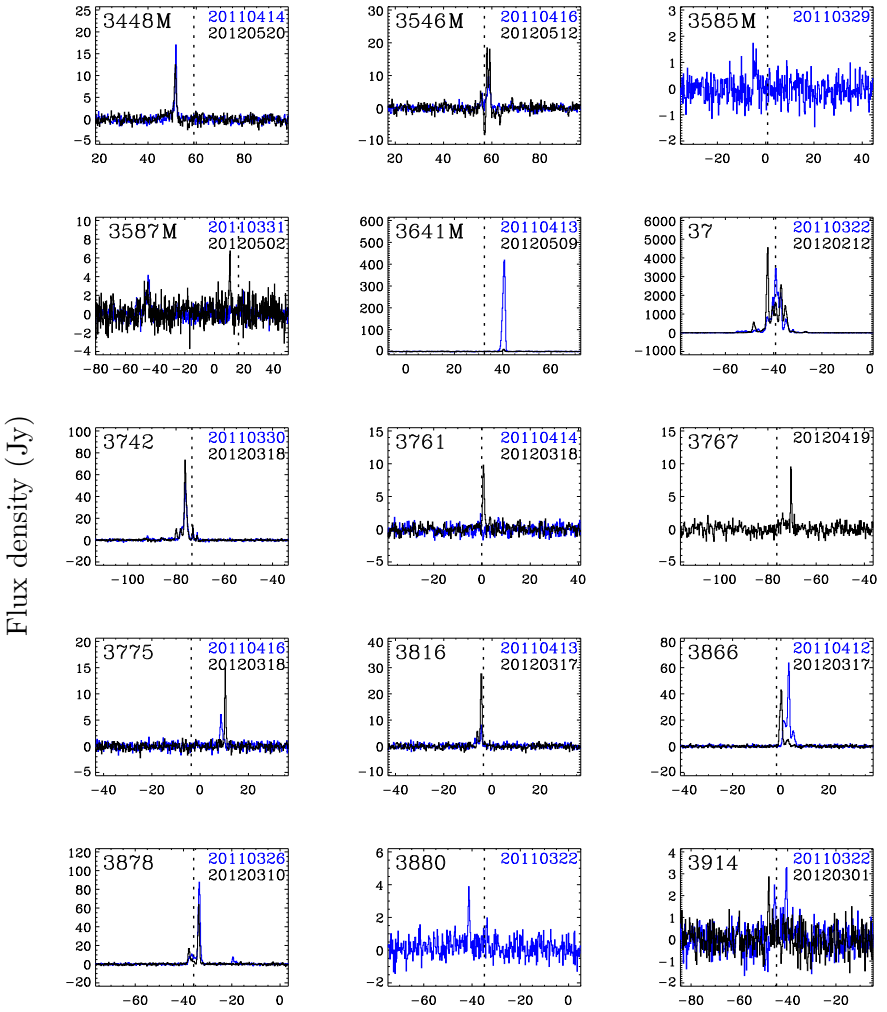

Figure 2.10: Continued

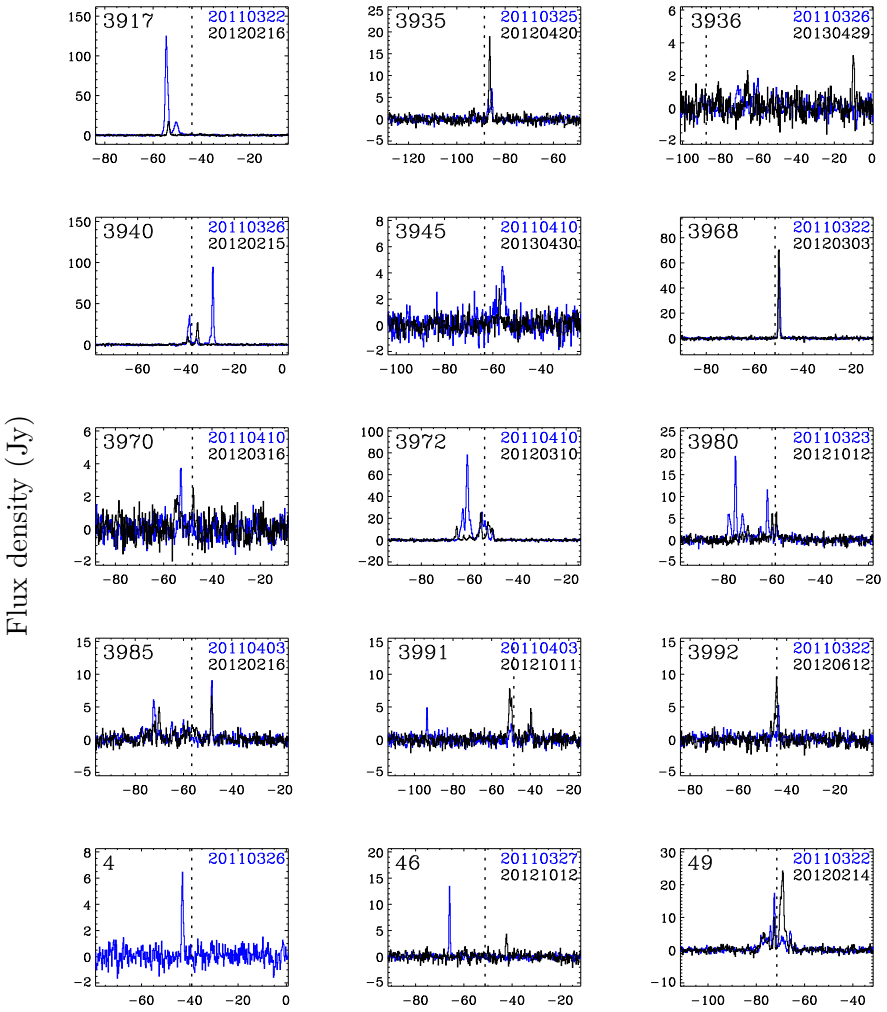

Figure 2.11: Continued

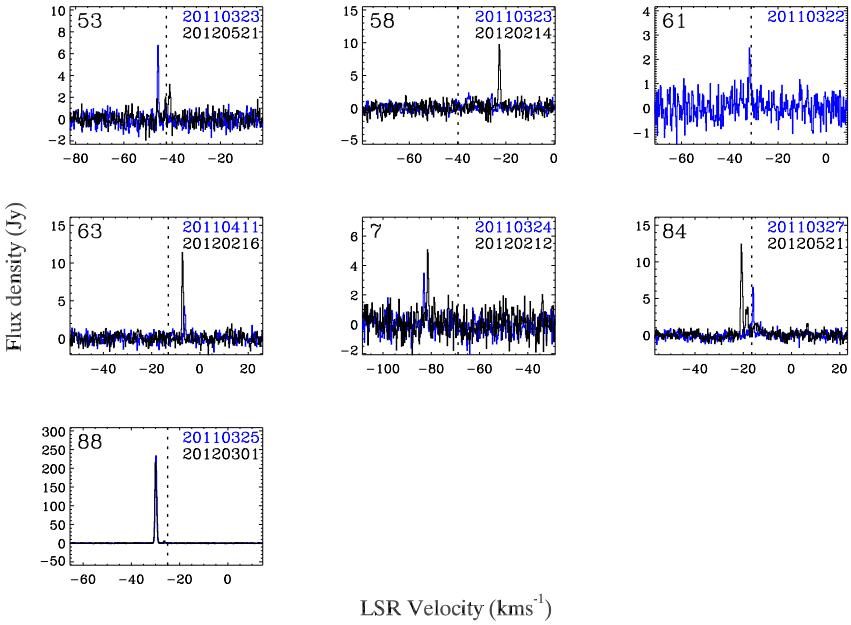

Figure 2.12: Continued

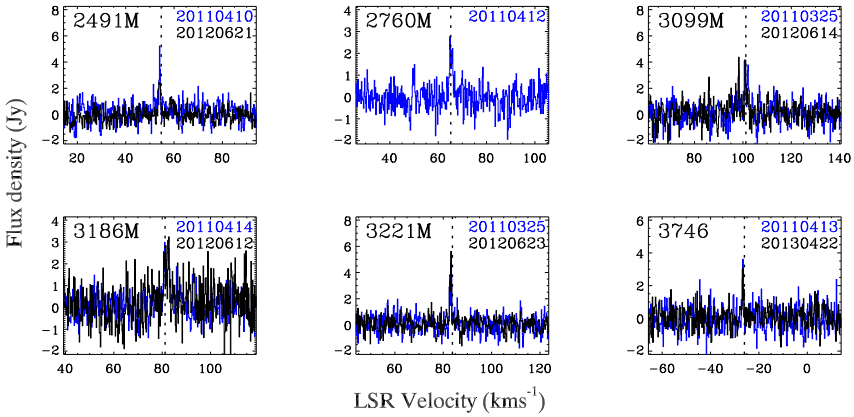

Figure 2.13: Same as in Figure 2.2 except for the source detected only at 44 GHz.

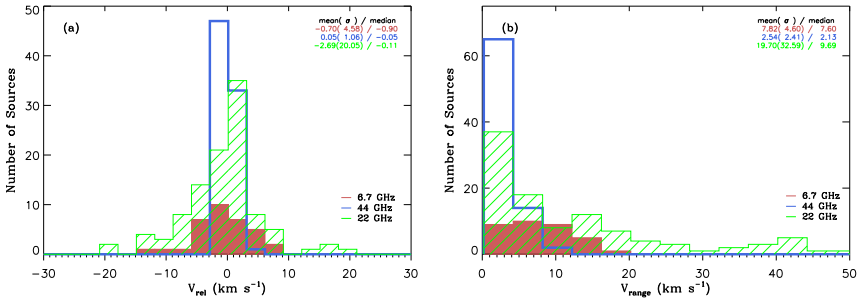

Figure 2.14: (a) Histogram of the relative peak velocities for the 22, 44, and 6.7 GHz maser sources in a bin size of 3 km s^{-1}. Blue, green, and brown colors represent 22, 44, and 6.7 GHz masers, respectively. The 22 and 44 GHz data are from the second epoch survey of this study, while the 6.7 GHz data are from the MMB survey. The mean and median values of each distribution are listed in the top-right corner of each panel. (b) Same as in (a) except for the velocity ranges in 4 km s^{-1} bin.

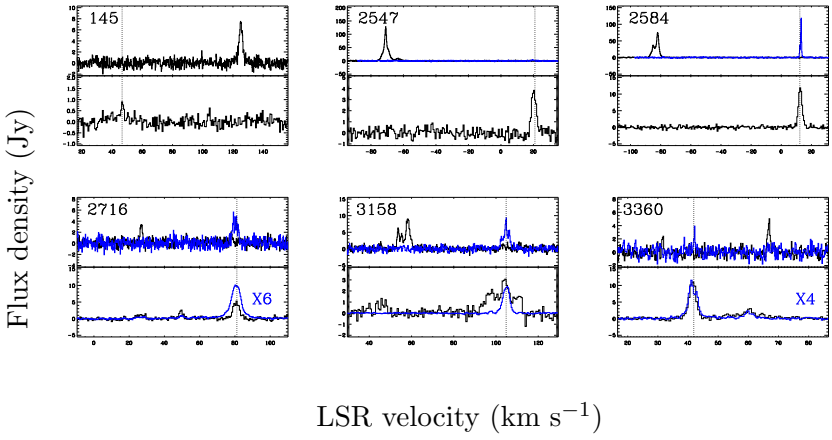

Figure 2.15: (Upper) The detected 22 GHz H_2O (*black*) and 44 GHz CH_3OH (*blue*) maser spectra and (Lower) ^{13}CO J=1−0 (*black*) and HCO^+ J=1−0 (*blue*) line spectra of dominant H_2O maser outflow source candidates (^{13}CO J=2−1 line spectrum only for RMS 3936). For each source, the source name is presented at the top-right corner of the upper panel and the systemic velocity is indicated by a vertical dotted line. The lower panel shows spectrum of $^{13}CO(J = 1-0)$(or $^{13}CO(J = 2-1)$ for RMS 3936, refers to Table 2.6.) and $HCO^+(J = 1-0)$ line for 13 H_2O maser sources with high velocity offset (> 30 km s^{-1}) from the systemic velocity. For comparison, corresponding the 22 GHz H_2O and 44 GHz CH_3OH maser spectrum are shown in the upper panel. For each panel, black line represent the ^{13}CO and H_2O maser and blue one stands for HCO^+ line and 44 GHz CH_3OH maser. Because of the systemic velocity modification in RMS database during the observation period, the systemic velocities are presented in two type of vertical line: long-dashed and dashed line for old and current version of them. It is noted that each panel have a different y-axis scale of Jy(upper) and T_A^*(lower).

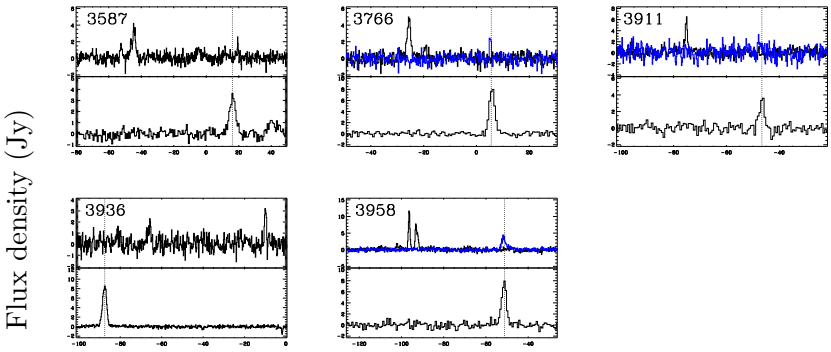

Figure 2.16: Continued

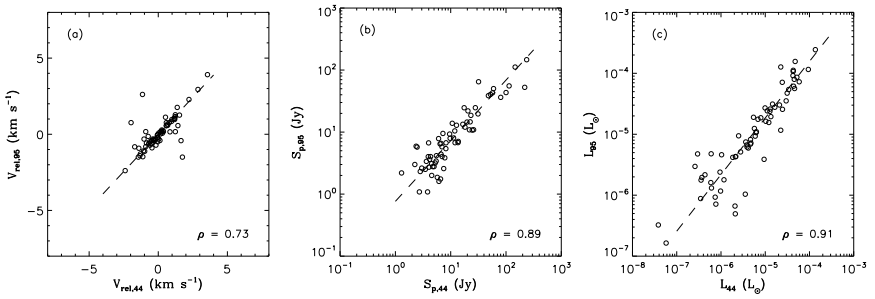

Figure 2.17: Comparison of (a) the relative peak velocities, (b) the peak flux densities, and (c) the isotropic luminosities of the 44 and 95 GHz class I CH_3OH maser sources. In each panel the least-squares fitted relation is displayed by a dashed line with the correlation coefficient in the bottom-right corner.

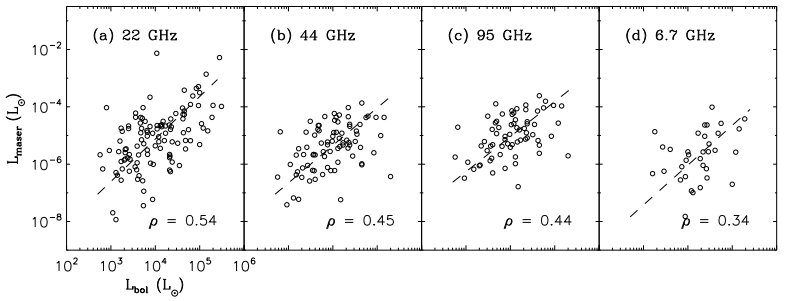

Figure 2.18: Comparison of the isotropic maser luminosity with the bolometric luminosity for (a) the 22 GHz, (b) 44 GHz, (c) 95 GHz, and (d) 6.7 GHz maser sources. The 22, 44, and 95 GHz data are from the second-epoch survey of this study, while the 6.7 GHz data are from the MMB survey (Breen et al., 2015). The Pearson correlation coefficient is shown in the bottom-right corner of each panel.

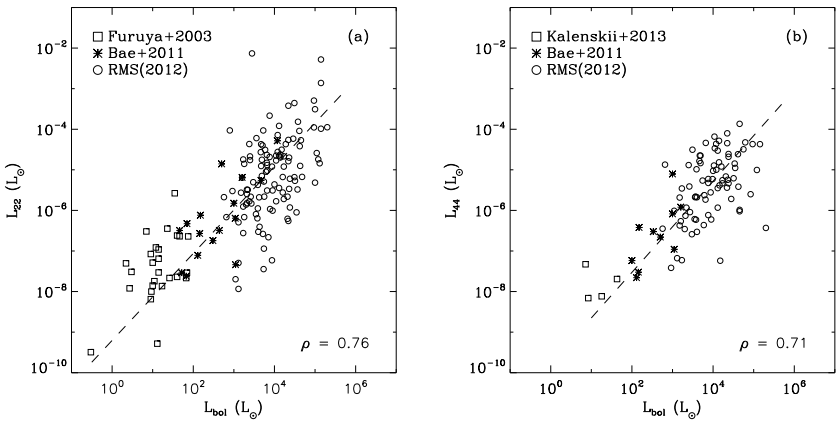

Figure 2.19: Comparison of the isotropic maser luminosity with the bolometric luminosity for (a) the 22 GHz and (b) 44 GHz maser sources. The data points in low- and intermediate-mass regime are added from the literature. In both panels open circles and asterisks are data points of this study in the second epoch and Bae et al. (2011), respectively. Open squares are data points from Furuya et al. (2003) in (a) and Kalenskii et al. (2013) in (b). The least-sqaures fitted relation is displayed by a dashed line with the correlation coefficient on the bottom-right corner in each panel.

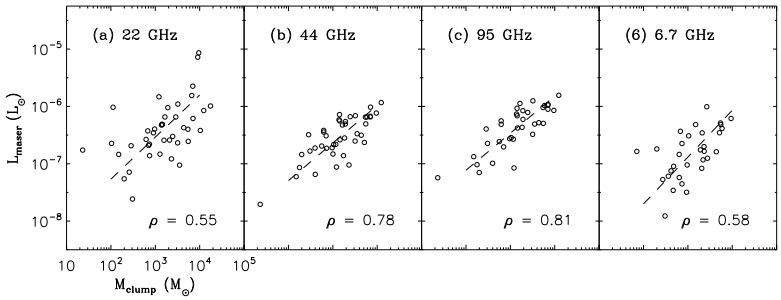

Figure 2.20: Same as in Figure 2.18 except for the associated ATLASGAL clump mass. In each panel the least-sqaures fitted relation is shown by a dashed line with the correlation coefficient on the bottom-right corner.

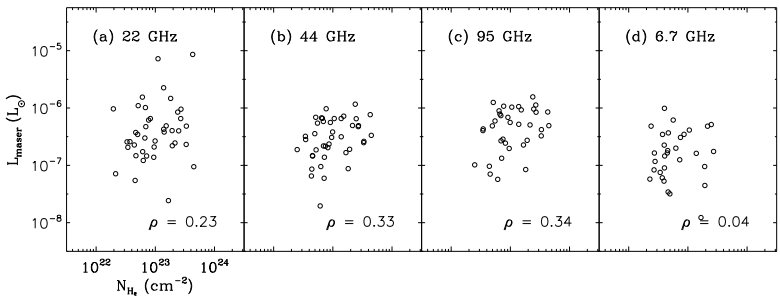

Figure 2.21: Same as in Figure 2.18 except for the peak H_2 column density.

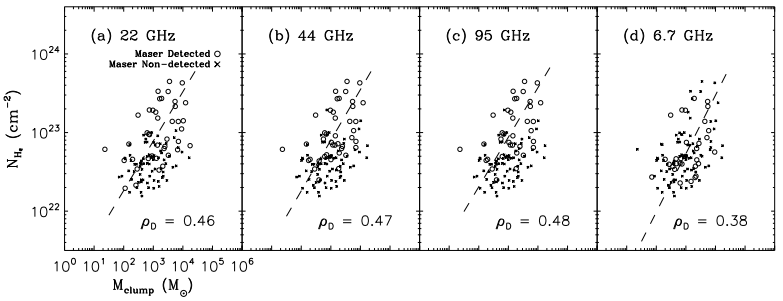

Figure 2.22: The peak H_2 column density versus the ATLASGAL clump mass for the four maser species. Open circles and crosses represent the sources with and without maser emission, respectively. In each panel the least-sqaures fitted relation is shown by a dashed line with the correlation coefficient on the bottom-right corner.

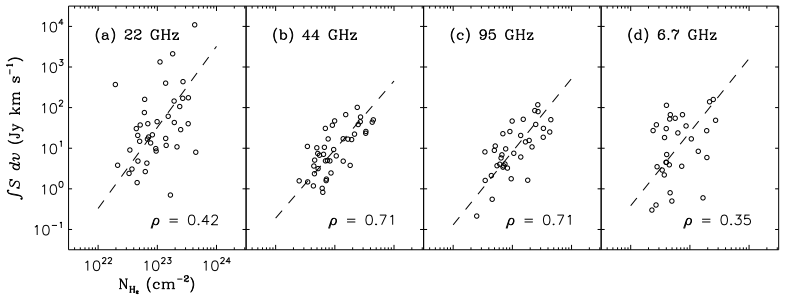

Figure 2.23: The integrated maser flux density versus the peak H_2 column density. In each panel the least-sqaures fitted relation is shown by a dashed line with the correlation coefficient in the bottom-right corner.

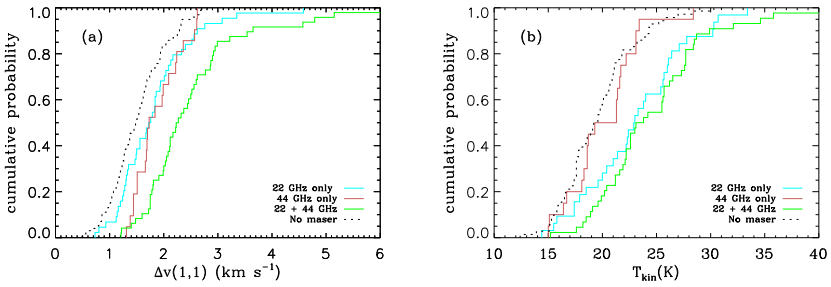

Figure 2.24: Cumulative probability of (a) the NH_3 linewidth and (b) the kinetic temperature for 4 subsamples, which are divided on the bassis of the second-epoch survey results. The subsamples and corresponding colors are displayed on the bottom-right corner in each panel.

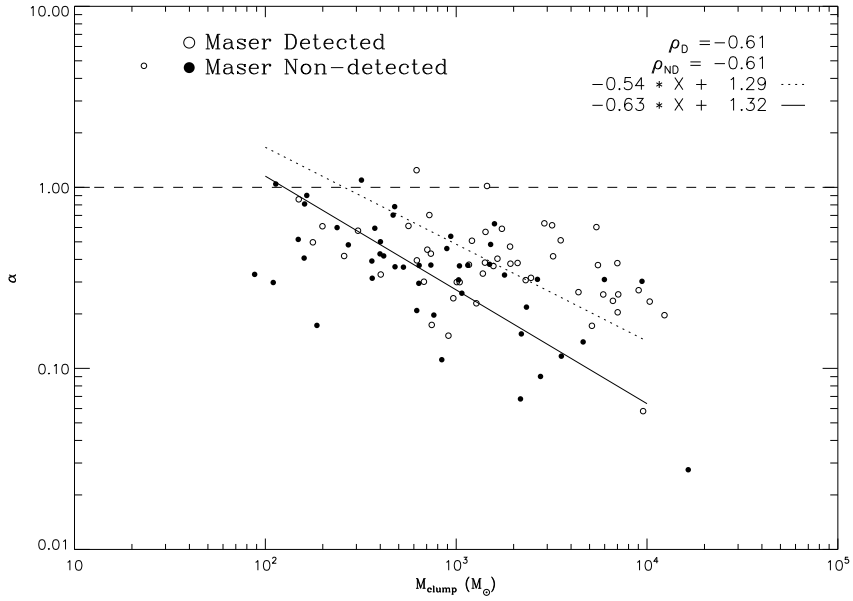

Figure 2.25: The virial parameter (α) versus the clump mass for the associated ATLASGAL clumps. Open and filled circles represent the sources with and without any maser emission, respectively. The dashed line indicates the critical value (α=1) for an isothermal sphere in hydrostatic equilibrium without magnetic support. The area of $\alpha < 1$ indicates the region where clumps are graviationally unstable and likely to be collapsing without additional support from strong magnetic field. The solid and dotted lines show the least-sqaures fitted relations for the filled and open circles, respectively. The Pearson correlation coefficients are shown in the right upper corner.

Chapter 3

Simultaneous Surveys of Water and Class I Methanol Masers toward High-mass Young stellar Objects in Different Evolutionary Stages

3.1 Introduction

High-mass stars are very important in the evolution of galaxies because they inject energy and matter into the interstellar medium

throughout their lifetimes. However, understanding the formation process of high-mass (>8 $M_{\odot}$) stars remains a challenge in modern astronomy. Detailed observational studies of high-mass star formation are difficult because high-mass young stellar objects (YSOs) are located at large distances and deeply embedded in molecular clouds and evolve fast. Furthermore, they usually form in clusters, which makes even theoretical studies difficult. Interstellar masers at centimeter and millimeter wavelengths enable us to study these high-mass star-forming regions unaffected by obscuration from dust.

There are four primary masers of H_2O, class I/II CH_3OH, and OH that are commonly observed in high-mass star-forming regions. Class I CH_3OH masers (e.g., at 44 GHz and 95 GHz) and H_2O masers (22 GHz) are collisonally pumped in shocked gas regions, while class II CH_3OH (e.g., at 6.7GHz and 12.2 GHz) and OH masers (ground state mainline at 1.6 GHz) are radiatively pumped by infrared emission from warm dust (e.g. Elitzur et al., 1989; Cragg et al., 2002). Among them H_2O maser are highly variable on various time scales (e.g., Felli et al., 2007) and often show high-velocity emission features offset by 30 km s^{-1} or more from the systemic velocity (e.g., Breen et al. 2010a; Caswell et al. 2010; Kim et al. 2016a). Investigations through single-dish and interferometric observations (e.g. Torrelles et al., 1997; Urquhart et al., 2011) revealed that H_2O masers are closely related with high-mass YSOs in various evolutionary stages and are usually associated with protostellar outflows (e.g. Torrelles et al., 2001; Codella et al., 2004). Some correlations have been reported between the properties of H_2O maser and those of the central (proto)stars and the parental clumps, including correlation between the maser luminosity and the bolometric luminosity over many orders

of magnitude (e.g., Urquhart et al., 2011; Bae et al., 2011). This suggests that H_2O masers can be used to investigate the properties of the central objects and the surrounding medium.

The CH_3OH masers are important tools for studying high-mass YSOs because they are predominantly observed in high-mass star-forming regions (e.g., Minier et al. 2003; Ellingsen 2006; Pandian et al. 2008). These masers have been empirically classified into class I and class II types. Radiatively pumped by infrared emission from warm dust, Class II CH_3OH masers are excited near the central (proto)stars (e.g., Cragg+05). The 6.7 GHz transition is the strongest and most common Class II CH_3OH maser and numerous searches have shown that these masers are not found toward low-mass YSOs (e.g., Minier et al. 2003; Bourke et al. 2005; Xu et al. 2008; Pandian et al. 2008). A number of surveys have been conducted for 6.7 GHz masers, resulting in the detection of 1600 sources in the Galaxy to date. The surveys include those that are summarized in the compilation of Pestalozzi et al. (2005) and the recent searches of Pandian et al. (2007), Ellingsen (2007), Xu et al. (2008), and the Parkes Methanol Multibeam (MMB) blind survey (Green et al. 2009). Class I CH_3OH masers are collisionally excited like H_2O masers and generally associated with the interface between bipolar outflows and the ambient medium (e.g., Plambeck & Menten 1990; Kurtz et al. 2004; Voronkov et al. 2006). In contrast to class II, class I CH_3OH masers are usually found offset by 0.1–1.0 pc from UCHII regions, infrared sources, and OH masers (e.g., Plambeck & Menten 1990; Kurtz et al. 2004). Surveys have revealed that class I methanol masers are associated not only with high-mass star formation but also with lower mass counterparts (Kalenskii et al. 2010; Bae et al. 2011). Compared to class II masers, class I masers

are relatively poorly studied and understood. There have been only a few large surveys for class I masers (mainly at 44 and 95 GHz), primarily undertaken with single-dish telescopes (e.g., Haschick et al. 1990; Slysh et al. 1994; Val'tts et al. 2000; Ellingsen 2005; Chen et al. 2012; Gan et al. 2013; Kang et al. 2015; Kim et al. 2016a) along with a few smaller scale interferometric searches (e.g., Kurtz et al. 2004; Cyganowski et al. 2009; Voronkov et al. 2014). These have resulted in the detection of about 500 class I maser sources in the Galaxy to date (e.g, Bayandina et al. 2012; Chen et al. 2011; Jordan et al. 2015; Kang et al.2015).

Many high-mass YSOs are associated with two or more different types of masers, each of which requires physical conditions within a specific range (e.g., Cragg et al. 2005). The most commonly observed maser transitions are those for which strong population inversion occurs for a relatively wide range of density and temperature. It has long been speculated that the presence and absence of different maser transitions could be used to infer details of the physical conditions in the surrounding regions of high-mass YSOs, and detailed modelling has been undertaken towards a small number of regions which show emission in a large number of different maser transitions (e.g., Cecaroni et al. 1991; Cragg et al. 2001). Ellingsen et al. (2007) and Breen et al. (2010b) suggested that the common maser species (H_2O, class I/II CH_3OH, and OH) may help identify the evolutionary phases of the central objects, and proposed possible evolutionary sequences of these maser species. Further searches suggested that class I masers may arise more than once during the high-mass star formation process (Voronkov et al. 2010; Chen et al. 2011). On the basis of current observations, however, the evolutionary phase scenario for both H_2O

and class I CH_3OH masers remains poorly determined.

In this study, we present simultaneous surveys of H_2O and class I CH_3OH masers toward high-mass YSOs in different evolutionary stages. The primary purposes are to investigate the relationship between the properties of these masers and those of the central (proto)stars and the natal clumps, and to study the hypothesis that these masers are plausible evolutionary tracers of high-mass star formation. In Section 2 we describe the source selection and the observations. In Section 3 we present the results of the survey. Discussion of analyses is given in Section 4, followed by a summary in Section 5.

3.2 Sources and Observations

3.2.1 Sources

Infrared Dark Clouds (IRDCs)

IRDCs were firstly discovered in mid-infrared images from the Infrared Space Observatory (ISO) and Midcourse Space Experiment (MSX) as dark shillouettes against the bright Galactic mid-infrared background (e.g., Perault et al., 1996; Egan et al., 1998). Early studies of IRDCs revealed that they are cold (<25 K), massive ($\sim 10^2 - 10^4$ $M_\odot$), and dense($\gtrsim 10^5$ cm^{-3}) molecular clouds with high column density ($\sim 10^{23}$ cm^{-2})(e.g., Carey et al., 1998, 2000). More recent studies of IRDC clumps showed that they have typical masses of ∼120 $M_\odot$, sizes of ∼0.5 pc (Rathborne et al., 2006), dust temperatures between 16 and 52 K, and luminosities between ∼10 and 5 × 10^4 $L_\odot$

(Rathborne et al., 2010). NH_3 rotational temperatures range from ∼10 to 20 K, which are typically lower than dust temperatures (Pillai et al., 2006; Sakai et al., 2008; Devine et al., 2011; Ragan et al., 2011). IRDCs also host massive, cold IR-dark clumps that show similar physical properties to high-mass star-forming clumps except lower temperatures and luminosities (Battersby et al., 2010; Rathborne et al., 2008; Chambers et al., 2009; Sanhueza et al., 2010; Wang et al., 2006, 2011). These characteristics suggest that IRDC clumps would form high-mass stars in the future. These objects seem to be the best candidates for the most elusive and earliest phase of high-mass star formation. Rathborne et al. (2006) selected the 38 highest contrast ones from the IRDC catalog of Simon et al. (2006). They mapped the 38 IRDCs in 1.2mm continuum emission and identified 190 cores. Chambers et al. (2009) proposed an evolutionary sequence for those IRDC cores: quiescent (no green fuzzy or 24 um point source), intermediate, active (green fuzzy and a 24 μm point source), and red (enhanced 8 μm emission) cores. In addition to these cores, they classified blue cores containing a region of bright 3.6 μm emission, which is probably not associated with IRDCs. We selected 130 of the 190 IRDC cores on the basis of star formation activities, i.e., intermediate and active ones and other types with 22 GHz H_2O and 44 GHz CH_3OH maser emission. Our sample consists of 13 quiescent, 43 intermediate, 37 active, 35 red, and 2 blue cores. Combining the 24 μm, 60–100 μm (from the *Spitzer Space Telescope*) and submillimeter continuum data, Rathborne et al. (2010) constructed the broadband spectral energy distribution(SED) for 157 of the 190 cores, using the simple graybody fits to SEDs. From the SEDs, they determined the dust temperature, emissivities, opacities, bolometric luminosity, and

masses for the the IRDC cores. Our sample includes 112 of the 157 cores.

Methanol Maser Sources (MMSs) at 6.7 GHz

The CH_3OH maser were found to be ideal tracer of the forming sites of high-mass stars. In the targeted survey at early decades, CH_3OH masers were exclusively observed near the UCHII regions and totally absent in other type of objects, including the low-mass star forming regions, AGB stars, and other galaxies. The subsequent observations have revealed a great number of 6.7 GHz masers without radio continuum counterparts and suggest that they could trace even earlier stages prior to UCH II stages.

Byun et al. (2012) carried out single-dish survey of 22 GHz H_2O and 44 GHz class I CH_3OH masers towards 284 6.7 class II CH_3OH maser sources with declinations $> -30^\circ$ in the catalog of Pestalozzi et al. (2005). We observed 116 of the 284 sources because they showed detectable 22 GHz H_2O or 44 GHz CH_3OH maser emission (Byun et al., 2012). Pestalozzi et al. (2007) modeled the luminosity function of those 6.7 GHz CH_3OH masers as a power-law between sharp cutoffs having an index α of —1.5 and –2. Comparing the synthetic data with the observed source, they suggested that sources showing a distance ambiguity lie probably at the near distances. All of 116 sources except 9 have associated IRAS Point Sources (Pestalozzi et al., 2005). We calculated the bolometric luminosity the formulation of Casoli et al.

(1986):

$$L_{5-1000\mu\mathrm{m}} = 5.52 \times 10^{-1} D^2_{\mathrm{kpc}} \\ (12.53S_{12} + 4.95S_{25} + 2.54S_{60} + S_{100}) \qquad (3.1)$$

Here S_λ is the flux density in the IRAS band λ and D_{kpc} is the distance to the object in kiloparsec. We did not apply the correction for the fraction of the total luminosity which is emitted at longer wavelengths than 100 μm. Many sources in the catalog of Pestalozzi et al. (2005) were originally selected from the catalogs of UCHII candidates, which had been identified using the characteristic IRAS colors (Wood & Churchwell , 1989b). From the Infrared data analysis for IRAS point sources with similar IRAS colors, the correction value may be less a factor of 2 which does not significantly influence analysis in the log-scale comparisons(Mottram et al., 2011).

HMPOs

The progenitors of ultracompact HII (UCH II) regions (sources that have not yet begun to ionize their environment in a detectable way) have been searched among IRAS point sources. The criteria generally used aim at selecting high-luminosity ($>10^3$ $L_\odot$) stellar embryos embedded in a massive envelope and associated with hot gas but no UCH II region (see Kurtz et al. 2000). In fact, most surveys focused on red IRAS sources with colors satisfying the Wood & Churchwell (1989b) criteria (originally set for selecting UCH II regions) but not detected in radio centimeter surveys. The presence of an envelope around the IRAS sources is confirmed by their association with high-density gas, and the existence of hot gas by the detection of a hot core

and water or methanol masers (e.g. Bronfman et al. 1996; Plume et al. 1997). In this way, studies by e.g., Molinari et al. (2000) and Sridharan et al. (2002) have identified massive young stellar objects harboring high-luminosity infrared protostars. We selected 135 samples from Sridharan et al. (2002)(69) and Molinari et al. (1996)(81). Sridharan et al. (2002) examined 69 sample of IRAS point source. Their sample are associated with CS $J = 2 - 1$ emission and satisfies the color criteria of UCH II regions. The source are bright with flux density $F_{100\mu m} > 500$ Jy and $F_{60\mu m} > 90$ Jy , but without radio continuum emission at 5 GHz. Combining the IRAS PSC database with 1.2 mm continuum(Beuther et al., 2002), the bolometric luminosities were derived by two component graybody fits to SEDs. They observed NH_3 line towards 69 samples and obtained (1,1) lines of 59 sources in a detection rate of $\sim 86\%$. Spectral lines of CO and NH_3, and maser emissions of H_2O and CH_3OH species revealed that most of the sources have characteristics of evolutionary stage prior to UCH II regions (Beuther et al., 2002). Molinari et al. (1996) investigate 163 IRAS point sources with IRAS colors similar to the compact molecular clouds from Palla et al. (1991). Their sample has flux density of $F_{60\mu m} > 100$ Jy and no radio continuum counterparts. The FIR luminosity was calculated by integrating the IRAS fluxes, estimating the contribution at long wavelength out of IRAS band by extrapolation according to a blackbody peaking at 100 μm. They also observed NH_3 lines and detected 103 of the 163 sources at least in the NH_3(1,1) line corresponding to a detection rate of $\sim 62\%$. The "Low" sources in the sample, selected with IRAS colors typical of very young stellar objects (YSOs), have associated mm continuum peaks, relatively narrow NH_3 line widths, smaller power law indices of the frequency

dependence of dust opacity, and a high molecular outflow detection rate (Molinari et al., 1998, 2000). They may be at an evolutionary stage earlier than the UCH II region phase.

UCHIIs

We selected 103 UCHIIs from WC89a and KCW94. WC89a performed subarcsecond-resolution radio continuum observations of 52 compact HII regions at 2 and 6 cm with Very Large Array (VLA), and detected ultracompact ionized gas structures (UCHIIs) in all the sources. Wood & Churchwell (1989b)(WC89b) found that known UCHIIs at that time have characteristic IRAS colors, $\log(F_{60}/F_{12}) \geq 1.30$ and $\log(F_{25}/F_{12}) \geq 0.57$, and then identified ∼1650 UCHII candidates from the IRAS point source catalog on the basis of the criteria. They computed the total luminosity for 42 UCHII candidates by integrating IRAS four fluxes, and did not contain the fraction of total luminosity contributed from emissions at long wavelength. Churchwell et al. (1990) observed NH_3 lines 49 subsamples of WC89a sources and obtained 42 sources at least in the NH_3(1,1) line. They KCW94 made VLA radio continuum observations of 59 UCHII candidates with F_{100} ≥1000 Jy and an HII region complex DR21, in order to validate the IRAS two-color selection criteria. They detected UCHIIs in 49 (82%) of the sources. Of the remaining 11 sources, IRAS05391–0152 and IRAS19410+2336 were observed to have UCHIIs afterward (Walsh et al., 1998; Carral et al., 1999). The sources in our sample consist of 52 UCHIIs of WC89a and 51 UCHIIs of KCW94. The bolometric luminosity was estimated toward 24 source of them by integrating IRAS fluxes with a fractional correction of 20% from the contribution at 100

μm –1mm. Note that we didn't correct this for MMSs.

3.2.2 Observations

We surveyed the 483 sources in three maser transitions: H_2O $6_{16} - 5_{23}$ (22.235080 GHz), CH_3OH $7_0 - 6_1$ A^+ (44.069430 GHz), and $8_0 - 7_1$ A^+ (95.169463 GHz). The observations were undertaken using the Korean VLBI Network (KVN) 21 m telescopes from 2011 Nov to 2012 Nov. The telescopes were equipped with multi-frequency receiving systems which made it possible to observe in the 22, 43, 86, and 129 GHz bands simultaneously (Han et al., 2008). We observed single polarization at 22 and 44 GHz and dual polarization at 95 GHz. The backend was a digital spectrometer that provided 4096 channels and 64 MHz bandwidth for each stream.

The full widths at half maximum (FWHMs) of the telescopes were about $130''$ at 22 GHz, $65''$ at 44 GHz, and $32''$ at 95 GHz. The telescope pointing and focus were checked every $\sim$2 hr by observing strong SiO maser sources at 43 or 86 GHz. The pointing accuracy was better than $5''$. Each spectrum was obtained in position-switching mode usually with an offset of +2 minutes in the right ascension. The total (ON+OFF) integration time was typically 30 minutes for source, which yielded typical noise (1σ) levels of about 0.7 Jy, 0.7 Jy, and 0.8 Jy at about 0.2 km s^{-1} resolution after smoothing for 22, 44, and 95 GHz, respectively. The data were calibrated with the standard chopper wheel method to provide the line intensity on the T_A^* scale, which converted to flux density using the conversion factors in Table 3.1. The KVN telescopes are of shaped Cassegraign type

and hence have quite high first-sidelobe levels of $\sim$ 14 dB at $\sim$ 1.5 times FWHM away from the pointing center (Kim et al., 2011; Lee et al., 2011). We thus mapped each detected source at the observing frequency to investigate contamination from nearby bright maser sources. The mapping area was 1.5 FWHM $\times$ 1.5 FWHM around a source with half-beam spacing at each frequency. Table 3.1 summarizes the observational details. All the spectral data were reduced and analyzed with the GILDAS/CLASS package.

3.3 Results

3.3.1 Detection Statistics

Table 3.4 summarizes the detection rates of this survey. The detection rates of at least one maser species are 32%, 61%, 96% and 67% toward IRDCs, HMPOs, MMSs, and UCHIIs, respectively. Since some of IRDC cores are closely located each other, we exclude the possible contamination from emission of nearby sources. By eliminating the contaminations, the numbers of detected maser sources are 54, 53, and 40 in original and reduced to 21, 22, and 21 for 22, 44, and 95 GHz, respectively. The detection rate is the highest for MMSs because they have a selection bias of 44 GHz CH_3OH maser emission. HMPOs and UCHIIs are believed be in different evolutionary stages, but there is no significant difference between the detection rates for the two samples. It should be noted that 98 soruces(73%) of HMPOs were satisfying IRAS colors of WC89b, selection criteria of UCHIIs.

Water Masers

The detection rates of 22 GHz H_2O maser emission are 21%, 50%, 79%, and 63% for IRDCs, HMPOs, MMSs, and UCHIIs, respectively (Table 3.4). The detection rate tends to increase as the central object evolve from IRDCs to HMPOs to UCHIIs. We compared our results with those of previous H_2O maser surveys toward various samples. Wang et al. (2006) observed H_2O maser emission toward 140 IRDC cores in the catalog of Rathborne et al. (2006) with the Very Large Array (VLA), and detected the emission in 17(12%) sources at a typical 1σ noise level of 0.1 Jy. Chambers et al. (2009) also surveyed all 190 IRDCs in the same catalog with the Green Band telescope (GBT) at a noise level of 0.05 Jy (1σ) and gave a detection rate of 35%. The detection rates of H_2O maser emission toward HMPOs were roughly 50%. Sridharan et al. (2002) reported a detection rate of 42% towards 69 HMPOs with a similar sensitivity to ours. We also obtained a very similar rate of 46% for their 69 sources in our sample. Kim et al. (2016) acquired a detection rate of 45% toward 299 red MSX sources (RMSs), which are HMPO candidates. Urquhart et al. (2011) also detected H_2O maser emission at a rate of 52% from 275 RMSs, which are in protostellar stage, with a 1 σ level of $\sim$0.12 Jy. The detection rate of UCHIIs is 63%, which is higher than those in IRDCs and HMPOs. Churchwell et al. (1990) searched for H_2O maser emission toward 84 UCHIIs and detected the emission at a rate of 67%. Kim et al. (2016, in prep.) obtained the same detection rate for 103 UCHIIs, including many sources in the sample of Churchwell et al. (1990).. Therefore the detection rates of H_2O maser emission in the present study appear to be comparable to those of the previous surveys.

Class I Methanol Masers

We detected 44 GHz class I CH_3OH maser emission toward IRDCs, HMPOs, MMSs, and UCHIIs at detection rates of 22%, 39%, 92%, and 34%, respectively (Table 3.4). The detection rate for IRDCs is significantly lower than those of HMPOs and UCHIIs, and there is no apparent difference between the detection rates of HMPOs and UCHIIs. We carried out comparison study with the detection rate of 44 GHz maser. There is a deficiency of a large 44 GHz maser survey toward IRDCs. Fontani et al. (2010) searched 44 GHz CH_3OH maser toward 88 HMPOs and obtained detection rate of 31% with a 1 σ noise level of $\sim$0.3 Jy. Kim et al. (2016) surveyed 44 GHz maser toward 299 RMSs and gave a detection rate of 28% with a similar sensitivity to this survey. Kim et al(2016) observed 44 GHz maser emission toward 103 UCHIIs at a similar sensitivity to ours, and offered a detection rate of 48%.

The detection rates of 95 GHz class I CH_3OH maser emission are 21%, 31%, 71%, and 29% for toward IRDCs, HMPOs, MMSs, and UCHIIs, respectively. We found no significant difference between the detection rates of HMPOs and UCHIIs, which are higher than that of IRDCs. Fontani et al. (2010) searched for 95 GHz CH_3OH maser toward 88 HMPOs and obtained a detection rate of 13% with a 1 σ noise level of $\sim$0.7–0.8 Jy. This value is much lower than our result. Kim et al. (2016) surveyed 95 GHz maser toward 299 RMSs and gave a detection rate of 23% with a similar sensitivity to ours. Chen et al. (2012) observed 95 GHz maser emission toward 214 GLIMPSE point sources associated with the Bolocam Northern Galactic Plane Survey (BGPS) clumps and gave a detection rate of 29% with a 1 σ noise

level of 1.0 Jy. Gan et al. (2013) also made a survey of 95 GHz maser toward molecular outflow sources, yielding a detection rate of 22%.

New Detections

We compared our detections of the 95 GHz CH_3OH maser with the previous survey (Val'tts et al., 2000; Chen et al., 2011; Gan et al., 2013). The adopted search radius is $30''$ considering Mopra 22m telescope(beamsize of $52''$). We identified new detections toward 24(89%) of 27, 37(88%) of 42, 62(76%) of 82, and 22(73%) of 30 for IRDCs, HMPOs, MMSs, and UCHIIs, respectively. The new detections are marked as "Y" in Table 3.5–3.8.

3.3.2 Maser Line Properties

Table 3.9–3.12 presents the informations of H_2O and CH_3OH masers that we detected. We listed the line parameters of the peak velocity($v_{\rm p}$), the peak flux density($S_{\rm p}$), the integrated flux density($\int S_v dv$), and the minimum and maximum of the velocity over which the maser lines are distributed above 3σ level($v_{\rm min}$ and $v_{\rm max}$), and including velocity range($v_{\rm range}$). In Table 3.15 we summarized the measurements of each maser lines with the mean, median, minimum, and maximum values of $S_{\rm p}$, the relative peak velocity with respect to the systemic velocity ($v_{\rm rel}$), and $v_{\rm range}$.

Water Masers

We detected 22 GHz H_2O maser emission toward 27, 67, 106, and 65 source for IRDCs, HMPOs, MMSs, and UCHIIs, respectively. The median values of the peak flux densities are 8.6, 8.6, 27.9, and 24.4 Jy and the maximum values are 458.2, 691.8, 7690.4, and 6973.7 Jy for IRDCs, HMPOs, MMSs, and UCHIIs, respectively. Thus, we found an increasing trend of the peak flux density of H_2O maser emission from IRDCs(and HMPOs) to UCHIIs. There is no significant difference among the $v_{\rm rel}$ distributions of the individual samples. A large percentage of the 22 GHz H_2O maser-detected sources in each sample has $v_{\rm range}$ <20 km s^{-1}, namely, 85%, 69%, 53%, and 63% for IRDCs, HMPOs, MMSs, and UCHIIs, respectively. The medians of the velocity ranges are 1.7, 10.1, 16.2, and 14.5 km s^{-1} for IRDCs, HMPOs, MMSs, and UCHIIs, respectively. We investigated the presence of high-velocity (>30 km s^{-1}) H_2O maser features. The detection rates are 37% (10), 18% (12), 35% (32), and 28% (18) for IRDCs, HMPOs, MMSs, and UCHIIs, respectively. We compared the isotropic maser luminosity with the velocity range for all the detected maser sources. Figure 3.6 shows that there is a good correlation between the two parameters all three maser species. Similar trend has been reported in previous studies on 22 GHz water maser (Anglada et al., 1996) and 6.7 GHz methanol maser (Breen et al., 2011).

Class I Methanol Masers

The CH_3OH maser emission was detected toward 29, 52, 106, and 35 sources at 44 GHz and 27, 42, 82, and 30 sources at 95 GHz for IRDCs,

HMPOs, MMSs, and UCHIIs, respectively. The medians of the peak flux densities of 44 GHz masers are 6.7, 6.8, 8.8, and 8.4 Jy, and the maximum values are 104.9, 560.3, 340.3, and 63.7 Jy for IRDCs, HMPOs, MMSs, and UCHIIs, respectively. As for 95 GHz masers, the medians are 5.0, 4.0, 8.2, and 6.4 Jy and the maximum values are 53.1, 91.2, 203.9, and 41.4 Jy for IRDCs, HMPOs, MMSs, and UCHIIs, respectively. The peak velocities of both masers are almost alwaysies very close to the systemic velocity, except some MMSs (Figure 3.2 (a)). The medians of the relative peak velocities of both masers are less than 1 km s^{-1}. With a criterion of 1 km s^{-1} for the velocity range by Ellingsen et al. (2005), percentages of the broad spectral feature appearance for 44/95 GHz masers are 59%/67%, 75%/67%, 88%/80%, and 86%/87% for for IRDCs, HMPOs, MMSs, and UCHIIs, respectively. (c.f.76%/78% for RMSs) They might include quasi-thermal emission, which means maser emission may be blended with the thermal component.

Figure 3.2 compares 44 GHz masers with 95 GHz masers in the relative peak velocity, the peak flux density, and the isotropic maser luminosity. There appear to be strong correlations in all three parameters between the too masers. The least-squares fitting results are as follows:

$$\mathrm{V_{rel}} = 1.01(\mathrm{V_{rel}}) - 0.04 \ (\rho = 0.87), \tag{3.2}$$

$$\log(\mathrm{S_{p,95}}) = 0.91\log(\mathrm{S_{p,44}}) - 0.12 \ (\rho = 0.85), \tag{3.3}$$

$$\log(\mathrm{L_{95}}) = 0.98\log(\mathrm{L_{44}}) + 0.09 \ (\rho = 0.91). \tag{3.4}$$

Val'tts et al. (2000) and Jordan et al. (2015) estimated the peak flux density ratio of 44 and 95 GHz masers to be 0.31–0.32, while Kang et

al. (2015) derived the ratio to be about 0.71. Our result of best fit in linear scale plot is $S_{\mathrm{p},95} = 0.43 \times S_{\mathrm{p},44} + 2.16$ ($\rho = 0.79$).

3.3.3 Individual Sources

G020.80–00.14

The 22 GHz maser emission was detected with 16.3 Jy peak similar to ATCA observations(Walsh+14) of 12 Jy peak, conducted on same epoch with ours. For class I CH_3OH maser, not the 44 GHz but the 95 GHz maser was emitted. The peak flux density of 95 GHz is 1.7 Jy comparable to 1.5 Jy by Chen et al. (2012). Previous observations for 44 GHz GHz was carried out by Jordan et al.(2008) using Haystack 37m telescope with rms noise level of 4.6 Jy, which are larger than our work by an order. They could not detect 44 GHz maser emissions.

IRAS18162–2048

IRAS18162–2048 also known as HH 80-81 only has EHV dominant blue shifted components at ~ -80 km s^{-1}offset from the systemic velocity(20 km s^{-1}). Furuya et al. (2003) reported the component around +10 km s^{-1} is the strongest one. About ten years later the H_2O maser observation made by Urquhart et al. (2011) showed that most emission are concentrated around at 40–50 km s^{-1}

3.4 Analysis and Discussion

3.4.1 Luminosity

In order to examine the relationship of maser emission with other indicators of star formation, we looked for correlations between the isotropic maser luminosity ($L_{\rm maser}$) and the bolometric luminosity the central (proto)stars ($L_{\rm bol}$). The maser luminosity is calculated using the total integrated maser flux density and the source distance in the same way as in Kim et al. (2016a). The source distance and bolometric luminosity adopted for each source are presented in Table 3.3. The results of least-square analyses between the two parameters are listed in Table 3.16. For 22 GHz H_2O and 44/95 GHz CH_3OH masers, we obtained positive good correlations, although the bolometric luminosity ranges of the individual samples are different. For each sources in different evolutionary stages with maser emissions, we plot together the isotropic luminosities of three masers against $L_{\rm bol}$) (Figure 3.3). The maser luminosity tends to increase with the bolometric luminosity for all maser species. Linear regression analyses yield the following relations with correlation coefficients of 0.52–0.58:

$$\log(\mathrm{L_{22}}) = 1.16\ \log(\mathrm{L_{bol}}) - 9.89\ (\rho = 0.58), \tag{3.5}$$

$$\log(\mathrm{L_{44}}) = 0.94\ \log(\mathrm{L_{bol}}) - 9.19\ (\rho = 0.52), \tag{3.6}$$

$$\log(\mathrm{L_{95}}) = 0.94\ \log(\mathrm{L_{bol}}) - 9.00\ (\rho = 0.53). \tag{3.7}$$

There are a number of previous studies on the relationship between the isotropic maser luminosity and the bolometric or far infrared(FIR) luminosity of the central object. For H_2O masers, the relation between $L_{\rm H_2O}$ and $L_{\rm bol}$ was proposed by Furuya et al. (2003) ($\rho = 0.28$) for

low-mass YSOs ($L_{\rm bol} \sim 0.1 - 10^2 L_{\odot}$), Bae et al. (2011) ($\rho = 0.72$) for intermediate-mass YSOs ($L_{\rm bol} \sim 10^1 - 10^4 L_{\odot}$), Kim et al. 2016 ($\rho = 0.54$) for high-mass YSOs($L_{\rm bol} \sim 10^3 - 10^6 L_{\odot}$), and Felli et al. (1992) ($\rho = 0.7$) for low-to high-mass YSOs ($L_{\rm bol} \sim 10^1 - 10^6 L_{\odot}$). For comparison, we plot our data together with H_2O maser data of low-and intermediate-mass YSOs from Furuya et al. (2003) and Bae et al. (2011). We obtained a relation of $L_{22} = 5.40 \times 10^{-10} (L_{\rm bol})^{1.02}$ with a considerably higher correlation coefficient ($\rho = 0.75$). which is consistent with the results of the previous studies such as Felli et al. (1992) and Bae et al. (2011).

In the case of 44 GHz CH_3OH masers, the correlation between L_{44} and $L_{\rm bol}$ was reported by Kalenskii et al. (2013) for low-mass YSOs ($L_{\rm FIR} \sim 0.1 - 10^2 L_{\odot}$) and Bae et al. (2011) for intermediate-mass YSOs ($L_{\rm bol} \sim 10^1 - 10^3 L_{\odot}$). We combine our data with the data of Kalenskii et al. (2013) and Bae et al. (2011) to widen the range of $L_{\rm bol}$. The best-fit line of 44 GHz data is $L_{44} = 3.94 \times 10^{-10} (L_{\rm bol})^{0.98} (\rho = 0.65)$. For 95 GHz CH_3OH masers, Gan et al. (2013) presented a relation of $L_{95} = 1.74 \times 10^{-8} (L_{\rm bol})^{0.51} (\rho = 0.66)$ from low- to high-mass YSOs ($L_{\rm bol} \sim 10^1 - 10^6 L_{\odot}$). The slope is almost twice lower than ours, although the correlation coefficient is very similar.

3.4.2 Clump Mass

We search for the dense clumps associated with our targets using the 870 μm continuum data of APEX Telescope Large Area Survey of the Galaxy(ATLASGAL) with a threshold radius of $30''$. For each sample, we find at least $\sim 75\%$ of the sources in the ATLASGAL coverage are

associated with the ATLASGAL sources.The sources with associated ATLASGAL clumps have higher detection rates then those without associated ATLASGAL clumps (Table 3.13). Assuming that 870 μm emission is optically thin, we calculate the ATLASGAL clump mass using the following equation:

$$M_{\rm clump} = \frac{S_{\rm int} D^2}{k_\nu B_\nu(T_{\rm d}) R_{\rm d}}. \tag{3.8}$$

Here $S_{\rm int}$ is the integrated flux density, D is the distance to the source, k_ν is the mass absorption coefficient per unit mass of dust, $B_\nu(T)$ is the Planck function, $T_{\rm d}$ is the dust temperature, and $R_{\rm d}$ is the dust−to−gas mass ratio. We take $S_{\rm int}$ from the ATLASGAL catalog and adopt k_ν=1.85 cm^2 g^{-1}, $T_{\rm d}$=20 K, and $R_{\rm d}$=0.01 as in Schuller et al. (2009).

For each sample, we perform least-square regression of the clump mass $M_{\rm clump}$ versus the maser luminosity $L_{\rm maser}$ (Table 3.16). The fit results show that the correlation coefficients of 44 and 95 GHz CH_3OH masers are higher than that of H_2O maser except IRDCs. Figure 3.4 presents a log–log plot of $M_{\rm clump}$ versus $L_{\rm maser}$ for the entire sample. The equations of best linear fit are following:

$$\log(\mathrm{L}_{22}) = 1.23\ \log(\mathrm{M}_{\rm clump}) - 8.61\ (\rho = 0.66), \tag{3.9}$$

$$\log(\mathrm{L}_{44}) = 1.06\ \log(\mathrm{M}_{\rm clump}) - 8.26\ (\rho = 0.73), \tag{3.10}$$

$$\log(\mathrm{L}_{95}) = 1.07\ \log(\mathrm{M}_{\rm clump}) - 8.01\ (\rho = 0.78). \tag{3.11}$$

Chen et al. (2012) found a strong correlation ($\rho = 0.84$) with a slope of 0.81 between the isotropic luminosity of 95 GHz CH_3OH maser emission and the mass of the Bolocam Galactic Plane Survey (BGPS)

clump. Similar correlations between L_{95} and the BGPS clump mass were measured for extended green objects (EGOs) by Chen et al. (2011)($\rho = 0.6$) and molecular outflow sources by Gan et al. (2013)($\rho = 0.73$) with lower slopes of 0.5 and 0.6 in the log scale fit, respectively.

We investigate the relationship between the maser luminosity and the peak H_2 column density of the associated ATLASGAL clumps. The peak H_2 column density per beam can be derived by :

$$N_{\mathrm{H_2}} = \frac{S_{\mathrm{p}}}{\Omega_{\mathrm{b}} \mu_{\mathrm{H_2}} m_{\mathrm{H}} k_{\nu} B_{\nu}(T_{\mathrm{d}}) R_{\mathrm{d}}}, \tag{3.12}$$

where S_{p} is the peak flux density, Ω_{b} is the beam solid angle, $\mu_{\mathrm{H_2}}$ is the mean molecular weight, and m_{H} is the mass of hydrogen atom. We adopt Ω_{b}=6.8 $\times$ 10^{-9} Sr and $\mu_{\mathrm{H_2}}$=2.8 (e.g., Kauffmann et al., 2008). We carry out the least square regression analysis of each sample and the best fit results are listed in Table 3.16.

Figure 3.5 plots $N_{\mathrm{H_2}}$ against the luminosity of each maser emission for the entire sample. The lines of best fit result are given by:

$$\log(\mathrm{L_{22}}) = 2.03 \log(\mathrm{N_{H_2}}) - 51.57 \ (\rho = 0.42), \tag{3.13}$$

$$\log(\mathrm{L_{44}}) = 1.48 \log(\mathrm{N_{H_2}}) - 39.08 \ (\rho = 0.41), \tag{3.14}$$

$$\log(\mathrm{L_{95}}) = 1.47 \log(\mathrm{N_{H_2}}) - 38.63 \ (\rho = 0.49). \tag{3.15}$$

We also examine the dependence between the integrated flux density($\int S_{\nu}\, dv$) of each maser emission and $N_{\mathrm{H_2}}$. Because both $\int S_{\nu}\, dv$ and $N_{\mathrm{H_2}}$ are independent of distance and other physical parameters of the sources, the relationship is meaningful for the future maser survey based on

ATLASGAL sources (Chen et al., 2012). The linear regression analysis for the entire sample gives the best fit line of

$$\log(\int S_{22}\ dv) = 1.75\ \log(N_{H_2}) - 38.98\ (\rho = 0.42), \tag{3.16}$$

$$\log(\int S_{44}\ dv) = 1.34\ \log(N_{H_2}) - 29.92\ (\rho = 0.48), \tag{3.17}$$

$$\log(\int S_{95}\ dv) = 1.37\ \log(N_{H_2}) - 30.86\ (\rho = 0.59). \tag{3.18}$$

The linear fit for H_2O maser emission has a slight higher slope and a lower correlation coefficient than those of 44 and 95 GHz CH_3OH masers. The threshold column density for star formation in local clouds is generally $\sim 100\ M_\odot\ pc^{-2}$ (Lada et al., 2010; Heiderman et al., 2010), corresponding to $4.5 \times 10^{21} cm^{-2}$. Filling this threshold of column density into the above relations, we can obtain lower limits of 0.12, 0.11, and 0.07 Jy km s^{-1} for 22, 44, and 95 GHz masers, respectively. Furthermore, maser sources associated with the ATLASGAL sources have column densities larger than $\sim 2 \times 10^{22} cm^{-2}$.

3.4.3 NH_3 $\Delta v(1,1)$ and T_k

Using the available NH_3 data from the literatures (see the Table 3.3), we derive the physical properties of the dense gas environments where massive stars are forming. We find the associated NH_3 clumps of 260 sources in a search radius of $30''$ and 40% of them contained maser emissions. The measured linewidths (FWHM) of the $NH_3(1,1)$ lines for each sample are divided into two groups, *narrow* and *wide* ones. The *narrow* group contains IRDCs, RMSs, and HMPOs with medians

of 1.75, 1.73, and 1.79 km s^{-1}, respectively, which agree with the results of Wienen et al. (2012) and Chira et al. (2013). The *wide* group includes MMSs and UCHIIs with medians of 2.62 and 2.52 km s^{-1}, respectively. For each sample, we investigate any difference among the NH_3 linewidth distributions of 22, 44, and 95 GHz maser sources, but find no significant difference. Figure 3.7 shows the NH_3 (1,1) linewidth distribution of each maser species for the individual samples. There is a clear difference between the linewidth distributions of narrow and wide groups. To examine the statistical significance in the linewidth distributions, we perform a Kolmogorov-Smirnov(KS) test for different samples. The KS test indicates that both *narrow* and *wide* groups are significantly different in the linewidth distributions ($p = 2.4 \times 10^{-10}$).

We compare the distributions of kinetic temperature for maser-detected sources in each sample. The kinetic temperature cannot be derived for 5 of the 260 sources due to the non-detection of NH_3 (2,2) line emission. We estimate the rotation temperature $T_{\rm rot}$ using the below equation (Ho et al., 1983):

$$T_{\rm rot} = -41.5 \left(\ln \left\{ -\frac{0.282}{\tau_{\rm m}(1,1)} \ln \left[1 - \frac{T_b(2,2)}{T_b(1,1)} \left(1 - e^{-\tau_{\rm m}(1,1)} \right) \right] \right\} \right)^{-1} \tag{3.19}$$

with the optical depth of the (1,1) main line, $\tau_{\rm m}(1,1)$, and the brightness temperatures, $T_{\rm b}$, of the (1,1) and (2,2) inversion transitions. The kinetic temperature is related to the rotational temperature through the following equation citepswi05.

$$T_{\rm rot} = T_{\rm kin} \left\{ 1 + \frac{T_{\rm kin}}{T_{\rm o}} \ln \left[1 + 0.6 \, \exp(1 - 15.7/T_{\rm kin}) \right] \right\}, \tag{3.20}$$

where $T_o = (E(2,2) - E(1,1))/k_B \approx 41.5K$. It is noticeable that if the kinetic temperature is much higher than T_o, the rotational

temperature may be significantly underestimated (Walmsley et al., 1983). The medians of kinetic temperature are 16.4, 21.1, 22.8, 25.7, and 28.5 K for IRDCs, RMSs, HMPOs, MMSs, and UCHIIs, respectively. The KS test on combinations of the kinetic distribution for each objects showed that $T_{\rm kin}$ is increasing as the source evolves from IRDCs,RMSs,HMPOs to MMSs and UCHIIs. MMSs and UCHIIs are indistinct in the kinetic temperature distribution..

We compare the maser luminosity with the linewidth and kinematic temperature of the associated NH_3 clump. and and the physical physical properties from associated NH_3 data. H_2O maser sources have a moderate positive correlation ($\rho = 0.48$) between the NH_3 linewidth and maser luminosity, while 44 and 95 GHz CH_3OH masers do not show any significant correlation (Fig. 3.8). The slope of the best fit for H_2O masers is 4.51, which is comparable to the result of Anglada et al. (1996). On the other hand, we find no correlation between the kinetic temperature and any maser luminosity (Fig. 15).

3.4.4 Luminosity to Mass Ratio

The luminosity–mass ($L_{\rm bol}$–$M_{\rm clump}$) plots are known to be a well-established diagnostic tool to separate different evolutionary phases of star formation both in low- and high-mass star-forming regions (Saraceno et al., 1996; Molinari et al., 2008). We compare the clump mass with the bolometric luminosity toward different maser sources. The $L_{\rm bol}/M_{\rm clump}$ ratios are usually higher for maser-detected sources than for maser-nondetected sources. The medians of the ratios are about 14.1 and $\sim$8.5 $L_\odot/M_\odot$ for the former and the latter groups,

respectively, with $p \simeq 0.004$ by the KS test. The medians of the L_{bol}/M_{clump} ratios for maser-detected sources are 1.7, 10.1, 11.5, 18.3, and 27.5 $L_{\odot}/M_{\odot}$ toward IRDCs, RMSs, HMPOs, MMSs, and UCHIIs, respectively. According to KS tests for combinations of five samples, we can separate them into three groups: IRDC, RMSs+HMPOs, MMSs+UCHIIs. IRDCs has statistically different($p \leqq 4.1 \times 10^{-5}$) and the lowest $L_{\odot}/M_{\odot}$. Both group of RMSs+HMPOs and MMSs+UCHIIs significantly different($p \leqq 0.001$) in L_{bol}/M_{clump} distribution and there are no differences in its distribution within a group.

We perform the KS tests to examine the significance of differences among the L_{bol}/M_{clump} distributions for different combinations of 5 samples in each maser with a significance level of 0.01. For H_2O maser sources, there are three groups that have significant differences between their L_{bol}/M_{clump} distributions with a significant level ($p < 0.001$): IRDCs,RMSs+HMPOs+MMSs, MMSs+UCHIIs. In the case of 44 GHz CH_3OH maser sources, they are divided into three groups with a statistical significance ($p < 0.002$): IRDCs, RMSs+HMPOs, MMSs+UCHIIs. As for 95 GHz maser sources, we obtain the same result as for 44 GHz maser. We attempt the same analyses for the sources detected in only one maser species. Figure 3.10*a* plots the L_{bol}/M_{clump} distributions of 5 samples for the sources detected only at 22 GHz. There is no difference in the distributions of different samples. Figure 3.10*b* shows the same distributions for the sources detected only at 44 GHz. Although there seems to be distinct three group in the distribution, it is impossible to test a statistical significance due to a deficiency of source number.

Urquhart et al. (2015) proposed another evolutionary model of the

maser luminosity–mass ratio ($L_{maser}/M_{\rm clump}$) based on the correlation of 6.7 GHz methanol maser luminosity and bolometric luminosity. Adopting this model to the observed 3 maser species in the present studty, we compare the $\rm L_{\it maser}/M_{clump}$ distributions for different combinations of the 5 samples . There is no statistical difference for 22 GHz H_2O maser sources. For class I CH_3OH maser sources, there are statistically significant differences among a few combinations, including RMSs+HMPOs+MMSs vs. UCHIIs and IRDCs+RMSs+HMPOs vs. MMSs However, it is still unclear whether these differences are reflecting the evolutionary effects or not.

3.4.5 Virial Mass

The virial parameter (α), defined as the ratio of virial mass to clump mass, is commonly used to investigate whether a clump is gravitational bound or stable to collapse. The virial mass or virial parameter can be calculated from the clump size and the linewidth (FWHM) of NH_3(1,1) assuming a constant density distribution by the following equation (Bertoldi et al., 1992):

$$\begin{aligned}\alpha &= \frac{M_{\rm vir}}{M} = \frac{5}{8{\rm ln2G}}\frac{R_{eff}{\Delta v_{\rm TOT}}^2}{a_1 a_2 M} \\ &= \frac{1}{a_1 a_2}\left(\frac{R_{eff}}{\rm pc}\right)\left(\frac{\Delta v_{\rm TOT}}{\rm km\ s^{-1}}\right)^2\left(\frac{M}{210 M_\odot}\right)^{-1}, \qquad (3.21)\end{aligned}$$

$$a_1 = \frac{1-p/3}{1-2p/5}\ \text{for p} < 2.5, \quad \text{a}_2 = \text{y}\frac{\text{arcsinh}(\text{y}^2-1)^{\frac{1}{2}}}{(\text{y}^2-1)^{\frac{1}{2}}} \qquad (3.22)$$

where R_{eff} is the effective radius of the clump, G is the gravitational constant, a_1 is the correction for the power-law density distribution $\rho(r) \sim r^{-p}$, a_2 accounts for the effect of the clump ellipticity, and y is the aspect ratio of the clump. We adopt the mean power value

determined by Mueller et al. (2002), <p>=1.8 (i.e. a_1=1.43), by modeling the 350 μm continuum emission maps of 31 massive star-forming clumps, and the mean aspect ratio of the associated ATLASGAL clumps in each sample: y=1.67, 1.55, 1.45, 1.65, and 1.53 corresponding to a_2=1.34, 1.27, 1.23, 1.32, and 1.26 for IRDCs, RMSs, HMPOs, MMSs, and UCHIIs, respectively. We make a correction for the measured linewidth of the NH_3(1,1) transition to estimate a linewidth of the average molecules according to the equation of Fuller et al. (1992):

$$\Delta v^2_{\rm TOT} = \Delta v^2_{\rm T} + \Delta v^2_{\rm NT} = \Delta v^2_{\rm obs} + 8\ln 2 \, \frac{\rm k_b T_{kin}}{\rm m_H} \left(\frac{1}{\mu_{\rm p}} - \frac{1}{\mu_{\rm NH_3}} \right). \quad (3.23)$$

Here $\Delta v_{\rm obs}$ is the observed linewidth, k_b is the Boltzmann constant, $T_{\rm kin}$ is the kinetic temperature of gas, taken to be 20 K, $\mu_{\rm p}$ and $\mu_{\rm NH_3}$ are the mean molecular mass of molecular hydrogen and ammonia taken as 2.33 and 17, respectively.

Figure 3.11 plots the virial parameter α against $M_{\rm clump}$ in log–log scales for all 224 sources that have the associated ATLASGAL sources and detectable NH_3 line emission. The clumps below $\alpha = 1$ line are gravitationally unstable when we do not account for the magnetic energy. If we are allowing for an equal amount of magnetic and kinetic support (Bertoldi et al., 1992), clumps with $\alpha < 2$ are supercrtical and unstable to collapse. The virial parameter is less than 1 for 182 (81%) sources while it is larger than 2 only for 12 (5%) soruces. For maser-detected sources, the portion of the sources with $\alpha \geq 1$ in each sample tends to decrease as the central sources evolve: 33%, 30%, 24%, 25%, and 17% for IRDCs, RMSs, HMPOs, MMSs, and UCHIIs, respectively. We cannot find such a trend in maser-nondetected sources. Furthermore, more massive clumps are more virialized and sources

with maser emission are less gravitationally bound than those without it. The sources with and without maser emission have mean α values of 0.90 and 0.37, respectively. The difference is statistically significant according to the KS test, $p = 7.5 \times 10^{-9}$. These findings suggest that massive clumps with maser emission are affected by more feedback from the central objects or the surroundings than those without it.

We also examine the gravitational stability of the associated ATLASGAL clumps by the Larson's second law. This analysis aims to investigate whether the presence of maser can affect the stability of the clump and there is an evolutionary effect depending on the associated maser species. Figure 3.12 plots $\Delta v(NH_3(1,1))$ versus M_{clump} in log–log scale. The original larson's relation is maked as dotted line. The most sources are locaed below the larson'd line, which is gavitationally unstable to copplapse. Both clumps with and without maser emission show moderate ($\rho = 0.4$) correlations and the solpe of the best fit line for both samples are not significnatly different.

3.4.6 Evolutionary Sequence

Figure 3.13 displays plots of L_{maser}/L_{bol} against L_{bol}/M for the 224 maser sources in the combined catalog. The linear regression fit of their distributions are similar each other: slopes of –1.5 to –1.3 and correlation coefficients of 0.56–0.75. The distribution of H_2O maser sources are more scattered than those of 44 and 95 GHz CH_3OH class I masers, i.e., 1σ of the slope is 0.14 and 0.08 for H_2O and class I CH_3OH masers, respectively. It is noticeable that IRDCs occupy a

distinct region in upper-left part of each panel for all three masers and UCHIIs reside a lower-right area of the panel of H_2O maser. These plots show that L_{maser}/L_{bol} could be a another indicator of massive star formation. It should be noted that they can be biased because the bolomeric lumminosity appears both in the ordinate and the abscissa. In the Figure 3.14, we plot L_{maser} versus L_{bol}/M_{clump}. These plots show no trend seen in Figure 3.13 but increasing tendency of the maser luminosity against L_{bol}/M_{clump} at the early phase of $< 10(L_{\odot}/M_{\odot})$.

The flux density ratio of different class I CH_3OH maser transitions can be an excellent probe of the physical condition of the maser emitting region (McEwen et al., 2014). We compare the peak flux density ratio of 44 and 95 GHz masers $S_{p,44}/S_{p,95}$ with the peak H_2 column density and L_{bol}/M_{clump} to test whether there is any relation between the ratio and the physical parameters. In the Figure 3.15*a*, we plot the flux density ratio against N_{H_2}. There is no linear trend in the distributions but we find that the peak of $S_{p,44}/S_{p,95}$ value monotonically decreases from ~ 10 to ~ 1 as the peak column density grows up. Figure 3.15*b* plots the flux ratio versus L_{bol}/M_{clump}. The maximum value of $S_{p,44}/S_{p,95}$ appears to increase until the phase goes up to ~ 10 $L_{\odot}/M_{\odot}$ and then starts to decrease. The modeling of class I CH_3OH masers by McEwen et al. (2014) predicts the $S_{p,44}/S_{p,95}$ ratios for various physical conditions. The estimated $S_{p,44}/S_{p,95}$ ratios range from 0.4 to 19.0 with an average of 1.2, which limits the density regimes to $\sim 10^5$ from Figure 5 of McEwen et al. (2014). The H_2 volume number density can be computed by using the mass and size of the associated ATLASGAL clump determined in § 4.2. The average volume density is 3×10^4, which is comparable to the model predictions.

3.5 Summary

We performed simultaneously surveys of 22 GHz H_2O and 44 and 95 GHz class I CH_3OH masers toward 483 massive YSOs. Our sample consists of 130 IRDCs, 135 HMPOs, 116 MMSs, and 103 UCHIIs and covers a wide range of evolutionary phases. The main findings of this study are as follows.

1. The overall detection rates are 32%, 61%, 96%, and 67% toward IRDCs, HMPOs, MMSs, and UCHIIs, respectively. We identified 145 new detections of 95 GHz CH_3OH maser. IRAS18162–2048 in the sample of UCHIIs is the only H_2O maser source with dominant blue shifted components.

2. The 22 GHz H_2O masers show significant differences in the line parameter distributions of different evolutionary stages but both class I CH_3OH masers are not. As the central source evolves, the peak flux density and the velocity range of H_2O maser tend to increase. The velocity ranges of both class I CH_3OH masers reveal a weak increasing tendency with evolutionary phase.

3. The 44 and 95 GHz class I CH_3OH masers have very similar properties on a wide range of evolutionary stage. The line parameters of both lines have a strong correlations in the relative peak velocity, the peak flux density, and the isotropic maser luminosity. The slope of dependence between the peak flux densities ($S_{\rm p,95}/S_{\rm p,44}$) of the two masers is 0.43. Seven sources that have detections of both lines are different $v_{\rm p}$ by > 2 km s^{-1}. Their spectra appear to have multiple components of narrow maser lines along with broad thermal-like

features.

4. We examined the relationship between the maser luminosity and physical condition of parental clumps(cores). We found good ($\rho >$ 0.5) correlations between the maser luminosity and the bolometric luminosity and the clump mass for all three masers.

5. As for the linewidth (FWHM) of $NH_3(1,1)$, five samples are divided into two distinct groups: *narrow* and *wide* groups. The former group consists of IRDCs, RMSs and HMPOs with a mean of 1.76 km s^{-1}, while the latter group contains MMSs and UCHIIs with a mean of 2.57 km s^{-1}. Two subgroup are statistically different by KS test. There is no difference in the combinations of subgroups between presence of maser emissions. As for the kinematic temperature, we found a weak increasing trend with evolutionary phase.

6. Using the $L_{\rm bol}/M_{\rm clump}$ ratio, we compared the distribution on each type of central object. Generally we can divide five different type of source into three distinct group (IRDCs / RMSs and HMPOs / MMSs and UCHII) in $L_{\rm bol}/M_{\rm clump}$ space. Sources associated with any maser emission are clearly separated into the same three group as well. There is no robust difference in the distribution on the combinations with each maser emission.

7. Our investigation on the virial parameter against $M_{\rm clump}$ suggested that ATLASGAL clumps with any maser emission are more gravitationally stable than those with no maser emissions in a wide range of clump mass.

8. We find that $L_{\rm maser}/L_{\rm bol}$ appear to decrease as driving source

evolves. The peak of flux ratio($S_{p,44}$ /$S_{p,95}$) for class I CH_3OH maser seem to have no significant variation as for the evolutionary sequence.

Bibliography

Anglada G., Estalella R., Pastor J., et al. 1996, ApJ, 463, 205

Battersby, C., Bally, J., Jackson, J. M., et al. 2010, ApJ, 721, 222

Bae, J.-H., Kim, K.-T., Youn, S.-Y., et al. 2011, ApJS, 196, 21

Batrla W., Menten K. M. 1988, ApJ, 329, L117

Bayandina O. S., Val'tts I. E., Larionov G. M. 2012, Astron. Rep., 56, 553

Bertoldi, F., & McKee, C. F. 1992, ApJ, 395, 140

Beuther, H., Schilke, P., Menten, K. M., et al. 2002, ApJ, 566, 945

Breen, S. L., Caswell, J. L., Ellingsen, S. P., & Phillips, C. J. 2010a, MNRAS, 406, 1487

Breen, S. L., Ellingsen, S. P., Caswell, J. L., et al. 2010b, MNRAS, 401, 2219

Breen S. L., Ellingsen S. P., Caswell J. L., et al. 2011, ApJ, 733, 80

Breen, S. L., Fuller, G. A., Caswell, J. L., et al. 2015, MNRAS, 450, 4109

Byun, D.-Y., Kim, K.-T., & Bae, J.-H. 2012, in IAU Symp. 287, Cosmic Masers from OH to H_0 (Cambridge: Cambridge Univ. Press), 284

Carey, S. J., Clark, F. O., Egan, M. P., et al. 1998, ApJ, 508, 721

Carey, S. J., Feldman, P. A., Redman, R. O., et al. 2000, ApJ, 543, L157

Carral, P., Kurtz, S., Rodrguez, L. F., et al. 1999, RMxAA, 35, 97

Casoli, F., Combes, F., Dupraz, C., Gerin, M., & Boulanger, F. 1986, A&A, 169, 281

Caswell, J. L., & Phillips, C. J. 2008, MNRAS, 386, 1521

Caswell J. L., Breen S. L., 2010, MNRAS, 407, 2599

Chambers, E. T., Jackson, J. M., Rathborne, J. M., et al. 2009, ApJ, 181, 360

Chen X., Ellingsen S. P., Shen Z.-Q., et al. 2011, ApJS, 196, 9

Chen, X., Ellingsen, S. P., He, J.-H., et al. 2012, ApJS, 200, 5

Chira R.-A., Beuther H., Linz H., et al. 2013, A&A, 552, A40

Churchwell, E., Walmsley, C. M., & Cesaroni, R. 1990, A&AS, 83, 119

Codella C., Lorenzani A., Gallego A. T., et al. 2004, A&AS, 417, 615

Cragg, D. M., Johns, K. P., Godfrey, P. D., et al. 1992, MNRAS, 259, 203

Cragg, D. M., Sobolev, A. M., & Godfrey, P. D. 2002, MNRAS, 331, 521

Cyganowski, C. J., Brogan, C. L., Hunter, T. R., et al. 2009, ApJ, 702, 1615

Devine, K. E., Chandler, C. J., Brogan, C., et al. 2011, ApJ, 733, 44

Egan, M. P., Shipman, R. F., Price, S. D., et al. 1998, ApJ, 494, L199

Elitzur, M., Hollenbach, D. J., & McKee, C. F. 1989, ApJ, 346, 983

Ellingsen, S. P. 2005, MNRAS, 359, 1498

Ellingsen, S. P., Voronkov, M. A., Cragg, D. M., et al. 2007, in IAU Symp. 242, Astrophysical Masers and their Environments, ed. J. M. Chapman & W. A. Baan (Cambridge: Cambridge Univ. Press), 213

Erickson, N. R., Goldsmith, P. F., Novak, G., Viscuso, P. J., Erickson, R. B., & Predmore, C. R. 1992, IEEE Trans. Microwave Theory Tech., MTT-40, 1

Felli, M., Palagi, F., & Tofani, G. 1992, A&A, 255, 293

Felli, M., Brand, J., Cesaroni, R., et al. 2007, A&A, 476, 373

Fontani, F., Cesaroni, R., & Furuya, R. S. 2010, A&A, 517, A56

Fuller G. A., Myers P. C. 1992, ApJ, 384, 523

Furuya, R. S., Kitamura, Y., Wootten, A., et al. 2003, ApJS, 144, 71

Gan C.-G., Chen X., Shen Z.-Q., et al. 2013, ApJ, 763, 2

Green J. A., Caswell, J. L., Fuller, G. A., et al. 2009, MNRAS, 392, 783

Han, F., Mao, R. Q., Lei, C. M., et al. 1995, PPMtO, 14, 185

Han, F., Mao, R. Q., Lu, J., et al. 1998, A&AS, 127, 181

Han, S.-T., Lee, J.-W., Kang, J., et al. 2008, IJIMW, 29, 69

Heiderman, A., Evans, N. J., II, Allen, L. E., Huard, T., & Heyer, M. 2010, ApJ, 723, 1019

Ho, P., & Townes, C. 1983, ARA&A, 21, 239

Jackson, J. M., Rathborne, J. M.; Shah, R. Y., et al. 2006, ApJS, 163, 145

Jordan, C. H., Walsh, A. J., Lowe, V., et al. 2015, MNRAS, 448, 2344

Kim, K.-T., Byun, D.-Y., Je, D.-H., et al. 2011, JKAS, 44, 81

Kim, C,-H, Kim, K.-T., Park, Y.-S., 2016, ApJS, 00, 00

Kalenskii, S. V., Kurtz, S., & Bergman, P. 2013, ARep, 57, 120

Kang, H., Kim, K.-T., Byun, D.-Y., et al. 2015, ApJS, 221, 6

Kauffmann, J., Bertoldi, F., Bourke, T. L., Evans, II, N. J., & Lee,C. W. 2008, A&A, 487, 993

Kauffmann J., Pillai T., Goldsmith P. F. 2013, ApJ, 779, 185

Kurtz, S., Churchwell, E., & Wood, D. O. S. 1994, ApJS, 91, 659

Kurtz, S., Hofner, P., & Alvarez, C. V. 2004, ApJS, 155, 149

Lada, C. J., Lombardi, M., & Alves, J. F. 2010, ApJ, 724, 687

Lee, S.-S., Byun, D.-Y., Oh, C. S., et al. 2011, PASP, 123, 1398

Lumsden, S. L., Hoare, M. G., Oudmaijer, R. D., & Richards, D. 2002, MNRAS, 336, 621

Lumsden, S. L., Hoare, M. G., Urquhart, J. S., et al. 2013, ApJS, 208, 11

Menten K. M., 1991, ApJ, 380, L75

McEwen, B. C., Pihlström, Y. M., & Sjouwerman, L. O. 2014, ApJ, 793, 133

Molinari S., Pezzuto S., Cesaroni R., et al. 2008, A&A, 481, 345

Mottram, J. C., Hoare, M. G., Urquhart, J. S., et al. 2011, A&A, 525, A149

Mueller, K. E., Shirley, Y. L., Evans, N. J., II, et al. 2002, ApJS, 143, 469

Rathborne, J. M., Jackson, J. M., & Simon, R. 2006, ApJ, 641, 389

Molinari S., Brand J., Cesaroni R., & Palla F., 1996, A&AS, 308, 573

Molinari S., Brand J., Cesaroni R., et al. 1998, A&AS, 336, 339

Molinari, S., Brand, J., Cesaroni, R., & Palla, F. 2000, A&A, 355, 617

Palla F., Brand J., Comoretto G., et al. 1991, A&AS, 246, 249

Perault, M., Omont, A., Simon, G., et al. 1996, A&A, 315, L165

Pestalozzi, M., Minier, V., & Booth, R. S. 2005, A&A, 432, 737

Pestalozzi, M. R., Chrysostomou, A., Collett, J. L., et al. 2007, A&A, 463, 1009

Pillai, T., Wyrowski, F., Carey, S. J., & Menten, K. M. 2006, A&A, 450, 569

Ragan, S. E., Bergin, E. A., & Wilner, D. 2011, ApJ, 736, 163

Ramesh B., Sridharan T. K., 1997, MNRAS, 284, 1001

Rathborne, J. M., Jackson, J. M., & Simon, R. 2006, ApJ, 641, 389

Rathborne, J. M., Jackson, J. M., Zhang, Q., & Simon, R. 2008, ApJ, 689, 1141

Rathborne, J. M., Jackson, J. M., Chambers, E. T., et al. 2010, ApJ, 715, 310

Rosolowsky, E., Dunham, M. K., Ginsburg, A., et al. 2010, ApJS, 188, 123

Sakai, T., Sakai, N., Kamegai, K., et al. 2008, ApJ, 678, 1049

Sanhueza, P., Garay, G., Bronfman, L., et al. 2010, ApJ, 715, 18

Saraceno P., Andre P., Ceccarelli C., et al. 1996, A&A, 309, 827

Schuller, F., Menten, K. M., Contreras, Y., et al. 2009, A&A, 504, 415

Seth, A. C., Greenhill, L. J., & Holder, B. P. 2002, ApJ, 581, 325

Simon, R., Jackson, J. M., Rathborne, J. M., & Chambers, E. T. 2006, ApJ, 639, 227

Sridharan, T. K., Beuther, H., Schilke, P., et al. 2002, ApJ, 566, 931

Sunada, K., Nakazato, T., Ikeda, N., et al. 2007, PASJ, 59, 1185

Swift, J. J., Welch, W. J., & Di Francesco, J. 2005, ApJ, 620, 823

Slysh V. I., Kalenskii S. V., Val'tts I. E., et al. 1994, MNRAS, 268, 464

Szymczak, M., Pillai, T., & Menten, K. M. 2005, A&A, 434, 613

Testi, L., Palla, F., & Natta, A. 1998, A&AS, 133, 81

Torrelles, J. M., Gómez, J. F., Rodríguez, L. F., et al. 1997, ApJ, 489, 744

Torrelles, J. M., Patel, N. A., Gómez, J. F., et al. 2001, ApJ, 560, 853

Urquhart, J. S., Hoare, M. G., Purcell, C. R., et al. 2009, A&A, 501, 539

Urquhart, J. S., Morgan, L. K., Figura, C. C., et al. 2011, MNRAS, 418, 1689

Urquhart J. S., Figura C. C., Moore T. J. T., et al. 2014a, MNRAS, 437, 1791

Urquhart J. S., Moore, T. J. T., Csengeri, T., et al., 2014b, MNRAS, 443, 1555

Urquhart, J. S., Moore, T. J. T., Menten, K. M., et al. 2015, MNRAS, 446, 3461

Valdettaro, R., Palla, F., Brand, J., et al. 2001, A&A, 368, 845

Val'tts, I. E., Dzyura, A. M., Kalenskii, S. V., et al. 1995, AZh, 72, 22

Val'tts I. E., Ellingsen S. P., Slysh V. I., et al. 2000, MNRAS, 317, 315

Val'tts, I. E., & Larionov, G. M. 2007, Astron. Rep., 51, 519

Voronkov, M. A., Brooks, K. J., Sobolev, A. M., et al. 2006, MNRAS, 373, 411

Walsh, A. J., Burton, M. G., Hyland, A. R., & Robinson, G. 1998, MNRAS, 301, 640W

Wang, Y., Zhang, Q., Rathborne, J. M., et al. 2006, ApJ, 651, L125

Wienen, M., Wyrowski F., Schuller F., et al. 2012, A&A, 544, A146

Walmsley C. M., Ungerechts H., 1983, A&A, 122, 164

Wang, Y., Zhang, Q., Rathborne, J. M., Jackson, J., & Wu, Y. 2006, ApJ, 651, L125

Wang, K., Zhang, Q., Wu, Y., & Zhang, H. 2011, ApJ, 735, 64

Wood, Douglas O. S., & Churchwell, Ed. 1989a, ApJS, 69, 831

Wood, Douglas O. S., & Churchwell, Ed. 1989b, ApJ, 340, 265

Table 3.1. Summary of Observations with KVN 21m telescopes

Maser Transition	Frequency (GHz)	FWHM ($''$)	η_A	Velocity Resolution (km s^{-1})	Velocity Coverage (km s^{-1})	T_{sys} (K)	f[a] (Jy K^{-1})
H_2O 6_{16}–5_{23}	22.235080	120	0.6	0.105	431	60–200	13.3
CH_3OH 7_0–6_1A^+	44.069430	62	0.6	0.053	218	120–350	13.3
CH_3OH 8_0–7_1A^+	95.169463	32	0.5	0.025	101	160–470	16.0

[a]The conversion factor from T_A^* to flux density.

Table 3.2. Summary of Targets

Name	Number of Sources Observed	In reference	References	Notes
IRDC	130	190	Rathborne et al. (2006)	15 of Quiescent cores
RMS	299	∼800	Lumsden et al. (2013)	HMPOs with L $\geq 10^3$ $L_\odot$, $\delta \geq -30^\circ$
HMPO	135	69, 81	Sridharan et al. (2002), Molinari et al. (1996)	15 sources are overlapped in both catalogs
MMS	116	284	Pestalozzi et al. (2005)	Previously detected 44 GHz maser emission
UCHII	103	82, 60	Wood & Churchwell (1989a), Kurtz et al. (1994)	Radio continuum detected

Note. — 1. Palla+91 : 260 (Richard+87 + WC89)
2. Molanari+96 : 163 of 260 (Palla+91)
3. Kurtz+94 : 59 [WC89, −(F_{60},F_{25} with upper limits), $F_{100} > 2000$ Jy, −(observed WC89)]
4. Fontanii+10 : 260 (Palla+91) + 36 (rejected in Palla+91 but be with known HII)
5. Sridharan+02 : 69 [CS(2-1) drom Bonfman+96 (satisfying WC+89), $F_{60} > 90$ Jy, $F_{100} > 500$ Jy, no known HII)

Table 3.3. List of Physical Properties

Name	L_{bol} from ($L_\odot$)		References	Clump mass from ($M_\odot$)	References	Δv,$T_{\rm kin}$ from (km s^{-1},K)		References	Distance Ambiguity
IRDC	SED-MIPS	112	Rathborne et al. (2010)	98/130	Rathborne+06	NH_3 (Eff,GBT)	46,1	A, Chira+13	Near[c]
RMS	SED-HiGAL	297	Lumsden+13	116/135	Urquhart+14	NH_3 (GBT)	257	Uruqhart+11	Solved
HMPO	SED-IRAS	31	Sridharan+02	69/77	Beuther+02	NH_3 (Eff)	39	Beuther+02	Partly Solved(1/3)
	SED-IRAS	81	Molinari+96		Molinari+00(11/19)	NH_3 (Eff)	79	Molinari+96	Partly Solved(1/4) by d_z
MMS	SED-IRAS	105	In this study	83/100	Hill+05	NH_3 (Parkes)	38,17	A, Hill+10	Near(?)
UCHII	SED-IRAS	32	WC+89,C90	53/69	Thompson+06(SCUBA)	NH_3 (Eff)	48,40	A, Churchwell+90(84)	Mostly Solved
	SED-IRAS	19	Kurtz+94[a]	850 μm (SCUBA)	Thompson+06(SCUBA)	NH_3 (Eff)		A, Churchwell+90(84)	Mostly Solved

Note. — A. Wienen+13, Dunham+10, Urquraht+11

2. Other submm continuum survey : BGPS, ATLASGAL

[a]Molinari+96(5) and three of 5 sources are overlaped with HMPO of Zhang+01, Miralles+94(3) and One of 3 sources are overlaped with HMPO of Zhang+01

Table 3.4. Summary of Detections

Source Name	Total Number	Detections (%)			
		Any	22 GHz	44 GHz	95 GHz
IRDCs	130	41(32)	27(21)	27(21)	26(20)
RMSs	299	151(51)	135(45)	83(28)	69(23)
HMPOs	114	83(61)	67(50)	52(39)	42(31)
MMSs	135	110(96)	91(79)	106(92)	82(71)
UCHIIs	103	69(67)	65(63)	35(34)	30(29)

Table 3.5. Summary of target sources(IRDC)

Col. No.	MSX[a] ID	R.A. (J2000.0)	Decl. (J2000.0)	Distance (kpc)	L_{bol} ($L_\odot$)	V_{LSR} (km s^{-1})	Detections 22 GHz	44 GHz	95 GHz
1	G015.05 MM1	18:17:50.4	-15:53:38	3.2	268	24.70	n	n	n
2	G015.05 MM2	18:17:40.0	-15:48:55	3.2	29	24.70	n	n	n
3	G015.31 MM1	18:18:56.4	-15:45:00	3.2	56	31.10	n	n	n
4	G015.31 MM2	18:18:50.4	-15:43:19	3.2	16	31.10	n	n	n
5	G018.82 MM1	18:25:56.1	-12:42:48	4.8	4526	42.20	y	y	Y
6	G018.82 MM2	18:26:23.4	-12:39:37	4.8	8990	42.20	n	n	n
7	G018.82 MM3	18:25:52.6	-12:44:37	4.8	11356	42.20	n	n	n
8	G018.82 MM4	18:26:15.5	-12:41:32	4.8	198	42.20	n	n	n
9	G018.82 MM5	18:26:21.0	-12:41:11	4.8	237	42.20	n	n	n
10	G019.27 MM1	18:25:58.5	-12:03:59	2.4	1998	26.20	n	n	Y
11	G019.27 MM2	18:25:52.6	-12:04:48	2.4	760	26.20	y	n	n
12	G022.35 MM1	18:30:24.4	-09:10:34	4.3	138	50.70	y	y	Y
13	G022.35 MM2[12]	18:30:24.2	-09:12:44	4.3	267	50.70	n	n	n
14	G023.60 MM1	18:34:11.6	-08:19:06	3.9	764	106.10	y	y	Y
15	G023.60 MM2	18:34:21.1	-08:18:07	3.9	1788	53.50	n	y	Y
16	G023.60 MM3[14]	18:34:10.0	-08:18:28	3.9	470	53.50	n	n	n
17	G023.60 MM4[15]	18:34:23.0	-08:18:21	3.9	323	53.50	n	y	n
18	G023.60 MM5	18:34:09.5	-08:18:00	3.9	1272	53.50	n	n	n
19	G023.60 MM7[15]	18:34:21.1	-08:17:11	3.9	137	53.50	n	n	n
20	G024.08 MM1	18:34:57.0	-07:43:26	3.8	14847	52.50	n	n	n
21	G024.33 MM1	18:35:07.9	-07:35:04	3.8	47387	113.60	y	y	y[4]
22	G024.33 MM2[24]	18:35:34.5	-07:37:28	3.8	150	113.60	y	y	n
23	G024.33 MM3	18:35:27.9	-07:36:18	3.8	317	113.60	n	y	Y
24	G024.33 MM5	18:35:33.8	-07:36:42	3.8	155	113.60	y	y	Y
25	G024.33 MM6[21]	18:35:07.7	-07:34:33	3.8	238	113.60	y	y	y
26	G024.33 MM9[23]	18:35:26.5	-07:36:56	3.8	697	113.60	n	y	n

Table 3.5 (cont'd)

Col. No.	MSX[a] ID	R.A. (J2000.0)	Decl. (J2000.0)	Distance (kpc)	$L_{\rm bol}$ ($L_\odot$)	$V_{\rm LSR}$ (km s^{-1})	Detections 22 GHz	44 GHz	95 GHz
27	G024.33 MM10[23]	18:35:27.9	-07:35:32	3.8	187	113.60	n	n	n
28	G024.60 MM1	18:35:40.2	-07:18:37	3.7	964	51.70	y	y	y[4]
29	G024.60 MM2[28]	18:35:35.7	-07:18:09	3.7	3544	51.70	y	n	n
30	G024.60 MM3[28]	18:35:41.1	-07:18:30	3.7	337	51.70	y	y	y[4]
31	G025.04 MM1	18:38:10.2	-07:02:34	3.4	498	63.50	n	y	n
32	G025.04 MM2	18:38:17.7	-07:02:51	3.4	37	63.50	n	y	n
33	G025.04 MM4[32]	18:38:13.7	-07:03:12	3.4	226	63.50	n	n	n
34	G027.75 MM1	18:41:19.9	-04:32:20	5.3	224	79.10	n	n	n
35	G027.75 MM3[34]	18:41:16.8	-04:31:55	5.3	109	79.10	n	n	n
36	G027.94 MM1	18:44:03.6	-04:38:00	3.2	1260	45.70	y	y	y[4]
37	G027.94 MM2[36]	18:44:03.1	-04:37:25	3.2	25	45.70	y	y	n
38	G027.97 MM1	18:43:52.8	-04:36:13	3.2	890	45.90	n	n	n
39	G027.97 MM2	18:43:58.0	-04:34:24	3.2	2743	45.90	y	n	n
40	G027.97 MM3[38]	18:43:54.9	-04:36:08	3.2	...	45.90	n	y	n
41	G028.04 MM1	18:44:08.5	-04:33:22	3.2	1160	45.50	n	y	Y
42	G028.08 MM1	18:42:20.3	-04:16:42	4.9	47	75.80	n	n	n
43	G028.23 MM2	18:43:29.0	-04:12:16	5.1	116	79.60	n	n	n
44	G028.23 MM3[43]	18:43:30.0	-04:12:33	5.1	48	79.60	n	n	n
45	G028.28 MM1	18:44:15.0	-04:17:54	3.3	4768	47.40	n	y	Y
46	G028.28 MM2	18:44:21.3	-04:17:37	3.3	4565	47.40	n	n	n
47	G028.28 MM3[45]	18:44:13.4	-04:18:05	3.3	2951	47.40	y	y	n
48	G028.28 MM4[45]	18:44:11.4	-04:17:22	3.3	...	47.40	y	n	n
49	G028.37 MM1	18:42:52.1	-03:59:45	5.0	26062	78.60	y	y	Y
50	G028.37 MM2[49]	18:42:37.6	-04:02:05	5.0	23329	78.60	y	y	y
51	G028.37 MM3	18:43:03.1	-04:06:24	5.0	...	99.70	n	y	Y
52	G028.37 MM4[54]	18:42:50.7	-04:03:15	5.0	2113	78.60	y	y	y

Table 3.5 (cont'd)

Col. No.	MSX[a] ID	R.A. (J2000.0)	Decl. (J2000.0)	Distance (kpc)	$L_{\rm bol}$ ($L_\odot$)	$V_{\rm LSR}$ (km s^{-1})	Detections 22 GHz	44 GHz	95 GHz
53	G028.37 MM5	18:42:26.8	-04:01:30	5.0	...	78.60	y	n	n
54	G028.37 MM6	18:42:49.0	-04:02:23	5.0	727	78.60	y	y	Y
55	G028.37 MM7[49]	18:42:56.3	-04:07:31	5.0	...	78.60	n	n	n
56	G028.37 MM8[49]	18:42:49.7	-04:09:54	5.0	...	78.60	n	n	n
57	G028.37 MM10[54]	18:42:54.0	-04:02:30	5.0	1200	78.60	y	y	y
58	G028.37 MM11[49]	18:42:42.7	-04:01:44	5.0	353	78.60	y	n	n
59	G028.37 MM13[49]	18:42:41.8	-03:57:08	5.0	...	78.60	y	n	n
60	G028.37 MM15[53]	18:42:32.4	-04:01:16	5.0	...	78.60	y	n	n
61	G028.37 MM16[49]	18:42:40.2	-04:00:23	5.0	288	78.60	y	n	n
62	G028.37 MM17[49]	18:43:00.0	-04:01:34	5.0	82	78.60	y	y	n
63	G028.37 MM18[49]	18:43:12.9	-04:01:16	5.0	...	78.60	n	n	n
64	G028.53 MM2	18:44:15.7	-03:59:41	5.7	502	87.00	n	y	n
65	G028.53 MM5	18:44:17.0	-04:02:04	5.7	1283	87.00	n	n	n
66	G028.53 MM6	18:44:17.8	-04:00:05	5.7	123	87.00	y	y	n
67	G028.53 MM9[68]	18:44:19.3	-03:58:05	5.7	112	87.00	y	n	n
68	G028.53 MM10[66]	18:44:18.5	-03:58:43	5.7	154	87.00	y	n	n
69	G028.67 MM1	18:43:03.1	-03:41:41	5.1	11997	79.50	n	n	n
70	G028.67 MM2	18:43:07.1	-03:44:01	5.1	145	79.50	n	y	n
71	G028.67 MM3	18:42:58.2	-03:48:20	5.1	...	79.50	n	n	n
72	G028.67 MM6	18:43:12.2	-03:45:39	5.1	102	79.50	n	n	n
73	G030.14 MM1	18:46:35.7	-02:31:03	5.5	163	86.70	n	n	n
74	G030.57 MM1	18:48:00.0	-02:07:20	5.5	...	86.20	n	n	Y
75	G030.57 MM2	18:47:58.7	-02:15:20	5.5	...	86.20	n	n	n
76	G030.57 MM3	18:47:54.5	-02:11:15	5.5	357	86.20	n	n	n
77	G030.57 MM6	18:47:59.4	-02:13:13	5.5	...	86.20	n	n	n
78	G030.97 MM1	18:48:21.6	-01:48:27	5.1	4416	78.80	n	y	Y

Table 3.5 (cont'd)

Col. No.	MSX[a] ID	R.A. (J2000.0)	Decl. (J2000.0)	Distance (kpc)	$L_{\rm bol}$ ($L_\odot$)	$V_{\rm LSR}$ (km s^{-1})	Detections 22 GHz	44 GHz	95 GHz
79	G031.97 MM1	18:49:36.3	-00:45:45	6.9	36427	96.70	y	y	Y
80	G031.97 MM3	18:49:32.3	-00:47:02	6.9	1267	96.70	y	n	Y
81	G031.97 MM4	18:49:33.0	-00:47:33	6.9	638	96.70	y	y	Y
82	G031.97 MM5	18:49:21.9	-00:50:35	6.9	534	96.70	n	y	Y
83	G031.97 MM8	18:49:29.1	-00:48:12	6.9	871	96.70	n	n	n
84	G033.69 MM1	18:52:58.8	+00:42:37	7.1	2003	105.90	y	y	Y
85	G033.69 MM2	18:52:49.9	+00:37:57	7.1	22373	105.90	n	n	n
86	G033.69 MM3[88]	18:52:50.8	+00:36:43	7.1	5108	105.90	n	n	n
87	G033.69 MM4[84]	18:52:56.4	+00:43:08	7.1	246	105.90	n	y	n
88	G033.69 MM5	18:52:47.8	+00:36:47	7.1	18213	105.90	y	n	n
89	G033.69 MM9[84]	18:52:58.1	+00:41:20	7.1	5621	105.90	n	n	n
90	G033.69 MM10[85]	18:52:52.7	+00:38:35	7.1	426	105.90	n	y	y
91	G034.43 MM1[92]	18:53:18.0	+01:25:24	3.7	24360	57.10	y	y	y[4]
92	G034.43 MM2	18:53:18.6	+01:24:40	3.7	14304	57.10	y	y	Y
93	G034.43 MM3	18:53:20.4	+01:28:23	3.7	934	57.10	y	y	Y
94	G034.43 MM4[92]	18:53:19.0	+01:24:08	3.7	1164	57.10	n	y	y[4]
95	G034.43 MM5[92]	18:53:19.8	+01:23:30	3.7	177	57.10	y	y	y
96	G034.43 MM6[93]	18:53:18.6	+01:27:48	3.7	47	57.10	y	y	y
97	G034.43 MM7[93]	18:53:18.3	+01:27:13	3.7	101	57.10	y	y	y
98	G034.43 MM8[92]	18:53:16.4	+01:26:20	3.7	79	57.10	y	y	n
99	G034.77 MM1	18:56:48.2	+01:18:47	2.9	...	43.50	n	n	Y
100	G034.77 MM3	18:56:44.7	+01:20:42	2.9	...	43.50	n	n	n
101	G035.39 MM1	18:56:41.2	+02:09:52	2.9	...	44.70	y	n	n
102	G035.39 MM2	18:56:59.2	+02:04:53	2.9	...	44.70	y	n	n
103	G035.39 MM3	18:57:05.3	+02:06:29	2.9	6495	55.30	y	y	Y
104	G035.39 MM4	18:57:06.7	+02:08:23	2.9	116	44.70	y	n	n

Table 3.5 (cont'd)

Col. No.	MSX[a] ID	R.A. (J2000.0)	Decl. (J2000.0)	Distance (kpc)	$L_{\rm bol}$ ($L_\odot$)	$V_{\rm LSR}$ (km s^{-1})	Detections 22 GHz	44 GHz	95 GHz
105	G035.39 MM5[104]	18:57:08.8	+02:08:09	2.9	45	44.70	y	n	n
106	G035.39 MM6[104]	18:57:08.4	+02:09:09	2.9	327	44.70	n	n	n
107	G035.39 MM7	18:57:08.1	+02:10:50	2.9	242	44.70	n	n	n
108	G035.39 MM8[104]	18:57:07.0	+02:08:54	2.9	25	44.70	y	n	n
109	G035.59 MM1	18:57:02.3	+02:17:04	2.9	1685	44.70	n	n	n
110	G035.59 MM2	18:57:07.4	+02:16:14	2.9	128	44.70	n	n	n
111	G035.59 MM3[110]	18:57:11.6	+02:16:08	2.9	28	44.70	n	n	n
112	G038.95 MM1	19:04:07.4	+05:08:48	2.7	40	41.60	n	n	n
113	G038.95 MM2	19:04:03.4	+05:07:56	2.7	2031	41.60	n	n	n
114	G038.95 MM4	19:04:00.6	+05:09:06	2.7	320	41.60	n	n	n
115	G048.65 MM1	19:21:49.7	+13:49:30	2.5	537	34.00	y	n	n
116	G048.65 MM2[115]	19:21:47.6	+13:49:22	2.5	48	34.00	y	n	n
117	G053.11 MM1	19:29:17.2	+17:56:21	1.8	4473	22.00	y	y	Y
118	G053.11 MM2[117]	19:29:20.2	+17:57:06	1.8	325	22.00	y	n	n
119	G053.11 MM3	19:29:00.6	+17:55:11	1.8	...	22.00	n	n	n
120	G053.11 MM4	19:29:20.4	+17:55:04	1.8	178	22.00	n	n	n
121	G053.11 MM5	19:29:26.3	+17:54:53	1.8	192	22.00	n	n	n
122	G053.25 MM1[125]	19:29:39.0	+18:01:42	1.9	306	23.90	y	y	y
123	G053.25 MM2[125]	19:29:33.0	+18:01:00	1.9	46	23.90	y	n	n
124	G053.25 MM3	19:29:44.0	+17:58:47	1.9	49	23.90	n	n	n
125	G053.25 MM4	19:29:34.5	+18:01:39	1.9	188	23.90	y	n	n
126	G053.25 MM5	19:29:39.4	+17:58:40	1.9	46	23.90	n	n	n
127	G053.25 MM6	19:29:31.5	+17:59:50	1.9	393	23.90	y	n	n
128	G053.31 MM1	19:29:50.0	+18:05:07	2.0	7	24.00	n	n	n
129	G053.31 MM2	19:29:42.1	+18:03:57	2.0	17	24.00	n	n	n
130	G053.31 MM3[128]	19:29:49.7	+18:04:39	2.0	21	24.00	n	n	n

Table 3.6. Summary of target sources(HMPO)

Col. No.	HMPO ID	R.A. (J2000.0)	Decl. (J2000.0)	Distance (kpc)	L_{bol} ($L_{\odot}$)	V_{LSR} (km s^{-1})	Detections		
							22 GHz	44 GHz	95 GHz
1	HM00117+6412	00:14:27.7	+64:28:46	1.8	1400	-37.00	y	n	n
2	HM00420+5530	00:44:57.6	+55:47:18	7.7	52000	-51.00	y	n	n
3	HM04579+4703	05:01:39.7	+47:07:23	2.5	3900	-17.00	y	n	n
4	HM05137+3919	05:17:13.3	+39:22:23	10.8	56000	-25.00	y	n	n
5	HM05168+3634	05:20:16.2	+36:37:21	6.1	24000	-15.00	y	n	n
6	HM05274+3345	05:30:45.6	+33:47:52	1.5	4400	-4.00	y	y	Y
7	HM05345+3157	05:37:47.8	+31:59:24	1.8	1400	-18.00	y	n	n
8	HM05358+3543	05:39:10.4	+35:45:19	1.8	...	-18.00	y	y	n
9	HM05373+2349	05:40:24.4	+23:50:54	1.2	660	2.00	y	y	Y
10	HM05490+2658	05:52:12.9	+26:59:33	2.1	...	1.00	n	y	n
11	HM05553+1631	05:58:13.9	+16:32:00	2.5	...	6.00	y	n	n
12	HM06056+2131	06:08:41.0	+21:31:01	1.5	5800	3.00	y	y	Y
13	HM06584-0852	07:00:51.5	-08:56:29	4.5	9100	41.00	n	n	n
14	HM17450-2742	17:48:09.3	-27:43:21	23.5	16	-17.00	n	n	n
15	HM18014-2428	18:04:29.3	-24:28:47	2.9	17000	13.00	n	n	n
16	HM18018-2426	18:04:53.9	-24:26:41	1.5	6600	11.00	n	y	y[1]
17	HM18024-2119	18:05:25.4	-21:19:41	5.2	20655	1.00	y	y	Y
18	HM18024-2231	18:05:30.6	-22:31:36	2.9	5600	16.00	n	n	n
19	HM18089-1732	18:11:51.3	-17:31:28	13.0	398107	33.00	y	y	y[1]
20	HM18090-1832	18:12:01.9	-18:31:56	10.0	31622	110.00	n	n	n
21	HM18102-1800	18:13:12.2	-17:59:35	14.0	199526	21.00	n	y	n
22	HM18144-1723	18:17:24.4	-17:22:13	4.3	13000	47.00	y	y	Y
23	HM18151-1208	18:17:57.1	-12:07:22	3.0	...	33.00	y	y	y[1]
24	HM18159-1550	18:18:47.6	-15:48:54	11.7	100000	60.00	n	n	n
25	HM18162-1612	18:19:07.5	-16:11:21	4.9	29000	62.00	n	y	Y
26	HM18182-1433	18:21:07.9	-14:31:53	11.8	125892	60.00	y	y	Y

Table 3.6 (cont'd)

Col. No.	HMPO ID	R.A. (J2000.0)	Decl. (J2000.0)	Distance (kpc)	L_{bol} ($L_{\odot}$)	V_{LSR} (km s^{-1})	Detections 22 GHz	44 GHz	95 GHz
27	HM18223-1243	18:25:10.9	-12:42:17	12.4	199526	46.00	n	n	n
28	HM18247-1147	18:27:31.1	-11:45:56	9.3	100000	122.00	n	y	Y
29	HM18256-0742	18:28:20.5	-07:40:22	2.9	11000	37.00	n	n	n
30	HM18264-1152	18:29:14.3	-11:50:26	12.5	125892	44.00	y	y	y[4]
31	HM18272-1217	18:30:02.7	-12:15:27	2.9	...	34.00	n	n	n
32	HM18278-1009	18:30:35.2	-10:07:12	5.7	17000	116.60	n	y	n
33	HM18288-0158	18:31:26.7	-01:56:35	0.5	190	6.00	n	n	n
34	HM18290-0924	18:31:44.8	-09:22:09	10.5	100000	84.00	y	y	n
35	HM18306-0835	18:33:21.8	-08:33:38	10.7	63095	77.00	y	y	Y
36	HM18308-0841	18:33:31.9	-08:39:17	10.7	79432	77.00	y	y	Y
37	HM18310-0825	18:33:47.2	-08:23:35	10.4	63095	84.00	n	n	n
38	HM18337-0743	18:36:29.0	-07:40:33	11.5	100000	58.00	n	y	Y
39	HM18345-0641	18:37:16.8	-06:38:32	9.5	...	96.00	n	y	Y
40	HM18348-0616	18:37:29.0	-06:14:15	9.0	125892	110.00	y	n	n
41	HM18363-0554	18:39:03.7	-05:52:15	4.3	13000	65.00	n	n	n
42	HM18372-0541	18:39:56.0	-05:38:49	13.4	199526	23.00	y	n	n
43	HM18385-0512	18:41:12.0	-05:09:06	13.1	199526	26.00	y	n	n
44	HM18396-0431	18:42:18.8	-04:28:37	6.1	42000	97.00	n	n	n
45	HM18424-0329	18:45:03.3	-03:26:49	3.4	5100	48.00	n	n	n
46	HM18426-0204	18:45:12.8	-02:01:12	13.5	100000	15.00	y	y	n
47	HM18431-0312	18:45:46.9	-03:09:24	8.2	31622	105.00	n	n	n
48	HM18437-0216	18:46:22.7	-02:13:24	7.3	...	111.00	n	n	n
49	HM18440-0148	18:46:36.3	-01:45:23	8.3	...	98.00	n	n	n
50	HM18445-0222	18:47:10.8	-02:19:06	9.4	158489	87.00	n	n	n
51	HM18447-0229	18:47:23.7	-02:25:55	8.2	39810	103.00	n	n	n
52	HM18454-0136	18:48:03.7	-01:33:23	11.9	63095	39.00	n	n	n

Table 3.6 (cont'd)

Col. No.	HMPO ID	R.A. (J2000.0)	Decl. (J2000.0)	Distance (kpc)	L_{bol} ($L_\odot$)	V_{LSR} (km s^{-1})	Detections 22 GHz	44 GHz	95 GHz
53	HM18454-0158	18:48:01.3	-01:54:49	5.6	...	53.00	y	n	n
54	HM18460-0307	18:48:39.2	-03:03:53	9.5	39810	84.00	n	n	n
55	HM18470-0044	18:49:36.7	-00:41:05	8.2	...	97.00	y	n	n
56	HM18472-0022	18:49:50.7	-00:19:09	11.1	79432	49.00	n	n	n
57	HM18488+0000	18:51:24.8	+00:04:19	8.9	79432	83.00	n	y	Y
58	HM18507+0121	18:53:17.4	+01:24:55	3.9	48000	57.00	y	y	Y
59	HM18511+0146	18:53:38.1	+01:50:27	3.9	20000	57.00	n	n	n
60	HM18517+0437	18:54:13.8	+04:41:32	2.9	...	44.00	y	y	Y
61	HM18521+0134	18:54:40.8	+01:38:02	9.0	39810	76.00	n	n	n
62	HM18527+0301	18:55:16.5	+03:05:07	5.3	16000	76.00	y	n	n
63	HM18530+0215	18:55:34.2	+02:19:08	8.7	251188	78.00	n	y	Y
64	HM18532+0047	18:55:50.6	+00:51:22	4.0	13000	59.00	y	n	n
65	HM18540+0220	18:56:35.6	+02:24:54	10.6	79432	50.00	n	n	n
66	HM18551+0302	18:57:42.1	+03:06:05	4.0	24000	58.00	n	n	n
67	HM18553+0414	18:57:52.9	+04:18:06	0.6	251	10.00	y	n	n
68	HM18565+0349	18:59:03.4	+03:53:22	6.8	26000	92.00	y	y	n
69	HM18566+0408	18:59:09.9	+04:12:14	6.7	...	85.00	y	y	Y
70	HM18567+0700	18:59:13.6	+07:04:47	2.2	8400	29.00	n	n	n
71	HM18571+0349	18:59:40.0	+03:53:35	3.9	18000	56.00	n	n	n
72	HM18586+0106	19:01:10.6	+01:11:16	2.7	4800	38.00	n	n	n
73	HM19012+0505	19:03:43.5	+05:09:49	2.9	17000	40.00	y	n	n
74	HM19012+0536	19:03:45.1	+05:40:40	8.6	50118	66.00	n	y	y[4]
75	HM19035+0641	19:06:01.1	+06:46:35	2.2	...	32.00	y	n	n
76	HM19043+0726	19:06:47.7	+07:31:38	4.4	14000	59.00	n	y	Y
77	HM19074+0752	19:09:53.3	+07:57:22	8.9	63095	55.00	n	n	n
78	HM19088+0902	19:11:15.9	+09:07:27	4.7	30000	60.00	y	y	Y

Table 3.6 (cont'd)

Col. No.	HMPO ID	R.A. (J2000.0)	Decl. (J2000.0)	Distance (kpc)	L_{bol} ($L_\odot$)	V_{LSR} (km s^{-1})	Detections 22 GHz	44 GHz	95 GHz
79	HM19092+0841	19:11:37.4	+08:46:30	4.5	17000	60.00	y	y	n
80	HM19094+0944	19:11:52.0	+09:49:46	6.1	37000	65.00	n	n	n
81	HM19175+1357	19:19:49.1	+14:02:46	10.6	...	15.00	n	n	Y
82	HM19198+1423	19:22:07.7	+14:29:20	5.5	22000	60.00	y	n	n
83	HM19213+1723	19:23:37.0	+17:28:59	4.1	28000	42.00	y	n	n
84	HM19217+1651	19:23:58.8	+16:57:37	10.5	...	4.00	y	y	Y
85	HM19220+1432	19:24:19.7	+14:38:03	5.5	...	69.00	y	n	n
86	HM19266+1745	19:28:54.0	+17:51:56	10.0	50118	5.00	n	y	n
87	HM19282+1814	19:30:28.1	+18:20:53	8.2	79432	24.00	n	n	n
88	HM19368+2239	19:38:58.1	+22:46:32	4.4	8600	36.00	n	y	Y
89	HM19374+2352	19:39:33.2	+23:59:55	4.3	27000	37.00	y	y	n
90	HM19388+2357	19:40:59.4	+24:04:39	4.3	15000	35.00	y	y	Y
91	HM19403+2258	19:42:27.2	+23:05:12	6.3	50118	27.00	n	n	n
92	HM19410+2336	19:43:11.4	+23:44:06	6.4	100000	22.40	y	y	Y
93	HM19411+2306	19:43:18.1	+23:13:59	5.8	19952	29.00	y	n	n
94	HM19413+2332	19:43:28.9	+23:40:04	6.8	25118	21.00	n	n	n
95	HM19471+2641	19:49:09.9	+26:48:52	2.4	...	21.00	y	n	n
96	HM20050+2720	20:07:06.7	+27:28:53	1.1	390	6.00	y	y	Y
97	HM20051+3435	20:07:03.8	+34:44:35	3.7	10000	12.00	n	n	n
98	HM20056+3350	20:07:31.5	+33:59:39	1.7	4000	9.00	y	n	n
99	HM20062+3550	20:08:09.8	+35:59:20	1.7	5	1.00	y	y	Y
100	HM20081+2720	20:10:11.5	+27:29:06	0.7	...	6.00	n	n	n
101	HM20099+3640	20:11:46.4	+36:49:37	8.7	42000	-36.00	y	n	n
102	HM20106+3545	20:12:31.3	+35:54:46	1.6	1800	8.00	n	n	n
103	HM20126+4104	20:14:26.0	+41:13:32	1.7	...	-4.00	y	y	Y
104	HM20188+3928	20:20:39.3	+39:37:52	1.4	340	2.00	y	y	Y

Table 3.6 (cont'd)

Col. No.	HMPO ID	R.A. (J2000.0)	Decl. (J2000.0)	Distance (kpc)	L_{bol} ($L_\odot$)	V_{LSR} (km s^{-1})	Detections 22 GHz	44 GHz	95 GHz
105	HM20205+3948	20:22:21.9	+39:58:05	4.5	...	-2.00	n	n	n
106	HM20216+4107	20:23:23.8	+41:17:40	1.7	...	-2.00	n	n	n
107	HM20217+3947	20:23:31.7	+39:57:23	3.7	7100	-1.00	n	n	n
108	HM20220+3728	20:23:55.7	+37:38:10	4.5	81000	-3.00	n	y	n
109	HM20278+3521	20:29:46.9	+35:31:39	5.0	11000	-5.00	n	n	n
110	HM20286+4105	20:30:27.9	+41:15:48	3.7	39000	-4.00	y	y	Y
111	HM20293+3952	20:31:10.7	+40:03:10	2.0	6309	6.00	y	y	Y
112	HM20319+3958	20:33:49.3	+40:08:45	1.6	...	9.00	n	n	n
113	HM20332+4124	20:35:00.5	+41:34:48	3.9	...	-2.00	y	n	n
114	HM20333+4102	20:35:09.5	+41:13:18	0.1	46	8.00	n	n	n
115	HM20343+4129	20:36:07.1	+41:40:01	1.4	...	11.50	n	n	n
116	HM20444+4629	20:46:08.3	+46:40:41	2.4	3300	-4.00	n	n	n
117	HM21078+5211	21:09:25.2	+52:23:44	1.5	13000	-6.00	y	n	n
118	HM21307+5049	21:32:31.5	+51:02:22	4.9	12000	-47.00	y	y	Y
119	HM21391+5802	21:40:42.4	+58:16:10	0.8	94	0.00	y	y	Y
120	HM21519+5613	21:53:39.2	+56:27:46	7.3	19000	-63.00	n	n	n
121	HM22134+5834	22:15:09.1	+58:49:09	2.6	...	-20.00	y	n	n
122	HM22172+5549	22:19:09.0	+56:04:45	2.9	4800	-44.00	n	n	n
123	HM22198+6336	22:21:27.6	+63:51:42	1.3	1200	-11.00	y	n	n
124	HM22305+5803	22:32:24.3	+58:18:58	5.4	14000	-52.00	n	n	n
125	HM22506+5944	22:52:38.6	+60:00:56	5.7	22000	-52.00	y	y	Y
126	HM22551+6221	22:57:05.2	+62:37:44	0.7	...	-13.00	n	n	n
127	HM22570+5912	22:59:06.4	+59:28:28	5.1	...	-47.00	y	n	n
128	HM23026+5948	23:04:45.7	+60:04:35	5.8	18000	-51.00	n	n	n
129	HM23033+5951	23:05:25.7	+60:08:08	3.5	...	-53.00	y	y	Y
130	HM23139+5939	23:16:09.3	+59:55:23	4.8	...	-45.00	y	y	Y

Table 3.6 (cont'd)

Col. No.	HMPO ID	R.A. (J2000.0)	Decl. (J2000.0)	Distance (kpc)	L_{bol} ($L_\odot$)	V_{LSR} (km s^{-1})	Detections 22 GHz	44 GHz	95 GHz
131	HM23140+6121	23:16:11.7	+61:37:45	6.4	44000	-52.00	n	n	n
132	HM23151+5912	23:17:21.0	+59:28:49	5.7	...	-54.00	y	y	Y
133	HM23314+6033	23:33:44.4	+60:50:30	2.8	11000	-45.00	y	n	n
134	HM23385+6053	23:40:53.2	+61:10:21	6.9	76000	-50.00	y	y	Y
135	HM23545+6508	23:57:05.2	+65:25:11	0.8	...	-20.00	n	n	n

Table 3.7. Summary of target sources(MMS)

Col. No.	MMS ID	R.A. (J2000.0)	Decl. (J2000.0)	Distance (kpc)	L_{bol} ($L_\odot$)	V_{LSR}[b] (km s^{-1})	Detection[c] 22 GHz	44 GHz	95 GHz
1	0.21-0.00	17:46:07.660	-28:45:20.00	8.4	426000	49.20	n	y	Y
2	0.31-0.20	17:47:09.120	-28:46:16.00	8.0	515000	18.00	y	n	n
3	0.49+0.18	17:46:04.000	-28:24:51.50	2.6	16800	0.80	n	y	Y
4	0.64-0.04	17:47:18.650	-28:24:25.00	8.1	3700000	49.10	y	y	Y
5	0.66-0.02	17:47:18.610	-28:22:56.00	8.3	3880000	72.20	y	y	Y
6	0.67-0.02	17:47:19.230	-28:22:14.50	8.3	3880000	73.40	y	y	Y
7	0.69-0.03	17:47:24.810	-28:21:43.50	8.2	3790000	68.50	y	y	Y
8	0.83+0.18	17:46:52.820	-28:07:35.00	4.5	27200	3.50	y	y	Y
9	1.14-0.12	17:48:48.470	-28:01:12.00	...	...	-21.00	y	n	n
10	2.53+0.19	17:50:46.480	-26:39:45.00	2.7	2630	4.50	n	n	n
11	5.90-0.42	18:00:40.870	-24:04:20.50	2.7	302000	6.60	y	y	Y
12	6.78-0.27	18:01:57.200	-23:12:37.00	4.5	32800	26.90	y	y	Y
13	8.68-0.36	18:06:23.500	-21:37:23.00	5.0	157000	43.00	y	y	n
14	9.62+0.19	18:06:14.659	-20:31:31.57	5.2	310000	1.00	y	y	Y
15	10.32-0.26	18:09:24.200	-20:08:07.00	4.5	27300	39.00	n	y	Y
16	10.47+0.02	18:08:38.210	-19:51:49.50	6.0	411000	75.00	y	y	Y
17	10.62-0.38	18:10:29.240	-19:55:41.50	0.9	21300	5.00	y	y	y[1]
18	12.20-0.10	18:12:39.920	-18:24:17.50	2.7	36800	24.50	y	y	Y
19	12.68-0.18	18:13:54.200	-18:01:44.00	4.7	...	52.00	y	y	y[4]
20	12.79-0.19	18:14:11.100	-17:55:57.00	3.9	...	36.00	y	y	y[1]
21	12.89+0.49	18:11:51.400	-17:31:30.00	4.0	60000	39.00	y	y	y[1]
22	12.90-0.26	18:14:39.520	-17:52:00.00	4.0	123000	39.00	y	y	y[4]
23	13.18+0.06	18:14:00.800	-17:28:05.00	4.5	119000	48.50	n	y	n
24	14.33-0.63	18:18:53.370	-16:47:39.50	2.5	20200	22.00	y	y	y[1]
25	14.60+0.01	18:17:01.140	-16:14:39.00	2.8	19700	24.80	y	y	y[1]
26	15.03-0.67	18:20:24.790	-16:11:35.50	2.4	524000	21.00	y	y	y[1]

Table 3.7 (cont'd)

Col. No.	MMS ID	R.A. (J2000.0)	Decl. (J2000.0)	Distance (kpc)	L_{bol} ($L_\odot$)	V_{LSR} [b] (km s^{-1})	Detection[c] 22 GHz	44 GHz	95 GHz
27	15.67-0.48	18:20:58.300	-15:32:34.00	17.0	232000	-3.40	y	y	n
28	16.58-0.05	18:21:09.130	-14:31:48.50	4.6	28100	59.00	y	y	Y
29	16.86-2.15	18:29:24.410	-15:16:04.00	1.7	4390	14.60	y	y	y[1]
30	17.01-2.39	18:30:33.900	-15:14:53.00	2.4	2580	23.30	y	y	n
31	18.46-0.00	18:24:36.350	-12:51:08.00	3.9	37000	49.00	n	n	n
32	18.65+0.04	18:24:48.700	-12:39:17.00	5.3	30400	80.20	y	y	n
33	19.36-0.03	18:26:25.790	-12:03:53.00	2.5	6930	26.30	n	y	y[4]
34	19.48+0.15	18:26:00.390	-11:52:22.50	2.1	14700	23.30	y	y	Y
35	19.61-0.13	18:27:16.520	-11:53:38.50	4.0	45400	53.00	n	y	Y
36	19.61-0.23	18:27:37.200	-11:56:27.00	3.1	118000	36.00	y	y	y[1]
37	19.70-0.26	18:27:55.520	-11:52:39.00	3.5	8720	43.60	y	n	n
38	19.88-0.52	18:29:11.700	-11:49:58.00	3.7	15500	46.80	y	y	n
39	20.08-0.13	18:28:10.320	-11:28:47.00	3.5	47800	44.00	y	n	n
40	21.87+0.01	18:31:01.750	-09:49:01.00	1.9	6370	21.00	y	y	n
41	22.05+0.22	18:30:35.700	-09:34:26.00	3.9	15800	53.80	y	y	y[4]
42	22.36+0.06	18:31:44.130	-09:22:12.50	5.1	31100	79.70	y	y	Y
43	23.01-0.41	18:34:40.200	-09:00:36.00	4.8	96800	75.00	y	y	y[1]
44	23.24-0.24	18:34:31.260	-08:42:47.00	4.3	39400	64.10	n	y	Y
45	23.32-0.29	18:34:49.900	-08:40:34.00	4.3	22800	63.80	n	y	Y
46	23.39+0.19	18:33:13.100	-08:23:56.00	4.8	23000	74.10	n	y	n
47	23.43-0.18	18:34:39.270	-08:31:39.00	6.0	349000	103.00	n	y	y[1]
48	23.48+0.08	18:33:44.050	-08:21:20.50	5.4	20200	87.40	y	y	Y
49	23.98-0.08	18:35:22.900	-08:01:11.00	4.6	15400	70.90	y	y	y[4]
50	24.33+0.14	18:35:09.200	-07:35:06.00	6.4	30100	110.00	y	y	y[4]
51	24.50-0.03	18:36:08.700	-07:30:55.00	6.7	200000	114.40	n	y	n
52	24.67-0.14	18:36:48.400	-07:24:25.00	6.6	203000	113.10	y	y	n

Table 3.7 (cont'd)

Col. No.	MMS ID	R.A. (J2000.0)	Decl. (J2000.0)	Distance (kpc)	L_{bol} ($L_\odot$)	V_{LSR}[b] (km s^{-1})	Detection[c] 22 GHz	44 GHz	95 GHz
53	24.78+0.08	18:36:12.570	-07:12:11.50	6.6	228000	110.20	y	y	Y
54	24.93+0.08	18:36:29.200	-07:05:05.00	3.8	9620	53.40	y	y	n
55	25.41+0.10	18:37:16.920	-06:38:28.00	5.7	18000	96.00	n	y	Y
56	25.65+1.04	18:34:20.910	-05:59:40.50	3.1	30300	41.90	y	y	Y
57	25.70+0.04	18:38:03.150	-06:24:15.00	5.6	85100	92.80	n	y	Y
58	25.82-0.17	18:39:03.630	-06:24:09.50	5.5	...	91.20	y	y	Y
59	26.60-0.22	18:40:38.550	-05:43:56.00	6.6	33300	107.50	n	y	Y
60	27.28+0.15	18:40:34.480	-04:57:13.50	2.6	14700	34.60	y	y	Y
61	27.36-0.16	18:41:50.980	-05:01:28.00	6.0	86900	99.40	y	y	Y
62	27.78+0.05	18:41:47.500	-04:33:11.00	7.2	31100	111.80	y	y	n
63	27.78-0.25	18:42:57.200	-04:41:59.00	5.9	16900	97.90	n	y	Y
64	28.20-0.05	18:42:58.200	-04:13:59.50	6.0	186000	95.70	y	y	Y
65	28.39+0.08	18:42:54.500	-04:00:04.00	4.5	22400	71.10	y	y	Y
66	28.81+0.36	18:42:37.490	-03:30:12.50	5.6	...	91.30	y	y	n
67	28.83-0.25	18:44:51.090	-03:45:48.00	5.3	64700	86.00	n	y	n
68	28.86+0.07	18:43:45.100	-03:35:29.00	6.6	202000	105.00	y	y	Y
69	29.91-0.03	18:46:03.690	-02:41:52.50	6.1	892000	96.80	y	y	Y
70	30.20-0.17	18:47:03.500	-02:30:31.00	7.3	200000	108.00	n	n	n
71	30.22-0.18	18:47:07.800	-02:29:43.00	7.3	200000	113.00	n	n	n
72	30.30+0.06	18:46:23.700	-02:17:56.00	2.6	5900	36.70	y	y	n
73	30.40-0.29	18:47:51.200	-02:23:15.00	6.3	...	98.40	y	y	n
74	30.53+0.01	18:47:00.100	-02:07:26.00	3.6	33800	53.00	y	y	Y
75	30.70-0.07	18:47:36.900	-02:01:05.00	5.5	156000	88.00	y	y	y[1]
76	30.79+0.20	18:46:48.090	-01:48:46.00	5.4	34600	86.00	y	y	Y
77	30.82-0.05	18:47:46.200	-01:54:14.00	6.7	1350000	101.00	y	y	Y
78	30.86+0.16	18:47:09.130	-01:44:10.50	6.9	57000	102.00	n	y	Y

Table 3.7 (cont'd)

Col. No.	MMS ID	R.A. (J2000.0)	Decl. (J2000.0)	Distance (kpc)	L_{bol} ($L_\odot$)	V_{LSR}[b] (km s^{-1})	Detection[c] 22 GHz	44 GHz	95 GHz
79	31.28+0.06	18:48:12.390	-01:26:22.60	7.3	209000	110.00	y	y	Y
80	31.41+0.31	18:47:34.310	-01:12:47.00	7.3	178000	96.90	y	y	Y
81	32.03+0.06	18:49:37.300	-00:45:47.00	6.0	52600	92.80	y	y	Y
82	32.74-0.08	18:51:22.800	-00:12:15.00	2.7	7590	39.00	y	y	Y
83	33.86+0.01	18:53:05.200	+00:49:36.00	4.2	1850	64.00	y	y	Y
84	34.10+0.01	18:53:31.900	+01:02:26.00	3.7	1050	55.90	n	n	n
85	34.24+0.13	18:53:21.500	+01:13:43.00	3.7	536000	55.00	y	y	Y
86	34.39+0.24	18:53:21.500	+01:24:09.00	3.7	31400	55.80	y	y	n
87	34.78-1.38	18:59:44.700	+01:01:12.00	3.2	5140	46.90	y	y	Y
88	35.02+0.35	18:54:00.600	+02:00:50.00	3.0	35500	44.00	y	y	n
89	35.20-0.74	18:58:12.700	+01:40:50.00	2.0	16300	28.00	y	y	y[4]
90	35.20-1.74	19:01:45.600	+01:13:28.00	2.9	222000	43.50	y	y	Y
91	35.79-0.17	18:57:16.100	+02:27:44.00	4.0	4920	60.80	y	y	n
92	37.54+0.21	18:59:11.600	+04:12:08.00	6.7	84000	83.70	y	y	n
93	38.91-0.35	19:03:40.000	+05:09:29.00	2.3	7830	32.30	y	y	n
94	39.10+0.48	19:00:59.500	+05:42:28.00	1.1	277	15.30	n	y	n
95	40.25-0.19	19:05:40.600	+06:26:08.00	5.8	29900	74.00	y	y	y[4]
96	43.15+0.02	19:10:09.700	+09:05:35.00	11.1	28500	13.00	y	y	n
97	49.47-0.37	19:23:39.821	+14:31:04.47	5.5	932000	59.50	y	y	Y
98	49.49-0.39	19:23:44.500	+14:30:31.00	5.5	932000	59.00	y	y	Y
99	59.78+0.06	19:43:11.248	+23:44:03.34	2.6	18700	25.00	y	y	Y
100	59.84+0.66	19:40:59.400	+24:04:39.00	4.3	12100	38.40	y	y	Y
101	75.76+0.34	20:21:40.100	+37:25:37.00	4.9	330000	-2.90	y	y	Y
102	78.10+3.64	20:14:26.044	+41:13:33.39	4.7	75700	-6.10	n	y	Y
103	81.72+0.57	20:39:00.700	+42:22:50.00	2.9	...	0.00	y	y	Y
104	81.76+0.59	20:39:03.500	+42:25:53.00	3.1	...	-1.00	y	y	Y

Table 3.7 (cont'd)

Col. No.	MMS ID	R.A. (J2000.0)	Decl. (J2000.0)	Distance (kpc)	L_{bol} ($L_\odot$)	V_{LSR}[b] (km s^{-1})	Detection[c] 22 GHz	44 GHz	95 GHz
105	81.87+0.78	20:38:36.452	+42:37:36.06	1.2	...	6.00	y	y	Y
106	109.86+2.10	22:56:18.095	+62:01:49.45	0.5	8130	-11.10	y	y	Y
107	111.53+0.76	23:13:45.364	+61:28:10.55	2.7	183000	-56.20	y	y	Y
108	121.28+0.65	00:36:42.200	+63:28:30.00	2.1	4300	-22.40	n	n	n
109	133.94+1.04	02:27:03.849	+61:52:25.42	4.5	430000	-44.60	y	y	Y
110	173.49+2.42	05:39:13.059	+35:45:51.29	11.0	247000	-13.60	y	y	Y
111	188.95+0.89	06:08:53.350	+21:38:28.70	4.4	54800	11.00	y	y	Y
112	192.60-0.05	06:12:54.020	+17:59:23.00	1.1	11400	5.00	y	y	Y
113	203.05-14.5	05:41:44.150	-01:54:44.90	...	...	-1.00	y	y	Y
114	359.43-0.10	17:44:40.660	-29:28:17.60	8.2	...	-52.00	y	y	n
115	359.61-0.24	17:45:39.080	-29:23:29.00	...	...	22.50	y	y	Y
116	359.89-0.06	17:45:38.200	-29:03:28.00	...	...	10.00	y	y	y[1]

Table 3.8. Summary of target sources(UCHII)

Col. No.	UCHII ID	R.A. (J2000.0)	Decl. (J2000.0)	Distance (kpc)	L_{bol} ($L_\odot$)	V_{LSR} (km s^{-1})	Detections 22 GHz	44 GHz	95 GHz
1	IRAS02232+6138	02:27:01.0	+61:52:14	3.0	206000	-46.40	y	y	Y
2	IRAS02575+6017	03:01:32.3	+60:29:12	3.8	30831	-38.00	n	n	n
3	IRAS03035+5819	03:07:25.6	+58:30:52	4.2	55462	-39.40	y	n	n
4	IRAS05391-0152	05:41:38.7	-01:51:19	0.7	...	10.00	y	n	n
5	IRAS05393-0156	05:41:49.5	-01:55:17	0.5	13000	10.00	y	n	n
6	Mon R2	06:07:46.6	-06:22:59	10.8	...	9.50	y	n	n
7	IRAS06056+2131	06:08:41.0	+21:31:01	0.8	...	0.00	y	n	n
8	IRAS06058+2138	06:08:54.1	+21:38:25	2.2	...	2.50	y	y	Y
9	IRAS06061+2151	06:09:07.8	+21:50:39	4.1	...	-0.70	y	n	n
10	IRAS06063+2040	06:09:21.9	+20:39:28	2.8	27000	9.50	n	n	n
11	IRAS06084-0611	06:10:51.0	-06:11:54	1.0	11000	10.00	y	n	n
12	IRAS06099+1800	06:12:53.3	+17:59:22	2.5	61000	10.00	y	y	Y
13	G5.48-0.24	17:59:03.0	-24:20:59	14.3	745000	75.00	n	n	n
14	G5.89-0.39	18:00:30.4	-24:04:00.20	2.0	300000	10.00	y	y	y[1]
15	G5.97-1.17	18:03:40.5	-24:22:44.37	2.7	84000	10.00	n	n	n
16	G6.55-0.10	18:00:49.6	-23:20:23	16.7	1280000	15.00	n	n	n
17	G8.14+0.23	18:03:00.4	-21:48:05	4.2	192000	19.70	y	n	n
18	G8.67-0.36	18:06:19.0	-21:37:32.32	4.8	264000	38.00	y	y	y[1]
19	G10.10+0.74	18:05:13.1	-19:50:34.88	4.4	...	38.60	n	n	n
20	IRAS18032-2032	18:06:13.5	-20:31:47	5.7	...	5.00	y	y	Y
21	G10.15-0.34	18:09:25.1	-20:19:15	4.4	...	5.00	n	n	n
22	G10.30-0.15	18:08:56.1	-20:05:53.76	6.0	734000	11.00	y	y	Y
23	G10.47+0.03	18:08:38.4	-19:51:52	7.3	679000	66.20	y	y	Y
24	IRAS18073-2046	18:10:17.1	-20:45:43	3.9	...	28.00	n	n	n
25	G10.62-0.38	18:10:23.5	-19:56:14.7	17.6	...	-3.00	y	n	n
26	IRAS18085-1931	18:11:33.2	-19:30:39	5.2	...	-1.10	n	n	n

Table 3.8 (cont'd)

Col. No.	UCHII ID	R.A. (J2000.0)	Decl. (J2000.0)	Distance (kpc)	L_{bol} ($L_\odot$)	V_{LSR} (km s^{-1})	Detections 22 GHz	44 GHz	95 GHz
27	G11.94-0.62	18:14:01.1	-18:53:24.2	5.2	193000	38.90	y	y	y[1]
28	G12.21-0.10	18:12:39.7	-18:24:21	16.1	1440000	20.00	y	y	Y
29	G12.43-0.05	18:12:54.6	-18:11:08.33	16.7	173000	40.00	n	n	n
30	IRAS18162-2048	18:19:11.9	-20:47:34	1.9	28000	12.20	y	y	y[1]
31	G15.04-0.68	18:20:24.8	-16:11:35.0	2.1	433000	21.10	y	y	y[1]
32	IRAS18222-1317	18:25:02.3	-13:15:51	4.2	248000	54.90	n	n	n
33	IRAS18228-1312	18:25:42.3	-13:10:20	2.9	...	33.30	n	n	n
34	IRAS18232-1154	18:26:03.0	-11:52:34	2.0	...	24.10	y	n	n
35	G19.07-0.27	18:26:47.0	-12:26:32	5.4	262000	63.00	n	y	n
36	G19.61-0.23	18:27:38.0	-11:56:42	4.5	261000	41.60	y	y	y[1]
37	G20.08-0.14	18:28:10.6	-11:28:45	12.3	73000	40.70	y	n	Y
38	IRAS18316-0602	18:34:19.8	-05:59:44	3.0	...	41.40	y	y	Y
39	G23.46-0.20	18:34:44.9	-08:31:07.4	9.0	875000	65.00	n	n	n
40	G23.71+0.17	18:33:52.5	-08:07:32	9.2	...	115.00	y	y	n
41	G23.96+0.15	18:34:24.9	-07:54:48	6.0	249000	79.60	y	n	n
42	G25.72+0.05	18:38:02.8	-06:23:47.3	14.0	594000	54.50	n	n	n
43	G27.28+0.15	18:40:34.0	-04:57:48	12.8	...	31.70	n	n	n
44	IRAS18403-0417	18:42:58.2	-04:14:00	9.1	476000	97.40	y	y	Y
45	IRAS18416-0420	18:44:18.6	-04:17:53	3.3	117000	48.10	n	n	n
46	G29.96-0.02	18:46:03.9	-02:39:21.9	7.4	1980000	96.00	y	y	y[1]
47	G30.54+0.02	18:46:59.1	-02:07:32	13.8	516000	48.00	y	n	n
48	G31.41+0.31	18:47:34.6	-01:12:43	8.5	279000	98.50	y	y	Y
49	IRAS18456-0129	18:48:15.1	-01:26:25	7.3	...	109.90	y	y	n
50	IRAS18469-0132	18:49:34.7	-01:29:08	7.3	...	87.70	n	y	n
51	IRAS18479-0005	18:50:30.9	-00:01:59	12.9	1339676	15.00	y	n	n
52	G33.50+0.20	18:51:46.7	+00:35:32.3	...	...	11.00	n	n	n

Table 3.8 (cont'd)

Col. No.	UCHII ID	R.A. (J2000.0)	Decl. (J2000.0)	Distance (kpc)	L_{bol} ($L_\odot$)	V_{LSR} (km s^{-1})	Detections 22 GHz	44 GHz	95 GHz
53	IRAS18496+0004	18:52:09.9	+00:08:40	7.1	128000	76.90	n	n	n
54	G33.92+0.11	18:52:50.0	+00:55:29	7.1	310000	107.60	y	y	n
55	G34.26+0.15	18:53:18.5	+01:14:57.9	4.0	593000	58.30	y	y	Y
56	IRAS18515+0157	18:54:04.2	+02:01:34	10.0	...	51.90	y	n	n
57	IRAS18534+0218	18:56:00.7	+02:22:52	10.2	...	49.60	y	n	n
58	IRAS18538+0216	18:56:23.5	+02:20:38	10.1	...	53.20	y	n	n
59	G35.05-0.52	18:57:09.0	+01:39:03.37	12.7	399000	49.60	n	y	y[1]
60	IRAS18592+0108	19:01:47.0	+01:13:08	3.2	...	43.60	y	n	n
61	IRAS18593+0408	19:01:53.0	+04:12:50	9.2	726000	60.70	y	n	n
62	G37.55-0.11	19:00:15.7	+04:03:13	9.9	475000	53.70	n	n	n
63	G41.71+0.11	19:07:09.8	+07:51:36.10	...	...	-10.00	n	n	n
64	G41.74+0.10	19:07:15.5	+07:52:43.90	12.6	...	-13.00	n	n	n
65	G42.42-0.27	19:09:49.5	+08:18:43.67	5.2	94623	64.90	y	n	n
66	G42.90+0.57	19:07:42.0	+09:07:20.0	...	...	-20.60	n	n	n
67	IRAS19081+0903	19:10:35.0	+09:08:31	11.7	...	6.70	y	y	n
68	IRAS19095+0930	19:11:53.3	+09:35:46	9.0	...	44.10	y	n	n
69	G43.18-0.52	19:12:23.2	+08:32:12.2	...	...	57.20	n	n	n
70	G43.89-0.78	19:14:26.2	+09:22:34.0	10.3	276000	52.90	y	n	n
71	G44.26+0.10	19:11:56.5	+10:07:02.1	8.1	...	60.00	y	n	n
72	G45.07+0.13	19:13:22.1	+10:50:53.4	6.0	1424000	58.30	y	y	Y
73	G45.12+0.13	19:13:27.9	+10:53:36.74	6.9	1660000	58.60	y	n	n
74	G45.45+0.06	19:12:00.1	+11:03:59.50	...	...	57.60	y	n	n
75	G45.47+0.05	19:12:04.4	+11:04:11.00	...	...	57.60	y	n	n
76	G45.48+0.13	19:14:08.5	+11:12:16	9.7	975000	60.80	y	n	n
77	IRAS19181+1349	19:20:28.1	+13:55:26	9.7	...	17.70	y	n	n
78	W51d	19:23:40.0	+14:30:51	5.1	...	59.60	y	y	Y

Table 3.8 (cont'd)

Col. No.	UCHII ID	R.A. (J2000.0)	Decl. (J2000.0)	Distance (kpc)	L_{bol} ($L_\odot$)	V_{LSR} (km s^{-1})	Detections 22 GHz	44 GHz	95 GHz
79	G50.23+0.33	19:22:34.7	+15:30:10.01	...	...	30.00	n	n	n
80	G50.31+0.68	19:21:27.6	+15:44:21.3	1.9	87700	26.00	y	n	n
81	IRAS19282+1814	19:30:28.1	+18:20:53	2.3	...	23.60	n	n	n
82	G54.10-0.06	19:31:42.3	+18:42:52	7.9	175000	39.90	y	n	n
83	IRAS19410+2336	19:43:11.6	+23:44:06	2.2	...	22.40	y	y	Y
84	IRAS19442+2427	19:46:20.0	+24:35:24	5.8	268534	21.70	n	n	n
85	G61.48+0.09	19:46:47.3	+25:12:43.6	4.1	...	21.90	y	n	n
86	IRAS19598+3324	20:01:45.6	+33:32:44	8.3	1803017	-25.20	y	n	n
87	IRAS20081+3122	20:10:09.1	+31:31:34	3.0	...	11.60	y	y	Y
88	IRAS20178+4046	20:19:39.3	+40:56:30	3.3	70000	0.90	n	n	n
89	G75.78+0.34	20:21:44.1	+37:26:40	5.6	446000	-0.10	y	y	Y
90	G75.83+0.40	20:21:39.3	+37:31:03.6	5.5	603000	0.00	y	n	n
91	IRAS20220+3728	20:23:55.7	+37:38:10	4.4	...	-2.70	n	n	n
92	IRAS20255+3712	20:27:26.6	+37:22:48	1.0	32000	-1.70	y	n	n
93	IRAS20264+4042	20:28:12.4	+40:52:28	1.5	...	-41.90	n	n	n
94	IRAS20277+3851	20:29:36.4	+39:01:17	4.4	...	-2.90	n	n	n
95	IRAS20306+4005	20:32:28.7	+40:16:05	1.0	...	3.70	n	n	n
96	IRAS20350+4126	20:36:52.6	+41:36:32	2.1	...	-3.10	n	n	n
97	DR21	20:39:01.1	+42:19:43	1.5	...	0.00	y	y	Y
98	IRAS22176+6303	22:19:18.2	+63:18:46	0.9	20796	-7.19	n	y	Y
99	IRAS22543+6145	22:56:19.1	+62:01:57	0.7	34753	-11.10	y	y	Y
100	IRAS22551+6221	22:57:05.2	+62:37:44	0.7	...	-13.40	n	n	n
101	NGC7538	23:13:45.7	+61:28:21	3.5	690240	-57.20	y	y	Y
102	IRAS23133+6050	23:15:31.5	+61:07:09	2.5	186000	-56.30	n	n	n
103	IRAS23138+5945	23:16:04.8	+60:02:00	2.5	31000	-44.10	y	y	Y

Table 3.9. Detected Maser Line Parameters(IRDC)

RMS ID	Line	Epoch	Station	v_p (km s^{-1})	S_p (Jy)	$\int S_\nu dv$ (Jykm s^{-1})	$v_{\rm min}$ (km s^{-1})	$v_{\rm max}$ (km s^{-1})	$v_{\rm rel}$ (km s^{-1})	$L_{\rm maser}$ (L$_\odot$)	notes
G018.82 MM1	22	20121107	US	33.88	136.9	363.3	31.14	60.42	29.28	1.94E-04	
	44	20121107	US	39.81	3.3	13.3	38.53	44.49	5.95	1.41E-05	
	95	20121107	US	39.81	4.5	14.6	38.04	43.36	5.32	3.34E-05	
	95	20120309	YS	27.16	7.7	5.5	26.18	27.16	0.98	3.14E-06	
G019.27 MM2	22	20120311	YS	28.62	13.7	12.7	27.99	29.25	1.26	1.69E-06	
G022.35 MM1	22	20121107	US	50.59	24.8	22.3	49.96	51.23	1.26	9.57E-06	
	44	20121107	US	52.77	2.7	7.1	51.07	54.90	3.83	6.04E-06	
	95	20121107	US	54.22	2.9	9.2	51.07	55.79	4.73	1.69E-05	
G023.60 MM1	22	20121108	US	108.10	3.1	1.5	107.89	108.10	0.21	5.41E-07	
	44	20121108	US	106.26	7.2	15.1	104.13	109.87	5.74	1.06E-05	
	95	20121108	US	106.08	7.4	14.3	105.68	109.03	3.35	2.15E-05	
G023.60 MM2	44	20120307	YS	50.47	16.5	20.8	50.26	56.21	5.95	1.45E-05	
	95	20120307	YS	52.88	3.2	6.2	50.33	54.66	4.33	9.39E-06	
G023.60 MM4	44	20121108	US	52.81	5.5	5.4	50.26	53.02	2.76	3.80E-06	
G024.33 MM1	22	20121113	US	110.97	44.1	96.3	32.60	112.02	79.42	3.23E-05	
	44	20121113	US	113.33	43.4	76.4	111.85	116.74	4.89	5.07E-05	
	95	20121113	US	113.38	53.1	98.5	111.61	116.92	5.32	1.41E-04	
G024.33 MM2	22	20121128	US	121.08	1.7	0.5	120.87	121.08	0.21	1.63E-07	
	44	20121128	US	119.50	2.1	0.9	119.29	119.71	0.43	6.22E-07	
G024.33 MM3	44	20121114	US	118.86	3.0	2.5	118.86	121.63	2.76	1.69E-06	
	95	20121114	US	118.89	3.3	2.2	117.91	119.09	1.18	3.09E-06	
G024.33 MM5	22	20121114	US	118.13	2.5	1.3	117.50	118.13	0.63	4.35E-07	
	44	20121114	US	119.71	2.8	2.6	117.59	119.71	2.13	1.69E-06	
	95	20121114	US	119.88	1.4	0.9	119.48	119.88	0.39	1.32E-06	
G024.33 MM6	22	20121114	US	110.97	40.5	84.7	32.81	112.02	79.21	2.84E-05	
	44	20121114	US	113.33	30.9	54.1	111.85	116.95	5.10	3.59E-05	

Table 3.9 (cont'd)

RMS ID	Line	Epoch	Station	v_p (km s^{-1})	S_p (Jy)	$\int S_\nu dv$ (Jykm s^{-1})	$v_{\rm min}$ (km s^{-1})	$v_{\rm max}$ (km s^{-1})	$v_{\rm rel}$ (km s^{-1})	$L_{\rm maser}$ (L$_\odot$)	notes
	95	20121114	US	113.38	8.2	11.7	112.79	115.35	2.56	1.67E-05	
G024.33 MM9	44	20121114	US	119.71	2.2	0.5	119.71	119.71	0.21	3.08E-07	
G024.60 MM1	22	20121114	US	52.44	38.0	37.8	51.59	53.28	1.69	1.20E-05	
	44	20121114	US	50.80	6.2	6.0	50.58	52.50	1.91	3.77E-06	
	95	20121114	US	50.89	6.0	9.8	50.30	52.86	2.56	1.33E-05	
G024.60 MM2	22	20121115	US	52.44	15.0	16.4	51.59	53.28	1.69	5.19E-06	
G024.60 MM3	22	20121114	US	52.44	35.2	36.3	51.59	53.49	1.90	1.15E-05	
	44	20121114	US	51.01	5.4	5.8	50.58	52.71	2.13	3.66E-06	
	95	20121114	US	50.89	3.7	4.5	50.69	53.45	2.76	6.14E-06	
G025.04 MM1	44	20120229	YS	65.55	5.2	2.1	65.34	65.55	0.21	1.12E-06	
G025.04 MM2	44	20121115	US	63.45	1.4	0.6	63.45	63.45	0.21	3.27E-07	
G027.94 MM1	22	20120301	YS	58.66	31.1	26.7	58.02	62.24	4.21	6.33E-06	
	44	20120301	YS	45.22	20.5	17.0	44.58	46.71	2.13	7.97E-06	
	95	20120301	YS	45.28	14.7	13.3	44.10	45.68	1.58	1.35E-05	
G027.94 MM2	22	20121115	US	42.43	5.8	4.4	42.22	43.07	0.84	1.04E-06	
	44	20121115	US	45.22	6.2	5.0	44.58	45.65	1.06	2.34E-06	
G027.97 MM2	22	20120301	YS	58.86	2.0	0.7	58.43	58.86	0.42	1.65E-07	
G027.97 MM3	44	20120319	YS	44.15	1.5	1.2	44.15	44.15	0.21	5.88E-07	
G028.04 MM1	44	20120301	YS	45.02	104.9	68.0	44.38	45.87	1.49	3.20E-05	
	95	20120301	YS	45.08	5.5	2.0	44.88	45.28	0.39	2.06E-06	
G028.28 MM1	44	20120309	YS	48.20	8.5	1.8	48.20	48.20	0.21	9.07E-07	
	95	20120309	YS	48.16	5.2	2.2	47.97	48.36	0.39	2.43E-06	
G028.28 MM3	22	20121125	US	31.92	2.1	2.0	31.71	58.67	26.97	5.09E-07	
	44	20121125	US	48.41	3.1	1.7	47.98	48.41	0.43	8.66E-07	
G028.28 MM4	22	20121125	US	31.92	1.7	0.4	31.71	31.92	0.21	9.10E-08	
G028.37 MM1	22	20120307	YS	77.65	458.2	455.0	-3.46	88.40	91.85	2.64E-04	

Table 3.9 (cont'd)

RMS ID	Line	Epoch	Station	v_p (km s^{-1})	S_p (Jy)	$\int S_\nu dv$ (Jykm s^{-1})	$v_{\rm min}$ (km s^{-1})	$v_{\rm max}$ (km s^{-1})	$v_{\rm rel}$ (km s^{-1})	$L_{\rm maser}$ (L$_\odot$)	notes
	44	20120307	YS	76.63	63.0	117.4	76.00	80.04	4.04	1.35E-04	
	95	20120307	YS	76.41	27.1	69.6	73.65	81.33	7.68	1.73E-04	
G028.37 MM2	22	20120310	YS	77.65	10.1	8.6	77.02	78.28	1.26	4.98E-06	
	44	20120310	YS	82.37	9.0	7.7	81.52	82.37	0.85	8.90E-06	
	95	20120310	YS	82.12	5.5	4.9	81.53	82.32	0.79	1.21E-05	
G028.37 MM3	44	20120310	YS	101.35	6.7	10.3	99.65	101.35	1.70	1.19E-05	
	95	20120310	YS	99.68	5.0	6.3	99.28	101.25	1.97	1.57E-05	
G028.37 MM4	22	20120310	YS	77.65	26.9	21.0	77.02	78.07	1.05	1.22E-05	
	44	20120310	YS	78.55	3.6	3.1	78.55	78.55	0.21	3.56E-06	
	95	20120310	YS	79.76	2.6	4.7	78.58	80.54	1.97	1.16E-05	
G028.37 MM5	22	20120311	YS	29.41	8.6	6.9	28.78	30.04	1.26	3.97E-06	
G028.37 MM6	22	20120310	YS	77.65	9.1	5.3	77.23	77.86	0.63	3.09E-06	
	44	20120310	YS	79.40	9.2	9.4	78.97	79.82	0.85	1.08E-05	
	95	20120310	YS	79.76	4.8	3.5	79.17	79.95	0.79	8.64E-06	
G028.37 MM10	22	20120310	YS	77.65	7.8	5.2	77.23	77.86	0.63	3.00E-06	
	44	20120310	YS	79.82	5.8	12.8	76.42	79.82	3.40	1.47E-05	
	95	20120310	YS	79.36	4.3	5.7	78.77	80.94	2.17	1.42E-05	
G028.37 MM11	22	20120311	YS	77.65	22.7	17.4	77.02	78.07	1.05	1.01E-05	
G028.37 MM13	22	20120312	YS	77.65	14.9	11.6	77.02	78.07	1.05	6.74E-06	
G028.37 MM15	22	20120314	YS	29.20	4.0	3.0	28.99	29.83	0.84	1.76E-06	
G028.37 MM16	22	20120315	YS	77.65	31.7	28.8	76.81	81.44	4.63	1.67E-05	
G028.37 MM17	22	20120318	YS	77.44	6.4	4.8	77.23	78.07	0.84	2.81E-06	
	44	20120318	YS	79.40	3.2	1.2	79.40	79.61	0.21	1.35E-06	
G028.53 MM2	44	20121127	US	85.88	2.4	6.6	83.12	88.22	5.10	9.92E-06	
G028.53 MM6	22	20120310	YS	92.16	4.6	3.3	91.74	92.58	0.84	2.52E-06	
	44	20120310	YS	87.37	4.8	2.1	87.37	87.37	0.21	3.07E-06	

Table 3.9 (cont'd)

RMS ID	Line	Epoch	Station	v_p (km s^{-1})	S_p (Jy)	$\int S_\nu dv$ (Jykm s^{-1})	$v_{\rm min}$ (km s^{-1})	$v_{\rm max}$ (km s^{-1})	$v_{\rm rel}$ (km s^{-1})	$L_{\rm maser}$ (L$_\odot$)	notes
G028.53 MM9	22	20121123	US	66.04	2.4	0.5	66.04	66.04	0.21	3.83E-07	
G028.53 MM10	22	20120318	YS	92.16	3.6	5.6	82.89	92.37	9.48	4.21E-06	
G028.67 MM2	44	20121123	US	73.49	1.2	0.5	73.49	73.49	0.21	5.84E-07	
	95	20120310	YS	90.31	4.0	2.7	89.52	90.51	0.98	8.13E-06	
G030.97 MM1	44	20121108	US	77.05	2.8	1.0	76.83	77.05	0.21	1.17E-06	
	95	20120318	YS	77.20	1.7	0.7	76.83	77.05	0.21	1.77E-06	
G031.97 MM1	22	20120310	YS	96.17	4.7	15.1	90.49	102.28	11.80	1.67E-05	
	44	20120310	YS	95.37	9.8	8.6	94.52	95.58	1.06	1.87E-05	
	95	20120310	YS	95.10	7.2	23.3	91.56	98.05	6.50	1.10E-04	
G031.97 MM3	22	20120311	YS	98.07	3.5	7.1	82.90	98.28	15.38	7.89E-06	
	95	20120311	YS	98.05	4.2	3.8	98.05	99.43	1.38	1.82E-05	
G031.97 MM4	22	20121124	US	100.39	3.7	4.6	98.07	101.02	2.95	5.08E-06	
	44	20121124	US	98.13	4.1	11.2	93.88	98.35	4.46	2.44E-05	
	95	20121124	US	95.89	1.6	3.1	95.49	97.86	2.36	1.45E-05	
G031.97 MM5	44	20121124	US	95.37	1.5	1.8	95.37	96.22	0.85	4.00E-06	
	95	20121124	US	92.74	1.0	3.3	92.74	95.10	2.36	1.57E-05	
G033.69 MM1	22	20120307	YS	97.79	1.4	1.4	97.79	98.63	0.84	1.68E-06	
	44	20120307	YS	106.48	8.1	13.9	104.78	107.33	2.55	3.23E-05	
	95	20120307	YS	105.48	4.7	12.3	104.50	110.01	5.51	6.13E-05	
G033.69 MM4	44	20121124	US	106.48	2.6	2.3	105.85	106.91	1.06	5.24E-06	
G033.69 MM5	22	20121124	US	110.01	1.2	0.5	109.59	110.01	0.42	6.11E-07	
G033.69 MM10	44	20120311	YS	104.57	6.5	2.8	104.57	104.57	0.21	6.40E-06	
	95	20120311	YS	104.50	6.8	3.7	103.91	104.69	0.79	1.84E-05	
G034.43 MM1	22	20120315	YS	56.36	203.7	699.3	29.61	90.70	61.09	2.22E-04	
	44	20120315	YS	57.68	10.5	35.5	54.92	60.66	5.74	2.24E-05	
	95	20120315	YS	57.47	9.5	44.4	52.55	62.98	10.43	6.02E-05	

Table 3.9 (cont'd)

RMS ID	Line	Epoch	Station	v_p (km s^{-1})	S_p (Jy)	$\int S_\nu dv$ (Jykm s^{-1})	$v_{\rm min}$ (km s^{-1})	$v_{\rm max}$ (km s^{-1})	$v_{\rm rel}$ (km s^{-1})	$L_{\rm maser}$ (L$_\odot$)	notes
G034.43 MM2	22	20120229	US	56.36	128.9	509.5	45.41	90.70	45.29	1.62E-04	
	44	20120229	US	60.24	36.8	65.8	56.20	60.66	4.46	4.14E-05	
	95	20120229	US	60.23	21.6	52.6	55.50	60.62	5.12	7.15E-05	
G034.43 MM3	22	20120311	YS	56.36	8.8	28.5	48.15	62.47	14.33	9.04E-06	
	44	20120311	YS	59.17	38.5	44.2	58.11	60.66	2.55	2.78E-05	
	95	20120311	YS	59.24	30.2	44.6	56.88	61.80	4.92	6.06E-05	
G034.43 MM4	44	20121124	US	60.02	22.6	56.8	54.71	61.94	7.23	3.57E-05	
	95	20121124	US	58.06	6.3	15.1	56.09	60.03	3.94	2.04E-05	
G034.43 MM5	22	20121124	US	56.36	28.1	121.2	37.61	65.63	28.02	3.85E-05	
	44	20121124	US	57.90	3.0	3.6	57.47	58.75	1.28	2.27E-06	
	95	20121124	US	58.26	0.8	0.3	57.86	57.86	0.20	4.18E-07	
G034.43 MM6	22	20121125	US	56.36	3.4	13.9	51.52	62.68	11.17	4.42E-06	
	44	20121125	US	59.17	19.1	21.6	56.83	60.45	3.61	1.36E-05	
	95	20121125	US	59.24	3.1	3.1	57.86	59.83	1.97	4.16E-06	
G034.43 MM7	22	20121125	US	56.36	38.9	119.8	48.15	159.38	111.23	3.80E-05	
	44	20121125	US	59.39	3.7	5.5	57.26	59.81	2.55	3.48E-06	
	95	20121125	US	60.23	0.6	0.5	59.44	59.44	0.20	6.94E-07	
G034.43 MM8	22	20121125	US	56.36	295.6	923.8	45.41	160.64	115.24	2.93E-04	
	44	20121125	US	60.24	3.9	8.4	57.26	60.45	3.19	5.30E-06	
	95	20121108	US	44.26	2.1	4.1	43.48	45.84	2.36	3.45E-06	
G035.39 MM1	22	20121107	US	66.71	2.7	3.9	66.71	77.67	10.95	7.65E-07	
G035.39 MM2	22	20120301	YS	55.34	12.8	10.3	54.71	58.92	4.21	2.01E-06	
G035.39 MM3	22	20121113	US	53.86	5.0	18.9	44.17	57.23	13.06	3.69E-06	
	44	20121127	US	55.06	1.8	0.7	55.06	55.28	0.21	2.58E-07	
	95	20121113	US	55.70	1.8	3.2	54.91	55.70	0.79	2.68E-06	
G035.39 MM4	22	20121114	US	47.75	5.8	6.1	46.70	48.18	1.47	1.18E-06	

Table 3.9 (cont'd)

RMS ID	Line	Epoch	Station	v_p (km s^{-1})	S_p (Jy)	$\int S_\nu dv$ (Jykm s^{-1})	$v_{\rm min}$ (km s^{-1})	$v_{\rm max}$ (km s^{-1})	$v_{\rm rel}$ (km s^{-1})	$L_{\rm maser}$ (L$_\odot$)	notes
G035.39 MM5	22	20121125	US	47.75	3.8	4.4	46.49	48.18	1.69	8.57E-07	
G035.39 MM8	22	20121124	US	48.39	1.3	0.5	47.97	48.39	0.42	1.04E-07	
G048.65 MM1	22	20120315	YS	32.84	9.1	13.2	30.73	33.47	2.74	1.92E-06	
G048.65 MM2	22	20120319	YS	32.84	5.4	7.0	30.95	33.26	2.32	1.01E-06	
G053.11 MM1	22	20120301	YS	17.05	25.7	20.8	16.21	17.68	1.47	1.56E-06	
	44	20120301	YS	21.95	20.3	12.2	21.52	22.37	0.85	1.81E-06	
	95	20120301	YS	21.98	14.9	18.9	18.63	22.96	4.33	6.07E-06	
G053.11 MM2	22	20120307	YS	16.42	2.2	3.8	13.89	24.00	10.11	2.89E-07	
G053.25 MM1	22	20121113	US	22.95	2.6	1.3	22.53	22.95	0.42	1.13E-07	
	44	20121113	US	25.12	3.2	2.2	24.91	25.76	0.85	3.68E-07	
	95	20121113	US	25.06	2.0	2.7	24.66	25.84	1.18	9.68E-07	
G053.25 MM2	22	20121115	US	22.95	4.3	9.9	16.63	32.01	15.38	8.26E-07	
G053.25 MM4	22	20121113	US	22.95	4.5	5.6	22.53	30.33	7.79	4.71E-07	
G053.25 MM6	22	20121107	US	32.22	2.7	0.6	32.22	32.22	0.21	4.68E-08	

Table 3.10. Detected Maser Line Parameters(MMS)

RMS ID	Line	Epoch	Station	v_p (km s^{-1})	S_p (Jy)	$\int S_\nu dv$ (Jykm s^{-1})	$v_{\rm min}$ (km s^{-1})	$v_{\rm max}$ (km s^{-1})	$v_{\rm rel}$ (km s^{-1})	$L_{\rm maser}$ (L$_\odot$)	notes
0.21-0.00	44	20120512	YS	45.75	10.9	7.4	45.32	46.17	0.85	NaN	
	95	20120512	YS	45.83	5.6	1.2	45.63	45.83	0.20	NaN	
0.31-0.20	22	20120512	YS	19.16	14.7	23.1	15.37	19.58	4.21	NaN	
0.49+0.18	44	20120518	YS	-7.12	3.6	0.8	-7.12	-7.12	0.21	NaN	
	95	20120518	YS	-7.10	3.0	0.6	-7.12	-7.12	0.20	NaN	
0.64-0.04	22	20120526	US	69.01	137.1	1634.9	-7.04	99.34	106.39	NaN	
	44	20120526	US	54.36	10.2	223.3	43.31	83.27	39.97	NaN	
	95	20120526	US	49.67	7.8	136.5	44.74	75.26	30.52	NaN	
0.66-0.02	22	20120511	YS	68.93	406.1	5344.7	-26.08	126.87	152.95	NaN	
	44	20120511	YS	60.45	23.5	453.3	47.06	80.65	33.59	NaN	
	95	20120511	YS	56.62	31.5	556.0	44.81	78.48	33.67	NaN	
0.67-0.02	22	20120511	YS	67.19	329.7	3581.2	-26.08	126.87	152.95	6.29E-03	
	44	20120511	YS	69.10	34.8	466.9	48.69	85.46	36.78	1.62E-03	
	95	20120511	YS	64.12	37.7	573.7	50.54	80.46	29.93	4.31E-03	
0.69-0.03	22	20120511	YS	54.07	141.8	2245.8	-6.60	126.12	132.72	4.03E-03	
	44	20120511	YS	72.27	7.4	126.8	45.28	77.59	32.31	4.51E-04	
	95	20120511	YS	58.83	6.3	60.6	55.68	77.93	22.25	4.66E-04	
0.83+0.18	22	20120520	YS	2.97	9.9	17.3	2.55	13.93	11.38	6.28E-05	
	44	20120520	YS	5.36	10.9	15.6	4.93	7.06	2.13	1.12E-04	
	95	20120520	YS	5.64	8.5	8.4	5.25	6.43	1.18	1.31E-04	
1.14-0.12	22	20120510	YS	-13.52	6.8	1.4	-13.73	-13.52	0.21	NaN	
5.90-0.42	22	20120510	YS	9.89	3.1	1.5	8.00	9.89	1.90	7.07E-06	
	44	20120510	YS	9.52	16.5	46.3	2.72	9.73	7.02	4.29E-04	
	95	20120510	YS	4.27	12.8	60.4	3.48	9.58	6.10	1.21E-03	
6.78-0.27	22	20120510	YS	12.47	14.3	22.0	11.63	16.26	4.63	7.85E-05	
	44	20120510	YS	19.83	8.4	16.4	19.62	24.72	5.10	1.16E-04	

Table 3.10 (cont'd)

RMS ID	Line	Epoch	Station	v_p (km s^{-1})	S_p (Jy)	$\int S_\nu dv$ (Jykm s^{-1})	$v_{\rm min}$ (km s^{-1})	$v_{\rm max}$ (km s^{-1})	$v_{\rm rel}$ (km s^{-1})	$L_{\rm maser}$ (L$_\odot$)	notes
	95	20120510	YS	19.79	5.8	9.4	19.39	22.94	3.54	1.43E-04	
8.68-0.36	22	20120509	YS	29.83	39.8	89.3	-23.26	39.10	62.36	2.88E-04	
	44	20120509	YS	37.63	3.6	2.4	37.42	38.27	0.85	1.54E-05	
9.62+0.19	22	20120416	YS	-6.06	27.9	160.5	-9.01	20.49	29.49	1.03E-03	
	44	20120416	YS	3.50	6.1	6.2	3.29	5.41	2.13	7.84E-05	
	95	20120416	YS	3.53	7.8	21.4	-0.40	5.90	6.30	5.85E-04	
10.32-0.26	44	20120513	YS	32.36	98.1	74.3	31.51	35.76	4.25	5.16E-04	
	95	20120513	YS	32.48	12.9	3.7	32.28	32.68	0.39	5.58E-05	
10.47+0.02	22	20120416	YS	61.83	89.7	666.1	38.03	167.38	129.35	1.80E-03	
	44	20120416	YS	66.66	7.4	30.1	61.98	71.33	9.35	1.61E-04	
	95	20120416	YS	67.10	10.0	78.8	59.42	74.38	14.96	9.11E-04	
10.62-0.38	22	20120419	YS	0.05	424.8	1221.2	-16.59	40.29	56.88	7.07E-03	
	44	20120419	YS	-6.75	88.6	94.8	-9.72	-3.77	5.95	1.09E-03	
	95	20120419	YS	-6.64	26.9	81.8	-10.38	-0.73	9.65	2.03E-03	
12.20-0.10	22	20120419	YS	28.95	401.1	1182.9	-12.34	34.01	46.35	5.30E-03	
	44	20120419	YS	23.77	5.4	15.9	21.43	27.60	6.16	1.42E-04	
	95	20120419	YS	25.09	5.6	22.2	20.37	26.47	6.10	4.26E-04	
12.68-0.18	22	20120509	YS	59.69	203.0	460.6	54.42	62.43	8.01	1.49E-03	
	44	20120509	YS	55.14	6.3	8.0	54.29	55.99	1.70	5.10E-05	
	95	20120509	YS	55.13	4.1	7.2	53.35	56.11	2.76	9.89E-05	
12.79-0.19	22	20120419	YS	-3.08	7.5	26.7	-3.50	38.21	41.71	9.99E-05	
	44	20120419	YS	32.76	39.8	71.1	31.91	39.99	8.08	5.26E-04	
	95	20120419	YS	32.83	29.1	27.9	32.04	37.16	5.12	4.46E-04	
12.89+0.49	22	20120509	YS	29.41	79.9	126.5	28.15	32.57	4.42	4.58E-04	
	44	20120509	YS	31.51	16.0	18.6	31.08	34.27	3.19	1.34E-04	
	95	20120509	YS	31.49	12.5	26.1	31.10	36.81	5.71	4.05E-04	

Table 3.10 (cont'd)

RMS ID	Line	Epoch	Station	v_p (km s^{-1})	S_p (Jy)	$\int S_\nu dv$ (Jykm s^{-1})	$v_{\rm min}$ (km s^{-1})	$v_{\rm max}$ (km s^{-1})	$v_{\rm rel}$ (km s^{-1})	$L_{\rm maser}$ (L$_\odot$)	notes
12.90-0.26	22	20120509	YS	36.58	12.7	38.1	-10.82	37.00	47.82	1.38E-04	
	44	20120509	YS	36.61	8.8	20.9	35.76	39.80	4.04	1.50E-04	
	95	20120509	YS	36.42	10.1	21.7	35.04	39.76	4.73	3.36E-04	
13.18+0.06	44	20120513	YS	49.30	20.8	40.4	46.75	51.21	4.46	2.67E-04	
14.33-0.63	22	20120509	YS	4.25	15.1	22.3	3.83	23.63	19.80	1.02E-04	
	44	20120509	YS	23.50	87.7	183.8	11.81	24.35	12.54	1.66E-03	
	95	20120509	YS	22.35	20.5	53.4	16.64	26.49	9.84	1.04E-03	
14.60+0.01	22	20120501	YS	26.17	19.5	38.6	19.85	33.33	13.48	1.68E-04	
	44	20120501	YS	25.17	16.8	27.1	22.83	26.45	3.61	2.34E-04	
	95	20120501	YS	24.97	4.0	2.4	23.59	24.97	1.38	4.45E-05	
15.03-0.67	22	20120501	YS	20.05	206.0	422.4	13.31	23.21	9.90	1.92E-03	
	44	20120501	YS	19.03	7.9	3.7	18.82	19.25	0.43	3.31E-05	
	95	20120501	YS	19.01	6.2	2.8	17.83	19.01	1.18	5.38E-05	
15.67-0.48	22	20120501	YS	-5.40	5.9	16.2	-124.43	-3.08	121.35	1.09E-04	
	44	20120501	YS	-5.37	6.8	6.5	-5.79	-4.52	1.28	8.57E-05	
16.58-0.05	22	20120419	YS	64.16	31.6	70.6	55.10	68.59	13.48	2.24E-04	
	44	20120419	YS	61.29	26.2	36.7	57.25	61.92	4.68	2.31E-04	
	95	20120419	YS	61.14	25.2	33.5	58.19	61.93	3.74	4.55E-04	
16.86-2.15	22	20120419	YS	19.97	30.5	80.0	-48.07	21.24	69.31	3.96E-04	
	44	20120419	YS	17.52	23.8	53.3	14.12	28.36	14.24	5.22E-04	
	95	20120419	YS	17.73	13.3	28.4	14.97	19.10	4.13	6.00E-04	
17.01-2.39	22	20120501	YS	18.56	4.2	5.7	18.56	21.09	2.53	2.51E-05	
	44	20120501	YS	19.85	3.8	0.8	19.85	19.85	0.21	7.15E-06	
18.65+0.04	22	20120518	YS	29.11	6.0	9.6	28.90	82.62	53.72	2.61E-05	
	44	20120518	YS	79.30	3.0	8.7	77.60	82.70	5.10	4.66E-05	
19.36-0.03	44	20120512	YS	26.46	108.4	186.8	24.97	30.07	5.10	1.59E-03	

Table 3.10 (cont'd)

RMS ID	Line	Epoch	Station	v_p (km s^{-1})	S_p (Jy)	$\int S_\nu dv$ (Jykm s^{-1})	$v_{\rm min}$ (km s^{-1})	$v_{\rm max}$ (km s^{-1})	$v_{\rm rel}$ (km s^{-1})	$L_{\rm maser}$ (L$_\odot$)	notes
	95	20120512	YS	26.08	60.4	106.4	24.90	28.44	3.54	1.95E-03	
19.48+0.15	22	20120415	YS	25.74	3.9	11.0	12.89	26.79	13.90	5.00E-05	
	44	20120415	YS	22.01	4.1	3.2	21.80	23.71	1.91	2.89E-05	
	95	20120415	YS	23.73	2.6	0.5	23.53	23.53	0.20	9.85E-06	
19.61-0.13	44	20120501	YS	56.35	5.1	6.5	56.14	58.47	2.34	4.28E-05	
	95	20120501	YS	56.91	2.3	3.5	56.13	56.91	0.79	4.99E-05	
19.61-0.23	22	20120415	YS	46.64	56.8	564.9	23.47	63.28	39.82	2.18E-03	
	44	20120415	YS	41.26	18.5	27.1	40.62	46.36	5.74	2.07E-04	
	95	20120415	YS	41.09	16.8	31.5	40.11	48.77	8.66	5.20E-04	
19.70-0.26	22	20120415	YS	43.07	5.5	10.6	40.55	44.34	3.79	3.84E-05	
19.88-0.52	22	20120415	YS	46.48	21.2	101.0	14.25	46.91	32.65	3.55E-04	
	44	20120415	YS	43.56	8.3	9.4	42.92	44.41	1.49	6.52E-05	
20.08-0.13	22	20120415	YS	46.42	16.8	32.7	36.73	46.84	10.11	1.17E-04	
21.87+0.01	22	20120416	YS	20.47	13.1	33.7	19.00	25.74	6.74	1.51E-04	
	44	20120416	YS	22.86	2.3	0.5	22.65	22.86	0.21	4.31E-06	
22.05+0.22	22	20120416	YS	53.48	6.8	2.1	53.27	53.69	0.42	6.85E-06	
	44	20120416	YS	51.62	40.5	77.5	47.58	54.38	6.80	4.96E-04	
	95	20120416	YS	51.61	7.3	11.1	49.84	52.59	2.76	1.53E-04	
22.36+0.06	22	20120416	YS	87.39	17.3	22.1	15.34	88.65	73.31	5.86E-05	
	44	20120416	YS	83.90	45.3	27.4	83.26	84.75	1.49	1.44E-04	
	95	20120416	YS	83.81	23.7	16.2	83.22	84.40	1.18	1.84E-04	
23.01-0.41	22	20120418	YS	73.21	123.6	299.5	55.09	87.11	32.02	8.10E-04	
	44	20120418	YS	76.01	7.7	9.0	75.80	79.62	3.83	4.83E-05	
	95	20120418	YS	75.96	6.2	8.5	75.37	77.73	2.36	9.86E-05	
23.24-0.24	44	20120512	YS	61.28	14.8	18.7	60.65	63.41	2.76	1.10E-04	
	95	20120512	YS	61.12	6.9	4.2	60.73	61.52	0.79	5.26E-05	

Table 3.10 (cont'd)

RMS ID	Line	Epoch	Station	v_p (km s^{-1})	S_p (Jy)	$\int S_\nu dv$ (Jykm s^{-1})	$v_{\rm min}$ (km s^{-1})	$v_{\rm max}$ (km s^{-1})	$v_{\rm rel}$ (km s^{-1})	$L_{\rm maser}$ (L$_\odot$)	notes
23.32-0.29	44	20120513	YS	75.86	35.2	57.5	55.67	77.56	21.90	3.37E-04	
	95	20120513	YS	76.18	3.3	0.7	75.98	75.98	0.20	8.25E-06	
23.39+0.19	44	20120513	YS	77.66	4.6	4.0	75.96	77.87	1.91	2.16E-05	
23.43-0.18	44	20120513	YS	99.76	59.0	158.1	95.51	104.22	8.72	6.69E-04	
	95	20120513	YS	99.63	16.3	46.6	95.69	103.96	8.27	4.26E-04	
23.48+0.08	22	20120418	YS	87.51	6.6	3.6	87.08	87.72	0.63	8.59E-06	
	44	20120418	YS	85.65	5.3	8.7	83.73	86.07	2.34	4.18E-05	
	95	20120418	YS	85.60	4.9	10.2	83.44	86.00	2.56	1.05E-04	
23.98-0.08	22	20120418	YS	75.85	4.9	16.6	31.40	76.06	44.66	4.59E-05	
	44	20120418	YS	72.97	7.3	7.5	72.12	74.25	2.13	4.07E-05	
	95	20120418	YS	72.65	2.8	4.9	70.88	73.04	2.17	5.73E-05	
24.33+0.14	22	20120418	YS	110.74	56.3	78.3	58.91	112.00	53.09	1.50E-04	
	44	20120418	YS	113.35	36.9	62.3	112.71	116.75	4.04	2.37E-04	
	95	20120418	YS	113.32	7.4	12.1	112.93	115.09	2.17	9.97E-05	
24.50-0.03	44	20120418	YS	111.16	3.0	3.0	110.31	111.58	1.28	1.05E-05	
24.67-0.14	22	20120512	YS	117.84	3.0	0.6	117.84	117.84	0.21	1.14E-06	
	44	20120512	YS	113.26	4.8	3.6	113.05	114.11	1.06	1.29E-05	
24.78+0.08	22	20120418	YS	113.11	281.2	550.1	5.87	116.27	110.39	9.88E-04	
	44	20120418	YS	114.86	31.2	68.4	107.63	115.92	8.29	2.43E-04	
	95	20120418	YS	108.05	10.6	52.7	106.28	114.94	8.66	4.05E-04	
24.93+0.08	22	20120418	YS	42.97	31.1	64.7	3.37	113.12	109.76	2.05E-04	
	44	20120418	YS	46.76	4.7	2.9	46.33	46.97	0.64	1.80E-05	
25.41+0.10	44	20120511	YS	95.31	9.2	11.4	94.88	97.22	2.34	4.83E-05	
	95	20120511	YS	95.19	7.9	10.0	94.99	97.55	2.56	9.13E-05	
25.65+1.04	22	20120419	YS	40.95	270.3	299.3	35.90	48.54	12.64	1.03E-03	
	44	20120419	YS	41.63	46.0	49.9	40.36	44.61	4.25	3.41E-04	

Table 3.10 (cont'd)

RMS ID	Line	Epoch	Station	v_p (km s^{-1})	S_p (Jy)	$\int S_\nu dv$ (Jykm s^{-1})	$v_{\rm min}$ (km s^{-1})	$v_{\rm max}$ (km s^{-1})	$v_{\rm rel}$ (km s^{-1})	$L_{\rm maser}$ (L$_\odot$)	notes
	95	20120419	YS	41.68	38.6	52.6	40.30	45.03	4.73	7.77E-04	
25.70+0.04	44	20120518	YS	95.51	2.7	2.1	95.51	96.36	0.85	9.10E-06	
	95	20120518	YS	96.32	3.2	4.3	95.73	98.09	2.36	4.00E-05	
25.82-0.17	22	20120419	YS	90.46	286.2	1354.8	64.13	138.28	74.16	3.02E-03	
	44	20120419	YS	90.30	97.8	118.1	89.87	99.44	9.57	5.21E-04	
	95	20120419	YS	90.19	58.2	110.1	89.60	99.25	9.65	1.05E-03	
26.60-0.22	44	20120511	YS	107.03	5.3	12.3	105.76	109.58	3.83	4.19E-05	
	95	20120511	YS	108.19	6.0	9.1	105.83	108.38	2.56	6.67E-05	
27.28+0.15	22	20120511	YS	-20.49	6.7	8.4	-20.70	-17.96	2.74	3.03E-05	
	44	20120511	YS	31.15	5.5	7.2	31.15	32.85	1.70	5.14E-05	
	95	20120511	YS	31.43	4.3	3.7	31.23	33.00	1.77	5.77E-05	
27.36-0.16	22	20120501	YS	94.66	19.3	55.9	87.71	96.56	8.85	1.07E-04	
	44	20120501	YS	94.03	120.5	205.5	87.87	96.16	8.29	7.82E-04	
	95	20120501	YS	94.06	49.1	113.4	87.96	96.03	8.07	9.31E-04	
27.78+0.05	22	20120501	YS	100.74	4.8	6.5	100.11	103.90	3.79	9.38E-06	
	44	20120501	YS	101.12	3.8	3.0	99.42	101.12	1.70	8.63E-06	
27.78-0.25	44	20120512	YS	104.22	8.6	7.8	102.95	104.65	1.70	2.98E-05	
	95	20120512	YS	103.98	5.1	4.9	102.99	104.37	1.38	4.00E-05	
28.20-0.05	22	20120501	YS	95.52	14.4	19.8	94.68	98.68	4.00	3.63E-05	
	44	20120501	YS	97.46	2.6	4.0	93.21	97.46	4.25	1.45E-05	
	95	20120501	YS	96.02	2.0	0.4	95.83	95.83	0.20	3.07E-06	
28.39+0.08	22	20120509	YS	77.53	362.4	339.3	73.94	87.85	13.90	8.51E-04	
	44	20120509	YS	79.34	37.0	44.6	76.15	81.04	4.89	2.22E-04	
	95	20120509	YS	79.34	17.8	6.8	79.15	79.74	0.59	7.35E-05	
28.81+0.36	22	20120509	YS	88.25	11.5	35.1	-67.44	88.67	156.11	7.05E-05	
	44	20120509	YS	85.93	3.3	3.8	85.72	87.42	1.70	1.52E-05	

Table 3.10 (cont'd)

RMS ID	Line	Epoch	Station	v_p (km s^{-1})	S_p (Jy)	$\int S_\nu dv$ (Jykm s^{-1})	$v_{\rm min}$ (km s^{-1})	$v_{\rm max}$ (km s^{-1})	$v_{\rm rel}$ (km s^{-1})	$L_{\rm maser}$ (L$_\odot$)	notes
28.83-0.25	44	20120511	YS	86.37	7.8	5.0	86.16	87.22	1.06	2.10E-05	
28.86+0.07	22	20120509	YS	105.11	103.9	325.0	88.25	108.48	20.22	5.19E-04	
	44	20120509	YS	103.46	8.8	12.8	101.97	104.73	2.76	4.06E-05	
	95	20120509	YS	103.20	4.4	7.5	103.01	105.17	2.17	5.13E-05	
29.91-0.03	22	20120509	YS	34.34	7.7	38.0	31.39	45.29	13.90	6.66E-05	
	44	20120509	YS	98.24	127.0	55.1	95.68	99.94	4.25	1.92E-04	
	95	20120509	YS	98.35	6.8	2.7	98.15	98.35	0.20	2.04E-05	
30.30+0.06	22	20120509	YS	49.02	7.9	6.5	48.18	49.45	1.26	2.15E-05	
	44	20120509	YS	45.15	5.1	2.5	44.73	45.15	0.43	1.66E-05	
30.40-0.29	22	20120511	YS	102.93	2.7	2.4	102.93	103.77	0.84	3.95E-06	
	44	20120511	YS	103.45	4.5	4.5	103.24	104.72	1.49	1.44E-05	
30.53+0.01	22	20120518	YS	-34.11	6.5	19.6	-40.01	-30.74	9.27	5.59E-05	
	44	20120518	YS	48.48	3.6	3.8	47.42	48.91	1.49	2.17E-05	
	95	20120518	YS	47.86	2.2	0.9	47.27	47.86	0.59	1.10E-05	
30.70-0.07	22	20120510	YS	97.59	3.3	7.9	88.74	97.80	9.06	1.51E-05	
	44	20120510	YS	89.43	32.6	54.5	88.16	95.60	7.44	2.07E-04	
	95	20120510	YS	89.55	17.8	29.7	87.98	94.08	6.10	2.44E-04	
30.79+0.20	22	20120510	YS	80.63	3.5	2.7	80.63	81.89	1.26	5.23E-06	
	44	20120510	YS	82.33	73.0	85.3	80.42	86.37	5.95	3.31E-04	
	95	20120510	YS	82.23	33.9	38.0	80.66	84.20	3.54	3.19E-04	
30.82-0.05	22	20120508	YS	97.10	117.5	850.8	61.92	129.76	67.84	1.23E-03	
	44	20120508	YS	96.91	42.0	137.9	93.29	103.07	9.78	3.95E-04	
	95	20120508	YS	96.64	19.0	72.9	94.08	102.35	8.27	4.51E-04	
30.86+0.16	44	20120518	YS	106.41	7.4	2.9	105.77	106.41	0.64	8.03E-06	
	95	20120518	YS	106.31	4.9	1.5	106.31	106.50	0.20	8.62E-06	
31.28+0.06	22	20120510	YS	106.95	6.2	10.6	106.52	114.53	8.01	1.31E-05	

Table 3.10 (cont'd)

RMS ID	Line	Epoch	Station	v_p (km s^{-1})	S_p (Jy)	$\int S_\nu dv$ (Jykm s^{-1})	$v_{\rm min}$ (km s^{-1})	$v_{\rm max}$ (km s^{-1})	$v_{\rm rel}$ (km s^{-1})	$L_{\rm maser}$ (L$_\odot$)	notes
	44	20120510	YS	109.31	11.3	32.0	105.70	111.65	5.95	7.84E-05	
	95	20120510	YS	109.19	9.5	33.7	105.64	111.94	6.30	1.78E-04	
31.41+0.31	22	20120510	YS	99.26	313.4	558.4	93.57	107.69	14.11	6.90E-04	
	44	20120510	YS	93.96	4.0	19.7	92.25	101.40	9.14	4.81E-05	
	95	20120510	YS	96.49	9.7	61.1	93.15	104.17	11.03	3.23E-04	
32.03+0.06	22	20120510	YS	92.91	7.8	26.8	91.43	102.17	10.74	4.39E-05	
	44	20120510	YS	95.30	16.9	25.0	92.75	97.42	4.68	8.11E-05	
	95	20120510	YS	95.33	8.2	17.7	93.37	97.70	4.33	1.24E-04	
32.74-0.08	22	20120508	YS	33.00	27.9	19.0	31.73	33.42	1.69	5.92E-05	
	44	20120508	YS	35.97	5.8	8.1	35.76	37.88	2.13	4.99E-05	
	95	20120508	YS	35.83	4.5	6.2	34.64	37.79	3.15	8.25E-05	
33.86+0.01	22	20120510	YS	62.42	3.1	1.9	62.00	62.42	0.42	4.42E-06	
	44	20120510	YS	60.12	5.7	5.1	59.91	61.82	1.91	2.29E-05	
	95	20120510	YS	64.76	3.1	0.6	64.76	64.76	0.20	6.01E-06	
34.24+0.13	22	20120419	YS	51.52	131.0	654.5	24.14	67.53	43.40	1.64E-03	
	44	20120419	YS	56.65	12.0	19.0	55.37	60.26	4.89	9.46E-05	
	95	20120419	YS	56.75	10.2	17.3	55.37	60.29	4.92	1.86E-04	
34.39+0.24	22	20120419	YS	62.44	69.2	204.1	45.79	63.28	17.49	5.02E-04	
	44	20120419	YS	58.72	8.4	20.5	57.02	60.42	3.40	9.98E-05	
34.78-1.38	22	20120510	YS	52.27	5.1	1.7	52.27	52.48	0.21	4.65E-06	
	44	20120510	YS	44.93	7.0	8.4	44.72	47.48	2.76	4.50E-05	
	95	20120510	YS	44.91	4.7	1.6	44.71	44.91	0.20	1.81E-05	
35.02+0.35	22	20120420	YS	44.53	66.4	68.6	35.47	59.48	24.02	1.89E-04	
	44	20120420	YS	52.66	3.3	2.4	51.60	52.66	1.06	1.30E-05	
35.20-0.74	22	20120420	YS	39.48	30.0	97.5	20.31	40.32	20.01	3.20E-04	
	44	20120420	YS	33.90	18.4	40.8	31.77	36.03	4.25	2.65E-04	

Table 3.10 (cont'd)

RMS ID	Line	Epoch	Station	v_p (km s^{-1})	S_p (Jy)	$\int S_\nu dv$ (Jykm s^{-1})	$v_{\rm min}$ (km s^{-1})	$v_{\rm max}$ (km s^{-1})	$v_{\rm rel}$ (km s^{-1})	$L_{\rm maser}$ (L$_\odot$)	notes
	95	20120420	YS	33.09	9.7	26.8	32.11	36.64	4.53	3.77E-04	
35.20-1.74	22	20120417	YS	37.29	32.5	102.1	33.07	54.56	21.49	2.87E-04	
	44	20120417	YS	41.11	4.6	8.6	40.05	44.08	4.04	4.80E-05	
	95	20120417	YS	42.69	2.6	3.0	39.93	42.69	2.76	3.54E-05	
35.79-0.17	22	20120417	YS	63.01	13.5	35.3	54.80	64.07	9.27	7.71E-05	
	44	20120417	YS	62.24	5.2	8.9	59.90	62.45	2.55	3.83E-05	
37.54+0.21	22	20120417	YS	85.70	3.5	6.6	27.77	86.12	58.36	6.85E-06	
	44	20120417	YS	86.41	3.0	4.4	83.86	86.62	2.76	9.06E-06	
38.91-0.35	22	20120418	YS	33.25	88.0	72.8	32.83	38.73	5.90	2.04E-04	
	44	20120418	YS	38.41	3.3	3.2	37.14	38.41	1.28	1.79E-05	
39.10+0.48	44	20120512	YS	26.30	9.0	12.6	21.41	26.94	5.53	8.50E-05	
40.25-0.19	22	20120420	YS	73.68	68.7	135.8	59.57	86.96	27.39	1.63E-04	
	44	20120420	YS	72.67	85.5	124.4	70.97	77.35	6.38	2.96E-04	
	95	20120420	YS	72.79	54.4	80.3	71.42	76.34	4.92	4.13E-04	
43.15+0.02	22	20120508	YS	-6.70	7690.4	87629.6	-200.94	128.76	329.70	2.69E-01	
	44	20120508	YS	1.68	2.4	0.5	1.68	1.68	0.21	3.11E-06	
49.47-0.37	22	20120416	YS	56.94	5772.5	28255.5	-54.92	162.70	217.62	1.98E-02	
	44	20120416	YS	59.91	12.3	45.9	54.17	66.92	12.76	6.38E-05	
	95	20120416	YS	58.46	8.2	67.3	53.93	66.93	12.99	2.02E-04	
49.49-0.39	22	20120416	YS	57.84	6692.5	30203.8	-59.71	167.60	227.31	2.12E-02	
	44	20120416	YS	49.17	76.1	277.6	47.68	66.60	18.92	3.86E-04	
	95	20120416	YS	54.64	37.7	299.1	47.75	65.28	17.52	8.97E-04	
59.78+0.06	22	20120416	YS	6.57	44.3	93.5	5.30	25.74	20.43	7.81E-05	
	44	20120416	YS	22.61	18.6	18.9	21.55	24.31	2.76	3.13E-05	
	95	20120416	YS	22.42	15.7	14.8	21.43	23.40	1.97	5.29E-05	
59.84+0.66	22	20120416	YS	34.92	8.3	8.4	32.19	35.77	3.58	3.62E-06	

Table 3.10 (cont'd)

RMS ID	Line	Epoch	Station	v_p (km s^{-1})	S_p (Jy)	$\int S_\nu dv$ (Jykm s^{-1})	$v_{\rm min}$ (km s^{-1})	$v_{\rm max}$ (km s^{-1})	$v_{\rm rel}$ (km s^{-1})	$L_{\rm maser}$ (L$_\odot$)	notes
	44	20120416	YS	34.95	4.0	1.4	34.95	35.16	0.21	1.19E-06	
	95	20120416	YS	35.23	3.4	2.2	34.44	35.23	0.79	3.98E-06	
75.76+0.34	22	20120418	YS	-4.69	285.7	657.9	-29.55	23.75	53.30	3.66E-04	
	44	20120418	YS	-2.32	31.6	49.6	-4.44	1.09	5.53	5.47E-05	
	95	20120418	YS	-2.33	6.9	13.6	-4.70	0.03	4.73	3.25E-05	
78.10+3.64	44	20120418	YS	-3.18	10.0	13.9	-4.45	-1.69	2.76	1.41E-05	
	95	20120418	YS	-3.17	13.3	27.1	-5.34	-0.42	4.92	5.93E-05	
81.72+0.57	22	20120416	YS	0.32	438.6	927.4	-12.96	7.27	20.22	1.81E-04	
	44	20120416	YS	-0.05	340.3	385.3	-6.86	2.07	8.93	1.49E-04	
	95	20120416	YS	-0.02	203.9	334.2	-8.10	2.34	10.43	2.79E-04	
81.76+0.59	22	20120416	YS	-5.95	13.0	58.9	-8.90	6.48	15.38	1.31E-05	
	44	20120416	YS	-5.09	42.7	53.8	-5.94	0.01	5.95	2.37E-05	
	95	20120416	YS	-5.16	33.4	48.1	-6.54	1.34	7.88	4.58E-05	
81.87+0.78	22	20120418	YS	9.90	534.8	1993.3	-7.59	21.48	29.07	6.66E-05	
	44	20120418	YS	8.92	28.9	41.1	6.16	12.75	6.59	2.72E-06	
	95	20120418	YS	7.55	15.3	64.4	4.60	13.26	8.66	9.20E-06	
109.86+2.10	22	20120416	YS	-9.14	1681.7	2206.8	-41.37	2.66	44.03	1.28E-05	
	44	20120416	YS	-13.18	7.4	3.0	-13.40	-12.97	0.43	3.45E-08	
	95	20120416	YS	-10.79	2.7	3.4	-11.38	-9.81	1.57	8.46E-08	
111.53+0.76	22	20120416	YS	-58.20	70.8	214.5	-72.95	-43.67	29.28	3.63E-05	
	44	20120416	YS	-57.32	22.9	30.0	-59.44	-53.49	5.95	1.01E-05	
	95	20120416	YS	-57.41	8.8	17.3	-58.78	-55.24	3.54	1.25E-05	
133.94+1.04	22	20120416	YS	-48.50	6229.7	7648.6	-68.72	-41.55	27.18	3.59E-03	
	44	20120416	YS	-46.78	4.1	7.4	-47.84	-45.08	2.76	6.93E-06	
	95	20120416	YS	-46.40	7.0	29.5	-51.52	-44.03	7.48	5.92E-05	
173.49+2.42	22	20120416	YS	-15.39	57.8	125.5	-28.03	-13.07	14.96	3.52E-04	

Table 3.10 (cont'd)

RMS ID	Line	Epoch	Station	v_p (km s^{-1})	S_p (Jy)	$\int S_\nu dv$ (Jykm s^{-1})	$v_{\rm min}$ (km s^{-1})	$v_{\rm max}$ (km s^{-1})	$v_{\rm rel}$ (km s^{-1})	$L_{\rm maser}$ (L$_\odot$)	notes
	44	20120416	YS	-16.63	22.4	27.6	-18.76	-14.72	4.04	1.53E-04	
	95	20120416	YS	-16.77	22.3	29.5	-18.94	-14.61	4.33	3.55E-04	
188.95+0.89	22	20120416	YS	8.37	18.7	52.0	-3.85	9.42	13.27	2.34E-05	
	44	20120416	YS	3.08	7.3	16.7	-0.32	4.78	5.10	1.49E-05	
	95	20120416	YS	3.49	5.9	17.1	0.54	5.07	4.53	3.29E-05	
192.60-0.05	22	20120416	YS	3.42	286.2	746.7	-0.58	15.64	16.22	2.10E-05	
	44	20120416	YS	7.29	7.0	14.0	6.65	11.54	4.89	7.77E-07	
	95	20120416	YS	10.88	6.8	21.0	5.96	11.47	5.51	2.52E-06	
203.05-14.5	22	20120416	YS	13.01	106.1	146.2	2.69	14.06	11.38	NaN	
	44	20120416	YS	10.64	3.3	2.8	9.79	10.85	1.06	NaN	
	95	20120416	YS	10.79	3.1	2.8	10.39	11.38	0.98	NaN	
359.43-0.10	22	20120513	YS	-57.58	14.5	28.3	-59.27	-56.74	2.53	5.07E-05	
	44	20120513	YS	-53.54	7.4	27.0	-55.45	-49.93	5.53	9.60E-05	
359.61-0.24	22	20120513	YS	22.39	46.7	62.9	19.23	54.42	35.18	NaN	
	44	20120513	YS	19.26	97.2	125.9	16.49	22.02	5.53	NaN	
	95	20120513	YS	19.33	58.2	96.6	16.57	23.07	6.50	NaN	
359.89-0.06	22	20120513	YS	28.64	4.7	2.8	28.01	28.64	0.63	NaN	
	44	20120513	YS	20.36	11.0	153.4	3.78	33.12	29.34	NaN	
	95	20120513	YS	21.59	9.7	83.1	12.14	25.14	12.99	NaN	

Table 3.11. Detected Maser Line Parameters(HMPO)

RMS ID	Line	Epoch	Station	v_p (km s^{-1})	S_p (Jy)	$\int S_\nu dv$ (Jykm s^{-1})	$v_{\rm min}$ (km s^{-1})	$v_{\rm max}$ (km s^{-1})	$v_{\rm rel}$ (km s^{-1})	$L_{\rm maser}$ (L$_\odot$)	notes
HM00117+6412	22	20120124	US	-35.00	3.8	2.6	-36.26	-34.79	1.47	1.97E-07	
HM00420+5530	22	20120123	YS	-51.32	32.5	44.1	-52.16	-43.31	8.85	6.09E-05	
HM04579+4703	22	20120122	YS	-14.16	5.8	6.4	-18.37	-13.95	4.42	9.03E-07	
HM05137+3919	22	20120122	YS	-29.95	305.9	265.4	-31.00	-25.74	5.27	7.18E-04	
HM05168+3634	22	20120122	YS	-20.16	104.9	192.6	-27.53	5.75	33.29	1.65E-04	
HM05274+3345	22	20120122	YS	-0.95	258.3	463.2	-13.37	3.06	16.43	2.58E-05	
	44	20120122	YS	-3.42	11.2	14.3	-4.48	-2.14	2.34	1.58E-06	
	95	20120122	YS	-3.43	9.0	11.6	-4.62	-2.25	2.36	2.76E-06	
HM05345+3157	22	20120122	YS	-16.42	77.6	130.4	-21.27	-13.89	7.37	9.80E-06	
HM05358+3543	22	20120122	YS	-18.53	123.7	257.1	-22.74	-14.73	8.01	1.93E-05	
	44	20120122	YS	-16.78	13.8	19.7	-18.90	-15.08	3.83	2.94E-06	
HM05373+2349	22	20120129	US	3.79	61.1	160.8	-3.16	17.48	20.65	5.11E-06	
	44	20120129	US	1.95	0.8	0.3	1.31	1.95	0.64	1.75E-08	
	95	20120129	US	2.37	1.3	1.8	0.99	2.57	1.58	2.42E-07	
HM05490+2658	44	20120122	YS	1.16	0.2	0.0	0.95	0.95	0.21	7.69E-09	
HM05553+1631	22	20120123	YS	-1.27	41.3	63.9	-5.27	24.22	29.49	9.26E-06	
HM06056+2131	22	20120125	YS	1.84	6.1	6.9	1.21	4.58	3.37	3.59E-07	
	44	20120125	YS	2.10	1.6	0.3	2.10	2.10	0.21	3.60E-08	
	95	20120125	YS	1.99	1.4	2.0	0.42	2.78	2.36	4.48E-07	
HM18018-2426	44	20120126	US	10.73	560.3	363.9	10.10	12.65	2.55	3.76E-05	
	95	20120126	US	10.78	91.2	55.7	10.19	11.37	1.18	1.24E-05	
HM18024-2119	22	20120128	US	-9.85	8.1	32.5	-19.54	3.63	23.17	2.04E-05	
	44	20120128	US	-0.12	15.9	19.8	-1.18	3.50	4.68	2.46E-05	
	95	20120128	US	-0.01	1.9	2.4	-0.80	0.78	1.58	6.48E-06	
HM18089-1732	22	20120127	US	29.10	168.1	140.3	21.52	33.11	11.59	5.50E-04	
	44	20120127	US	31.46	20.2	24.8	31.03	34.65	3.61	1.93E-04	

Table 3.11 (cont'd)

RMS ID	Line	Epoch	Station	v_p (km s^{-1})	S_p (Jy)	$\int S_\nu dv$ (Jykm s^{-1})	$v_{\rm min}$ (km s^{-1})	$v_{\rm max}$ (km s^{-1})	$v_{\rm rel}$ (km s^{-1})	$L_{\rm maser}$ (L$_\odot$)	notes
	95	20120127	US	31.40	12.5	24.5	30.81	35.34	4.53	4.12E-04	
HM18102-1800	44	20120208	US	19.46	4.1	11.0	19.25	24.14	4.89	9.90E-05	
HM18144-1723	22	20120129	US	53.00	40.8	69.3	38.68	54.06	15.38	3.01E-05	
	44	20120129	US	48.44	54.0	64.7	45.46	49.50	4.04	5.58E-05	
	95	20120129	US	48.35	26.9	35.4	45.60	49.34	3.74	6.58E-05	
HM18151-1208	22	20120128	US	31.84	6.3	3.7	31.42	32.05	0.63	7.74E-07	
	44	20120128	US	30.40	37.2	53.9	29.33	34.01	4.68	2.23E-05	
	95	20120128	US	33.76	4.6	12.1	29.43	33.96	4.53	1.08E-05	
HM18162-1612	44	20120130	US	62.37	10.4	7.6	61.95	63.01	1.06	8.36E-06	
	95	20120130	US	62.57	1.6	0.3	62.37	62.37	0.20	7.33E-07	
HM18182-1433	22	20120130	US	61.58	69.0	151.2	38.62	74.85	36.24	4.88E-04	
	44	20120130	US	61.22	27.4	32.9	58.46	61.86	3.40	2.11E-04	
	95	20120130	US	61.16	12.2	18.4	58.60	61.94	3.35	2.54E-04	
HM18247-1147	44	20120128	US	120.67	5.5	2.4	120.46	120.88	0.43	9.68E-06	
	95	20120128	US	120.79	4.2	1.8	120.40	120.79	0.39	1.54E-05	
HM18264-1152	22	20120129	US	42.84	146.2	221.4	2.60	47.27	44.66	8.02E-04	
	44	20120129	US	43.52	29.3	47.6	41.18	45.22	4.04	3.41E-04	
	95	20120129	US	43.19	39.7	69.9	40.83	45.94	5.12	1.08E-03	
HM18278-1009	44	20120131	US	111.80	2.8	1.0	111.80	112.02	0.21	1.56E-06	
HM18290-0924	22	20120128	US	87.27	7.0	33.5	18.38	88.53	70.15	8.58E-05	
	44	20120128	US	83.95	29.9	16.0	83.31	84.37	1.06	8.08E-05	
HM18306-0835	22	20120130	US	80.69	1.9	4.6	70.15	107.44	37.29	1.22E-05	
	44	20120130	US	78.01	19.2	35.4	76.31	80.56	4.25	1.86E-04	
	95	20120130	US	76.58	2.3	0.5	76.38	76.58	0.20	5.24E-06	
HM18308-0841	22	20120131	US	96.70	4.3	2.6	96.28	96.91	0.63	6.78E-06	
	44	20120131	US	76.31	17.0	19.8	75.25	77.37	2.13	1.04E-04	

Table 3.11 (cont'd)

RMS ID	Line	Epoch	Station	v_p (km s^{-1})	S_p (Jy)	$\int S_\nu dv$ (Jykm s^{-1})	$v_{\rm min}$ (km s^{-1})	$v_{\rm max}$ (km s^{-1})	$v_{\rm rel}$ (km s^{-1})	$L_{\rm maser}$ (L$_\odot$)	notes
	95	20120131	US	76.38	7.2	8.5	75.60	77.37	1.77	9.66E-05	
HM18337-0743	44	20120206	US	60.71	5.9	6.7	58.37	60.92	2.55	4.09E-05	
	95	20120206	US	60.93	2.9	0.7	60.73	60.93	0.20	9.09E-06	
HM18345-0641	44	20120206	US	95.52	9.4	11.5	94.67	96.37	1.70	4.78E-05	
	95	20120206	US	95.38	7.4	10.8	94.79	97.16	2.36	9.65E-05	
HM18348-0616	22	20120209	US	109.89	1.4	1.3	109.47	110.74	1.26	2.53E-06	
HM18372-0541	22	20120131	US	22.89	2.3	1.8	22.68	23.95	1.26	7.63E-06	
HM18385-0512	22	20120208	US	19.15	223.5	1216.1	13.04	62.76	49.72	4.84E-03	
HM18426-0204	22	20120209	US	11.10	2.8	8.2	4.57	13.42	8.85	3.46E-05	
	44	20120209	US	16.22	2.1	1.1	16.01	16.43	0.43	9.42E-06	
HM18454-0158	22	20120206	US	97.56	8.7	46.9	95.45	111.04	15.59	3.41E-05	
HM18470-0044	22	20120210	US	89.52	3.9	4.3	88.68	89.94	1.26	6.65E-06	
HM18488+0000	44	20120210	US	83.16	9.3	6.9	82.52	83.37	0.85	2.51E-05	
	95	20120210	US	83.37	3.3	1.6	82.78	83.37	0.59	1.24E-05	
HM18507+0121	22	20120210	US	56.26	165.0	703.0	37.51	90.81	53.30	2.44E-04	
	44	20120210	US	60.14	31.4	58.1	54.61	60.99	6.38	4.00E-05	
	95	20120210	US	60.13	6.1	14.3	55.60	60.32	4.73	2.12E-05	
HM18517+0437	22	20120128	US	41.16	7.0	17.9	36.94	41.79	4.85	3.49E-06	
	44	20120128	US	43.31	5.1	4.5	43.10	44.16	1.06	1.72E-06	
	95	20120128	US	43.78	4.6	5.2	42.99	44.37	1.38	4.31E-06	
HM18527+0301	22	20120205	US	83.48	12.7	26.1	78.21	90.64	12.43	1.67E-05	
HM18530+0215	44	20120206	US	79.86	1.8	6.1	67.96	80.71	12.76	2.14E-05	
	95	20120206	US	76.40	1.5	3.7	75.81	79.75	3.94	2.78E-05	
HM18532+0047	22	20120214	YS	61.00	8.6	7.2	60.37	61.42	1.05	2.63E-06	
HM18553+0414	22	20120215	YS	11.37	52.2	176.6	1.05	27.59	26.54	1.48E-06	
HM18565+0349	22	20120208	US	88.31	2.1	4.1	84.52	94.63	10.11	4.33E-06	

Table 3.11 (cont'd)

RMS ID	Line	Epoch	Station	v_p (km s^{-1})	S_p (Jy)	$\int S_\nu dv$ (Jykm s^{-1})	$v_{\rm min}$ (km s^{-1})	$v_{\rm max}$ (km s^{-1})	$v_{\rm rel}$ (km s^{-1})	$L_{\rm maser}$ (L$_\odot$)	notes
	44	20120208	US	90.25	2.4	0.7	90.25	90.46	0.21	1.57E-06	
HM18566+0408	22	20120129	US	85.95	5.7	17.4	29.49	94.59	65.10	1.81E-05	
	44	20120129	US	86.43	4.9	4.2	85.80	86.86	1.06	8.71E-06	
	95	20120129	US	86.94	3.2	6.3	83.60	87.14	3.54	2.82E-05	
HM19012+0505	22	20120216	YS	33.15	35.4	24.4	32.73	34.42	1.69	4.74E-06	
HM19012+0536	44	20120216	YS	65.10	4.1	8.3	65.10	77.00	11.90	2.83E-05	
	95	20120216	YS	66.37	3.4	2.9	65.58	66.37	0.79	2.13E-05	
HM19035+0641	22	20120216	YS	33.79	13.0	17.4	33.16	35.48	2.32	1.95E-06	
HM19043+0726	44	20120216	YS	58.31	9.2	5.1	58.10	58.52	0.43	4.48E-06	
	95	20120216	YS	58.19	7.2	3.5	57.79	58.38	0.59	6.57E-06	
HM19088+0902	22	20120131	US	-6.89	32.5	522.5	-121.70	82.44	204.14	2.69E-04	
	44	20120131	US	58.03	24.7	13.4	57.82	59.31	1.49	1.37E-05	
	95	20120131	US	58.01	7.1	3.0	57.81	58.40	0.59	6.69E-06	
HM19092+0841	22	20120208	US	45.78	6.6	13.4	45.15	61.37	16.22	6.23E-06	
	44	20120208	US	58.03	5.5	4.8	56.97	58.25	1.28	4.43E-06	
	95	20120130	US	13.99	1.7	1.4	13.20	13.99	0.79	1.60E-05	
HM19198+1423	22	20120208	US	58.21	3.1	1.6	58.21	58.63	0.42	1.17E-06	
HM19213+1723	22	20120208	US	-29.10	465.3	2468.6	-37.74	-24.68	13.06	9.72E-04	
HM19217+1651	22	20120209	US	9.79	77.9	86.1	0.95	21.17	20.22	2.20E-04	
	44	20120209	US	0.33	6.2	7.4	-0.30	4.37	4.68	3.73E-05	
	95	20120209	US	4.37	2.6	5.8	1.42	5.35	3.94	6.29E-05	
HM19220+1432	22	20120209	US	56.68	6.4	10.5	56.47	63.42	6.95	7.39E-06	
HM19266+1745	44	20120210	US	5.58	3.6	7.9	3.88	7.07	3.19	3.65E-05	
HM19368+2239	44	20120128	US	38.07	17.1	24.3	35.31	43.81	8.50	2.20E-05	
	95	20120128	US	35.98	4.0	5.2	35.78	37.94	2.17	1.01E-05	
HM19374+2352	22	20120129	US	35.00	30.5	49.8	32.05	39.21	7.16	2.14E-05	

Table 3.11 (cont'd)

RMS ID	Line	Epoch	Station	v_p (km s^{-1})	S_p (Jy)	$\int S_\nu dv$ (Jykm s^{-1})	$v_{\rm min}$ (km s^{-1})	$v_{\rm max}$ (km s^{-1})	$v_{\rm rel}$ (km s^{-1})	$L_{\rm maser}$ (L$_\odot$)	notes
	44	20120129	US	34.18	2.8	0.6	34.18	34.18	0.21	5.09E-07	
HM19388+2357	22	20120209	US	34.89	13.1	24.3	19.94	43.53	23.60	1.03E-05	
	44	20120209	US	35.16	3.2	2.1	34.10	35.16	1.06	1.73E-06	
	95	20120209	US	35.17	2.6	2.2	33.99	35.17	1.18	4.04E-06	
HM19410+2336	22	20120207	US	24.82	102.1	145.2	8.60	26.09	17.49	1.38E-04	
	44	20120207	US	22.56	20.5	18.0	21.71	23.83	2.13	3.39E-05	
	95	20120207	US	22.47	19.0	14.8	21.59	23.56	1.97	6.02E-05	
HM19411+2306	22	20120206	US	31.00	5.1	3.1	30.58	31.21	0.63	2.43E-06	
HM19471+2641	22	20120207	US	-31.35	2.5	2.2	-31.77	-30.72	1.05	2.90E-07	
HM20050+2720	22	20120131	US	-2.11	8.1	14.4	-15.38	-1.27	14.11	4.05E-07	
	44	20120131	US	7.43	1.5	0.3	7.43	7.43	0.21	1.74E-08	
	95	20120131	US	6.37	1.6	0.3	6.17	6.37	0.20	3.71E-08	
HM20056+3350	22	20120214	YS	7.21	77.6	79.9	6.58	8.26	1.69	5.17E-06	
HM20062+3550	22	20120214	YS	13.32	7.4	4.9	13.11	13.75	0.63	3.27E-07	
	44	20120214	YS	0.10	14.4	8.2	-0.12	0.52	0.64	1.09E-06	
	95	20120214	YS	0.19	9.6	4.7	-0.01	0.38	0.39	1.33E-06	
HM20099+3640	22	20120126	US	-36.95	1.3	0.3	-36.95	-36.95	0.21	4.72E-07	
HM20126+4104	22	20120125	US	-2.00	2.2	5.2	-6.21	-1.37	4.85	3.49E-07	
	44	20120125	US	-3.20	8.4	14.5	-4.90	-1.29	3.61	1.92E-06	
	95	20120125	US	-3.04	6.2	12.5	-4.81	-1.07	3.74	3.58E-06	
HM20188+3928	22	20120207	US	-2.11	7.3	14.1	-3.37	1.05	4.42	6.42E-07	
	44	20120207	US	2.37	2.9	4.2	0.46	5.14	4.68	3.81E-07	
	95	20120207	US	0.99	1.9	2.6	0.99	2.57	1.58	5.00E-07	
HM20220+3728	44	20120210	US	-1.57	1.7	0.5	-1.78	-1.57	0.21	4.84E-07	
HM20286+4105	22	20120131	US	-4.11	6.9	8.6	-54.03	-3.05	50.98	2.77E-06	
	44	20120131	US	-4.05	6.8	4.8	-4.27	-3.20	1.06	3.02E-06	

Table 3.11 (cont'd)

RMS ID	Line	Epoch	Station	v_p (km s^{-1})	S_p (Jy)	$\int S_\nu dv$ (Jykm s^{-1})	$v_{\rm min}$ (km s^{-1})	$v_{\rm max}$ (km s^{-1})	$v_{\rm rel}$ (km s^{-1})	$L_{\rm maser}$ (L$_\odot$)	notes
	95	20120131	US	-4.22	4.0	5.2	-4.42	-2.45	1.97	7.16E-06	
HM20293+3952	22	20120208	US	-99.65	26.1	98.0	-104.29	19.59	123.87	9.09E-06	
	44	20120208	US	4.88	10.7	18.4	4.67	7.65	2.98	3.37E-06	
	95	20120208	US	5.98	3.7	3.0	5.38	6.17	0.79	1.21E-06	
HM20332+4124	22	20120131	US	-5.05	3.9	6.9	-13.27	-4.63	8.64	2.42E-06	
HM21078+5211	22	20120128	US	-13.48	691.8	1784.6	-35.18	18.75	53.93	9.19E-05	
HM21307+5049	22	20120131	US	-65.85	1.6	1.8	-66.07	-63.54	2.53	9.93E-07	
	44	20120131	US	-47.90	1.3	1.3	-48.33	-47.27	1.06	1.41E-06	
	95	20120131	US	-48.01	1.0	0.8	-48.60	-47.42	1.18	2.06E-06	
HM21391+5802	22	20120125	US	11.90	23.7	58.1	-9.37	12.32	21.70	7.58E-07	
	44	20120125	US	-0.90	10.1	14.8	-1.12	7.17	8.29	3.81E-07	
	95	20120125	US	-1.01	5.4	5.8	-1.21	0.76	1.97	3.24E-07	
HM22134+5834	22	20120127	US	-13.57	2.0	0.4	-13.57	-13.57	0.21	6.70E-08	
HM22198+6336	22	20120128	US	-0.57	6.8	12.8	-11.32	0.48	11.80	4.87E-07	
HM22506+5944	22	20120127	US	-52.32	22.1	48.7	-59.06	-49.16	9.90	3.67E-05	
	44	20120127	US	-51.84	6.1	9.8	-52.48	-50.14	2.34	1.46E-05	
	95	20120127	US	-51.04	5.0	10.2	-54.19	-50.06	4.13	3.29E-05	
HM22570+5912	22	20120131	US	-55.74	2.6	4.5	-55.95	-46.89	9.06	2.69E-06	
HM23033+5951	22	20120128	US	-50.79	5.5	13.7	-61.11	-46.79	14.33	3.89E-06	
	44	20120128	US	-54.54	21.2	11.2	-54.97	-53.90	1.06	6.29E-06	
	95	20120128	US	-54.60	15.2	9.1	-54.99	-53.81	1.18	1.11E-05	
HM23139+5939	22	20120128	US	-47.00	47.8	76.5	-60.91	-39.00	21.91	4.09E-05	
	44	20120128	US	-45.48	1.9	2.1	-45.69	-44.20	1.49	2.26E-06	
	95	20120128	US	-46.01	2.4	2.5	-46.21	-45.02	1.18	5.78E-06	
HM23151+5912	22	20120128	US	-51.16	42.6	64.5	-76.65	-49.68	26.97	4.86E-05	
	44	20120128	US	-52.78	4.5	3.5	-54.69	-52.56	2.13	5.22E-06	

Table 3.11 (cont'd)

RMS ID	Line	Epoch	Station	v_p (km s^{-1})	S_p (Jy)	$\int S_\nu dv$ (Jykm s^{-1})	$v_{\rm min}$ (km s^{-1})	$v_{\rm max}$ (km s^{-1})	$v_{\rm rel}$ (km s^{-1})	$L_{\rm maser}$ (L$_\odot$)	notes
	95	20120128	US	-54.62	1.5	0.3	-54.81	-54.81	0.20	9.30E-07	
HM23314+6033	22	20120124	US	-38.36	5.5	10.1	-44.05	-36.89	7.16	1.82E-06	
HM23385+6053	22	20120129	US	-59.59	22.4	49.2	-65.06	-54.95	10.11	5.50E-05	
	44	20120129	US	-50.05	2.0	4.2	-53.88	-49.84	4.04	9.36E-06	
	95	20120129	US	-51.01	1.5	1.0	-51.99	-51.01	0.98	4.69E-06	

Table 3.12. Detected Maser Line Parameters(UCHII)

RMS ID	Line	Epoch	Station	v_p (km s^{-1})	S_p (Jy)	$\int S_\nu dv$ (Jykm s^{-1})	$v_{\rm min}$ (km s^{-1})	$v_{\rm max}$ (km s^{-1})	$v_{\rm rel}$ (km s^{-1})	$L_{\rm maser}$ (L$_\odot$)	notes
IRAS02232+6138	22	20111102	YS	-48.40	4822.7	7804.9	-97.91	-41.24	56.67	1.63E-03	
	44	20111102	YS	-46.45	4.7	7.8	-47.30	-45.18	2.13	3.21E-06	
	95	20111102	YS	-46.42	7.2	17.8	-48.00	-44.06	3.94	1.59E-05	
IRAS03035+5819	22	20111103	YS	-22.44	16.5	13.2	-23.07	-21.81	1.26	5.41E-06	
IRAS05391-0152	22	20120125	YS	13.69	2.4	1.1	13.48	13.90	0.42	1.36E-08	
IRAS05393-0156	22	20120124	YS	13.69	9.5	11.7	6.10	14.11	8.01	6.78E-08	
Mon R2	22	20111103	YS	11.29	1320.5	876.9	4.97	12.34	7.37	2.37E-03	
IRAS06056+2131	22	20120124	YS	1.79	4.6	5.2	1.37	4.53	3.16	7.66E-08	
IRAS06058+2138	22	20111102	YS	1.55	25.0	44.5	-3.71	8.29	12.01	4.99E-06	
	44	20111102	YS	3.08	7.5	13.5	1.38	4.36	2.98	3.01E-06	
	95	20111102	YS	3.26	5.3	10.2	1.29	4.64	3.35	4.91E-06	
IRAS06061+2151	22	20111103	YS	-7.55	685.9	1524.5	-17.87	-2.28	15.59	5.94E-04	
IRAS06084-0611	22	20111102	YS	13.69	4.8	11.5	-1.90	13.90	15.80	2.67E-07	
IRAS06099+1800	22	20111103	YS	3.57	224.0	414.5	2.10	14.74	12.64	6.01E-05	
	44	20111103	YS	11.01	8.6	18.4	6.76	11.44	4.68	5.27E-06	
	95	20111103	YS	11.16	10.2	21.7	7.02	11.55	4.53	1.35E-05	
G5.89-0.39	22	20111103	YS	11.79	65.7	179.6	-69.11	13.05	82.16	1.67E-05	
	44	20111103	YS	12.50	27.7	61.7	7.61	12.71	5.10	1.13E-05	
	95	20111103	YS	12.53	11.6	38.1	7.02	12.73	5.71	1.51E-05	
G8.14+0.23	22	20120115	YS	14.54	3.1	5.3	-5.05	22.12	27.18	2.17E-06	
G8.67-0.36	22	20111103	YS	35.37	83.0	183.8	-21.30	49.48	70.78	9.82E-05	
	44	20111103	YS	35.82	29.0	85.2	32.21	39.86	7.65	9.01E-05	
	95	20111103	YS	36.01	20.4	63.1	31.28	39.35	8.07	1.44E-04	
IRAS18032-2032	22	20120115	YS	-3.32	71.1	268.2	-40.19	25.33	65.52	2.02E-04	
	44	20120115	YS	3.67	4.7	6.1	3.25	5.58	2.34	9.08E-06	
	95	20120115	YS	3.79	2.8	7.0	1.83	6.55	4.73	2.25E-05	

Table 3.12 (cont'd)

RMS ID	Line	Epoch	Station	v_p (km s^{-1})	S_p (Jy)	$\int S_\nu dv$ (Jykm s^{-1})	$v_{\rm min}$ (km s^{-1})	$v_{\rm max}$ (km s^{-1})	$v_{\rm rel}$ (km s^{-1})	$L_{\rm maser}$ (L$_\odot$)	notes
G10.30-0.15	22	20120114	YS	20.80	1.9	3.9	5.84	22.48	16.64	3.28E-06	
	44	20120114	YS	13.50	15.1	36.7	7.55	14.77	7.23	6.06E-05	
	95	20120114	YS	13.53	6.0	18.6	8.22	15.70	7.48	6.66E-05	
G10.47+0.03	22	20111104	YS	62.30	104.6	659.5	46.71	206.82	160.11	8.15E-04	
	44	20111104	YS	66.78	7.7	17.3	65.51	69.76	4.25	4.23E-05	
	95	20111104	YS	68.14	12.0	56.4	61.84	70.90	9.06	2.98E-04	
G10.62-0.38	22	20120212	YS	0.05	105.5	318.8	-14.69	3.64	18.33	2.29E-03	
G11.94-0.62	22	20120115	YS	39.01	6.7	19.6	20.26	40.48	20.22	1.23E-05	
	44	20120115	YS	38.63	2.7	7.2	28.64	39.48	10.84	8.99E-06	
	95	20120115	YS	38.68	2.3	5.3	36.12	40.06	3.94	1.42E-05	
G12.21-0.10	22	20111104	YS	23.69	161.4	806.5	-11.92	31.06	42.98	4.85E-03	
	44	20111104	YS	23.56	7.2	17.7	21.22	25.69	4.46	2.11E-04	
	95	20111104	YS	23.52	14.0	28.3	23.32	28.64	5.32	7.29E-04	
IRAS18162-2048	22	20120213	YS	-82.91	3.2	6.7	-83.33	-80.17	3.16	5.62E-07	
	44	20120213	YS	13.14	122.8	96.4	12.08	13.78	1.70	1.60E-05	
	95	20120213	YS	13.08	41.4	32.6	12.10	13.87	1.77	1.17E-05	
G15.04-0.68	22	20120115	YS	19.94	559.1	766.3	11.51	23.73	12.22	7.84E-05	
	44	20120115	YS	19.13	7.6	5.2	18.07	19.35	1.28	1.05E-06	
	95	20120115	YS	19.11	2.7	2.8	18.71	20.09	1.38	1.21E-06	
IRAS18232-1154	22	20120114	YS	26.10	2.9	2.9	25.47	26.31	0.84	2.70E-07	
G19.07-0.27	44	20111103	YS	69.11	2.7	2.5	66.35	69.11	2.76	3.39E-06	
G19.61-0.23	22	20111103	YS	48.87	82.7	786.7	20.64	55.61	34.97	3.70E-04	
	44	20111103	YS	40.91	21.7	32.4	40.48	46.44	5.95	3.02E-05	
	95	20111103	YS	41.18	20.1	40.8	37.64	46.69	9.06	8.20E-05	
G20.08-0.14	22	20120115	YS	46.28	16.3	32.4	34.70	56.39	21.70	1.14E-04	
	95	20120115	YS	41.07	1.7	5.5	39.89	45.20	5.32	8.20E-05	

Table 3.12 (cont'd)

RMS ID	Line	Epoch	Station	v_p (km s^{-1})	S_p (Jy)	$\int S_\nu dv$ (Jykm s^{-1})	$v_{\rm min}$ (km s^{-1})	$v_{\rm max}$ (km s^{-1})	$v_{\rm rel}$ (km s^{-1})	$L_{\rm maser}$ (L$_\odot$)	notes
IRAS18316-0602	22	20111104	YS	40.87	208.1	408.2	-9.48	47.40	56.88	8.52E-05	
	44	20111104	YS	41.77	49.3	44.5	40.50	44.54	4.04	1.84E-05	
	95	20111104	YS	41.77	32.8	36.1	41.38	44.13	2.76	3.23E-05	
G23.71+0.17	22	20120216	YS	110.68	3.4	3.2	110.05	111.10	1.05	6.21E-06	
	44	20111104	YS	113.03	4.8	2.0	113.03	113.25	0.21	7.70E-06	
G23.96+0.15	22	20120112	YS	74.65	7.9	10.6	74.02	82.23	8.22	8.85E-06	
IRAS18403-0417	22	20111104	YS	95.61	17.9	15.8	94.98	96.03	1.05	3.03E-05	
	44	20111104	YS	97.77	3.8	0.8	97.77	97.77	0.21	3.11E-06	
	95	20120216	YS	95.21	3.2	8.8	93.83	97.57	3.74	7.23E-05	
G29.96-0.02	22	20111104	YS	99.27	114.7	343.1	91.26	110.85	19.59	4.36E-04	
	44	20111104	YS	98.29	10.6	16.4	95.95	99.35	3.40	4.12E-05	
	95	20120121	YS	96.96	8.6	22.2	96.37	99.91	3.54	1.20E-04	
G30.54+0.02	22	20120217	YS	-33.85	2.6	7.4	-36.16	-32.37	3.79	3.26E-05	
G31.41+0.31	22	20111102	YS	98.82	359.4	763.7	85.33	133.16	47.82	1.28E-03	
	44	20111102	YS	97.81	3.6	16.3	93.77	101.21	7.44	5.40E-05	
	95	20111102	YS	98.48	6.4	36.8	93.95	102.41	8.47	2.64E-04	
IRAS18456-0129	22	20111102	YS	105.79	21.2	27.7	105.16	114.22	9.06	3.42E-05	
	44	20111102	YS	110.06	3.5	7.5	107.72	111.12	3.40	1.83E-05	
IRAS18469-0132	44	20120217	YS	86.16	3.1	1.2	86.16	86.37	0.21	3.04E-06	
IRAS18479-0005	22	20120115	YS	14.68	28.2	110.6	-5.33	22.48	27.81	4.27E-04	
G33.92+0.11	22	20120217	YS	109.18	2.1	2.6	105.18	109.18	4.00	3.01E-06	
	44	20111103	YS	108.61	2.8	0.6	108.61	108.61	0.21	1.38E-06	
G34.26+0.15	22	20111103	YS	60.72	408.0	2154.9	-33.66	138.67	172.33	8.00E-04	
	44	20111103	YS	56.33	28.3	92.0	54.42	62.71	8.29	6.76E-05	
	95	20111103	YS	56.50	16.9	87.0	54.14	64.18	10.04	1.38E-04	
IRAS18515+0157	22	20120114	YS	44.63	52.9	55.0	40.42	59.59	19.17	1.28E-04	

Table 3.12 (cont'd)

RMS ID	Line	Epoch	Station	v_p (km s^{-1})	S_p (Jy)	$\int S_\nu dv$ (Jykm s^{-1})	$v_{\rm min}$ (km s^{-1})	$v_{\rm max}$ (km s^{-1})	$v_{\rm rel}$ (km s^{-1})	$L_{\rm maser}$ (L$_\odot$)	notes
IRAS18534+0218	22	20120214	YS	-12.23	3.3	1.6	-12.23	-12.02	0.21	3.78E-06	
IRAS18538+0216	22	20120214	YS	45.30	110.5	179.3	42.56	55.41	12.85	4.24E-04	
G35.05-0.52	44	20111104	YS	49.97	28.7	20.8	49.33	50.61	1.28	1.54E-04	
	95	20111104	YS	50.17	16.1	7.4	49.97	50.56	0.59	1.18E-04	
IRAS18592+0108	22	20111104	YS	36.96	25.3	105.1	32.75	48.13	15.38	2.50E-05	
IRAS18593+0408	22	20120215	YS	57.65	4.6	5.6	57.22	59.33	2.11	1.11E-05	
G42.42-0.27	22	20120216	YS	63.03	2.9	21.3	-6.71	68.50	75.21	1.33E-05	
IRAS19081+0903	22	20111103	YS	-6.89	168.6	2685.6	-206.18	68.32	274.50	8.53E-03	
	44	20111103	YS	3.67	2.4	0.5	3.46	3.46	0.21	3.27E-06	
IRAS19095+0930	22	20111104	YS	41.05	711.6	1187.1	29.25	50.53	21.28	2.23E-03	
G43.89-0.78	22	20120215	YS	50.27	23.0	36.4	47.53	51.53	4.00	8.96E-05	
G44.26+0.10	22	20120215	YS	56.31	3.9	2.2	56.10	56.52	0.42	3.37E-06	
G45.07+0.13	22	20120115	YS	60.09	25.1	54.7	53.56	67.46	13.90	4.57E-05	
	44	20120115	YS	59.10	2.3	3.8	58.25	62.07	3.83	6.31E-06	
	95	20120115	YS	59.06	2.2	4.7	57.29	61.23	3.94	1.69E-05	
G45.12+0.13	22	20120115	YS	59.97	1.6	4.5	50.70	61.87	11.17	4.93E-06	
G45.45+0.06	22	20120112	YS	51.39	17.3	21.4	46.75	52.02	5.27	NaN	
G45.47+0.05	22	20120214	YS	51.39	7.4	5.7	50.96	51.81	0.84	NaN	
G45.48+0.13	22	20120114	YS	66.80	4.3	8.8	53.95	67.44	13.48	1.93E-05	
IRAS19181+1349	22	20120213	YS	17.17	110.3	476.5	6.01	36.77	30.76	1.04E-03	
W51d	22	20111103	YS	56.76	6973.7	37955.3	-59.32	167.57	226.89	2.29E-02	
	44	20111103	YS	49.13	20.6	116.7	48.07	66.77	18.71	1.39E-04	
	95	20111103	YS	61.74	5.0	34.4	53.87	66.86	12.99	8.86E-05	
G50.31+0.68	22	20120112	YS	24.00	4.2	9.4	23.58	27.79	4.21	7.88E-07	
G54.10-0.06	22	20120112	YS	36.21	9.6	37.7	34.53	42.53	8.01	5.45E-05	
IRAS19410+2336	22	20111103	YS	22.72	51.7	193.6	11.76	27.35	15.59	2.17E-05	

Table 3.12 (cont'd)

RMS ID	Line	Epoch	Station	v_p (km s^{-1})	S_p (Jy)	$\int S_\nu dv$ (Jykm s^{-1})	$v_{\rm min}$ (km s^{-1})	$v_{\rm max}$ (km s^{-1})	$v_{\rm rel}$ (km s^{-1})	$L_{\rm maser}$ (L$_\odot$)	notes
	44	20111103	YS	22.56	21.4	17.5	21.50	23.41	1.91	3.89E-06	
	95	20111103	YS	22.77	15.5	10.4	21.78	22.97	1.18	5.01E-06	
G61.48+0.09	22	20111104	YS	15.90	93.0	173.3	14.00	28.54	14.54	6.76E-05	
IRAS19598+3324	22	20120121	YS	-23.20	4.7	14.4	-27.20	-15.19	12.01	2.30E-05	
IRAS20081+3122	22	20120121	YS	14.87	137.7	203.6	-76.78	55.74	132.51	4.25E-05	
	44	20111102	YS	11.33	12.7	15.7	9.63	12.61	2.98	6.47E-06	
	95	20111102	YS	11.58	4.7	3.0	11.38	12.17	0.79	2.65E-06	
G75.78+0.34	22	20120121	YS	-4.63	656.8	1727.9	-30.12	23.39	53.51	1.26E-03	
	44	20120121	YS	3.67	8.4	17.3	-2.28	3.89	6.16	2.49E-05	
	95	20120121	YS	3.62	6.2	17.2	-1.50	3.81	5.32	5.34E-05	
G75.83+0.40	22	20120124	YS	-4.53	4.3	3.6	-5.16	-4.11	1.05	2.55E-06	
IRAS20255+3712	22	20120121	YS	-7.70	24.4	72.8	-15.92	8.31	24.23	1.69E-06	
DR21	22	20111102	YS	-6.43	6.9	13.7	-7.48	-3.69	3.79	7.15E-07	
	44	20111102	YS	-3.67	63.7	51.9	-5.37	0.58	5.95	5.37E-06	
	95	20111102	YS	-3.57	21.3	29.9	-5.73	-0.02	5.71	6.68E-06	
IRAS22176+6303	44	20111102	YS	-8.35	10.5	8.3	-8.35	-6.23	2.13	3.09E-07	
	95	20111102	YS	-8.06	3.9	6.2	-8.25	-5.89	2.36	4.96E-07	
IRAS22543+6145	22	20111103	YS	-9.10	1091.5	1253.4	-48.49	10.70	59.20	1.42E-05	
	44	20111103	YS	-13.07	9.8	5.7	-13.28	-12.22	1.06	1.28E-07	
	95	20111103	YS	-12.90	2.2	0.4	-13.09	-12.90	0.20	2.13E-08	
NGC7538	22	20111102	YS	-58.15	67.5	175.2	-72.89	-43.82	29.07	4.98E-05	
	44	20111102	YS	-57.25	13.3	17.8	-58.10	-54.28	3.83	1.00E-05	
	95	20111102	YS	-57.42	3.4	8.9	-59.39	-55.06	4.33	1.08E-05	
IRAS23138+5945	22	20120125	YS	-46.73	5.2	5.0	-47.15	-44.42	2.74	7.30E-07	
	44	20120125	YS	-44.37	1.4	1.6	-44.37	-42.67	1.70	4.50E-07	
	95	20111103	YS	-43.93	2.1	0.4	-44.12	-44.12	0.20	2.56E-07	

Table 3.13. Summary of ATLASGAL

Source Name	Number within region	Matches	Detections (%) Any	22 GHz	44 GHz	95 GHz
IRDCs	130	98(75)	39(40)	26(27)	26(27)	26(27)
RMSs	135	116(86)	57(49)	41(35)	42(36)	36(31)
HMPOs	77	69(90)	44(64)	31(45)	31(45)	25(36)
MMSs	100	83(83)	78(94)	62(75)	74(89)	62(75)
UCHIIs	69	53(77)	37(70)	34(64)	22(42)	18(34)
		No Matches				
IRDCs		32(25)	2(6)	1(3)	1(3)	1(3)
RMSs		19(14)	6(32)	5(26)	5(26)	2(11)
HMPOs		8(10)	3(38)	2(25)	1(13)	1(13)
MMSs		17(17)	17(100)	15(88)	17(100)	6(35)
UCHIIs		16(23)	9(56)	9(56)	2(13)	1(6)

Table 3.14. Summary of NH_3

Source Name	Number of matches	Non detection	Detections (%)			
			Any	22 GHz	44 GHz	95 GHz
IRDCs	47	28(60)	19(40)	13(28)	16(34)	15(32)
RMSs	218	99(45)	119(55)	98(45)	75(34)	62(28)
HMPOs	109	41(38)	68(62)	57(52)	43(39)	35(32)
MMSs	43	3(7)	40(93)	36(84)	37(86)	36(84)
UCHIIs	61	15(25)	46(75)	43(70)	27(44)	23(38)

Table 3.15. Summary of Maser Line Parameters

Source Name	Number	S_p mean	S_p median	S_p min	S_p max	V_{rel} mean	V_{rel} median	V_{rel} min	V_{rel} max	V_{range} mean	V_{range} median	V_{range} min	V_{range} max
22													
IRDCs	27	36.6± 91.0	5.8	1.2	458.2	1.36± 4.98	0.74	-8.32	12.96	12.8± 23.4	2.7	0.2	91.85
RMSs	112	144.4± 563.6	17.2	1.2	4552.1	-2.69± 20.05	-0.11	-92.86	79.11	19.7± 32.6	9.7	0.2	230.68
HMPOs	67	56.4± 113.5	8.6	1.3	691.8	-4.36± 20.12	-0.53	-105.65	44.56	20.1± 31.2	10.1	0.2	204.14
MMSs	91	389.1± 1362.6	27.9	2.7	7690.4	-3.82± 15.58	-0.74	-87.11	19.91	39.6± 56.6	16.2	0.2	329.70
UCHIIs	65	307.1± 1053.2	24.4	1.6	6973.7	-4.70± 17.54	-1.87	-95.11	16.96	33.1± 52.7	14.5	0.2	274.50
44													
IRDCs	27	15.8± 23.6	6.2	1.2	104.9	0.16± 2.46	-0.05	-6.01	6.11	2.4± 2.0	2.1	0.2	5.95
RMSs	81	21.5± 41.6	6.7	1.1	236.5	0.05± 1.06	-0.05	-2.39	3.56	2.5± 2.4	2.1	0.2	11.27
HMPOs	52	21.6± 77.0	6.8	0.2	560.3	-0.22± 1.53	-0.05	-4.80	3.14	2.8± 2.8	2.1	0.2	12.76
MMSs	106	25.1± 42.1	8.8	2.3	340.3	-0.37± 4.89	-0.69	-11.75	12.06	5.7± 7.4	4.0	0.2	39.97
UCHIIs	35	16.4± 23.1	8.4	1.4	122.8	-0.18± 2.68	-0.05	-10.47	6.11	4.0± 3.7	3.4	0.2	18.71
95													
IRDCs	26	9.3± 11.9	5.0	1.0	53.1	0.51± 2.38	-0.02	-3.96	6.28	3.0± 2.2	2.4	0.2	7.68
RMSs	68	16.2± 25.0	6.7	1.1	146.9	0.09± 1.08	-0.02	-2.39	3.91	3.0± 2.3	2.4	0.2	13.39
HMPOs	42	8.4± 15.0	4.0	1.0	91.2	-0.12± 1.14	-0.22	-1.99	3.13	1.9± 1.5	1.6	0.2	5.12
MMSs	82	16.3± 25.3	8.2	2.0	203.9	-0.70± 4.81	-0.81	-15.58	12.38	5.6± 6.6	4.1	0.2	33.67
UCHIIs	30	10.3± 9.6	6.4	1.7	41.4	0.21± 1.72	0.37	-3.57	3.72	4.7± 3.2	4.3	0.2	12.99

Table 3.16. Summary of Linear Regression Analyses

Parameters		Slope					intercept					ρ			
(log – log)	Line	IRDCs	RMSs	HMPOs	MMSs	UCHIIs	IRDCs	RMSs	HMPOs	MMSs	UCHIIs	IRDCs	RMSs	HMPOs	MM
$L_{\rm bol} - L_{\rm maser}$	22	1.13	1.48	1.12	1.46	1.74	-9.04	-11.00	-9.55	-11.49	-14.00	0.51	0.50	0.64	0
	44	0.92	1.25	1.09	1.11	1.51	-8.12	-10.31	-9.83	-10.17	-13.21	0.49	0.40	0.66	0
	95	0.95	1.17	0.93	1.20	1.80	-8.02	-9.70	-9.00	-10.44	-14.39	0.49	0.36	0.71	0
	6.7		1.39		1.24			-11.59		-11.33			0.34		0
$M_{\rm clump} - L_{\rm maser}$	22	1.17	1.66	1.31	1.79	1.84	-8.72	-10.11	-9.26	-10.79	-11.69	0.55	0.57	0.51	0
	44	1.26	1.29	1.33	1.08	1.37	-9.15	-9.16	-9.55	-8.48	-10.44	0.36	0.69	0.68	0
	95	1.17	1.38	1.30	1.35	1.16	-8.51	-9.10	-9.46	-9.24	-9.01	0.53	0.77	0.76	0
	6.7		1.63		1.45			-10.67		-10.26			0.58		0
$N_{\rm H_2} - L_{\rm maser}$	22	2.44	1.59	2.97	2.37	2.57	-61.07	-41.27	-73.37	-59.83	-64.95	0.70	0.19	0.47	0
	44	2.01	1.54	1.99	1.46	1.38	-51.24	-40.40	-50.80	-38.76	-37.63	0.49	0.32	0.41	0
	95	2.00	1.56	2.18	1.71	1.19	-50.68	-40.73	-55.38	-44.49	-32.57	0.63	0.30	0.52	0
	6.7		1.10		1.20			-30.76		-33.34			0.04		0

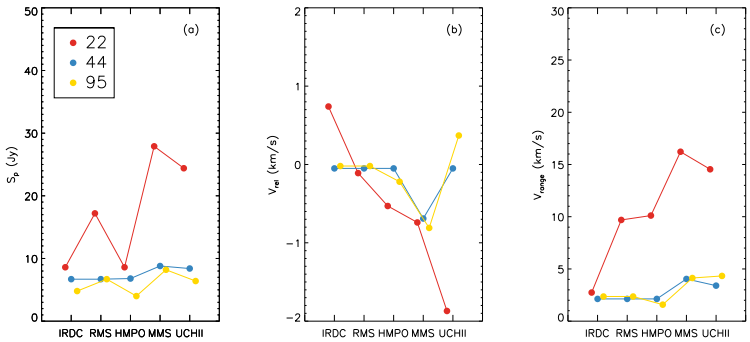

Figure 3.1: A median of (a) the peak flux density, (b) the relative velocity, and (c) the velocity range of the 22 GHz(red), 44 GHz(blue) and 95 GHz(yellow) masers for five type of objects.

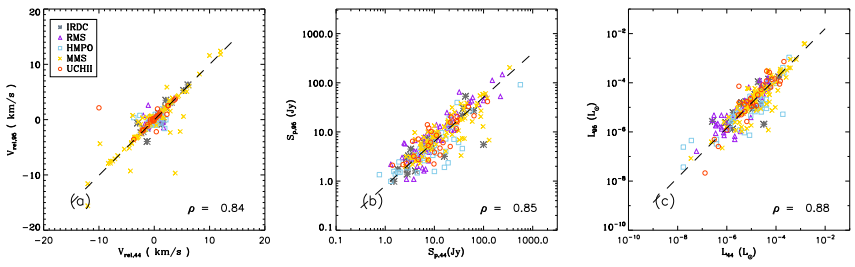

Figure 3.2: Comparison of (a) the relative peak velocities, (b) the peak flux densities, and (c) the isotropic luminosities of the 44 and 95 GHz class I CH_3OH maser sources. Symbols and colors of different type of object are presented in the upper-left corner of panel (a). In each panel the least-squares fitted relation is displayed by a dashed line with the correlation coefficient in the bottom-right corner.

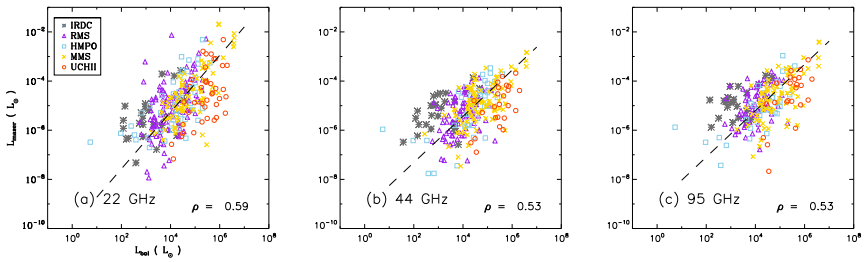

Figure 3.3: Comparison of the isotropic maser luminosity with the bolometric luminosity for (a) the 22 GHz, (b) 44 GHz, and (c) 95 GHz maser sources. In each panel the least-squares fitted relation is displayed by a dashed line with the correlation coefficient in the bottom-right corner.

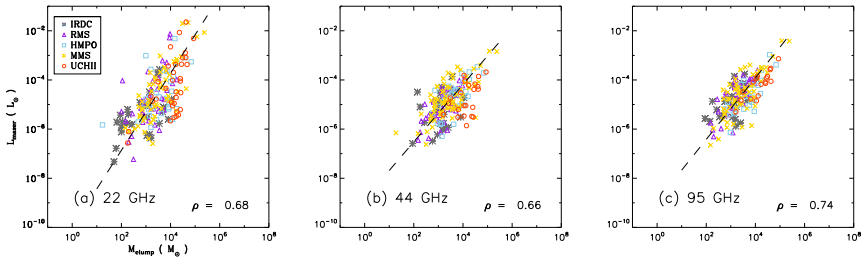

Figure 3.4: Same as in Figure 3.3 except for the associated ATLASGAL clump mass.

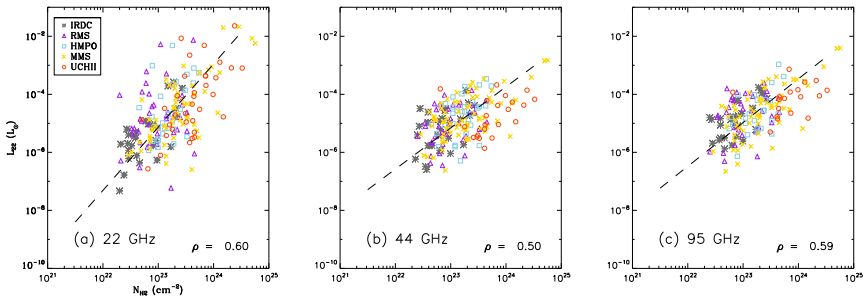

Figure 3.5: Same as in Figure 3.3 except for the associated ATLASGAL peak H_2 column density.

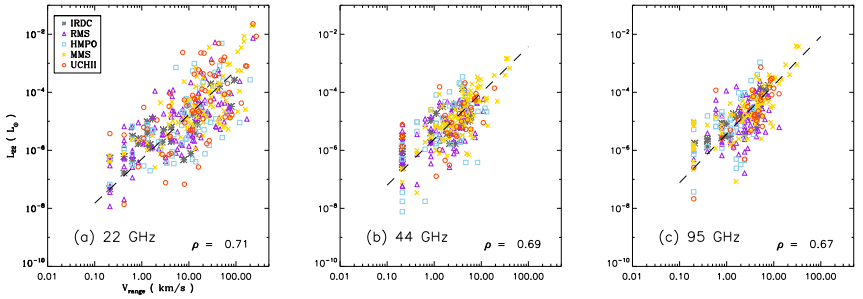

Figure 3.6: Same as in Figure 3.3 except for the velocity range of the detected maser lines.

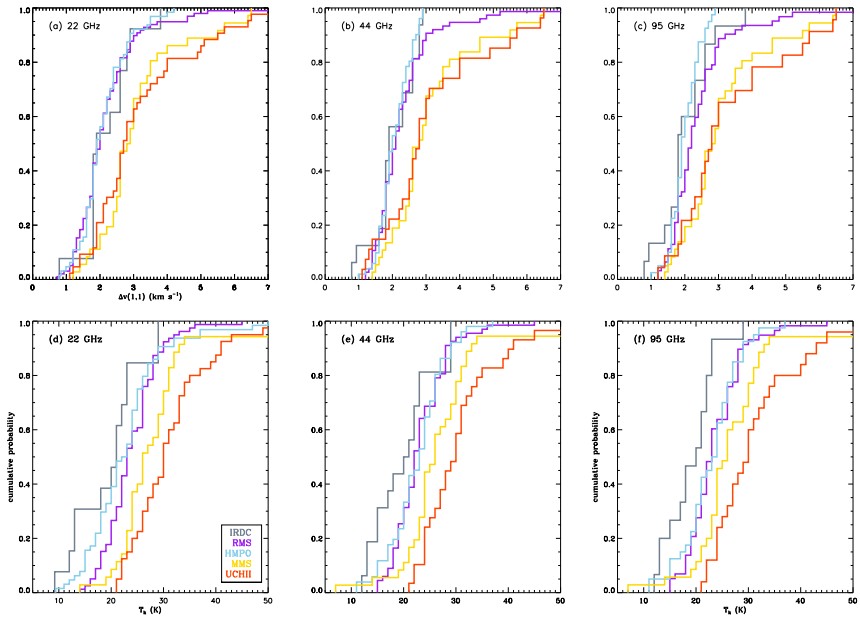

Figure 3.7: Cumulative probability of (Upper panel) the NH_3 linewidth and (Lower panel) the kinetic temperature for 5 type of objects. The detected maser lines are shown in upper-left corners on each panel. The source types and corresponding colors are displayed on the bottom-right corner in (d) panel.

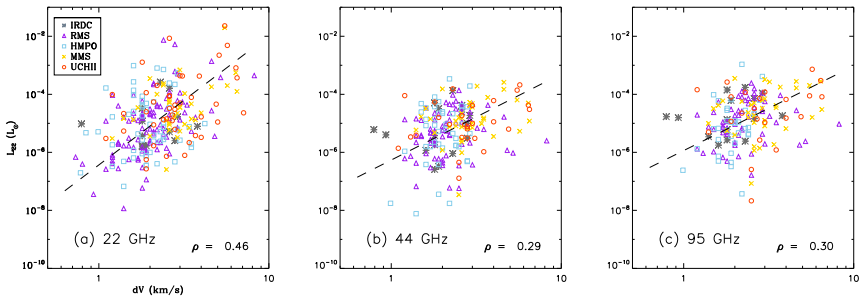

Figure 3.8: Same as in Figure 3.3 except for the NH_3 linewidth of the detected maser lines.

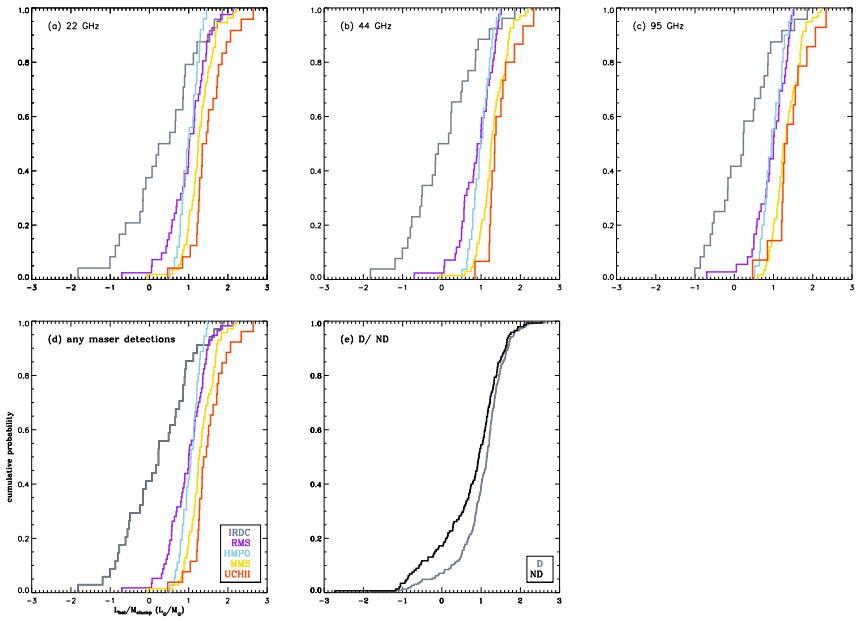

Figure 3.9: Cumulative probability of L_{bol}/M_{lump} for 5 type of objects regarding to the combinations of three maser detection and non-deection. The parameters of the distribution are displayed in upper-left corners on each panel. The source types and corresponding colors are displayed on the bottom-right corner in (d) and (e) panel.

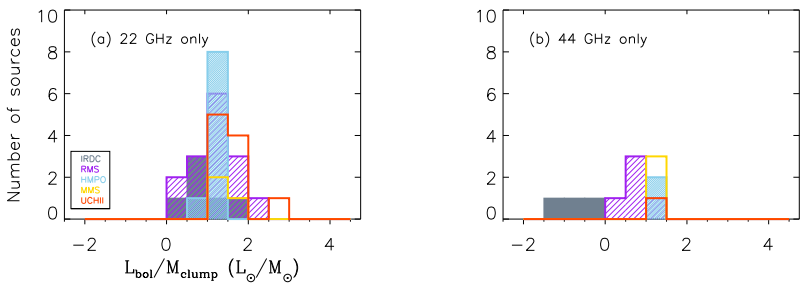

Figure 3.10: Histogram of L_{bol}/M_{lump} for the detected maser line of (a) 22 GHz only and (b) 44 GHz only. The source types and corresponding colors are displayed on the bottom-left corner in (a) panel.

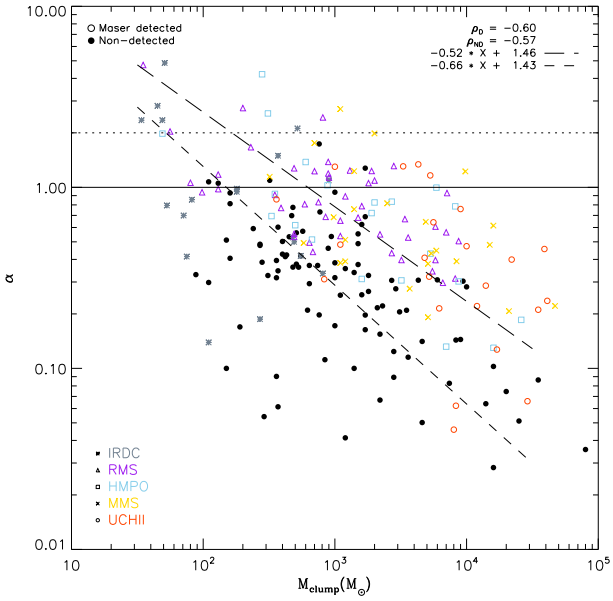

Figure 3.11: The virial parameter (α) versus the clump mass for the associated ATLASGAL clumps. Open and filled symbols represent the sources with and without any maser emission, respectively. The source types and corresponding colors are displayed in the bottom-right corner. The results of linear regression and correlation coefficient for the source with any maser emission and no maser emission are presented on the upper-right corner in the panel. The fitted line for maser detection and non-detection are shown as long-dashed and dashed line, respectively. The horizontal lines in solid and dotted style mark $\alpha = 1$ and $\alpha = 2$ (refer to Sec.4.5. for details)

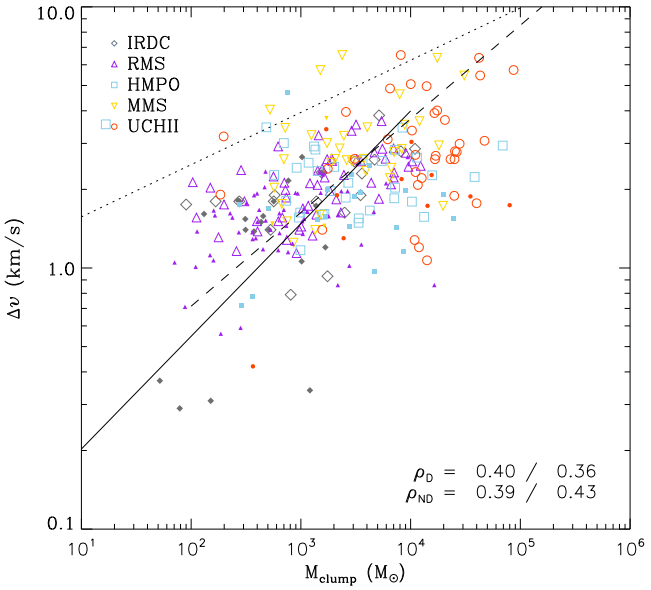

Figure 3.12: Comparison of FWHM linewidth of $NH_3(1,1)$ versus M_{clump} (Larson's 2nd law). In each panel the least-squares fitted relation is displayed by a dashed line with the correlation coefficient in the bottom-right corner. The best fit line for source with maser detections and non-detection are displayed in dashed and solid lines. The dotted line is original Larson's result of 0.42 $M^0.2$. The source types and corresponding colors are displayed on the upper-left corner in the panel.

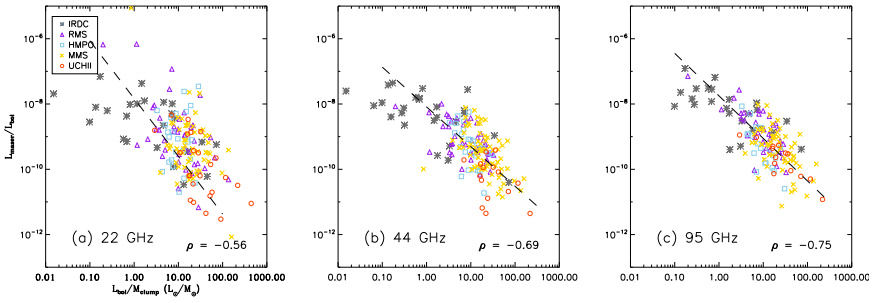

Figure 3.13: The maser luminosity to the bolometric luminosity against $L_{\rm bol}/M_{\rm clump}$ for the (a) 22 GHz, (b) 44 GHz, and (c) 95 GHz maser sources. In each panel the least-squares fitted relation is displayed by a dashed line with the correlation coefficient in the bottom-right corner. The source types and corresponding colors are displayed on the upper-left corner in (a) panel.

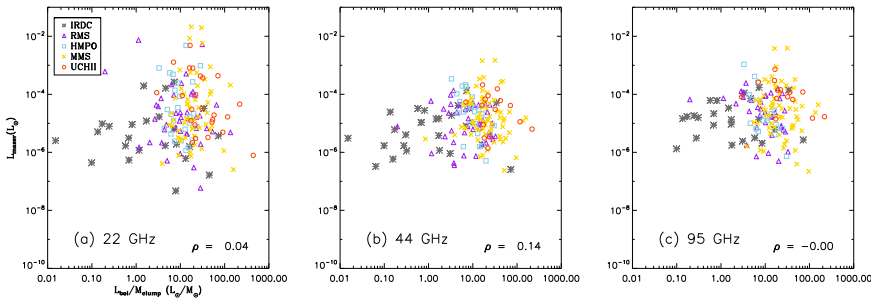

Figure 3.14: Same as in Figure 3.13 except for the maser luminosity against $L_{\rm bol}/M_{\rm clump}$.

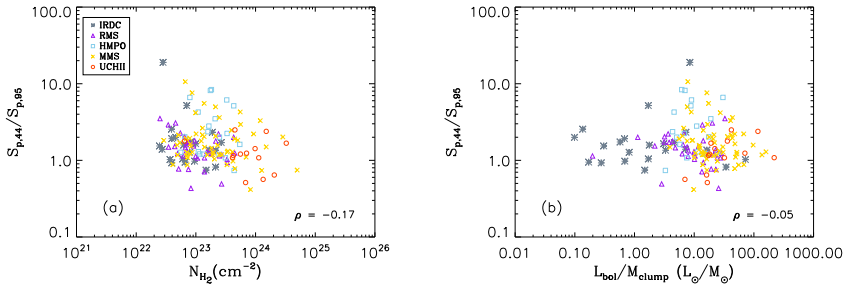

Figure 3.15: The peak flux ratio of 44 GHz to 95 GHz($S_{\rm p,44}/S_{\rm p,95}$) against (a) the peak column density and (b) $L_{\rm bol}/M_{\rm clump}$. The source types and corresponding colors are displayed on the upper-left corner in (a) panel.

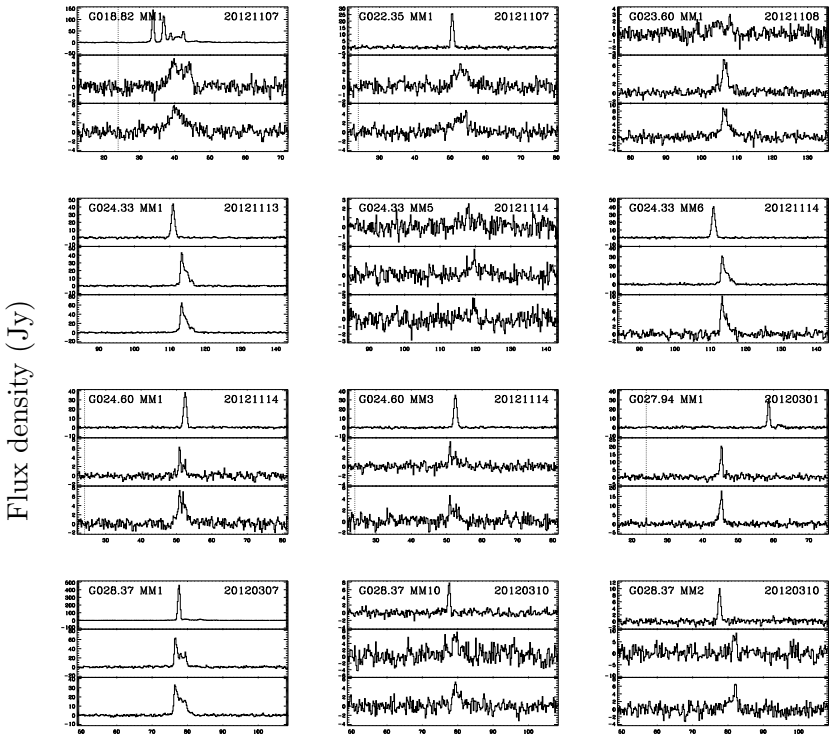

Figure 3.16: (Upper panel) The detected 22 GHz H_2O, (Middle panel) 44 GHz CH_3OH, and (Lower panel) 95 GHz CH_3OH maser spectra of the sources detected in all of three transitions. The source name is given in the top-left corner of the upper panel and the observing dates are shown in the top-right corner. The vertical dotted line indicates the systemic velocity.

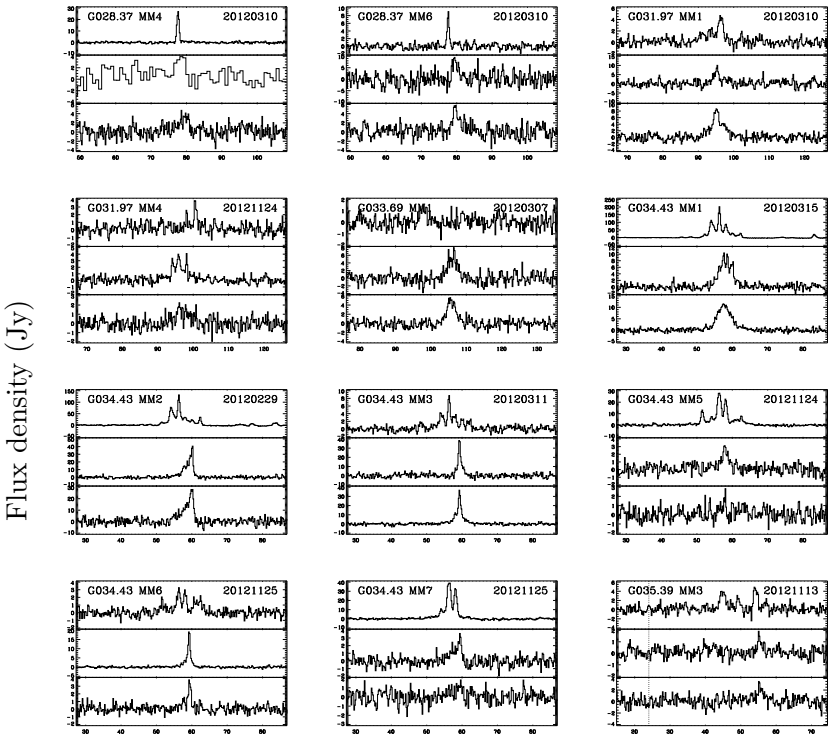

Figure 3.17: Continued

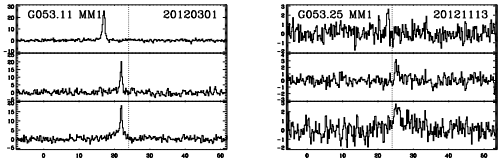

Figure 3.18: Continued

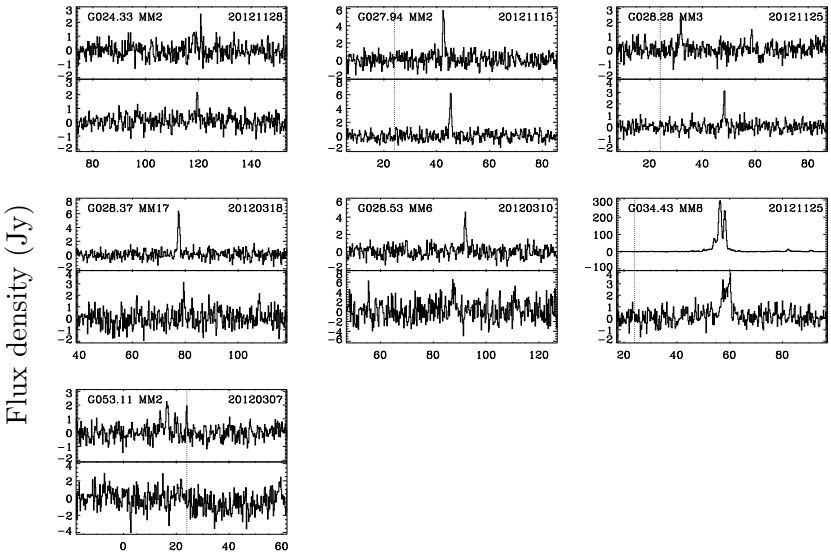

Figure 3.19: Same as in Figure 3.16 except for the source detected both at (Upper) 22 and (Lower) 44 GHz.

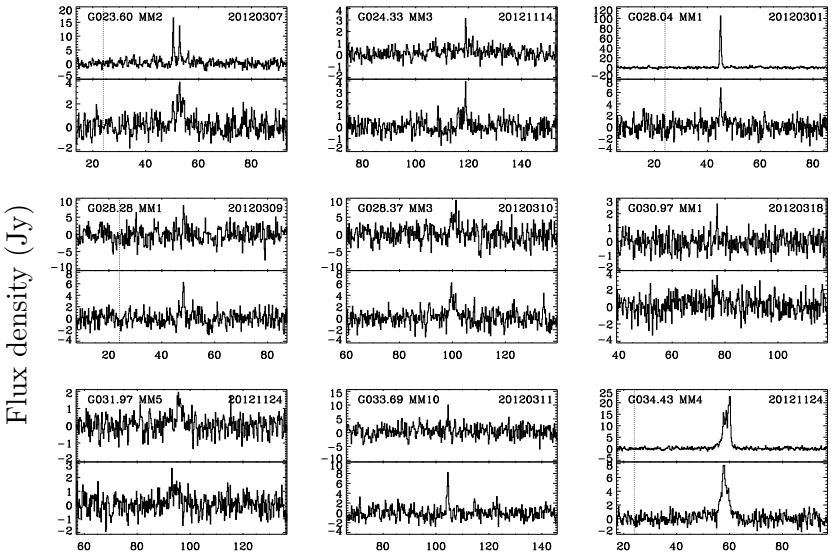

Figure 3.20: Same as in Figure 3.16 except for the source detected both at (Upper) 44 and (Lower) 95 GHz.

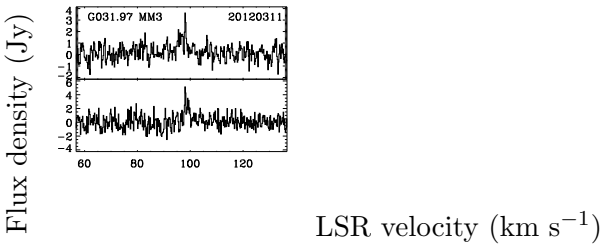

Figure 3.21: Same as in Figure 3.16 except for the source detected both at (Upper) 22 and (Lower) 95 GHz.

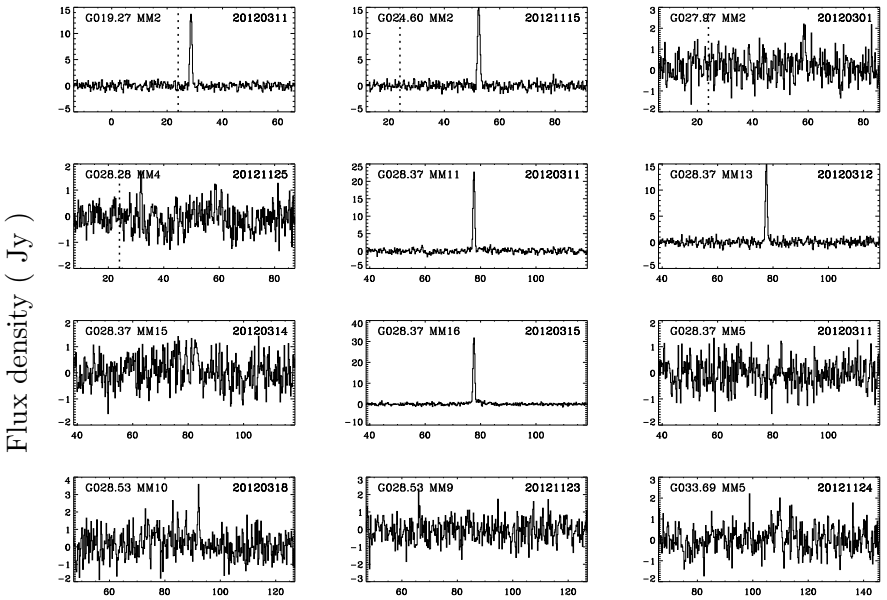

Figure 3.22: Same as in Figure 3.16 except for the source detected only at 22 GHz.

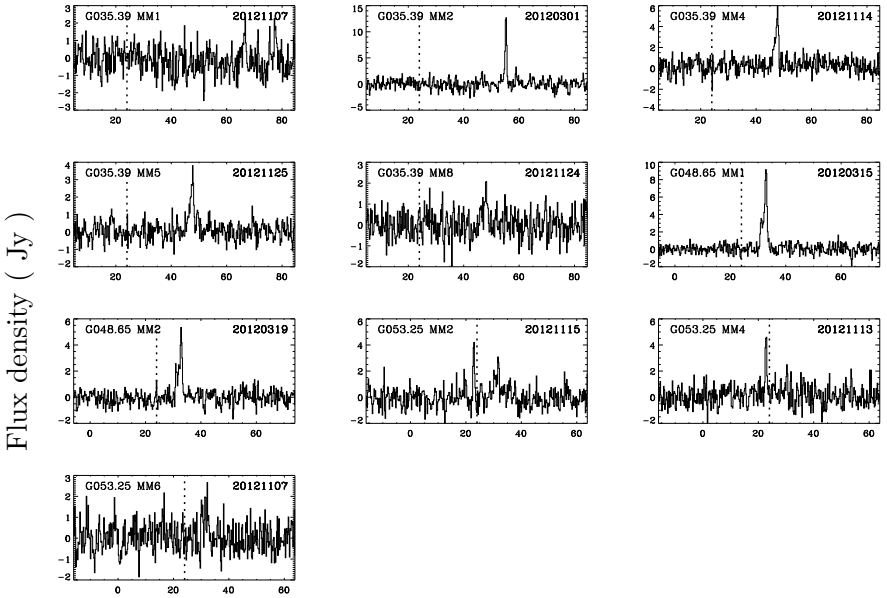

Figure 3.23: Continued

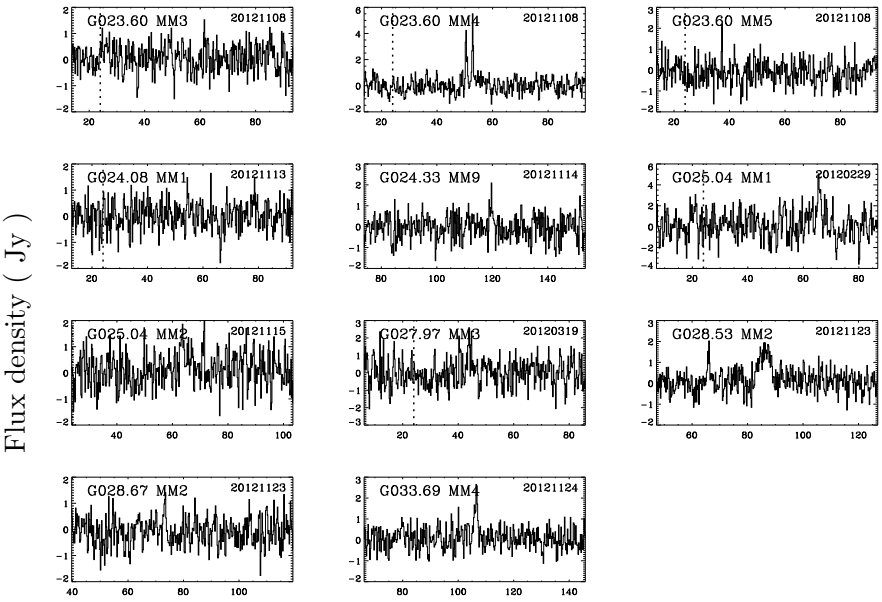

Figure 3.24: Same as in Figure 3.16 except for the source detected only at 44 GHz.

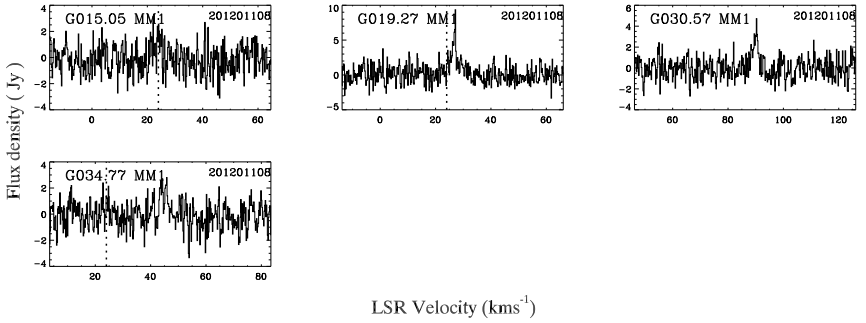

Figure 3.25: Same as in Figure 3.16 except for the source detected only at 95 GHz.

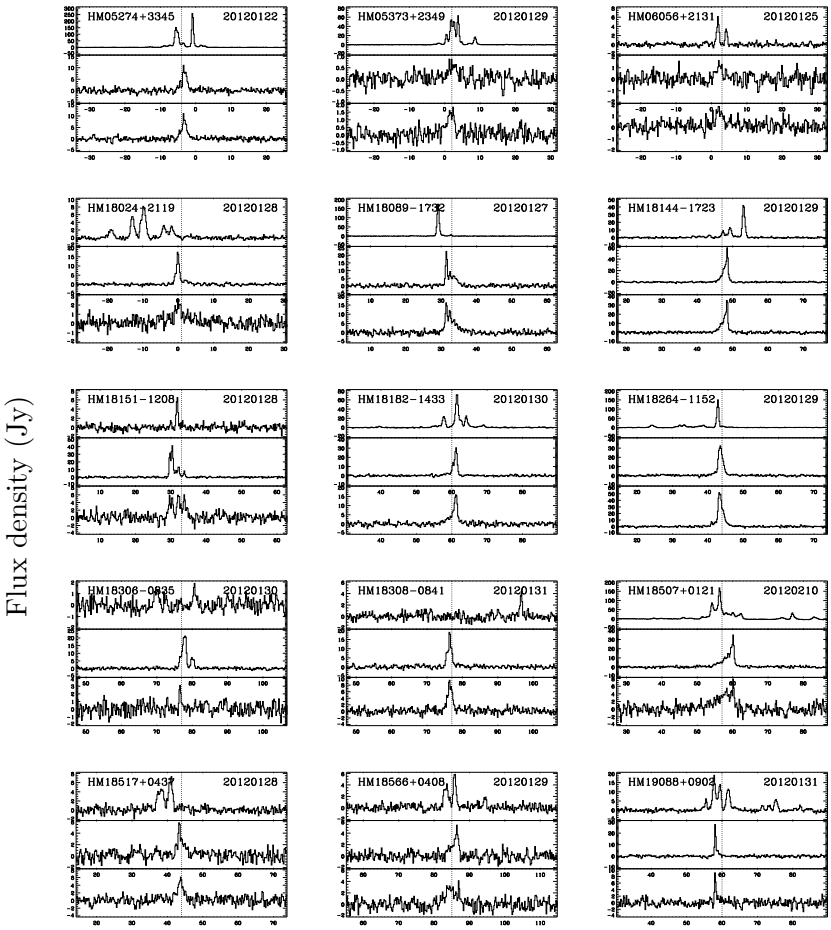

Figure 3.26: **HMPOs.** (Upper panel) The detected 22 GHz H_2O, (Middle panel) 44 GHz CH_3OH, and (Lower panel) 95 GHz CH_3OH maser spectra of the sources detected in all of three transitions. Other details are same as in Figure 3.16

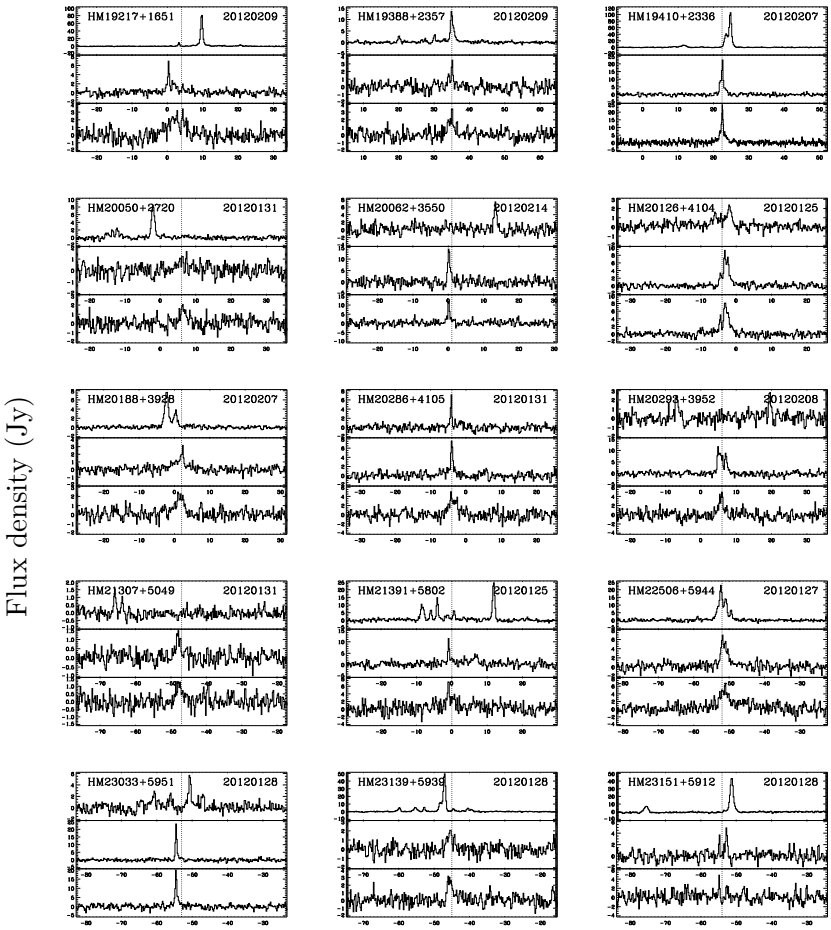

Figure 3.27: Continued

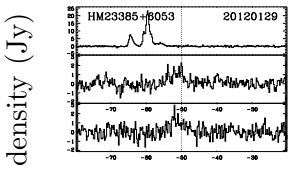

Flux density (Jy)

LSR velocity (km s^{-1})

Figure 3.28: Continued

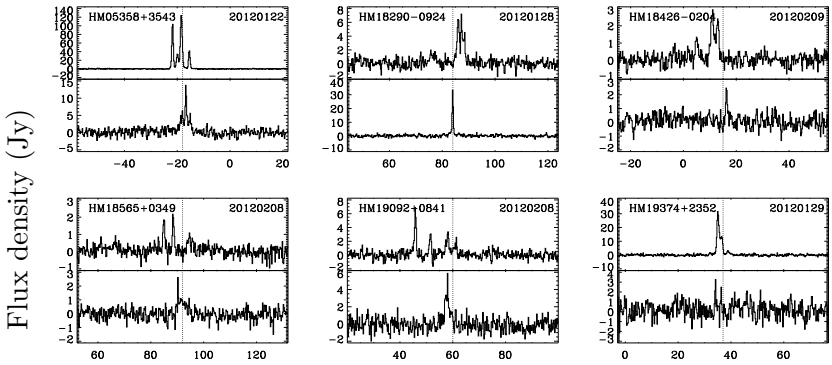

Figure 3.29: Same as in Figure 3.26 except for the source detected both at (Upper) 22 and (Lower) 44 GHz.

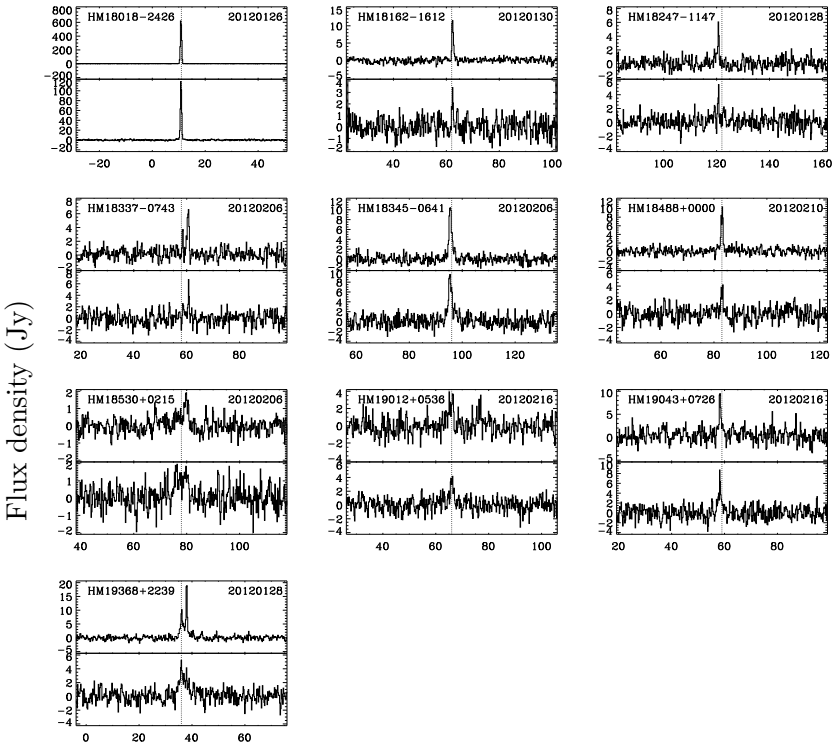

Figure 3.30: Same as in Figure 3.26 except for the source detected both at (Upper) 44 and (Lower) 95 GHz.

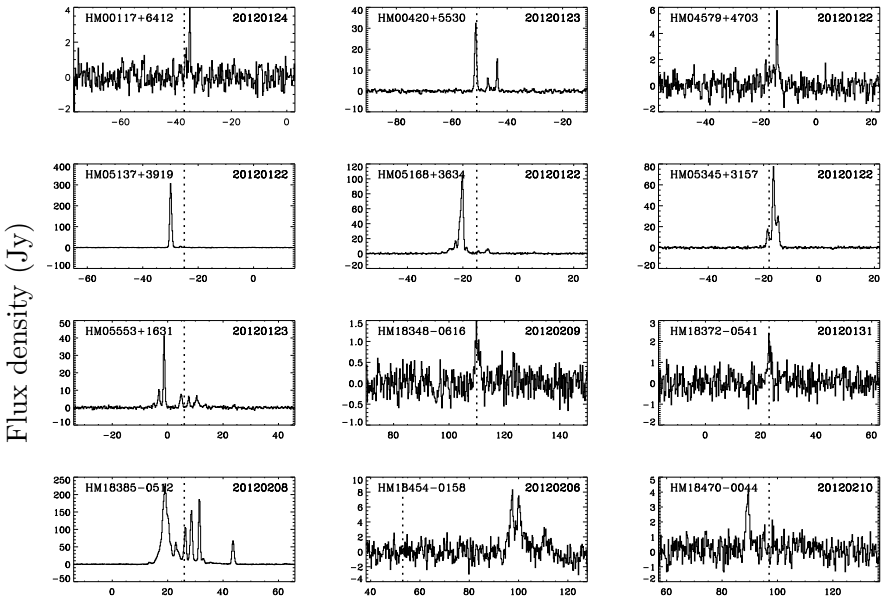

Figure 3.31: Same as in Figure 3.26 except for the source detected only at 22 GHz.

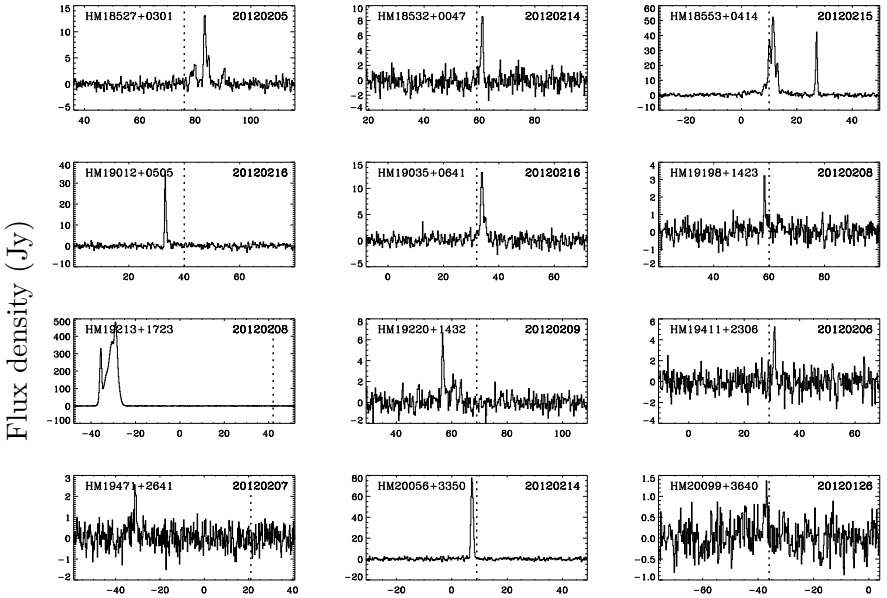

Figure 3.32: Continued

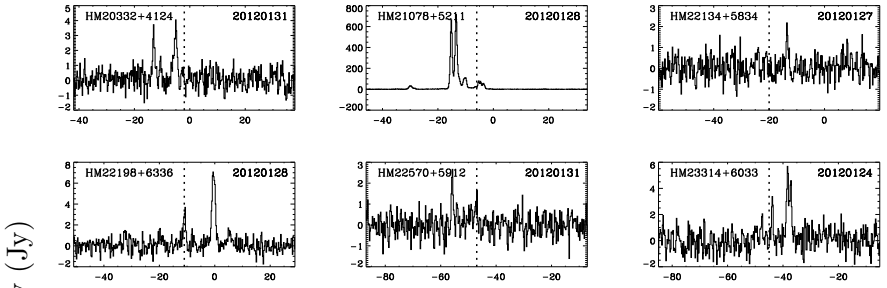

Figure 3.33: Continued

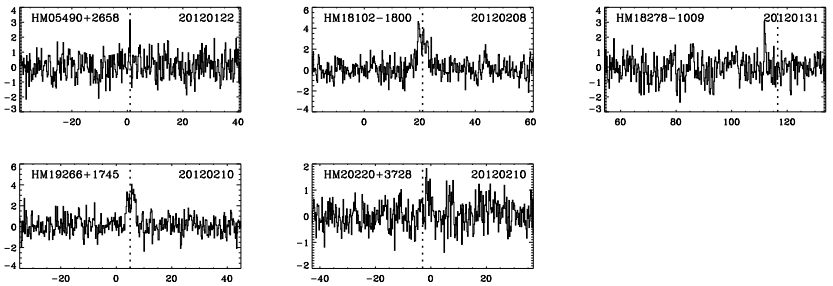

Figure 3.34: Same as in Figure 3.26 except for the source detected only at 44 GHz.

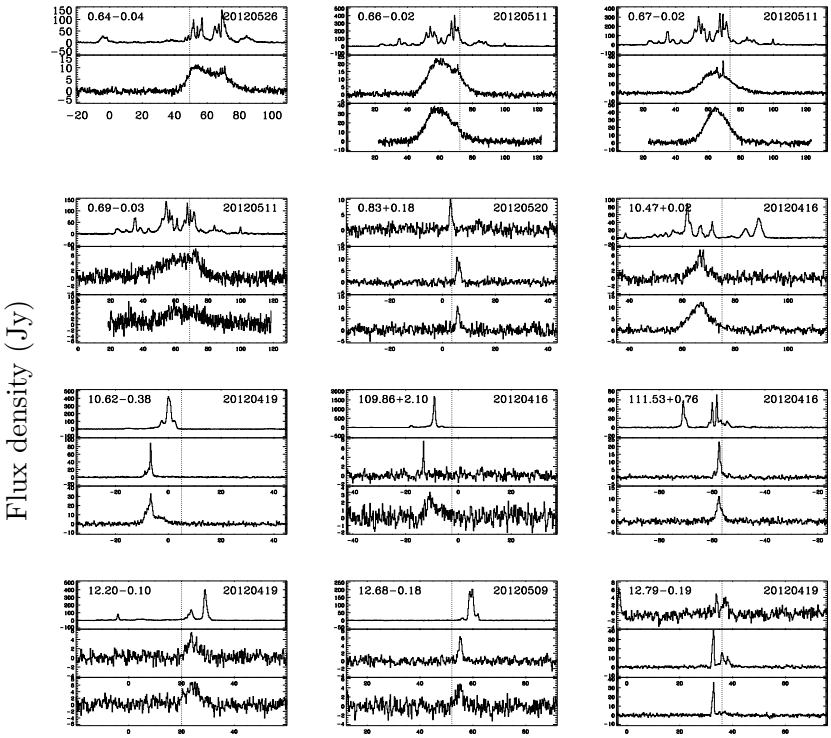

Figure 3.35: **MMSs.** (Upper panel) The detected 22 GHz H_2O, (Middle panel) 44 GHz CH_3OH, and (Lower panel) 95 GHz CH_3OH maser spectra of the sources detected in all of three transitions. Other details are same as in Figure 3.16

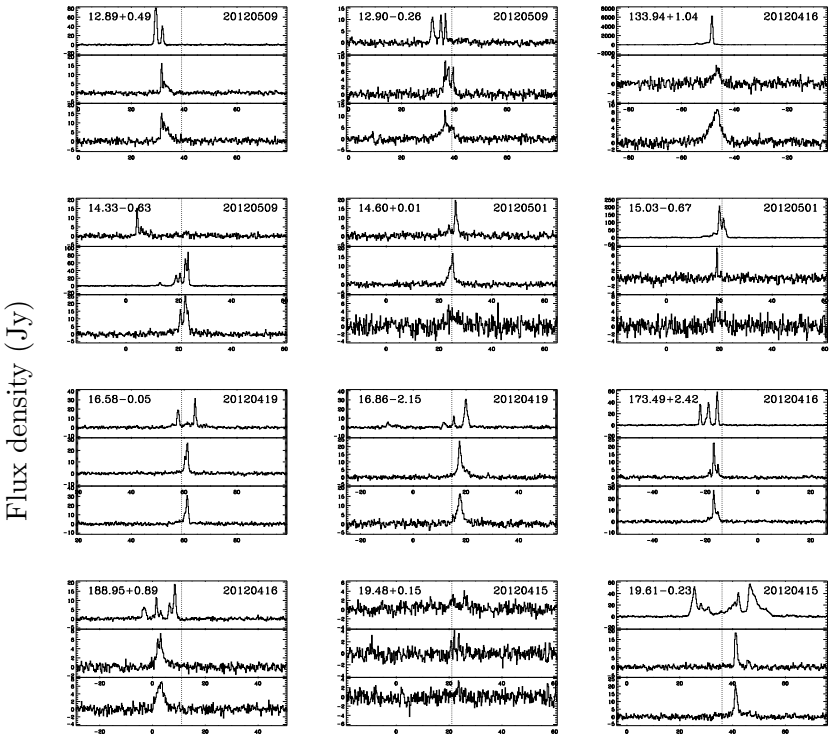

Figure 3.36: Continued

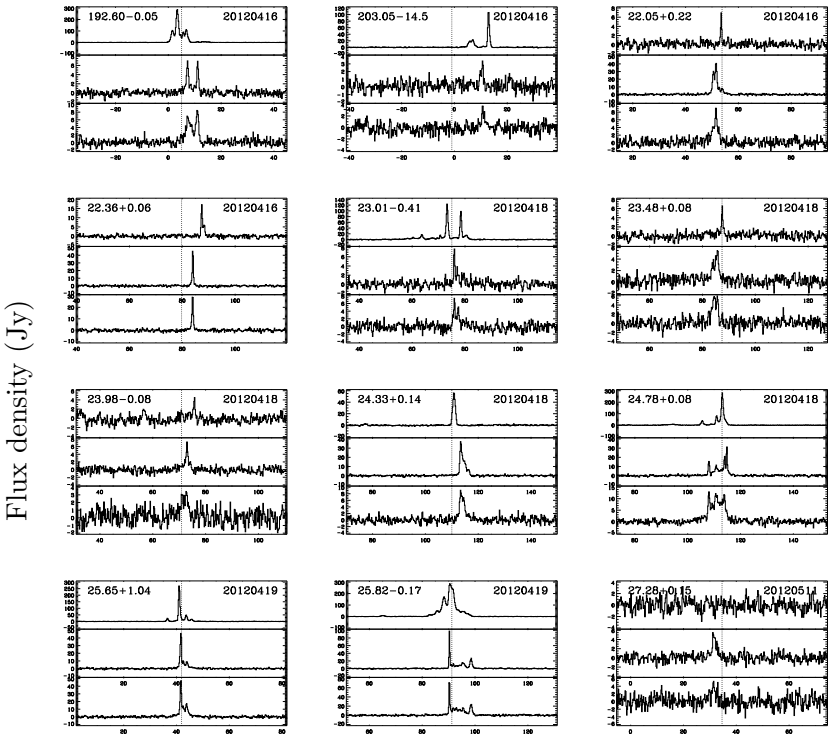

Figure 3.37: Continued

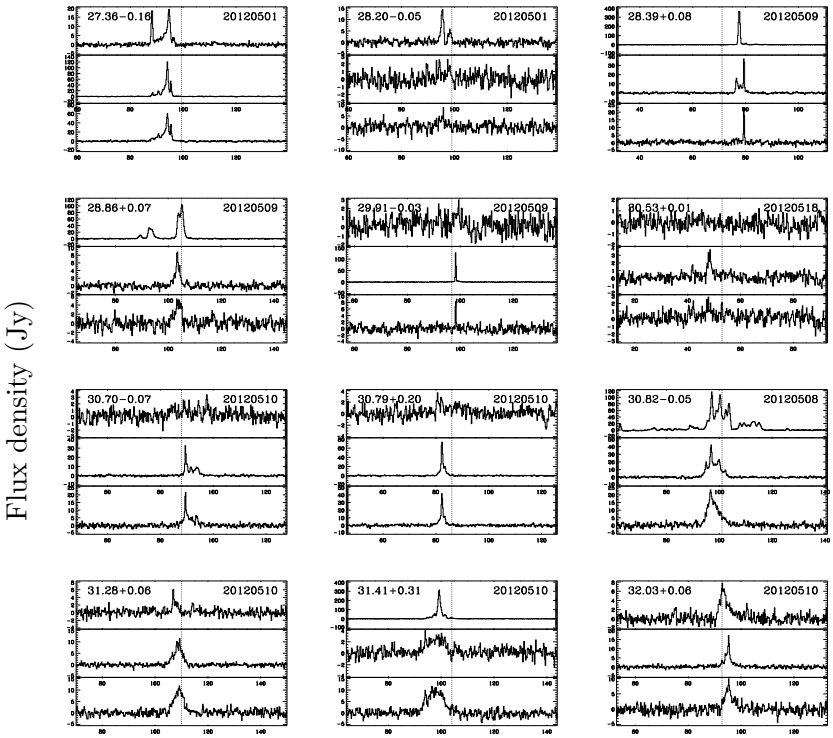

Figure 3.38: Continued

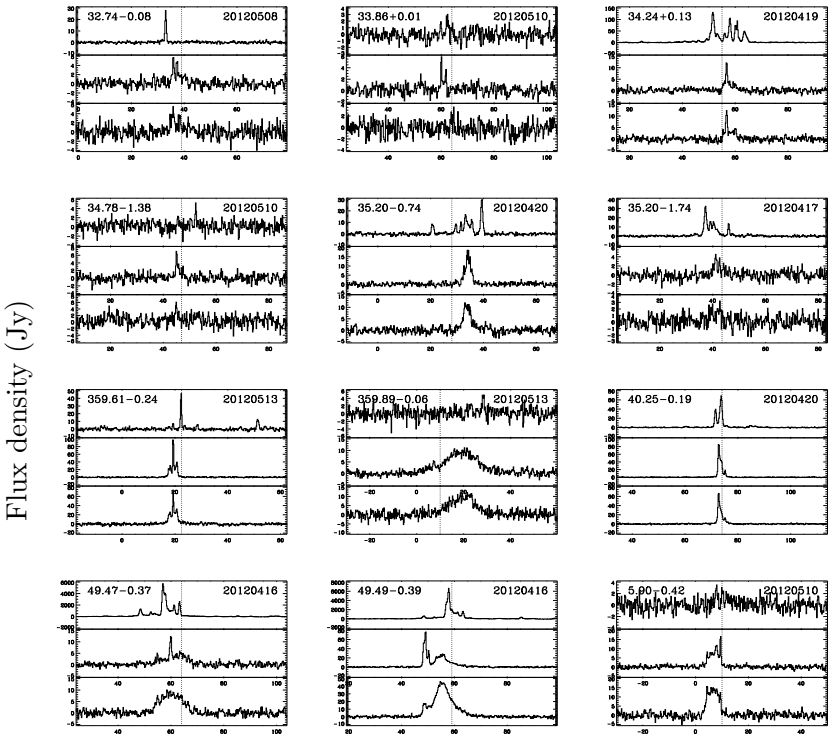

Figure 3.39: Continued

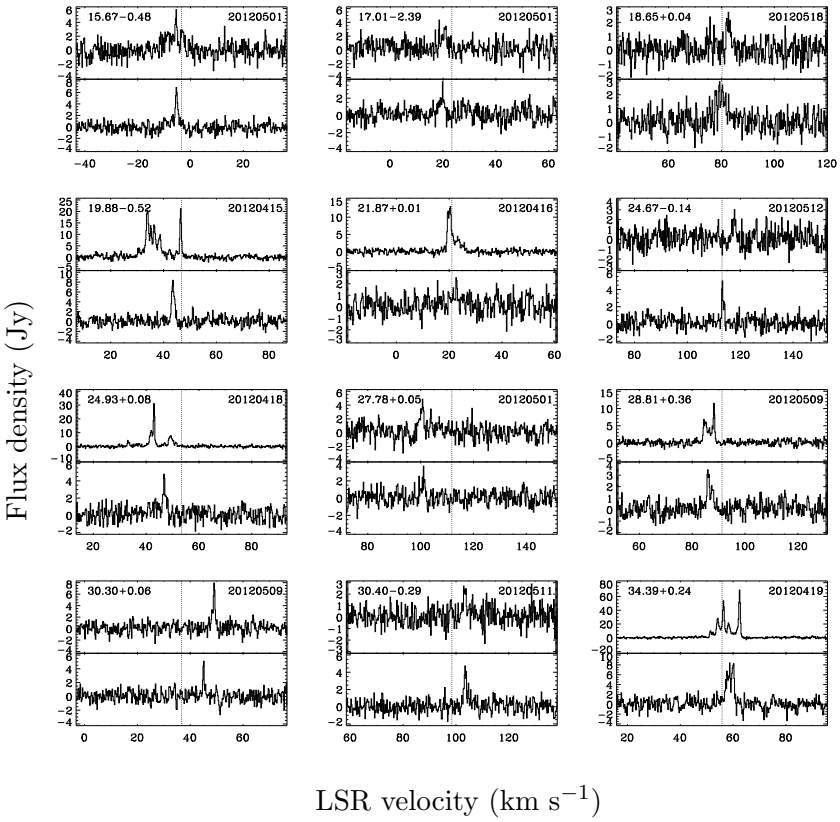

Figure 3.40: Same as in Figure 3.35 except for the source detected both at (Upper) 22 and (Lower) 44 GHz.

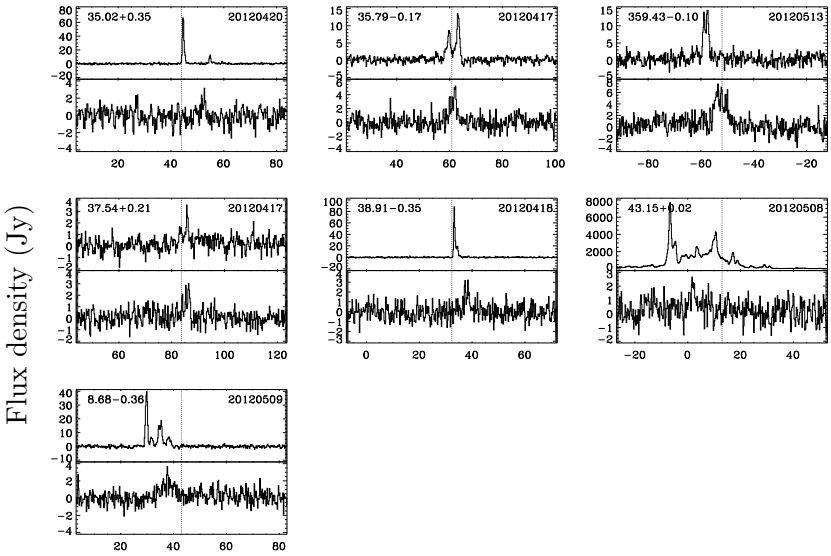

Figure 3.41: Continued

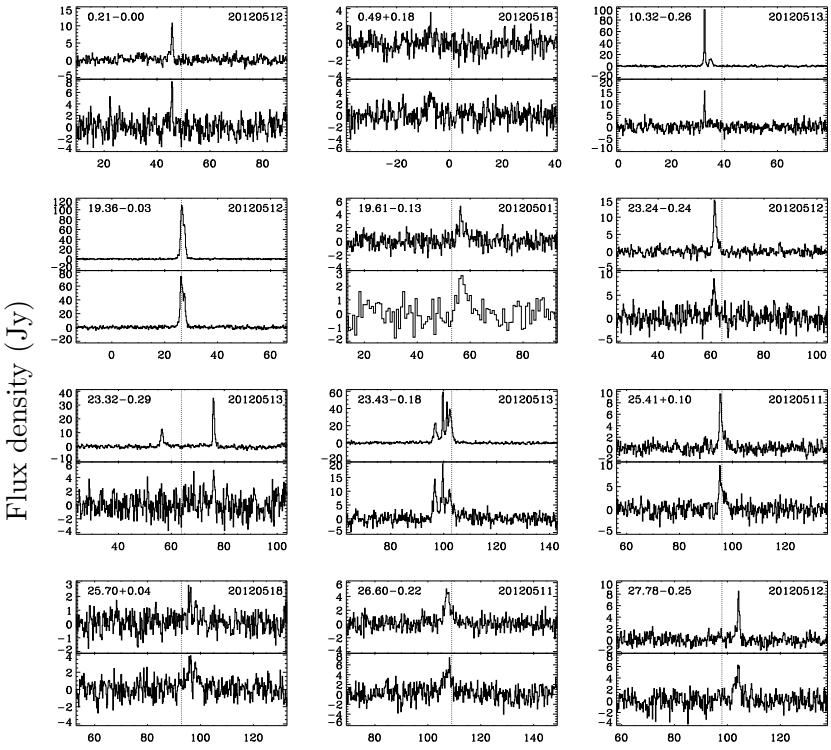

Figure 3.42: ame as in Figure 3.35 except for the source detected both at (Upper) 44 and (Lower) 95 GHz.

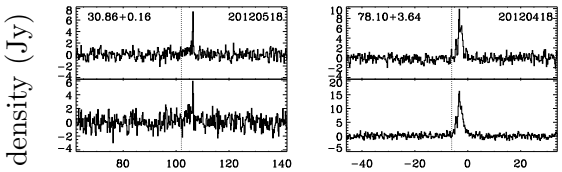

Figure 3.43: Continue

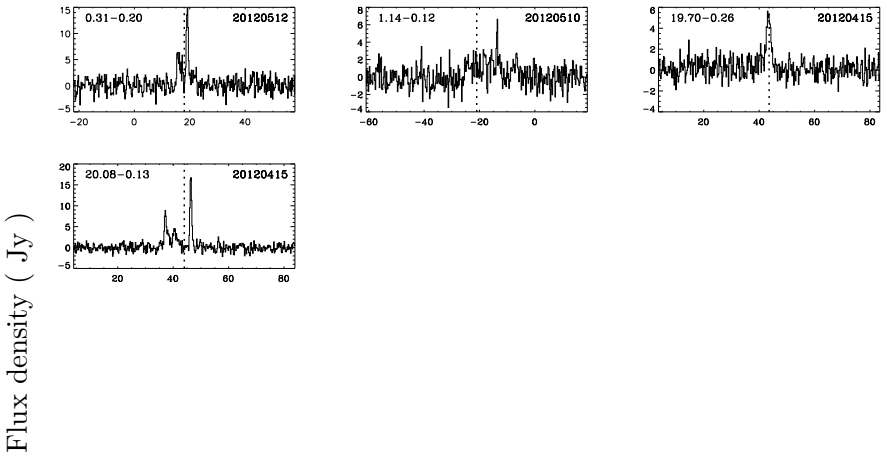

Figure 3.44: Same as in Figure 3.35 except for the source detected only at 22 GHz.

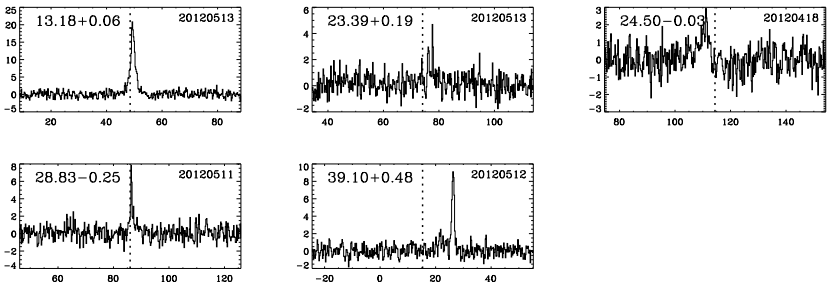

Figure 3.45: Same as in Figure 3.35 except for the source detected only at 44 GHz.

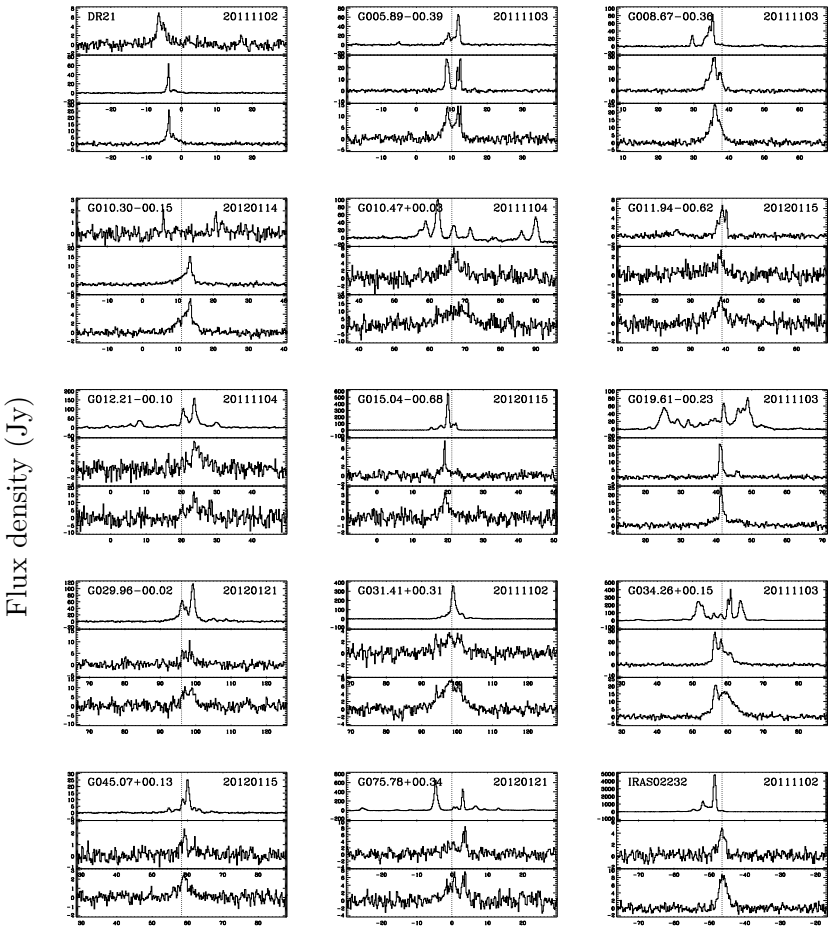

Figure 3.46: **UCHIIs.** Upper panel) The detected 22 GHz H_2O, (Middle panel) 44 GHz CH_3OH, and (Lower panel) 95 GHz CH_3OH maser spectra of the sources detected in all of three transitions. Other details are same as in Figure 3.16

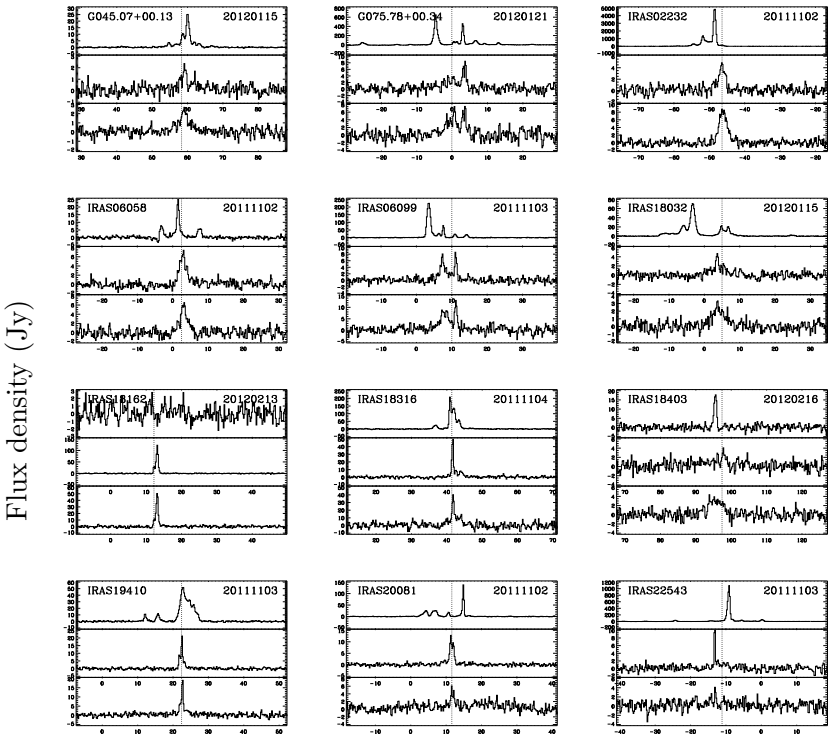

Figure 3.47: Continued

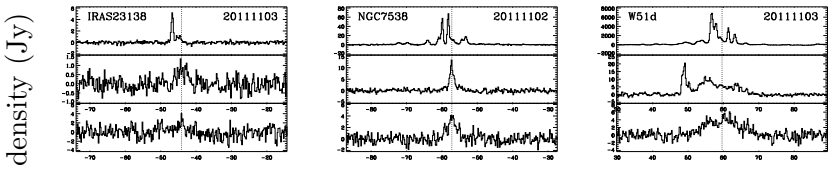

Figure 3.48: Continued

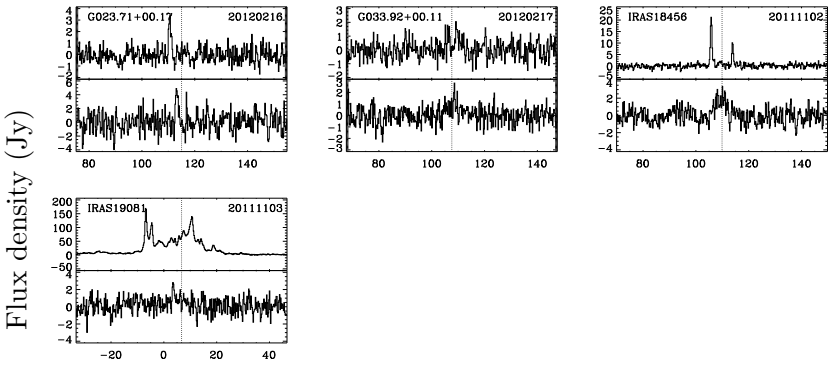

Figure 3.49: Same as in Figure 3.46 except for the source detected both at (Upper) 22 and (Lower) 44 GHz.

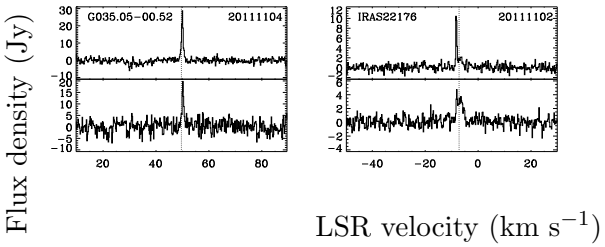

Figure 3.50: Same as in Figure 3.46 except for the source detected both at (Upper) 44 and (Lower) 95 GHz.

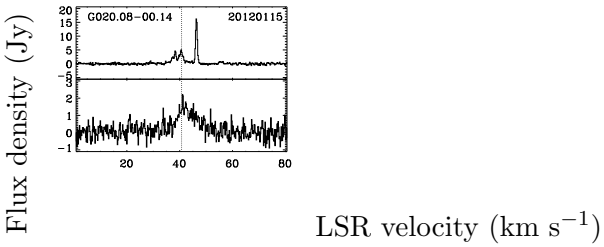

Figure 3.51: Same as in Figure 3.46 except for the source detected both at (Upper) 22 and (Lower) 95 GHz.

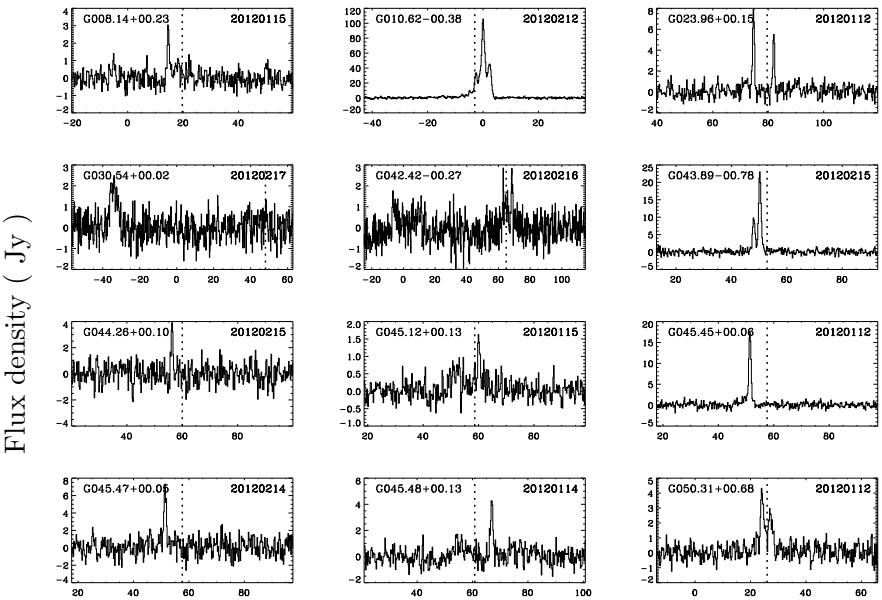

Figure 3.52: Same as in Figure 3.46 except for the source detected only at 22 GHz.

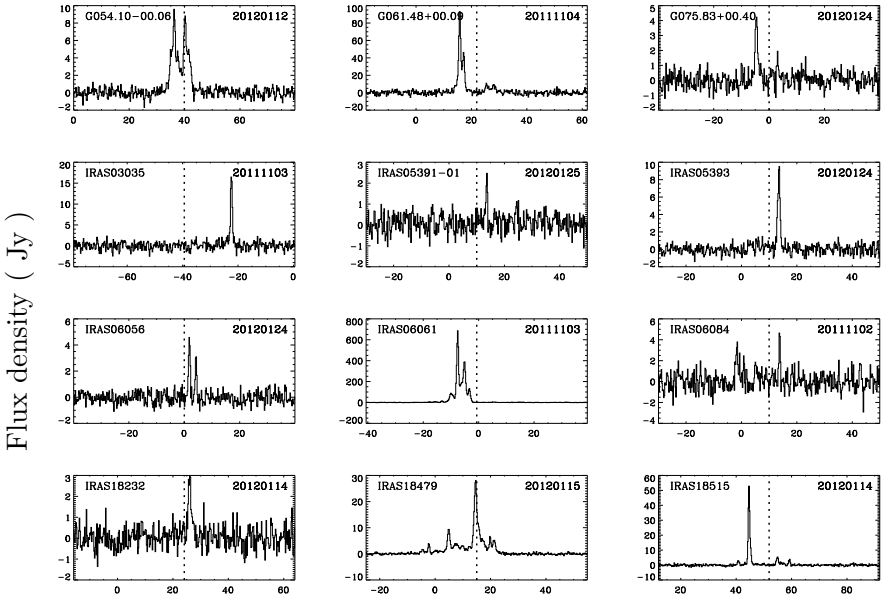

Figure 3.53: Continued

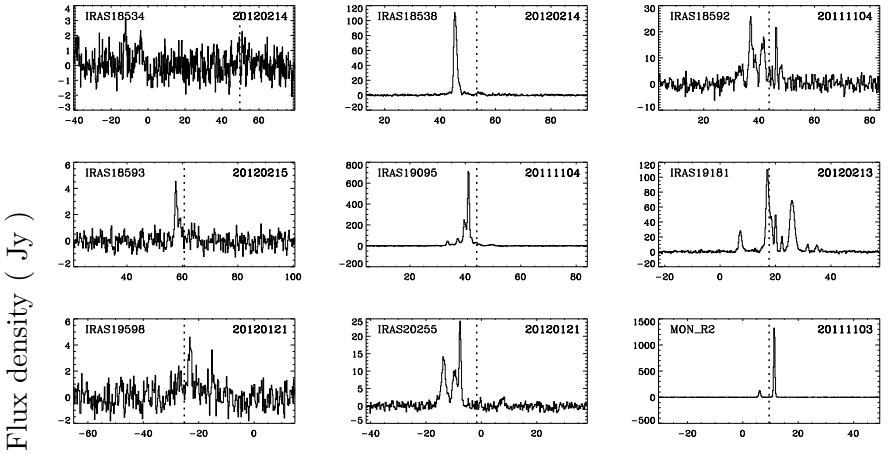

Figure 3.54: Continued

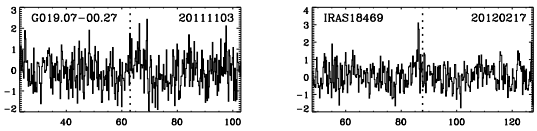

Figure 3.55: Same as in Figure 3.46 except for the source detected only at 44 GHz.

Chapter 4

Summary and Future Work

4.1 Summary

This thesis present a major investigation into the relationship between common masers of 22 GHz water (H_2O) and 44/95 GHz methanol (CH_3OH) and massive star forming regions in different evolutionary stages. Maser line data spanning two years of observations are used to probe the maser line property at sites of massive star forming regions. The overall goal is to identify maser signatures as an evolutionary indicator in massive star formation.

The KVN telescope was used to survey for maser emission of 22 GHz H_2O and 44 GHz / 95 GHz class I CH_3OH towards 782 massive star forming regions. Targets consist of 130 IRDCs, 299 RMSs, 135 HMPOs, 116 MMSs, and 103 UCHIIs and covers a wide range of

evolutionary phases.

The overall detection rates of any maser emissions are 32%, 51%, 61%, 96% and 67%toward IRDCs, RMSs, HMPOs, MMSs and UCHIIs, respectively. The 22 GHz, 44 GHz and 95 GHz maser detection rate for IRDCs are 22%, 22% and 21% compared to 63%, 34%, and 29% for UCHIIs, respectively. By these trends of detection rates, H_2O and class I CH_3OH maser are turn on at the very early stage of evolutions(IRDC) and survive as the central source evolves into UCHIIs. We identified 268 new maser sources: 15 at 22 GHz, 56 at 44 GHz and 197 at 95 GHz. We detected H_2O maser of high-velocity (> 30 km s^{-1}) features in 99 source of 386 H_2O maser emissions(26%): 10(37%), 27(20%), 12(18%), 32(35%), and 18(28%) for IRDCs, RMSs, HMPOs, MMSs, and UCHIIs, respectively. We discovered nine H_2O masers of being dominant H_2O maser outflow candidates from RMS samples.

The line parameter of the peak flux density(S_p), the relative peak velocity($V_{\rm rel}$) and the velocity range($v_{\rm range}$) for sources at a different stage of evolution. The 22 GHz H_2O masers show a significant increasing in the distributions of S_p and $v_{\rm range}$. The $v_{\rm range}$ of both class I CH_3OH masers reveal a weak increasing tendency with evolutionary phase. Both of 44 and 95 GHz class I CH_3OH masers have very similar properties. They have a strong correlation in the $S_{\rm p}$, $V_{\rm rel}$, and the isotropic maser luminosity. The slope of dependence between the peak flux densities of the two masers ($S_{\rm p,95}/S_{\rm p,44}$) is 0.43. Seven sources that were detected at both lines have different $v_{\rm p}$ by > 2 km s^{-1}. They turn out to have multiple components of narrow lines along with broad quasi-thermal feature.

We examined the relationship between the maser luminosity and

physical conditions of parental clumps(cores). As a result, there are strong ($\rho > 0.5$) correlations between the maser luminosity and the bolometric luminosity and the clump mass for all three masers. By the FWHM linewidth of $NH_3(1,1)$, the subsamples associated with NH_3 data can be divided into two distinct groups : *narrow* and *wide* group. The former group consists of IRDCs, RMSs and HMPOs with a mean of 1.76 km s^{-1}, while the latter group contains MMSs and UCHIIs with a mean of 2.57 km s^{-1}. As for the kinetic temperature, we find a weak increasing trend with evolutionary phase.

Using the L_{bol}/M_{clump} ratio, we compared the distribution on each type of central object. Generally we can divide five different type of source into three distinct group (IRDCs / RMSs and HMPOs / MMSs and UCHII) in $L_{rmbol}/M_{\ rmclump}$ space. Sources associated with any maser emission are clearly separated into the same three group as well. There is no robust difference in the distribution on the combinations with each maser emission.

Our investigation on the virial parameter against M_{clump} suggest that ATLASGAL clumps with any maser emission are more gravitationally stable than those with no maser emissions in a wide range of clump mass. We find that L_{maser}/L_{bol} appear to decrease as driving source evolves. The peak of flux ratio($S_{p,44}$ /$S_{p,95}$) for class I CH_3OH maser seem to have no significant variation as for the evolutionary sequence.

4.2 Future work

The works within this thesis present a number of ways for further investigation. The move to observations at high angular spatial resolution is expected to bring many exciting results and answers to the currently unanswered question. Interferometric observations of maser transitions (22 GHz H_2O and 44 / 95 GHz CH_3OH) for subsample of this work are required to allow a more detailed examination of the relationship between environment of massive SFRs and maser activity and diminish a false identification of driving source by single-dish observations. It would be interesting that the high resolution observations of maser spots compare the follow-up observations of outflow tracers like SiO molecular transition or near-IR H_2 imaging. Since 22 GHz H_2O and 44 / 95 GHz class I CH_3OH masers are known commonly to trace outflows, these comparison could yield a crucial information not only to distinguish if the picture suggested by Beuther & Shepherd (2005) holds, where the outflows decollimates with evolution, but also help to probe if there is a difference in the outflows between faint and strong maser sources. Sub-millimeter continuum mapping at high resolution would be a great asset to maser surveys in this thesis. The recently commissioned MUSTANG2 bolometer on the GBT will allow mm observations at a comparable resolution ($\sim 8''$) to the 70 μm Herschel data. To follow up these survey may help build on better global properties of massive SFRs in Galaxy. These follow-up observations by different type of observations will aid in a better understanding of a role of maser phenomenon in massive SFRs. As an evolutionary picture of maser emission, class I CH_3OH maser source within class II 6.7 GHz MMB survey area could be further investigated to test the

evolutionary scenario that the class I masers would be present before the class II(Ellingsen et al. 2006). Comparison maser spots of both CH_3OH masers with outflow morphologies will clarify the nature of driving sources for different class of CH_3OH masers. Moreover these follow-up observations at high resolution will provide a clue with the EHV dominant shifted source of H_2O maser emission.

초 록

우리 은하의 성간에는 물(22 GHz), 메탄올(44/95 GHZ) 등의 메이저가 발견되고, 관련된 기체 분자들은 차가운 성간 먼지에 있다가 충격파에 의해 증발해서 생성된다고 여겨진다. 이 메이저들은 주로 무거운 별 생성 영역들과 관련되어 있다고 알려진 지역에서 출현하므로, 메이저 탐사는 무거운 별 생성 영역에 대한 통계 연구를 가능하게 한다. 그런데 우리는 무거운 별 생성 과정에 나타나는 메이저 현상의 역할을 완전히 이해하지 못하고 있다. 이 논문의 주요 목적은 서로 다른 진화 단계에 있는 별 생성 영역과 대한 메이저 현상의 상관관계를 조사하여 밝히는 것이다. 우리는 782개의 무거운 별 생성 영역에 대한 물(22 GHz)과 메탄올(44/95 GHz) 메이저를 KVN 단일경 동시 관측을 수행했다. 관측된 천체는 다섯 종류인데, 이는 Infrared Dark Clouds (IRDCs), Red MSX Sources (RMSs), high-mass protostellar objects (HMPOs), Methanol Maser Sources (MMS), ultra-compact HII regions (UCHIIs) 등이다. 각 천체별 메이저 검출률은 32%(IRDCs), 51%(RMSs), 61%(HMPOs), 96%(MMSs), 67%(UCHIIs) 등이다. IRDCs에서 UCHIIs로 중심 천체가 진화 할수록 22 GHz 와 44 GHz 의 검출률이 증가하는 경향을 보인다. RMS 천체들에서 138

개는 6.7 GHz Methanol Multibeam (MMB) 탐사 영역과 중첩되고, 이중 25% 에서 6.7 GHz class II 메탄올 메이저가 검출되었다. 검출된 물 메이저에서 26%(99/386)는 30 km s^{-1} 이상의 고속선을 방출한다. 중심천체의 속도에는 방출선이 없고 30 km s^{-1} 이상의 고속선만 방출하는 물 메이저 천체가 있는데, 이러한 물 메이저원을 RMS 천체에서 9개 발견했다. 천이과정이 비슷한 그룹으로 분류되는 44 GHz와 95 GHz들의 스펙트럼을 비교하면 선 파라미터들이 서로 비슷하다. 따라서 이 메이저 방출선은 비슷한 환경에서 만들어 졌을 것이라 생각된다. 관측된 전체 샘플에 대해서 메이저의 등방광도(L_{maser})는 중심별의 광도(L_{bol})와 관계뿐 아니라, ATLASGAL 서브 밀리미터 자료에서 유도한 clump의 질량(M_{clump})과 좋은 상관관계($p > 0.5$)를 이루고 있음을 알 수 있었다. 문헌에서 찾은 암모니아 자료와 연관된 메이저원들의 선폭과 유도된 운동학적 온도를 보면 중심 천체가 진화함에 따라 선폭이 넓어지고 온도가 상승하는 경향을 보인다. 성간 분자운의 진화 척도로 알려진 L_{bol}/M_{clump} 비율을 다섯 가지 관측표본에 대하여 메이저 방출선과 조합들의 분포를 분석한 결과, 메이저 선을 방출 여부와 메이저 천이의 종류에 따른 분포의 차이를 볼 수 없었다. 비리알 파라미터를 계산하고 관측천체에 적용한 결과 메이저선을 방출하는 천체일수록 중력적으로 더 안정한 경향을 보이는 것을 발견했다. L_{maser}/L_{bol} 비가 진화된 천체일수록 감소하는 경향을 찾아냈다.

주요어 : 적외선:성간물질, 성간물질:분자, 메이저:성간물질. 별:생성

학 번 : 2006-30782